Exploring Sterically Constrained Achiral Gamma Amino Acids in the Design of Novel Peptide Foldamers

A thesis
Submitted in partial fulfillment of the requirements
of the degree of
Doctor of Philosophy

By

Rajkumar Misra

ID: 20123199

Indian Institute of Science Education and Research, Pune

Dedicated to My family ……

CERTIFICATE

This is to certify that the work incorporated in the thesis entitled "**Exploring Sterically Constrained Achiral Gamma Amino Acids in the Design of Novel Peptide Foldamers**" submitted by **Rajkumar Misra** carried out by the candidate at the Indian Institute of Science Education and Research (IISER), Pune, under my supervision. The work presented here or any part of it has not been included in any other thesis submitted previously for the award of any degree or diploma from any other University or Institution.

Date:

Dr. Hosahudya N. Gopi

(Research Supervisor)

Associate Professor, IISER-Pune

Pune-411008, India

Declaration

I hereby declare that the thesis entitled "**Exploring Sterically Constrained Achiral Gamma Amino Acids in the Design of Novel Peptide Foldamers**" submitted for the degree of Doctor of Philosophy in Chemistry at Indian Institute of Science Education and Research (IISER), Pune has not been submitted by me to any other University or Institution. This work was carried out at Indian Institute of Science Education and Research (IISER), Pune, India under the supervision of Dr. Hosahudya N. Gopi.

Date:

Rajkumar Misra

ID: 20123199

Senior Research Fellow

Dept. of Chemistry, IISER-Pune

Pune-411008

Acknowledgement

My first debt of gratitude must go to my advisor, Dr. Hosahudya N. Gopi. He patiently provided me the vision, encouragement and necessary advice to proceed through the doctorial program and complete my dissertation. He has been a strong and supportive adviser to me throughout my PhD tenure. His principles of life and dedication to work have always inspired me during my graduate studies. I would like to express my sincere gratitude to my supervisor for his valuable guidance, suggestion and developing me as researcher.

I would like to convey my sincere thank to our former Director Prof K. N. Ganesh for providing such excellent infrastructure and research facility here at IISER Pune. His enthusiasm about science was always source of inspiration.

I am sincerely thankful to my research advisory committee members Dr. Sudipta Basu and Dr. H. V. Thulasiram for their valuable suggestions during my RAC meetings which helped me a lot to shape my research projects. I also would like to present my sincere appreciation to all chemistry faculties of IISER, Pune for their cooperation and guidance. I would like to acknowledge CSIR India for providing financial support during the last five years.

I thank Dr. K. M. P. Raja (Madurai Kamaraj University), Gijo George (I.I.S.C Bangalore) for NMR modelling structures and Dr. T. S. Mahesh, Dr. Jeetender Chugh for their help in 2D NMR experiments. and Prof. Dr. Hans-Jörg Hofmann for quantum mechanical calculation (Institute of Biochemistry, Liepzig, Germany).

I am fortunate to work with excellent blend of talented and unique lab mates who helped me a lot in solving my research problems. Their moral support and helping nature gave me strength to move forward during my critical time. I have very special appreciation for Dr. Anupam Bandyopadhyay, Dr. Sandip Jadhav. Dr. Sachin Mali, Dr. Ganesh Kumar Mothukari, Dr. Susheel Benke who helped me a lot in my research career. I also thank my other lab mates Rahi M. Reja, Anindita, Rupal, Ankita and Shivani. Sumeet Kumar Singh, Shiva Shankar, Kuruva Veeresh, Sachin Nalawade, DR Puneeth Kumar, Sanjit Dey, Vivek Kumar, Saikat Pahan, Abhijith S. A and Rajat Patel for their direct or indirect inputs in my research.

I must acknowledge the help from Nitin for NMR analysis, Archana for X-ray instrument, Swati Dixit for MALDI TOF/TOF mass analysis. My Special thank to Mr. Nitin Dalvi and Mahesh Jadav

for assisting my research with purchase orders and other help. I am very thankful to Mayuresh for the administrative help.

Life becomes boring if I would not have met wonderful friends, Shayama and Arunava. As we have been together for long time and shared every moment and experience of life. They were always there for me whenever I required. Their kind and helping attitude always supported me in my difficult time. I present my deepest thank to both of you for bearing me for such a long time.

Further I would like to extend my special thank to Dr. Avishek, Dr. Barun, Dr. Tanmoy, Dr. Biplap, Sudev, Chandra, Debanjan, Avik, Dhruba, Shiva, Prabhakar, and all friend from chemistry department for their cooperation. Because of all these people all my five years in IISER passed just like few days.

It would have difficult to complete my PhD work without support from my family. I present my deepest gratitude to my family especially to my parents for their unconditional love and support. The care by my sisters and their love was always behind me during my PhD tenure.

Finally, I would like to sign off with pray to Lord Ma Kali for giving me strength and her blessing to complete my research work and submit this thesis.

Rajkumar Misra

CONTENTS

Chapter 1

General introduction of peptide Foldamers composed of β and γ amino acids and their hybrid sequences

Chapter 2

Artificial β-double helices from achiral γ-peptides

Chapter 3

Structural dimorphism of achiral α,γ-hybrid peptide foldamers: coexistence of 12- and 15/17-helices

Chapter 4

Modulating the structural properties of α,γ-hybrid peptides by α-amino acid residues: Uniform 12-helix *versus* "mixed" 12/10-helix

---

Chapter 5

Exploring structural features of folded peptide architectures in the construction of nanomaterials

Chapter 6

Ambidextrous α,γ-hybrid peptide foldamers with reversal of helix directionality

Abbreviations

Ac_2O = Acetic anhydride

ACN = Acetonitrile

AFM = Atomic Force Microscopy

AcOH = Acetic acid

Aib = α-Amino isobutyric acid

aq. = Aqueous

Bn = Benzyl

Boc = tert-Butoxycarbonyl

$(Boc)_2O$ = Boc anhydride

^tBu = tertiary Butyl

Calcd. = Calculated

Cbz-Cl = Benzyl chloroformate

CCDC no. = Cambridge Crystallographic Data Centre number

CD = Circular Dichroism

COSY = COrrelation SpectroscopY

CIF = Crystallographic Information File

dγ = dehydro gamma

DBU = 1,8-Diazabicyclo[5.4.0]undec-7-ene

DCC = N, N' –Dicyclohexylcarbodiimide

DCM = Dichloromethane

DiPEA = Diisopropylethyl Amine

DMAP = 4-Dimethylaminopyridine

DMF = Dimethylformamide

DLS = Dynamic Light Scattering

DMSO = Dimethylsulfoxide

DNA = Deoxyribonucleic acid

EtOH = Ethanol

Et = Ethyl

EDC=1-Ethyl-3-(3-dimethylaminopropyl)carbodiimide,

EtOAc = Ethyl acetate

Fmoc = 9-Fluorenylmethoxycarbonyl

Fmoc-OSu = N-(9-Fluorenylmethoxycarbonyloxy) succinimide

g = gram

h = hours

HBTU = 2-(1H-benzotriazol-1-yl)-1, 1, 3, 3-tetramethyluronium hexafluorophosphate

H-bond = Hydrogen bond

HOBt = Hydroxybenzotriazole

HCl = Hydrochloric acid

IR = Infrared spectroscopy

IBX = 2-Idoxybenzoic acid

LAH = Lithium Aluminium Hydride

M = Molar

MALDI-TOF/TOF = Matrix-Assisted Laser Desorption/Ionization-Time of Flight

MBHA = Methyl bezydrylamine

Me = Methyl

MeOH = Methanol

mg = Milligram

min = Minutes

µL = Micro liter

mL = Milliliter

mM = Millimolar

mmol = millimoles

m.p = Melting Point

MS = Mass Spectroscopy

N = Normal

NHS = N-hydroxy succinimide

NMP = N-methyl pyrrolidone

NMR = Nuclear Magnetic Resonance

NOE = Nuclear Overhauser Effect

ORTEP = Oak Ridge Thermal-Ellipsoid Plot Program

PG = Protecting Group

ppm = Parts per million

Py = Pyridine

ROESY = **R**otating-frame nuclear **O**verhauser **E**ffect correlation **S**pectroscop**Y**

RP- HPLC = Reversed Phase-High Performance Liquid Chromatography

RT = Room Temperature

SEM = Scanning Electron Microscopy

TEM = Transmission Electron Microscopy

TFA = Trifluoroacetic acid

THF = Tetrahydrofuran

UV = Ultraviolet–Visible Spectroscopy

TOCSY = TOtal **C**orrelation **S**pectroscopY

Abstract

The relationship between a well-defined structure and function of proteins inspire the creation of foldamers from non-natural building blocks. Various types of β-, γ- and their higher homologues have been widely explored to design protein structure mimetics. Inspired by the various types of folded architectures of β- and γ-peptides and their applications in chemical biology, medicinal chemistry and biomaterials, we have examined the helical architectures available to the sterically constrained gem-dialkyl substituted γ-amino acids. The single crystal and solution conformational analysis of the homooligomers of 4,4-dimethyl substituted (*E*)-vinylogous amino acids reveal a remarkable β-double helix structures. The beta-double helix structures are stabilized by the interstrand H-bonds. In continuation, we encountered a structural dimorphism in achiral α,γ-hybrid peptides composed of Aib (α-amino isobutyric acid) and 4,4-dimethyl substituted γ-amino acid, Aic (4-amino isocaproic acid) in 1:1 alternate order. The structural analysis shows two helix types, a novel 12- helical conformation in shorter sequences of 4-7 residues and an unprecedented 15/17-helix in longer sequences of nine residues. Interestingly, the 15/17- and 12-helices in alpha, gamma-hybrid peptides with their 5→1 and 4 →1 hydrogen bonding patterns can be recognized as backbone expanded analogs of the native α- and 3_{10}-helices, respectively. Further, replacement of Aib residues in 1:1 alternating α, γ-hybrid peptides composed of Aib and Aic with natural α-amino acids (leucine, alanine) leads to the mixed 12/10-helical conformations with alternating H-bonding directionality. This is in sharp contrast to the natural polypeptide helices. Instructively, replacing aliphatic amino acid residues with aromatic Phe residues in 1:1 alternating α,γ-hybrid peptides adopted β-sheet type extended conformations. The hybrid peptides with extended conformations were spontaneously self-assembled into remarkable capsules through multiple CH–π, π–π and H-bonds. As a proof of concept, we further showed the controlled release of encapsulated fluorescent molecules from peptide capsules using cationic dipeptide as a trigger. Further, we have the studied the conformational properties of achiral hybrid peptides composed 1:1 alternating Aib and 3,3-dimethyl substituted gamma-amino acid (Adb, 4-amino 3,3-dimethylbutanoic acid). The single crystal

and solution structure analysis revealed a rare co-existence of left and right-handed helical conformations (tendril perversion) and helix terminating property at the C-terminus within a single molecule. Overall, the conformational properties of sterically constrained gem-dimethyl substituted γ-amino acids presented in this thesis will provide wide opportunities to explore them as vital building blocks towards the design of new functional foldamers as well as templates for generation functional biomaterials.

Publications

1. Artificial β-double helices from achiral γ-peptides. **R. Misra**, S. Dey, R. M. Reja, H. N. Gopi *Angew Chem DOI: 10.1002/ange.201711124*
2. Modulating the structural properties of α,γ-hybrid peptides by alpha-amino acid residues Uniform 12-helix versus "mixed" 12/10-helix. **R. Misra**, K. M. P. Raja, H.-J. Hofmann, H. N. Gopi *Chem. Eur. J.* **2017**, 23, 16644
3. Structural dimorphism of achiral α,γ-hybrid peptide foldamers: coexistence of 12- and 15/17-helices. **R. Misra**, A. Saseendran, G. George, K. Veeresh, K. M. P. Raja, S. Raghothama, H.-J Hofmann, and H. N. Gopi *Chem. Eur. J.* **2017**, *23*, 3764
4. Backbone engineered γ-peptide amphitropic gels for immobilization of semiconductor quantum dots and 2D cell culture. **R. Misra**, A. Sharma, A. Shiras, and H. N Gopi *Langmuir*, **2017**, *33* , 7762.
5. Exploring structural features of folded peptide architectures in the construction of nanomaterials. **R. Misra**, R. M. Reja, L. V. Narendra, G. George, S. Raghothama and H. N. Gopi *Chem. Commun*., **2016**, *52*, 9597.
6. Structural features and molecular aggregations of designed triple-stranded β-sheets in single crystals. A. Bandyopadhyay, **R. Misra** and H. N. Gopi *Chem. Commun.*, **2016**, *52*, 4938.
7. Foldamers to nanotubes: influence of amino acid side chains in the hierarchical assembly of α,γ^4 hybrid peptide helices. S. V. Jadhav, **R. Misra** and H. N. Gopi *Chem. Eur. J*. **2014**, 20, 16523.
8. Efficient access to enantiopure γ^4-amino acids with proteinogenic side-chains and structural investigation of γ^4-Asn and γ^4-Ser in hybrid peptide helices. S.V. Jadhav, **R. Misra**, S. K. Singh, and H. N. Gopi *Chem. Eur. J*. **2013**, *19*, 16256.
9. pH sensitive coiled coils: a strategy for enhanced liposomal drug delivery. R. M Reja, M. Khan, S. K Singh, **R. Misra**, A. Shiras, H. N Gopi. *Nanoscale*. **2016**, *8*, 5139.

Chapter 1

General introduction of peptide foldamers composed of β and γ amino acids and their hybrid sequences

1.1 Introduction

Proteins play a crucial role in all biological events of life. The three dimensional structures of the proteins are mainly responsible for their function. Nature specifically chooses proteins to carry out these tasks because of their ability to fold into definite and rigid three dimensional conformations (Figure 1). Using 20 natural amino acids, Nature made a myriad of proteins with definite three dimensional structures and functions.

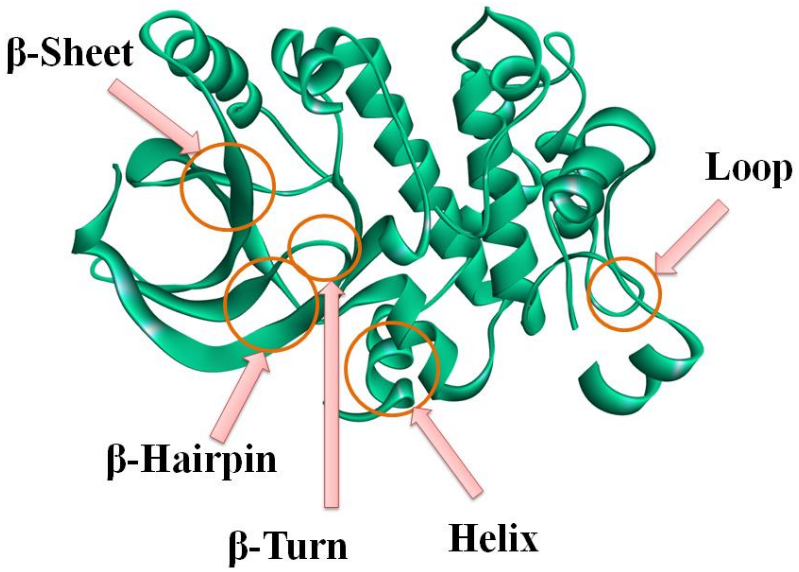

Figure 1 X-ray structure of the human mitogen-activated protein kinase 1 (MEK1). PDB code- 1s9j

The protein structures are mainly described at four levels, primary, secondary, tertiary and quaternary structures. The primary structure of a protein describes the number and sequence of amino acids arranged in the polypeptide chain. The hypothetical disintegration of protein three-dimensional structures leads to various secondary structures such as strands, helices, and reverse turns, which are assembled using loosely structured loops and associated with various noncovalent interactions.[1] The tertiary structure of a protein explains the 3D arrangements of the single polypeptide chain. The quaternary structure refers to how the protein subunits interact with each other and arrange themselves to form a larger aggregate protein complex through different noncovalent interaction like hydrogen bonding, disulphide bridge or charge interaction. The *de novo* design of protein secondary structures is not only important to understand the folding and functions of proteins but also provides enormous opportunities in the structure-based drug design.[2] Extensive efforts have been made over the past several decades to understand the conformational behaviour of polypeptides through

synthetic models composed of α-amino acids as well as stereochemically constrained amino acids.[3] Recently the introduction of backbone homologated α-amino acids such as β-, γ- and higher homologues have expanded the conformational space available to the polypeptides. The oligomers of these unnatural amino acids have shown the strong tendency to fold into specific conformations such as helices, sheets and reverse turns. These unnatural β- and γ-peptide foldamers provided a unique opportunity to design protein structure mimetics. Different types of structures adopted by the β- and γ-peptides and hybrid peptide foldamers composed of α,β-, α,γ- and β,γ-sequences are described below

1.2 Beta-peptide foldamers

In their seminal work, Seebach and Gellman introduced chiral acyclic β-amino acids and cyclic β-amino acids, respectively. The acyclic β-amino acids are backbone homologated analogues of α-amino acids. Depending on the position of the side chains on the backbone, they are classified as β^3- and β^2-amino acids. In continuation, Sharma and colleagues extensively investigated the β-peptide oligomers generated from carbo-β-amino acids. Further, Fulop and coworker, Aitkin et al and others have employed numerous types of cyclic β-amino acids in the design of β-peptide foldamers. The list of various β-amino acids used in the design of β-peptide foldamer is shown in Figure 2. The backbone conformations of these β-amino acids can recognize through the additional torsion variable θ along with ϕ and ψ. The local conformation of β-residues is shown in Figure 3.

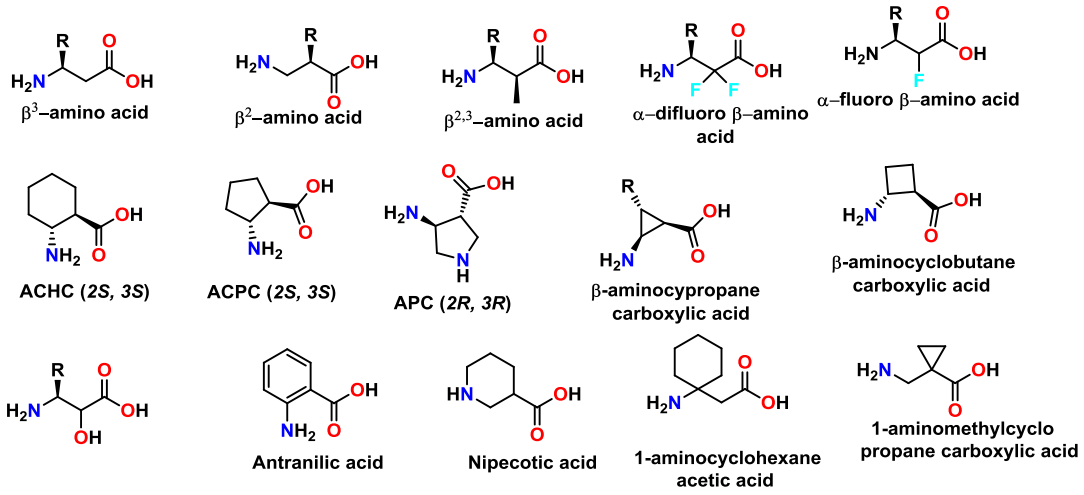

Figure 2 The list of β-amino acids used in the design of foldamers.

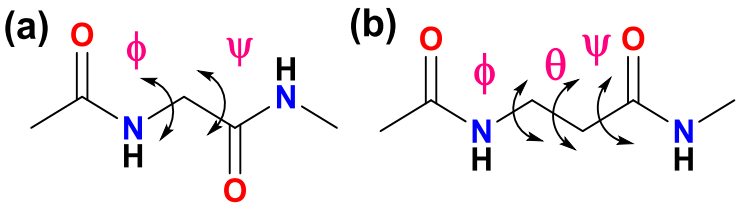

Figure 3 The torsional variables for (a) α and (b) β- amino acid were depicted.

The detailed conformational analysis of β-peptide homo-oligomers showed a variety of helical foldamers with different H-bonding pattern. The folding and H-bonding pattern is depending upon the nature of the β-residues. Gellman and colleagues reported the12- (C_{12}-, 12–membered H-bond pseudocycles) and 14-(C_{14}, 14-membered H-bond pseudocycles) helical conformations from the homooligomers of homooligomers of cyclic *trans*-2-amino cyclopentanecarboxylic acid (ACPC) and *trans*-2-aminocyclohexanecarboxylicacid (ACHC), respectively.[6] Instructively, the 12-helices have shown to adopt similar type of hydrogen bond directionality (C←N) as that of α-helix, whereas C_{14}-structures the hydrogen bond directions (N←C) are reversed. Similarly, Seebach and colleagues demonstrated the left-handed 14-helical conformations from the oligomers of acyclic β^3-amino acids. Further, they showed the right-handed 14-helix conformation from the oligomers of β^2-amino acids. In contrast to the 14-helical conformations, β-peptides composed of 1:1 alternating β^2-and β^3-amino acids have shown to adopt 12/10-helices with alternating H-bond directionality. Through extensive ab initio calculations, Hofman and colleagues provided various helical types available to the β-peptides.[7] The different types of helices available to the β-peptide as predicted by Hofmann and colleagues is shown Figure 4

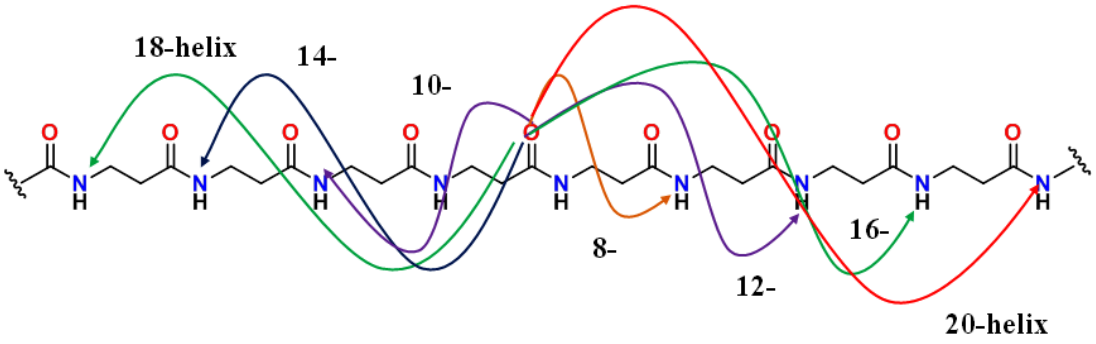

Figure 4 Possible H-bonding patterns observed of β-peptide oligomers using systematic quantum calculation.

Furthermore, Sharma and colleagues extensively investigated the conformations of the β-peptide oligomers generated from carbo-β-amino acids and shown mixed 12/10 or 10/12 helical structures.[8] Raiser et al. showed the utilization of the cyclic β-amino acids with different stereochemistry in the design of β-peptides.[9] In addition, Aitken and colleagues reported oligomers of trans-2-aminocyclobutane carboxylic acid fold into well-defined 12-helical conformation.[10] and Fulop *et al.*[11] showed utilization of various cyclic β-amino acids in the design of β-peptide foldamers. The crystal conformations of 14-helix from the β-peptide composed of *trans*-ACHA, 12-helices from the homooligomers of *trans*-ACPC and cyclobutane β-amino acid are shown in Figure 5.

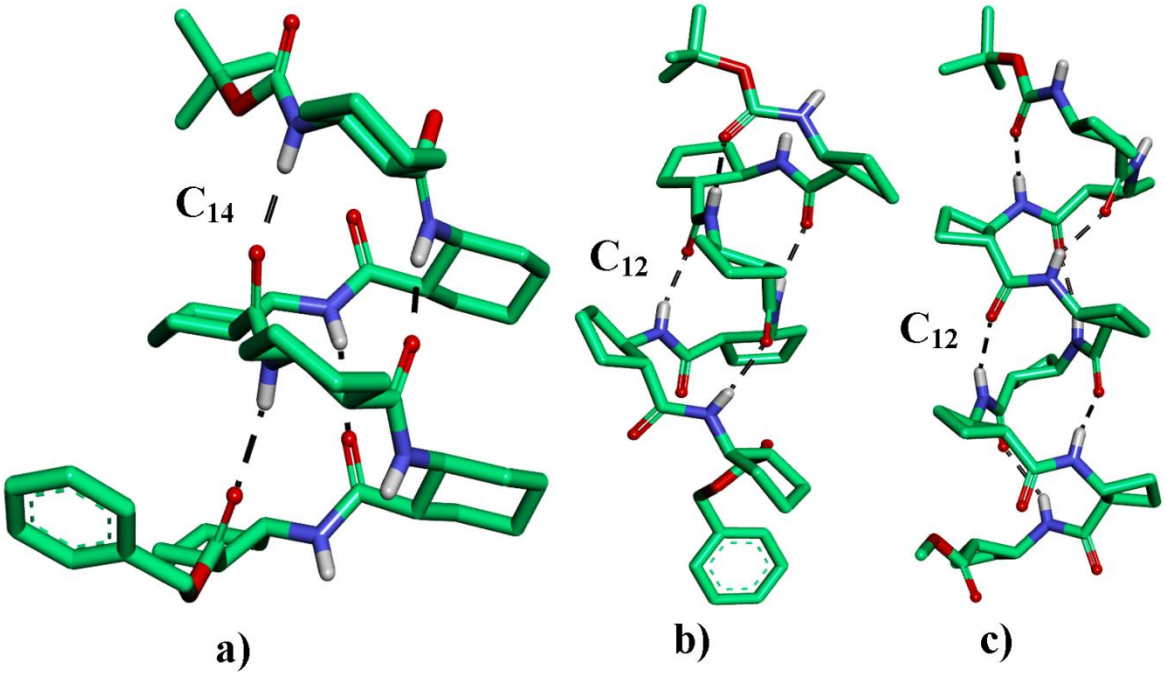

Figure 5 Helical crystal structure conformation oligomers of a) *trans*-ACHA (14-helix), b) *trans*-ACPC (12-helix), c) cyclobutane β-amino acid (12-helix)

In addition to the helices, β-amino acids have also been explored to design β-sheets type structures and reverse turns. Gellman and his colleagues observed the formation of polar antiparallel β-peptide sheets and further, they reported β-hairpin structures using different types of β-turn inducing segments.[12,13] In continuation, Balaram *et al*. examined the β-amino acids as guests into the host β-hairpin structures.[14] The design of hybrid β-hairpin with the combination of α, and β-amino acids also lead to the genesis of hybrid peptide foldamers. The major difference in the β-sheets formed by the β^3-amino acid and α-Amino acid is the directionality of the NH…O=C hydrogen bonds. In the case of α-peptide β-sheets, the H-

bonds are alternate in direction, whereas the β-residues have shown the H-bonds in the same direction leading to the polar sheets. Different types of β-amino acids utilized for the construct of the β-hairpin structure are shown in Figure 6. Further, Ortono *et al* reported homo-oligomers of *cis*-ACBC (cis-2-aminocyclobutane-1-carboxylic acid) residues exhibiting strand-like structures stabilized by the 6-membered intramolecular H-bonds. Interestingly, these strand-like structures facilitate supramolecular interactions and self-assembly, producing nanosized fibers or gels.[15]

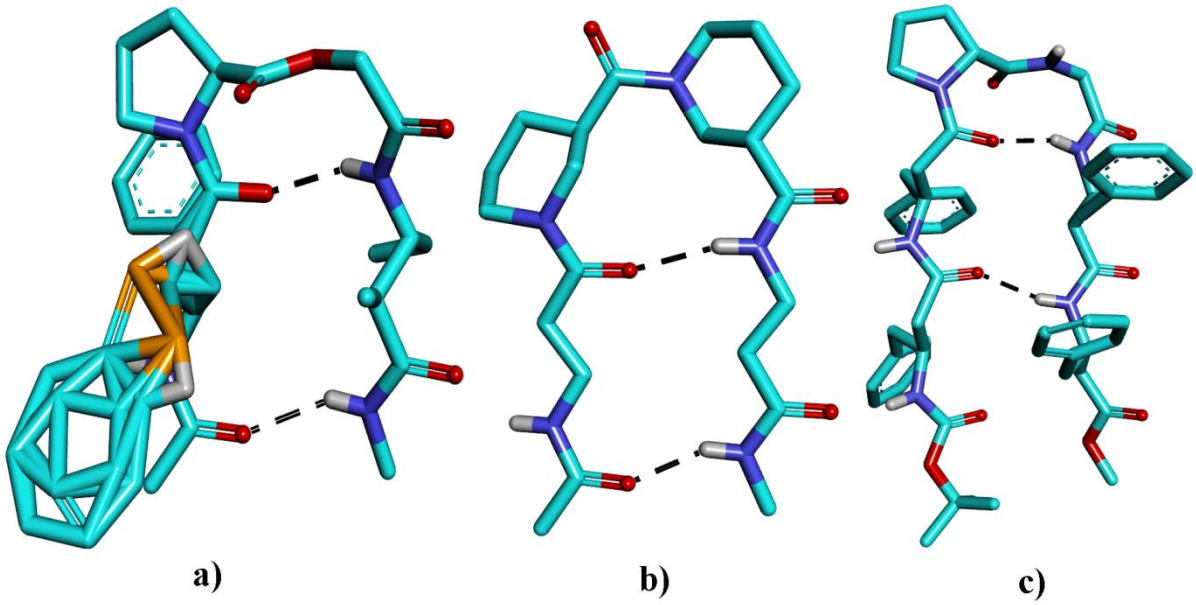

Figure 6 Different β-hairpin conformation constructed from β-amino acids containing α,β-disubstituted β-amino acids[12,13] and β^3-amino acids.[14]

1.2.1 Hybrid β-peptide foldamers

More recently, mixed heterogeneous peptides gained much attention over their homogeneous backbone counterparts. This is because it is possible to derive a variety of helical foldamers with different H-bonding patterns by varying the composition and order of amino acids in the peptide sequence. In their pioneering work, Balaram and colleagues demonstrated the hybrid peptide structures composed of β-amino acids and higher homologous amino acids into host α-peptide helices and β-hairpin structures.[16] Using systematic quantum chemical calculation Hofmann's groups predicted the different types of helices available to mixed α,β hybrid peptides.[17] Further, authors reported that α,β-peptides composed of unsubstituted glycine and β-alanine can fold into 8 different stable helical forms: 9-, 11/9, 9/11, 11, 15/14,12/13, 16/18 and18/16-helices. Sharma and colleagues reported 11/9 helical conformation from the hybrid

α,β sequence composed of α-amino acid and β^3-amino acid with alternating hydrogen bonding directionality.[18] In continuation, Jagadeesh *et. al* reported the dynamic equilibrium between 11 and 14/15 helical conformation in solution by α, β-hybrid peptide containing L-Ala and *cis*-FSAA (*cis*-β-furanoid sugar amino acid).[19] The Raiser and co-workers showed 3_{13}-helical conformation stabilized by *i*→*i+2* hydrogen bonds in α,β hybrid peptides composed of L-Ala and *cis*-Acc (*cis*-2-aminocyclopropanecarboxylic acid).[20] In an interesting study, Gellman and colleagues disclosed the crystallographic conformation of short α, β-hybrid peptides containing backbone constrained *trans*-ACPC amino acids (*trans*-2-aminocyclopentane carboxylic acid and its derivatives) and Aib. These hybrid peptides fold into 11-helix however, replacing *N*-terminal Aib with α-amino acid alanine it transformed into 14/15 helix suggesting the fine borderline energies between these two helices.[21a,21b] Recently, Amblard *et al*. showed the conformational conversion between 9/11-helix and 18/16-helix using tri-substituted β-amino acid [(*S*)-ABOC] in α,β-hybrid peptides.[22]Further, Gellman *et al*. demonstrated $C_{11/11/12}$-helix and $C_{10/11/11}$-helix formation in 1:2 and 2:1 α,β-hybrids.[23]Fulop and colleagues evaluated the stereochemical patterns in the folding of α,β-hybrid peptides.[24] In continuation, Gellman and colleagues reported spectacular helix bundle quaternary structures in oligomers composed of α-β-β-α-β-β and α-α-α-β-α-α-β repeats.[25] Different types of β-amino acids utilized in the protein structure mimetics with different H-bonding pattern are shown in Fig 7

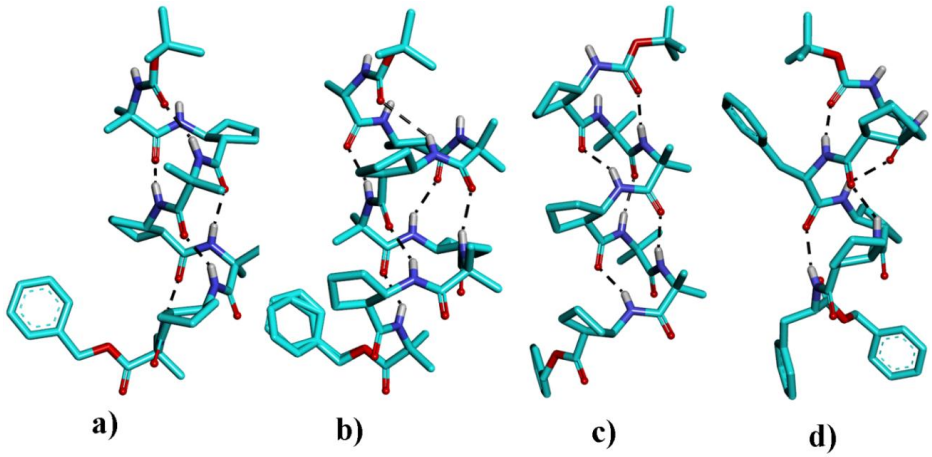

Figure 7 Examples of experimentally characterized hybrid peptides a) α, β 11-helix Boc-Aib-ACPC-Aib-ACPC-Aib-ACPC-Aib-ACPC-OBn,[21a] b) α,β 14/15-helix Boc-Ala-ACPC-Aib-ACPC-Aib-ACPC-Aib-ACPC-OBn,[21b] b) β,β,α 12/11/11 helix, Boc-ACPC-ACPC-Phe-ACPC-ACPC-Phe-OBn,[23] c) α,α,β with 10/11/11 helix, Boc-ACPC-Aib-Aib-ACPC-Aib-Aib-ACPC-OBn.[23]

1.2.2 Biologically active β- and hybrid β-peptides:

Though α-peptides can be easily designed to inhibit a variety of protein-protein interactions, protease inhibitors, antimicrobial candidates however their proteolytic susceptibility hindered their applications. In contrast, β-peptides are resistant to the proteolysis due to the presence of unnatural peptide backbone. These properties of β-peptides endorse them as very attractive candidates from the perspective of medicinal chemistry and chemical biology.[26] Due to higher helical propensity, the β-peptides have been explored to design antibacterial candidates. Gellman and colleagues designed cationic amphiphilic helical β-peptides and showed their specificity towards bacteria.[27] In addition to the β-peptides, Gellman and collogues have demonstrated potent antimicrobial properties of amphiphilic hybrid α, β-peptides and showed potent antibacterial activity against Gram-negative and Gram-positive bacteria.[28] In addition, these peptides also have shown good inhibitory profiles against biofilm formation of drug-resistant *candidaalbicans*. Recently, nylon-3 polymers made up of β-amino acids showed potent activity and selectivity against planktonic forms of multiple fungal species.[29] Further, Schepartz and coworkers designed p53(15-29) mimetics using β^3-peptides and demonstrated the inhibition of P53-MDM2 interactions.[30] In addition, same group also designed the fusion inhibitors for HIV-1 gp41-mediated fusion.[31]Gellman and co-workers developed β-peptides based entry inhibitors for HCMV (Human cytomegalovirus).[32] In addition, α, β-hybrid peptides have been explored to design inhibitors against the Bak/Bcl-xL interactions. The most active compound that inhibits the Bak/Bcl-xL interactions adopted a 15/14- helical conformation in solution.[33]

1.2.3 Ordered supramolecular assemblies of β-peptide helices:

In addition to the biological activity, the β-peptides have also attracted considerable attention recently due to their ordered supramolecular assemblies. In their seminal work, Gellman and his coworkers demonstrated self-assembled soluble aggregates of 14-helical β-peptides into tetrameric and, or hexameric bundles.[34] In addition, the same group has reported the quaternary bundles of α, β-peptides in aqueous solution as well as in crystalline state stabilized by close packing of the hydrophobic side chains and the charge interactions between polar residues.[35] The controlled lateral assembly of β-peptide 14-helices into tetrameric and octameric bundles were also reported by Schepartz and coworkers.[36]Ghadiri and coworkers reported the cyclic peptide derived from the acyclic β^3-amino acids and the peptide stack through extensive backbone-backbone H-bonding to form tubular channel

structures. The ability of channel-forming in lipid bilayer was further examined in the liposome-based proton transport assays and single-channel conductance experiments.[37] In their initial attempt Fülöp and his colleagues reported ordered supramolecular assembly of β-hexapeptide 10/12-helical structures into ribbon-like fibrils and vesicles.[38] In continuation, Gellman and his co-workers designed a series of β-peptides which self-assembled to form liquid crystals.[39] More recently, Lee and his colleagues reported a variety of self-assembled supramolecular architectures from β-peptides.[40] Furthermore, Perlmutter and his colleagues reported the self-assembled fibers from *N*-acetylated β-tri- and hexapeptides in aqueous as well as in organic solvents.[41]

1.3 γ-Peptide Foldamers

γ-Amino acids are double homologated α-amino acids having two -CH_2- groups between C^{α} and C=O carbon. The introduction of two methylene units leads two additional torsional variables θ_1 and θ_2 along with regular ϕ and ψ. Unlike β-amino acids, γ-amino acids have not been much explored probably due to the difficulties in the synthesis and isolation of stereochemically pure γ-amino acids. Nevertheless, in their seminal work Seebach[42] and Hannessian[43]simultaneously reported the stable 14-helical conformations from the homooligomers of monosubstituted γ-amino acids in solution. In contrast to the β^3-peptides, the γ^4-peptide have shown to adopt right-handed 14-helix (14-membered pseudocycles) stabilized by the H-bonds between the carbonyl group of residue i and the NH group of residue (i+3). Through extensive quantum calculations, Hofmann and colleagues predicted various types of helical conformations available to γ-peptides.[44] The helices with different hydrogen-bonded rings are illustrated in the Figure 8.

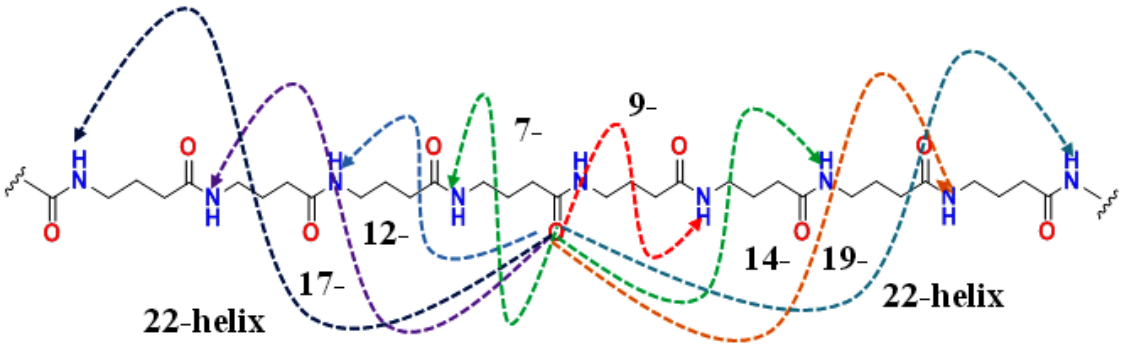

Figure 8 Possible H-bonding pattern observed of γ-peptide oligomers using systematic quantum calculation.

The 9-helix conformation predicted by the Hofmann was experimentally proved by Sharma and Kunwar.[45] In their pioneering work, Balaram and colleagues reported first crystal structure of 9-helix from the homooligomers of gabapentin (3, 3-dialkyl-γ-amino acid). The 9-helix of the Boc-Gpn-Gpn-Gpn-Gpn-NHMe is stabilized by three hydrogen bonds between the C=O moiety of residue i and the NH group of the residue (i +2).[46] Recently, Gellman and colleagues reported the C_{14} helical conformations in single crystals from the homooligomers of cyclic γ-amino acids.[47]

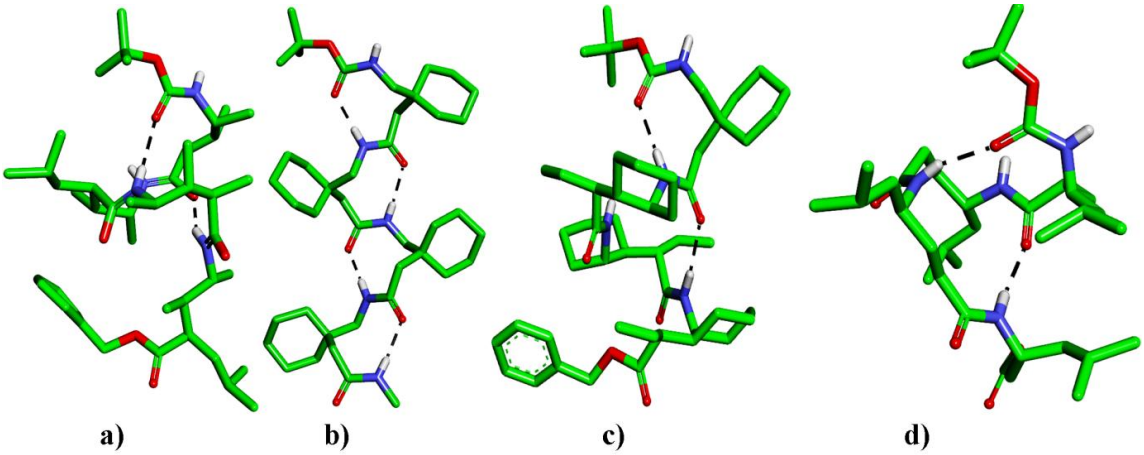

Figure 9 a) C_{14}-helix of γ^4-peptide,[48] b) C_9-helix of gabapentin oligomers,[46] c) C_{14} helical conformations of homooligomers of cyclic γ-amino acid[47] and d) C_{14}-helix of $\gamma^{2,3,4}$ -oligomer peptide.

In continuation, Balaram and co-workers reported atomic-resolution data of C_{14} helix formation by homooligomers of proteinogenic side chains containing γ^4 -residues (γ^4Leu, γ^4 Ile, and γ^4 Val).[48] Along with γ^4-amino acids, Seebach and colleagues demonstrated the 14-helical conformation of the trisubstituted $\gamma^{2,3,4}$-peptides.[49] The X-ray structures of γ-peptide 14- and 9-helices are shown in Figure 9. Various types of γ-amino acids explored in the design of γ-peptide foldamers are shown in the Figure 10.

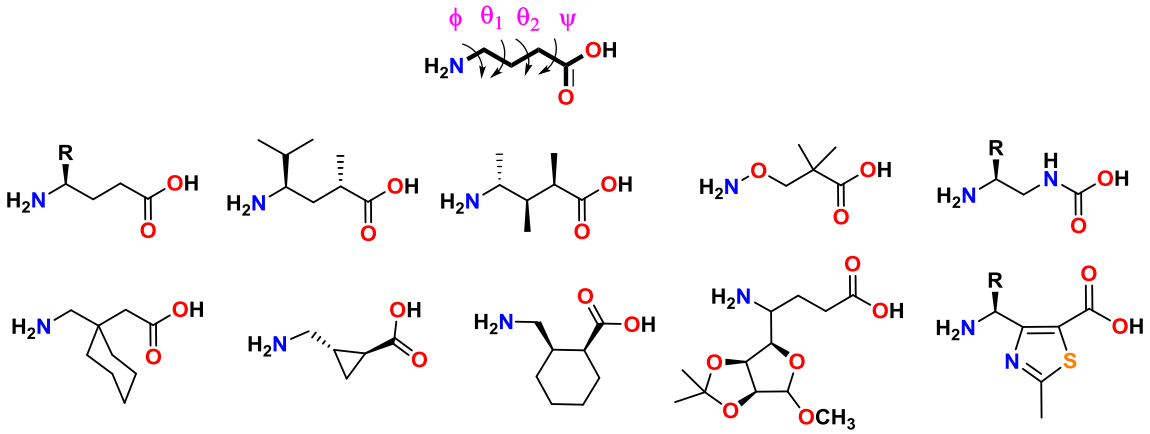

Figure 10 The torsional variables for γ- amino acid were depicted. The list of γ-amino acids used in the design of foldamers.

In continuation, Smith and colleagues synthesized and studied the conformational behaviour of cyclopropane γ-peptides.[50] In contrast to the helical signature, the short oligomer adopted an infinite parallel sheet structure in the solid state stabilized by bifurcated hydrogen-bonding between the carbonyl oxygen of the amide NH group and one CH of the cyclopropane ring (Figure 11a). Subsequently, they used this β-sheet promoting property to build a hairpin conformation with the help of a non-peptidic reverse turn.[50] In contrast to extended sheets, the homooligomers $\gamma^{2,3}$-trans-dioxolane-constrained γ-amino acids have shown to adopt C_7 helical conformations in solution.[51]

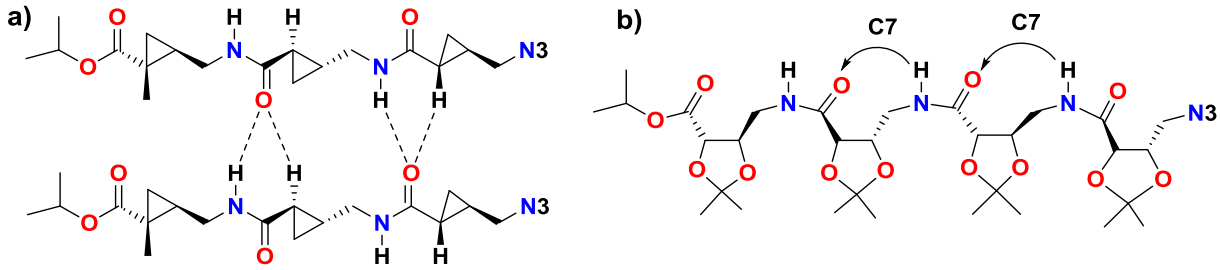

Figure 11 a) Parallel sheet based on cyclopropane γ-amino acids. b) C_7 bend-ribbon structure of $\gamma^{2,3}$-trans-dioxolane homooligomers

Besides these cyclic and acyclic γ-amino acids, there are also reports on the utilization of the γ-amino acids containing backbone heteroatoms such as O (Oxygen) and N (Nitrogen). Yang and colleagues demonstrated the conformational preference of both α-aminoxy peptides and

β-aminoxy peptides.[52] They observed C_8 helical conformations in α-aminoxy peptides and C_9 helices and turns in the case of β-aminoxy peptides. Further, LeGrel et al. reported insertion of NH moiety in the backbone of β^3-amino acids between the amine and β-carbon, which leads to the aza-amino acids.[53] Similar to the amino oxypeptides, the structures of azapeptides are stabilized by the short range turn like H-bonds. In continuation, Guichard and his colleagues studied the conformational properties of a variety of γ-peptide oligoureas (Figure 1.12a).[54] These γ-peptide oligoureas adopt a 14-helical conformation similar to other γ-peptide helices. Very recently, Millard and his co-workers reported well-defined 9-helices from γ-amino acids with thiazole backbone in solid state and in the solution (Figure 12b)[55]

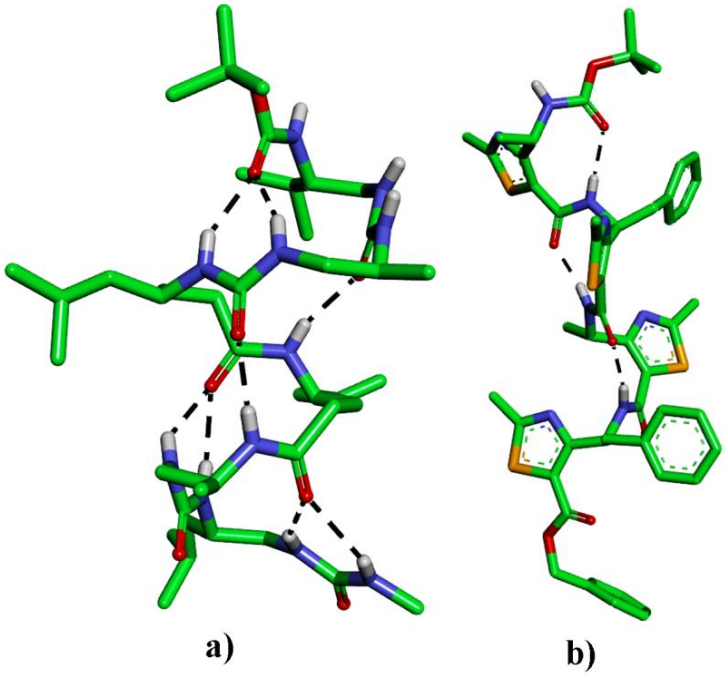

Figure 12 a) C_{14}-helical conformation of oligoureas,[54] b) C_9-helix of homologomers 4-amino-(methyl)-1,3-thiazole-5-carboxylic acids (ATCs).[55]

1.3.1 Heterogeneous foldamers containing γ-amino acids

Inspired by the structural diversity observed in the hybrid α,β-peptides, the structural properties of α,γ-hybrid peptides have also been examined. Through quantum chemical calculations, Hofmann and his colleagues predicted different helical types available to the oligomers of 1:1 alternatingα, and γ-amino acids. Among the various helix types, they proposed the most stable 12-helix conformation followed by mixed 12/10 or 18/20 helices.[56] In their seminal work, Balaram and his co-workers have shown the 12-helix conformation from the α,γ-hybrid tetrapeptide Boc-Aib-Gpn-Aib-Gpn-OMe. The structure is stabilized

4→1 H-bonds between the residues *i* and *i+3*.[57] In continuation Sharma *et.al* reported the mixed 12/10-helical conformations from several α,γ-peptides derived from repeating unit with alternating arrays of L-Ala and γ-Caa (C-linked carbo-γ-amino acid from D-mannose).[58] Further, the helix with 12/10-mixed hydrogen-bonding pattern was also observed in the single crystals.[59]

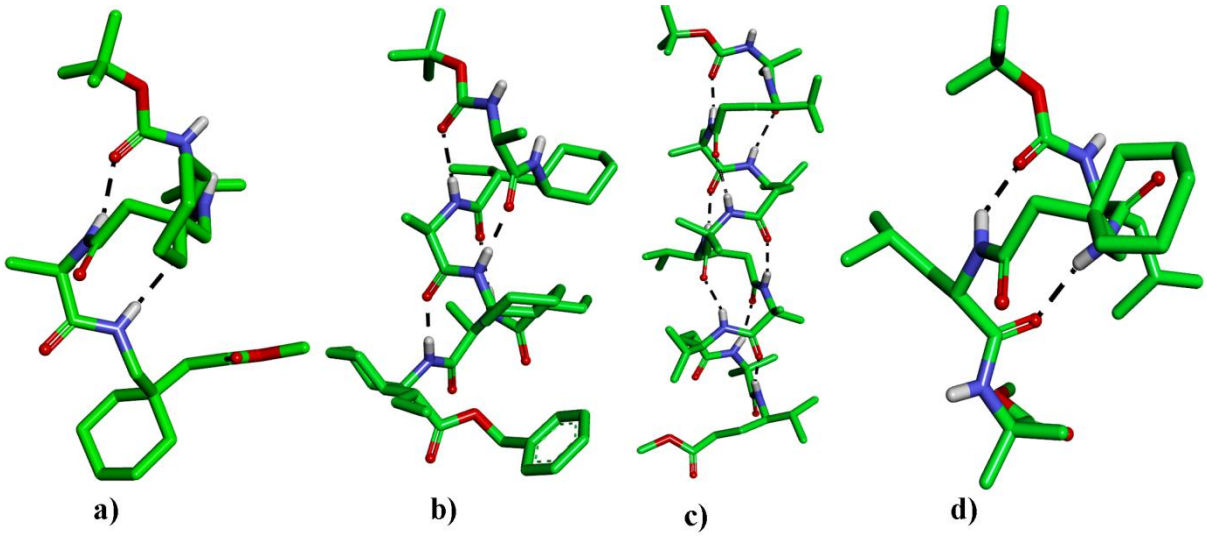

Figure 13 Examples of experimentally characterized hybrid peptides a) α, γ-12-helix: Boc-Aib-Gpn-Aib-Gpn-OMe.[57] b) α,γ-12-helix: Boc-DAla-EtACHA-DAla-EtACHA-DAla-EtACHA-OBn,[60b] b) α, γ-12-helix: Boc-Aib-γVal-Aib-γVal-Aib-γVal-Aib-γVal-OEt,[59b] c) α, γ, α with 10/12 helical conformation, Boc-Leu-Gpn-Aib-OMe.[59]

Gellman's group has designed, synthesized and studied the conformations of various α/γ-peptides containing sterically constrained cyclic γ-amino acids.[60] Apart from the helical structures, γ-amino acids have also been used in β-turns segment as well in the β-strands of β-hairpins. Balaram *et. al.* reported the single crystal conformation of the β-hairpin structurefrom Boc-Leu-Phe-Val-Aib-Gpn-Leu-Phe-Val-OMe.[61] The β-hairpin structure is stabilized by the four cross-strand hydrogen bonds with the Aib-Gpn segment forming a non-helical 12-membered turn. In addition, Roy *et. al.* demonstrated the β-hairpin conformation of the hybrid peptide (Boc-Leu-Val-γAbu-Val-^{D}Pro-Gly-Leu-γAbu-Val-Val-OMe) containing unsubstituted γ-amino acids in the anti-parallel β-strands.[62]

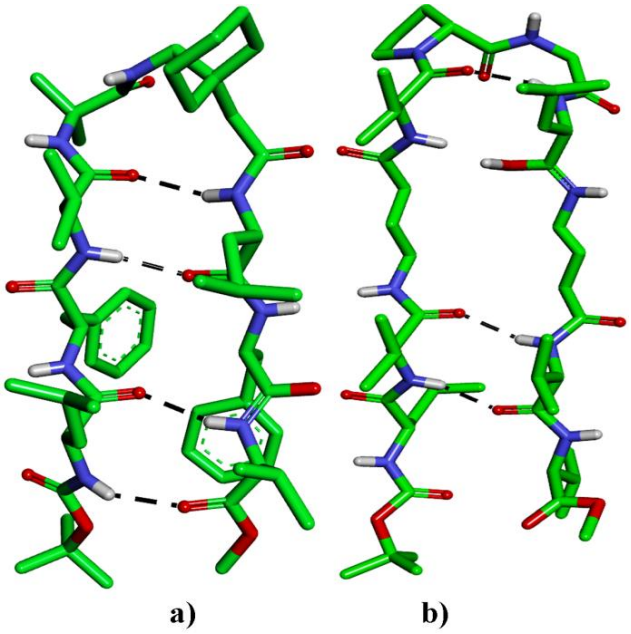

Figure 14: a) β-hairpin structure of peptide of Boc-Leu-Phe-Val-Aib-Gpn-Leu-Phe-Val-OMe[61] b) β-hairpin conformation of Boc-Leu-Val-γAbu-Val-DPro-Gly-Leu-γAbu-Val-Val-OMe.[62]

In addition to α, γ-hybrid peptides, there are few reports on the conformational properties of 1:1 alternating β, γ-hybrid peptides. The systematic quantum calculations by Hofmann and colleagues proposed stable 11-, 13-, mixed 11/13-, or 20/22- helices available to the β/γ-hybrid helices.[63] The H-bonding pattern in β/γ-hybrid peptides is shown Figure 15.

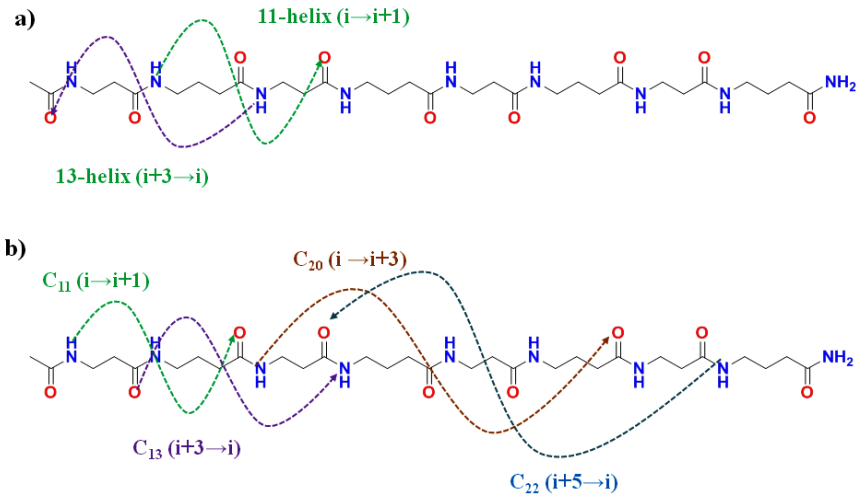

Figure 15 a) H-bonding in 11 helix and 13 helix b) H-bonding in mixed helices: 11/13 helix or in 20/22 helix of β, γ hybrid peptides.

Further, Sharma and Kunwar have shown the mixed 11/13 helical conformations in solution from β/γ-peptides composed of C-linked carbo-β- and γ-amino acids.[64] Furthermore, Balaram and colleagues characterizethe 13-membered H-bond the crystal structure of β, γ-hybrid peptide Boc-βLeu-Gpn-Val-OMe.[65] Continuous 13-helix in β/γ-hybrid peptides, similar to the α-helix, was successfully demonstrated by the Gellman and his co-workers in both solution as well as in single crystals.[66] The 13-helical conformations observed in the β, γ-hybrid peptides have displayed similar helical parameters as that of α-helix. The structural properties of β, γ-hybrid peptides provided unique opportunity to derive H-bond mimetics of α-helix. In continuation, Aitken and colleagues demonstrated the 9/8 ribbon from β, γ-hybrid peptides constituted with stereochemically constrained β-amino acids and unconstrained γ-amino acids, and the transformation of 9/8-ribbon structure into 13-helix by substituting unconstrained γ-amino acids with γ^4-amino acids.[67] Further, Koksch and colleagues have demonstrated the incorporation of β, γ-peptide fragments into the α-peptide coiled coil sequences.[68]

In contrast to the various unnatural γ-amino acids described above, a variety of naturally occurring non-ribosomal γ-amino acids such as α,β-unsaturated γ-amino acids, β-hydroxy γ-amino acids, β-keto-γ-amino acids have been found in many biologically active peptide natural products. However, little is known regarding the conformational properties of these amino acids.

1.4 Previous Work on Vinylogous amino acids as designing foldamer:

Vinylogous amino acids are α,β-unsaturated analogues of above described γ^4-amino acids. In contrast to the saturated γ^4-amino acids, (*E*)-α, β-Unsaturated γ-amino acids (insertion of –CH=CH- between $C_\alpha H$ and CO of α-amino acids, vinylogous amino acids) have been frequently found in many peptide natural products, such as cyclotheonamide (A, B, C, D, E), miraziridine A, gallinamideA.[69] Along with their synthetic analogues, these naturally occurring peptides containing vinylogous residues have shown the serine and cystine proteases inhibition activities.[70] In addition, the chemical reactivity of conjugated double bonds in (*E)*-vinylogous amino acids has been explored in various chemical reactions such as Diels-Alder reaction, epoxidation and Michael addition reactions to generate a variety of γ-amino acids.[71]In their preliminary work, Schreiber and colleagues reported the extended β-

sheet type structures from the dipeptides of (*E)*-vinylogus residues and unusual helical structure from the hybrid tetrapeptide.[72] In continuation, Chakraborty *et. al.*demonstrated the utility of *E*- vinylogous amino acids to induce reverse turns in β-hairpins.[73] Recently, Hofmann et al. provided a compressive overview of the possible helical structures formed by the unsubstituted vinylogous amino acids on the basis of a systematic computational analysis using ab initio MO theory.[74] They reported that vinylogous residues with (*E*)-double bonds favor the helices with larger hydrogen bond pseudocycles from 14- to 27-membered hydrogen-bond pseudocycles. The larger H-bond helices also provide an opportunity to design helical nanotubes as ion channels, however, these structures are yet to authenticate experimentally. The theoretically predicted 27-helix from homooligomers of *E*-vinylogous amino acids is shown in Figure 16a.

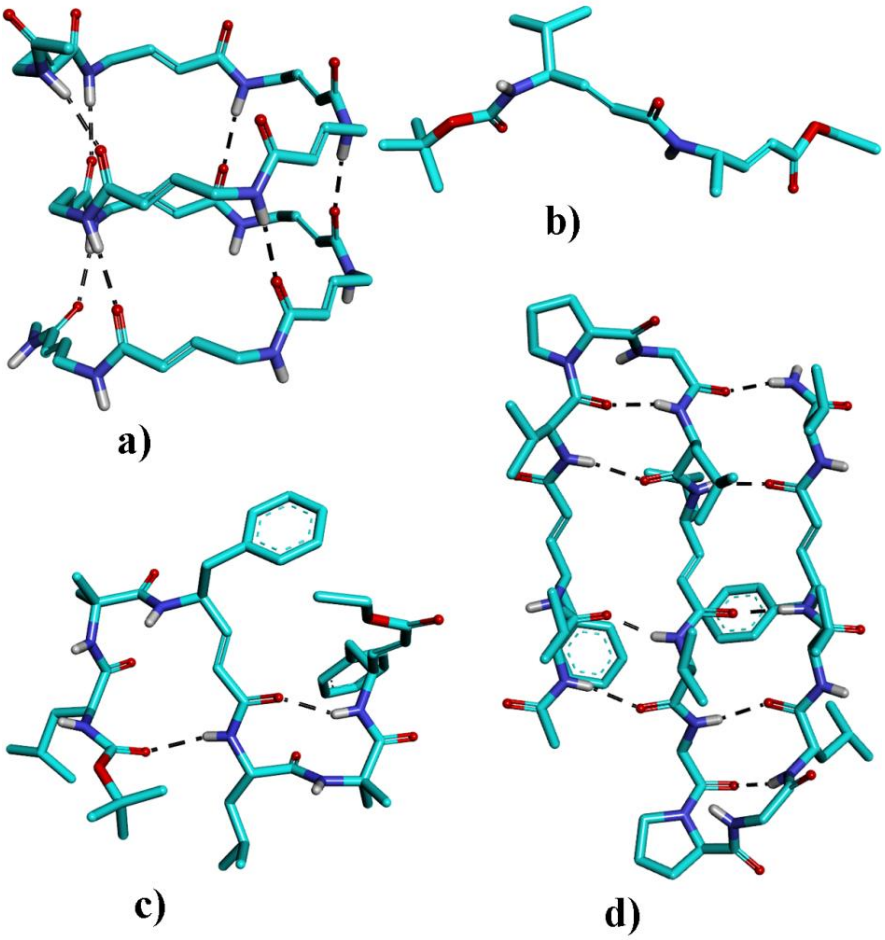

Figure 16 a) Theoretical models of C_{27}-helical structures,[74] **a)** Crystal structures: Boc-dγLeu-dγVal-OEt, [75] **b)** Ac-Val-dgF-Val-D Pro-Gly-Leu-dgL-Val-Ala- D Pro-Gly-LeuVal-dgF-Val-NH_2, [76] c) Boc-Leu-Aib-dgF-Leu-Aib-dgF-OEt.[77]

In contrast, the unsaturated amino acids with (*Z*)-configuration of the double bonds have shown to adopt seven- and nine-membered hydrogen bond pseudocycles. Recently, our group examined the utility of (*E*)-vinylogous amino acids design of stable β-hairpins, triple-stranded β-sheets and β-meander mimetics.[75-77] Furthermore, we also demonstrated the incorporation of Z-vinylogous amino acids into the α,γ-hybrid helices without deviating overall 12-helix folding.[78]

With this background on the structural and functional properties of β, γ- and vinylogous hybrid peptides motivated us to carry out the conformational analysis of achiral$\gamma^{4,4}$vinylogous amino acids with (*E*)-double bond and their homooligomers and hybrid peptides containing achiral dialkyl substituted γ-amino acids.

1.5 References

1. Linderstrom-Lang, K. U.; Schellman, J. A. (**1959**), *The Enzymes*, (P. D. Boyer, Ed.), *Vol. 1*, 2nd ed., 443-510. Academic Press, New York.
2. a) Karle, I. L.; Das, C.; Balaram, P. *Proc. Natl. Acad. Sci., USA.* **2000**, *97*, 3034; b) De Zotti, M.; Biondi, B.; Park, Y.; Hahm, K. S.; Crisma, M.; Toniolo, C.; Formaggio, F. *Amino Acids.* **2012**, *43*, 1761; c) Saragovi, H. U.; Greene, M. I.; Chrusciel, R. A.; Kahn, M. *Bio-Technol.* **1992**, *10*, 773.
3. a) Ramachandran, G. N.; Chandrasekaran, R. *Progress in Peptide Research*. Lande, S., Ed.; Gordon & Breach: New York, 1972; Vol. II (Proceedings of the Second American Peptide Symposium, Cleveland, 1970), 195; b) Marshall, G. R.; Bosshard, H. E. *Circ. Res*. **1972**, *31*, 143; c) Toniolo, C.; Benedetti, E. *ISI Atlas Sci. Biochem*. **1988**, *1*, 225. d) Bosch, R.; Schmitt, H.; Jung, G.; Winter, W. *Biopolymers*. **1985**, *24*, 961; e) Venkatraman, J.; Shankaramma, S. C.; Balaram, P. *Chem. Rev.* **2001**, *101*, 3131. f) Gehenn, K.; Stege, J.; Reed, J. *Anal. Biochem.* **2006**, 12, *356*; g) Narang, P.; Bhushan, K.; Bose, S.; Jayaram, B. *PhysChemChemPhys.* **2005**, *7*, 2364; h) Darbre, T.; Reymond, J. L. *Acc. Chem. Res.* **2006**, *39*, 925.
4. a) Seebach, D.; Gardiner, J. *Acc. Chem. Res.* **2008**, *41*, 1366; b) Horne, W. S.; Gellmann, S. H. *Acc. Chem. Res*. **2008**, *41*, 1399; c) Price, J. L.; Horne, W. S.; Gellman, S. H. *J. Am. Chem. Soc.* **2010**, *132*, 12378; d) Cheng, R. P.; Gellman, S. H.; DeGrado, W. F. *Chem. Rev*. **2001**, *101*, 3219; e) Vasudev, P. G., Chatterjee, S., Shamala, N., Balaram, P. *Chem. Rev.* **2011**, *111*, 657.

5. a) Hintermann, T.; Gademann, K.; Jaun, B.; Seebach, D. *Helv. Chim. Acta*. **1998**, *81*, 983; b) Seebach, D.; Beck, A. K.; Bierbaum, D. J. *Chem. Biodiv.* **2004**, *1*, 1111.
6. a) Appella, D. H.; Christianson, L. A.; Karle, I. L.; Powell, D. R.; Gellman, S. H. *J. Am. Chem. Soc.* **1996**, *118*, 13071; b) Appella, D. H.; Christianson, L. A.; Karle, I. L.; Powell, D. R.; Gellman, S. H. *J. Am. Chem. Soc.* **1999**, *121*, 6206; c) Appella, D. H.; Christianson, L. A.; Klein, D. A.; Richards, M. A.; Powell, D. R.; Gellman, S. H. *J. Am. Chem. Soc.* **1999**, *121*, 7574.
7. Günther, R., Hofmann, H.-J. & Kuczera, K. *J. Phys. Chem. B.* **2001**, *105*, 5559.
8. a) Sharma, G. V. M.; Reddy, R.; Krishna, P. R.; Ravi Sankar, A.; Narsimulu, K., Kumar, S. K.; Jayaprakash, P.; Jagannadh, B.; Kunwar, A. C. *J. Am. Chem. Soc.* **2003**, *125*, 13670; b) Sharma, G. V. M.; Chandramouli, N.; Choudhary, M.; Nagendar, P.; Ramakrishna, K. V. S.; Kunwar, A. C.; Schramm, P.; Hofmann, H. -J. *J. Am. Chem. Soc.* **2009**, *131*, 17335.
9. a) Guitot, K.; Carboni, S.; Reiser, O.; Piarulli, U. *J. Org. Chem.* **2009**, *74*, 8433. b) De Pol, S.; Zorn, C.; Klein, C. D.; Zerbe, O.; Reiser, O. *Angew. Chem., Int. Ed.* **2004**, *43*, 511; c) Berlicki, L.; Pilsl, L.; Weber, E.; Mandity, I. M.; Cabrele, C.; Martinek, T. A.; Fulop, F.; Reiser, O. *Angew. Chem., Int. Ed. Engl.* **2012**, *5*, 2208; d) Pilsl, L. K.; Reiser, O. *Amino Acids.* **2011**, *41*, 709.
10. Fernandes, C.; Faure, S.; Pereira, E.; Thery, V.; Declerck, V.; Guillot, R.; Aitken, D. J. *Org. Lett.* **2010**, *12*, 3606.
11. a) Martinek, T. A.; Fulop, F. *Chem. Soc. Rev*. **2012**, *41*, 687; b) Fulop, F.; Forro, E.; Toth, G. K. *Org. Lett*. **2004**, *6*, 4239.
12. Krauthauser, S.; Christianson, L. A.; Powell, D. R.; Gellman S. H. *J. Am. Chem. Soc.* **1997**, *119*, 11719,
13. Chung, Y. J.; Huck, B. R.; Christianson,L. A.; Stanger,H. E.; Krautha1user, S.; Powell, D. R.; Gellman S. H. *J. Am. Chem. Soc*. **2000**, *122*, 3995.
14. Karle, I.; Gopi, H. N.; Balaram P. *Proc. Natl. Acad. Sci., USA.* **2002**, *99*, 5161.
15. Rua, F.; Boussert, S.; Parella, T.; Diez-Perez, I.; Branchadell, V.; Giralt E.; Ortuno, R. M.; *Org. Lett*., **2007**, *9*, 3643.
16. a) Roy, R. S.; Karle, I. L.; Raghothama, S.; Balaram, P. *Proc. Natl. Acad. Sci.USA.* **2004**, *101*, 16478; b) Karle, I. L.; Pramanik, A.; Banerjee, A.; Bhattacharjya, S.; Balaram, P. *J. Am. Chem. Soc.* **1997**, *119*, 9087
17. Baldauf, C.; Günther, R; Hofmann, H.-J. *Pept. Sci*. **2006**, *84*, 408.

18. Srinivasulu, G.; Kumar, S. K.; Sharma, G. V. M.; Kunwar, A. C. *J. Org. Chem*. **2006**. *71*, 8395.
19. Jagadeesh, B.; Prabhakar, A.; Sarma, G. D.; Chandrasekhar, S.; Chandrashekar, G.; Reddy, M. S.; Jagannadh. B. *Chem. Commun*. **2007**, *371*, 371.
20. De Pol, S.; Zorn, C.; Klein, C. D.; Zerbe, O.; Reiser, O. *Angew. Chem. Int. Ed.* **2004**, *43*, 511.
21. a)Schmitt, M. A.; Choi, S. H.; Guzei, I. A.; Gellman, S. H. *J. Am. Chem. Soc.* **2005**, *127*, 13130; b) Choi, S. H.; Guzei, I. A.; Gellman, S. H. *J. Am. Chem. Soc.* **2007**, *129*, 13780.
22. Legrand, B.; Andre, C.; Moulat, L.; Wenger, E.; Didierjean, C.; Aubert, E.; Averlant-Petit, M. C.; Martinez, J.; Calmes, M.; Amblard, M. *Angew. Chem., Int. Ed*. **2014**, *53*, 13131.
23. Schmitt, M. A.; Choi, S. H.; Guzei, I. A.; Gellman, S. H. *J. Am. Chem. Soc*. **2006**, *128*, 4538.
24. Mándity, I. M.; Weber, E.; Martinek, T. A.; Olajos, G.; Tóth, G. K.; Vass, E.; Fülöp, F. *Angew. Chem., Int. Ed*. **2009**, *48*, 2171.
25. a)Horne, W. S.; Price, J. L.; Keck, J. L.; Gellman, S. H. *J. Am. Chem. Soc*. **2007**, *129*, 4178; b) Giuliano, M. W.; Horne, W. S.; Gellman, S. H. *J. Am. Chem. Soc*. **2009**, *131*, 9860.
26. Horne, W. S.; Price, J. L.; Gellman, S. H. *Proc. Natl. Acad. Sci. U.S.A.* **2008**, *105*, 9151; b) English, E. P.; Chumanov, R. S.; Gellman, S. H.; Compton, T. *J. Biol. Chem.* **2006**, *281*, 2661. c) Imamura, Y.; Watanabe, N.; Umezawa, N.; Iwatsubo, T.; Kato, N.; Tomita, T.; Higuchi, T.; *J. Am.Chem. Soc.* **2009**, *131*, 7353; d) Hook, D. F.; Bindschadler, P.; Mahajan, Y. R.; Sebesta, R.; Kast,¨ P.; Seebach, D. *Chem. Biodiversity* **2005**, *2*, 591; e) Rueping, M.; Mahajan, Y.; Sauer, M.; Seebach, D. *ChemBioChem* **2002**, *3*, 257.
27. Porter, E. A.; Weisblum, B.; Gellman, S. H. *J. Am. Chem. Soc*. **2002**, *124*, 7324.
28. Schmitt, M. A.; Weisblum, B.; Gellman, S. H. *J. Am. Chem. Soc.* **2007**, *129*, 417.
29. a) Liu, R.; Chen, X.; Falk, S. P.; Mowery, B. P.; Karlsson, A. J.; Weisblum, B.; Palecek, S. P.; Masters, K. S.; Gellman, S. H. *J. Am. Chem. Soc*. **2014**, *136*, 4333; b) Liu, R.; Chen, X.; Falk, S. P.; Masters, K. S.; Weisblum, B.; Gellman, S. H. *J. Am. Chem. Soc*. **2015**, *137*, 2183.

30. a) Kritzer, J. A.; Lear, J. D.; Hodsdon, M. E.; Schepartz, A. *J. Am. Chem. Soc*. **2004**, *126*, 9468; b) Kritzer, J. A.; Hodsdon, M. E.; Schepartz, A. *J. Am. Chem. Soc*. **2005**, *127*, 4118.
31. Stephens, O. M.; Kim, S.; Welch, B. D.; Hodsdon, M. E.; Kay, M. S.; Schepartz, A. *J. Am. Chem. Soc*. **2005**, *127*, 13126.
32. English E. P.; Chumanov, R. S.; Gellman S. H; Compton T. *J Biol Chem*. **2006**, *281*, 2661.
33. Sadowsky, J. D.; Fairlie, W. D.; Hadley, E. B.; Lee, H.-S. Umezawa, N.;Nikolovska-ColeskaZ.; Wang, S.; Huang, D. C. S.; Tomita, Y.; Gellman, S. H. *J. Am. Chem. Soc.*, **2007**, *129* , 139.
34. Raguse, T. L.; Lai, J. R.; LePlae, P. R.; Gellman, S. H. *Org. Lett.*, **2001**, *3* , 3963.
35. Horne, W. S.; Price, J. L.; Keck, J. L.; Gellman, S. H. *J. Am. Chem. Soc* **2007**, *129*, 4178.
36. Goodman, J. L.; Petersson, E. J.; Daniels, D. S.; Qiu, J. X.; Schepartz, A. *J. Am. Chem. Soc*. **2007**, *129*, 14746.
37. Clark, T.D., Buehler, L.K., Ghadiri, M. R. *J. Am. Chem. Soc*. **1998**, *120*, 651.
38. a) Hetenyi, A.; Mandity, I. M.; Martinek, T. A.; Toth, G. K.; Fulop, F.; *J. Am. Chem. Soc*. **2005**, 127, 547; b) Mandity, I. M.; Fulop, L.; Vass, E.; Toth, G. K.; Martinek, T. A.; Fulop, F. *Org. Lett.*, **2010**, *12*, 5584; c) Martinek, T. A.; Hetenyi, A.; Fulop, L.; Mandity, I. M.; Toth, G. K., Dekany, I., Fulop, F. *Angew. Chem. Int. Ed.*. **2006**, *45*, 2396.
39. Pomerantz, W. C.; Yuwono, V. M.; Drake, R.; Hartgerink, J. D.; Abbott, N. L.; Gellman, S.H. *J. Am. Chem. Soc*. **2011**, *133*, 13604.
40. a) Kwon, S.; Jeon, A.; Yoo, S. H.; Chung, I. S.; Lee, H. S. *Angew. Chem. Int. Ed.* **2010**, 49, 8232; b) Kwon, S.; Shin, H. S.; Gong, J.; Eom, J. H.; Jeon, A.; Yoo, S. H.; Chung, I. S.;Cho, S. J.; Lee, H. S. *J. Am. Chem. Soc*. **2011**, *133*, 17618.
41. Seoudi, R. S.; Dowd, A.; Del Borgo, M. P.; Kulkarni, K.; Perlmutter, P.; Aguilar, M.I.; Mechler, A. *Pure Appl Chem*. **2015a**, *87*, 1021.
42. Hintermann, T.; Gademann, K.; Seebach, D. *Helv. Chim. Acta.* **1998**, *81*, 893.
43. Hanessian, S.; Luo, X.; Schaum, R.; Michnick, S. *J. Am. Chem. Soc.* **1998**, *120*, 8569.
44. a) Baldauf, C.; Gunther, R.; Hofmann, H. J. *Helv. Chim. Acta*. **2003**, *86*, 2573; b) Baldauf, C.; Gunther, R.; Hofmann, H. -J. *J. Org. Chem.* **2006**, *71*, 1200.

45. a) Sharma, G. V. M.; Jayaprakash, P.; Narsimulu, K.; Sankar, A. R.; Reddy, K. R.; Kunwar, A. C. *Angew. Chem. Int. Ed.* **2006**, *45*, 2944.
46. Vasudev, P. G.; Shamala, N.; Ananda, K.; Balaram, P. *Angew. Chem., Int. Ed*. **2005**, *44*, 4972.
47. Guo, L.; Zhang, W.; Reidenbach, A.G.; Giuliano, M.W.; Guzei, I.A.; Spencer, L.C.; Gellman, S.H., *Angew. Chem. Int. Ed.* **2011,** *50*, 5843.
48. Basuroy, K.; Dinesh, B.; Reddy, M. B. M.; Chandrappa, S.; Raghothama, S.; Shamala, N.; Balaram, P. *Org. Lett*. **2013**, *15*, 4866.
49. Seebach, D.; Brenner, M.; Rueping, M.; Schweizer, B.; Jaun, B. *ChemCommun*, **2001**, 207
50. Khurram, M.; Qureshi, N.; Smith, M. D. *Chem. Commun*. **2006**, 5006
51. Kothari, A.; Khurram, M.; Qureshi, N.; Beck, E. M.; Smith, M. D. *Chem. Commun*. **2007**, 2814.
52. a) Lee, X.; Yang, D. *Chem. Commun*. **2006**, 3367; b) Chen, F.; Zhu, N.-Y.; Yang, D. *J. Am. Chem. Soc.* **2004**, *126*, 15980.
53. Cheguillaume, A.; Salaun, A.; Sinbandhit, S.; Potel, M.; Gall, P.; Baudy-Floch, M.; Le Grel, P. *J. Org. Chem.* **2001**, *66*, 4923.
54. Pendem, N.; Nelli, Y. R.; Douat, C.; Fischer, L.; Laguerre, M.; Ennifar, E.; Kauffman, B.; Guichard, G. *Angew. Chem.Int. Ed.* **2013**, *52*, 4147.
55. Mathieu, L.; Legrand, B.; Deng, C.; Vezenkov, L.; Wenger, E.; Didierjean, C.; Amblard, M.; Averlant-Petit, M. C.; Masurier, N.; Lisowski, V.; Martinez, J.; Maillard, L. T. *Angew. Chem. Int. Ed.* **2013**, *52*, 6006.
56. Baldauf, C.; Gunther, R.; Hofmann, H.-J. *J. Org. Chem.* **2006**, *71*, 1200.
57. Ananda, K.; Vasudev, P.G.; Sengupta, A.; Raja, K. M. P.; Shamala N.; Balaram, P. *J. Am. Chem. Soc.* **2005**, *127*, 168.
58. Sharma, G. V. M.; Jadhav, V. B.; Ramakrishna, K. V. S.; Jayaprakash, P.; Narsimulu, K.; Subash, V.; Kunwar, A. C. *J. Am. Chem. Soc.* **2006**, *128*, 14657.
59. a) Vasudev,P.G.; Chatterjee, S.; Ananda, K.; Shamala, N.; Balaram. P.; *AngewChem Int Ed.* **2008**, *41*, 6430. b) Sonti, R.; Dinesh, B.; Basuroy, K.; Raghothama, S.; Shamala, N.; Balaram; P. *Org. Lett.* **2014**, *16* , 1656.
60. a) Guo, L.; Zhang, W.; Guzei, I. A.; Spencer, L. C.; Gellman, S. H. *Org. Lett*. **2012**, *14*, 2582; b) Guo, L.; Chi, Y.; Almeida, A. M.; Guzei, I. A.; Parker, B. K.; Gellman, S. H. *J. Am. Chem. Soc.* **2009**, *131*, 16018.

61. Chatterjee, S.; Vasudev, P. G.; Raghothama, S.; Ramakrishnan, C.; Shamala, N.; Balaram, P. *J. Am. Chem. Soc.* **2009**, *131*, 5956.
62. Roy, R. S.; Gopi, H. N.; Raghothama, S.; Karle, I. L.; Balaram, P. *Chem Eur J* **2006**, *12*, 3295.
63. Baldauf, C.; Günther, R.; Hofmann, H.-J. *J. Org. Chem.* **2006**, *71*, 1200;
64. Sharma, G. V. M. Jadhav, V. B.; Ramakrishna, K. V. S.; Jayaprakash, P.; Narsimulu, K.; Subash, V.; Kunwar, A. C.; *J. Am. Chem. Soc*. **2006**, *128* , 14657.
65. Vasudev,P. G.; Ananda, K.; Chatterjee, S.; Aravinda, S.; Shamala, N.; Balaram, P. *J. Am. Chem. Soc*. **2007**, *129*, 4039.
66. Guo, L.; Almeida, A. M.; Zhang, W.; Reidenbach, A. G.; Choi, S. H.; Guzei, I. A.; Gellman S. H. *J. Am. Chem. Soc*. **2010**, *132* , 7868
67. a) Grison, C. M.; Robinab, S.; Aitken D. J. *Chem. Commun*. **2015**, *51*, 16233. b) Grison, C. M.; Robin, S.; Aitken, D. J. *Chem. Commun.* **2016**, *52*, 7802.
68. Nyakatu ra, E.K.; Mortier, J.; Radtke,V.; Wieczorek, S.; Araghi, R.R.; Baldauf, C.; Wolber, G.; Koksch, B. *ACS Med Chem Lett*. **2014**, *5* , 1300.
69. a) Linington, R. G.; Clark, B. R.; Trimble, E. E.; Almanza, A.; Uren, L.-D.; Kyle, D. E.; Gerwick, W. H. *J. Nat. Prod.* **2009**, *72*, 14; b) Coleman, J. E.; de Silva, E. D.; Kong, F.; Andersen, R. J.; Allen, T. M. *Tetrahedron*, **1995**, *51*, 10653; c) Schaschke, N. *Bioorg. Med. Chem. Lett.* **2004**, *14***,** 855; d) Lee, A. Y.; Hagihara, M.; Karmacharya, R.; Albers, M. W.; Schreiber, S. L.; Clardy, J. *J. Am. Chem. Soc.* **1993**, *115*, 12619; e) Hagihara M.; Schreiber, S. L. *J. Am. Chem. Soc.*, **1992**, *114*, 6570; f) Lee, A. Y.; Hagihara, M.; Karmacharya, R.; Albers, M. W.; Schreiber, S. L.; Clardy, J.*J. Am. Chem. Soc.*, **1993**, *115*, 12619; g) Nieman, J. A.; Coleman, J. E.; Wallace, D. J.; Piers, E.; Lim, L. Y.; Roberge, M.; Andersen, R. J. *J. Nat. Prod.*, **2003**, *66*, 183; h) Nakao, Y.; Matsunaga S.; Fusetani, N. *Bioorg. Med. Chem.***1995**, *3*, 1115; i) Fusetani, N.; Matsunaga, S.; Matsumoto, H.; Takebayashi, H. *J. Am. Chem. Soc.* **1990**, *112*, 7051.
70. a) Hanzlik, R. P.; Thompson, S. A. *J. Med. Chem.* **1984**, *27*, 711; b) Liu, S.; Hanzlik, R. P. *J. Med. Chem.* **1992**, *35*, 1067; c) Kong, J-S.; Venkatraman, S.; Furness, K.; Nimkar, S.; Shepherd, T. A.; Wang, Q. M.; Aube, J.; Hanzlik, R. P. *J. Med. Chem.*, **1998**, *41*, 2579; d) Santos, M. M. M.; Moreira, R. *Mini-Rev. Med. Chem.Lett*. **2007**, *7*, 1040. e) Breuning, A.; Degel, B.; Schulz, F.; Buchold, C.; Stempka, M.; Machon, U.; Heppner, S.; Gelhaus, C.; Leippe, M.; Leyh, M.; Kisker, C.; Rath, J.; Stich, A.; Gut,

J.; Rosenthal, P. J.; Schmuck, C.; Schirmeister, T. *J. Med. Chem.* **2010**, *53*, 1951; f) Schaschke N.; Sommerhoff, C. P. *Chem Med Chem*, **2010**, *5*, 367.

71. a) Plummer, J. S.; Emery, L. A.; Stier, M. A.; Suto, M. J. *Tetrahedron Lett.* **1993**, *34*, 7529. b) Fu, Y.; Xu, B.; Zou, X.; Ma, C.; Yang, X.; Mou, K.; Fu, G.; Lu, Y.; Xu, P. *Bioorg. Med. Chem. Lett*. **2007**, *17*, 1102; c) Reetz, M. T. *Angew. Chem., Int. Ed. Engl.* **1991**, *30*, 1531; d) Seebach, D.; Beck, A. K.; Bierbaum, D. J. *Chem. Biodiv.*,**2004**, *1*, 1111.
72. Hagihara, M.; Anthony, N. J.; Stout, T. J.; Clardy, J.; Schreiber, S. L. *J. Am. Chem. Soc*. **1992**, *114*, 6568.
73. Chakraborty, T. K.; Ghosh, A.; Kumar, S. K.; Kunwar, A. C. *J. Org. Chem*. **2003**, *68*, 6459.
74. Baldauf, C.; Gunther, R.; Hofmann, H.-J. *J. Org. Chem*. **2005**, *70*, 5351.
75. Mali, S. M.; Bandyopadhyay, A.; Jadhav, S. V.; Kumar, M. G.; Gopi, H. N. *Org. Biomol. Chem*., **2011**, *9*, 6566.
76. a) Bandyopadhyay, A.; Mali, S. M.; Lunawat, P.; Raja, K. M. P.; Gopi, H. N. *Org. Lett*. **2011**, *13*, 4482. b) Bandyopadhyay, A.; Gopi, H. N. *Org. Lett*. **2012**, *14*, 2770.
77. Kumar, M. G.; Benke, S. N.; Raja, K. M. P.; Gopi, H. N. *Chem. Commun*. **2015**, *51*, 13397.
78. Ganesh Kumar, M.; Thombare, V. J.; Katariya, M. M.; Veeresh, K.; Raja, K. M.P; Gopi, H. N. *Angew. Chem. Int. Ed*. **2016**, *55*, 7847.

Chapter 2

Artificial β-Double Helices from Achiral γ-Peptides

2.1 Introduction

Biopolymers such as nucleic acids and proteins, maintain a unique and specific ordered structures. These ordered structures of these biopolymers are mainly responsible for the sophisticated functions of these molecules in living systems. Double helix is a common structural feature in nucleic acids. The double helical structure of nucleic acids is extremely important for genetic information storage, replication, and transcription.[1] The double helical structures in nucleic acids are stabilized by the complementary hydrogen bonding between adjacent base pair of two anti-parallel polynucleotide strands and π-π staking between the base pair.[2] In comparison with nucleic acids and polysaccharides, intertwining conformationally identical polypeptide strands stabilized by the intermolecular H-bonds is relatively rare event in polypeptides, however with the exception of peptide antibiotic gramicidin A.[3] Over the decades, extensive efforts have been made in the literature to design β-double helix structures from the polypeptides composed of alternating L- and D-α-amino acids.[4] Influenced by the double helix structure in gramicidin A, Beneditti and colleagues examined the double helix formation using polypeptides consisting of 1:1 alternating L- and D-α-amino acids.[4a] In contrast to peptides, aromatic oligoamide foldamers[5] and synthetic polymers[6] have been shown to adopt double helical conformations. In their seminal work Lehn and his co-workers reported double-stranded helical metal complexes where two linear oligodonor ligands wrap around two or more metal centers and thus form a double helix.[7] Iverson and colleagues reported the double helical structures from alternating aromatic staking of electron rich 1,5-dialkoxy-naphthalene (DAN) and electron deficient1,4,5,8-naphthalene-tetracarboxylic diimide (NDI) in water.[8] Further, Yashima and co-workers demonstrated the double helix structures from the meta-terphenyl derivatives and these double helices are stabilized through amidinium–carboxylate salt bridges.[9] In continuation, Lehn and Huc reported the homo-dimeric double helical structures from the aromatic oligoamides stabilized by the π-π staking and H-bonds between the β-strands.[5a] The representative examples of double helical structures observed in the aromatic oligoamides, organic templates and L, D-peptides are shown in Figure 1. In this Chapter, we are demonstrating the double helix conformations from a new class of achiral γ-peptides.

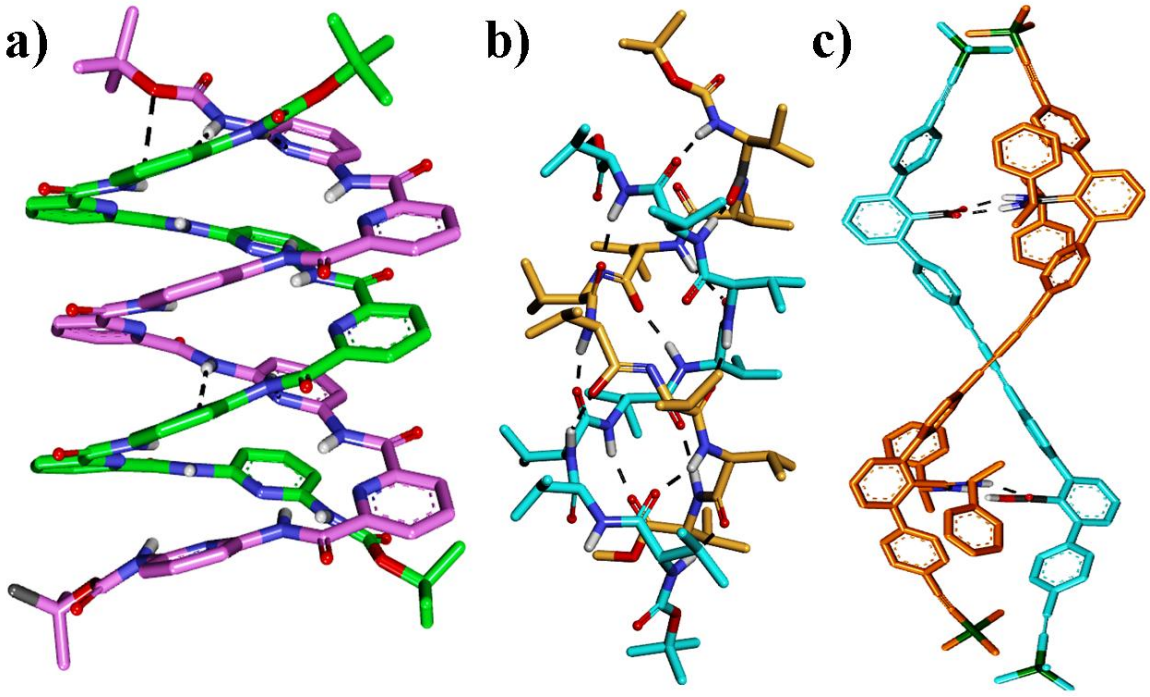

Figure 1 a) aromatic oligomides,[5a] b) polypeptide of L,-D, valine,[4a] c) meta-terphenyl derivatives through salt bridge interaction.[9a]

α,β-Unsaturated γ-amino acids (or vinylogous amino acids) have been often found in many peptide natural products.[10] Through extensive theoretical studies, Hofmann and colleagues predicted a variety of helical organizations available to the homo-oligomers of (*E*)- and (*Z*)-vinylogous residues.[11] Further, Maillard *et al.* described C_9 helices from thiazole γ-peptides analogous to the homo-oligomers of (*Z)*-vinylogous residues.[12] Recently, we demonstrated the accommodation of (*Z*)-vinylogous amino acids into C_{12} helices[13] and (*E*)-vinylogous amino acids into β-hairpins and three-stranded β-sheets.[14] The crystallographic analysis of (*E)*-vinylogous residues in short homo-oligomers[15,16] and in hybrid peptides[14,17] reveal that they promote extended β-sheet type structures. In comparison to the various folded architectures derived from the oligomers of backbone homologated α-amino acids such as β- and γ-amino acids,[18] the α,α-gem-dialkyl substituted α-amino acids have been extensively explored over the decades to design α- and 3_{10}-helices.[19] The Thorpe-Ingold effect imposes a marked conformational restriction on α,α-gem-dialkyl residues and confined them to adopt helical conformations in peptides.[18] We hypothesized that integration of the gem-dimethyl characteristic feature of the helix promoting α,α-dimethyl amino acid Aib (α-aminoisobutyric acid) with that of β-sheet promoting α,β-unsaturated γ-amino acid,[15,16] it may

be possible to realize β-double helix conformations. Though extensive efforts have been made in the literature to design various protein secondary structure types from β- and γ-peptide foldamers,[18] however β-double helical structures have never been authenticated.

2.2 Aim and rationale of the present work

We theorize that integration of the gem-dimethyl characteristic feature of the helix promotingα,α-dimethyl amino acid Aib (α-aminoisobutyric acid) with that of β-sheet promoting α,β-unsaturated γ-amino acid, it may be possible to realize β-double helix conformations from the oligomers of this monomer. In this Chapter, we are describing the design, synthesis and crystal conformations of new class of achiral γ-peptides constructed from achiral 4,4-dimethyl α, β-unsaturated γ-amino acid. As anticipated these achiral γ-peptides spontaneously intertwine into β-double helices.

2.3 Results and Discussion

2.3.1 Design and synthesis

As a part of our investigation and to test our hypothesis, we have synthesized peptides **P1**, **P2** and **P3**. The sequences of these peptides are shown in Scheme 1. The 4,4-gem-dimethyl α,β-unsaturated γ-amino acid (*trans*-α,β-unsaturated 4-aminoisocaproic acid, dγAic) was synthesized starting from the *N*-Boc-Aib aldehyde through Wittig reaction as reported earlier.[16] Boc-Aib aldehyde was obtained through reduction of corresponding *Weinreb amide* using LAH. Synthesis of dipeptide, tetrapeptide and pentapeptides were carried out through conventional solution-phase methods using a fragment-condensation strategy. The *tert*-butyloxycarbonyl group was used for *N*-terminus protection and the *C*-terminus was protected as an ethyl ester. Deprotections were performed with trifluoroacetic acid and saponification for the N- and C-termini, respectively. Couplings were mediated by the *N*-(3-dimethylaminopropyl)-*N′*-ethylcarbodiimide hydrochloride (EDC.HCl) and 1-hydroxybenzotriazole (HOBt) coupling agents. The dipeptide was synthesized by the coupling reaction between *N*-terminal Boc-dγAic-COOH and H_2N-dγAic-OEt. The tetrapeptide Boc-dγAic-dγAic-dγAic-dγAic-OEt (**P1**) was synthesized by the [2 +2] condensation involving *N*-terminal dipeptide acid Boc-dγAic-dγAic-COOH and H_2N-dγAic-dγAic-OEt. The pentapeptide Boc-dγAic-dγAic-dγAic-dγAic-dγAic-OEt (**P2**) was obtained by the [4+1] condensation involving *N*-terminal tetrapeptide acid Boc-dγAic-dγAic-dγAic-

dγAic-dγAic-COOH and H_2N-dγAic-OEt. The peptide Boc-dγAic-dγAic-dγAic- dγAic-dγAic-Pyr (**P3**) was synthesized by the [5 + 1] condensation involving *N*-terminal pentapeptide acid Boc-dγAic-dγAic-dγAic-dγAic-dγAic-COOH and H_2N-CH_2-Pyr. Finally, all peptides were purified through reversed-phase HPLC employing MeOH/H_2O gradient system.

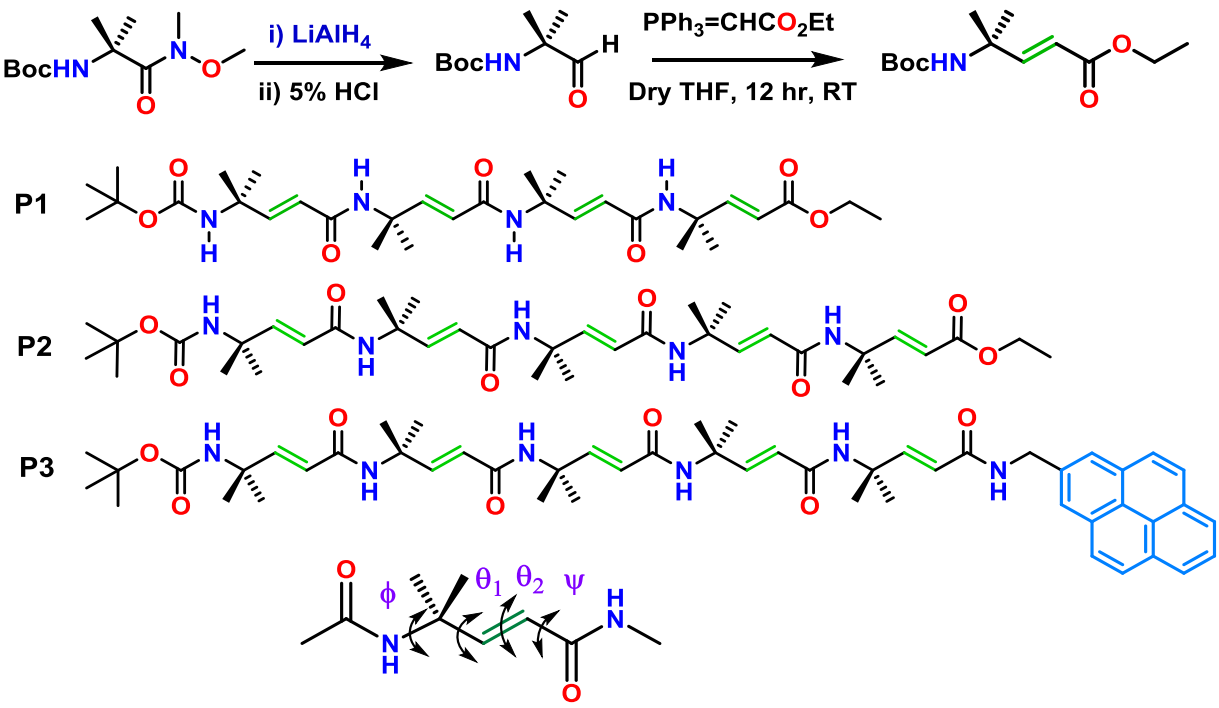

Scheme 1 a) Synthesis of *N*-Boc-dγAic from *N*-Boc-Aib. b) Chemical structures of dγAic homooligomers and local torsional variables of γ-residues.

2.3.2 Single crystal X-ray analysis of peptides P1 and P2.

To understand their unambiguous conformations, we subjected initially synthesized **P1** and **P2** for the crystallization in various solvent combinations. Both **P1** and **P2** gave diffraction-quality crystals in $CHCl_3$/n-heptane solution and their X-ray diffraction structures are shown in Figure 2a and 2b, respectively. Interestingly, both **P1** and **P2** adopted parallel β-double helix conformations in single crystals. The double helix hybridization in **P1** is stabilized by six independent interstrand H-bonds, (Figure 4a) while **P2** double helix hybridization is stabilized by eight independent interstrand H-bonds (Figure 4b) between the *i* (NH) and *i'-1*(CO) residues. The H-bond distances are in the range of 1.94-2.15 Å (N---O average dist. 2.77-3.07 Å) with an average ∠N-H---O 170°. Except for the BocNH and C-terminal ester

CO groups, all other amide NH and CO groups are involved in the interstrand H-bonding. The H-bond parameters of peptides **P1** and **P2** are tabulated in the Table 1 and Table 2, respectively.

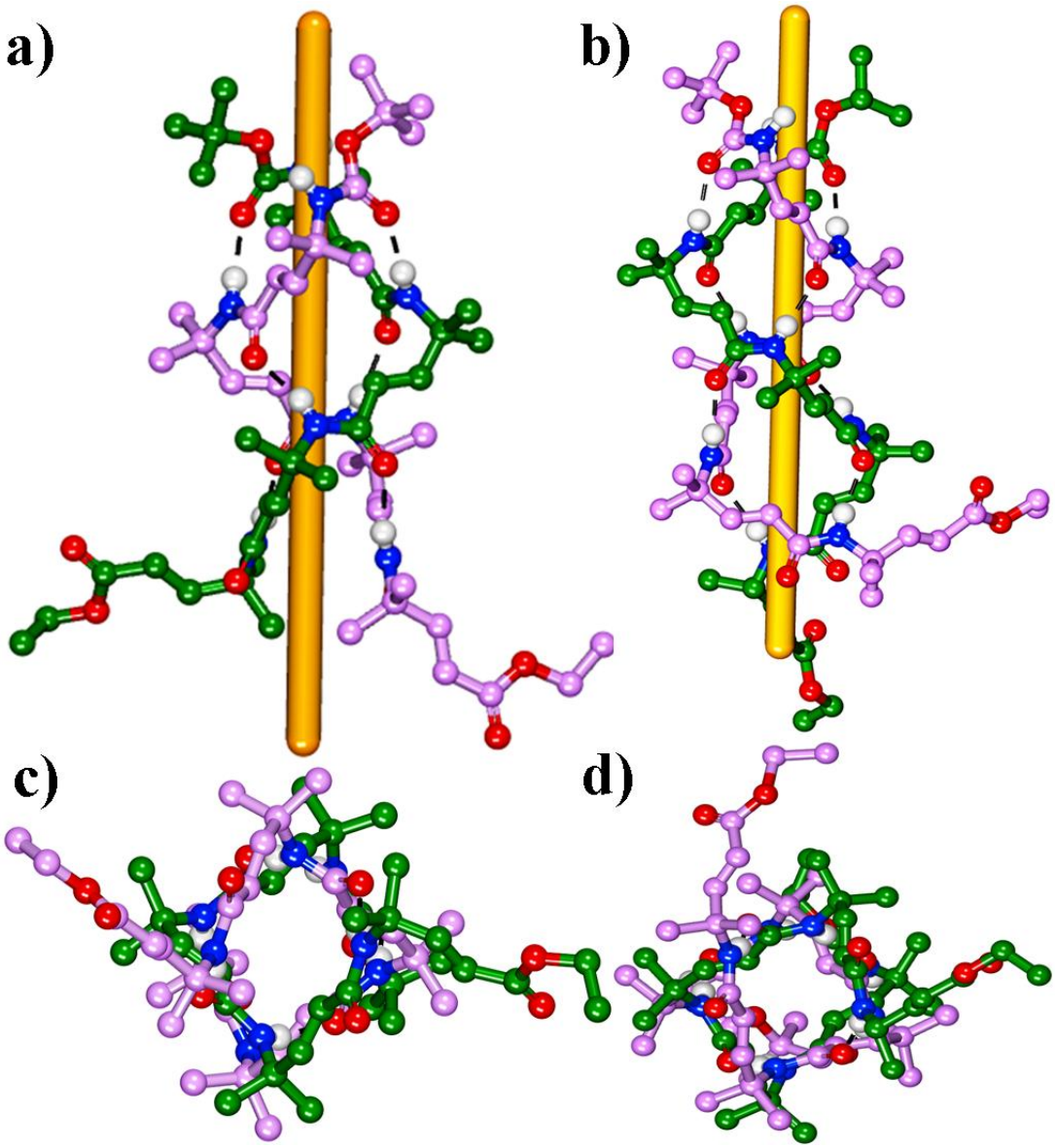

Figure 2: X-ray structures of a) **P1** and b) **P2.** To get a better view of parallel β-double helices, pictorially rods are created along the central axis. Green and magenta are used to represent two peptide strands. c) Top view of **P1** double helix. d) Top view of **P2** double helix.

The backbone conformation of the dγAic residues are described by the backbone torsion angles ϕ(N-C$^{\gamma}$), θ_1(C$^{\gamma}$-C$^{\beta}$), θ_2(C$^{\beta}$-C$^{\alpha}$) and ψ(C$^{\alpha}$-C=O) (Scheme 1). The average torsion angles

of γ-residues involved in the β-double helix conformation of **P1** and **P2** are tabulated in the Table 3. Analysis of the backbone torsion angles suggested that similar to the obvious extended conformation of C^{β}-C^{α} (θ_2), the C^{α}-CO (ψ) bond also adopted extended conformation (*s-cis*). In our previous studies, we have shown the general trend of (*E)*-vinylogous amides to adopt *s-cis* conformation along C^{α}-CO bond.[17] The torsion angle θ_1 displayed nearly eclipsed conformation with the values ranging from 3 to 35° in both **P1** and **P2**.

Table 1: Hydrogen Bond Parameters of **P1**

Donor (D)	**Acceptor (A)**	**D….A (Å)**	**DH….A (Å)**	**NH….O (deg)**
N6	O2	3.07	2.15	178
N7	O3	2.80	1.99	156
N8	O4	2.82	1.97	167
N2	O9	2.90	2.04	175
N3	O10	2.85	2.00	167
N4	O11	2.96	2.11	168

Table 2: Hydrogen Bond Parameters of **P2**

Donor (D)	**Acceptor (A)**	**D….A (Å)**	**DH….A (Å)**	**NH….O (deg)**
N7	O2	2.94	2.14	167
N8	O3	2.80	1.95	174
N9	O4	2.79	1.95	165
N10	O5	2.90	2.05	170
N2	O10	2.91	2.05	176
N3	O11	2.80	1.94	176

N4	O12	2.93	2.07	174
N5	O13	2.82	1.97	168

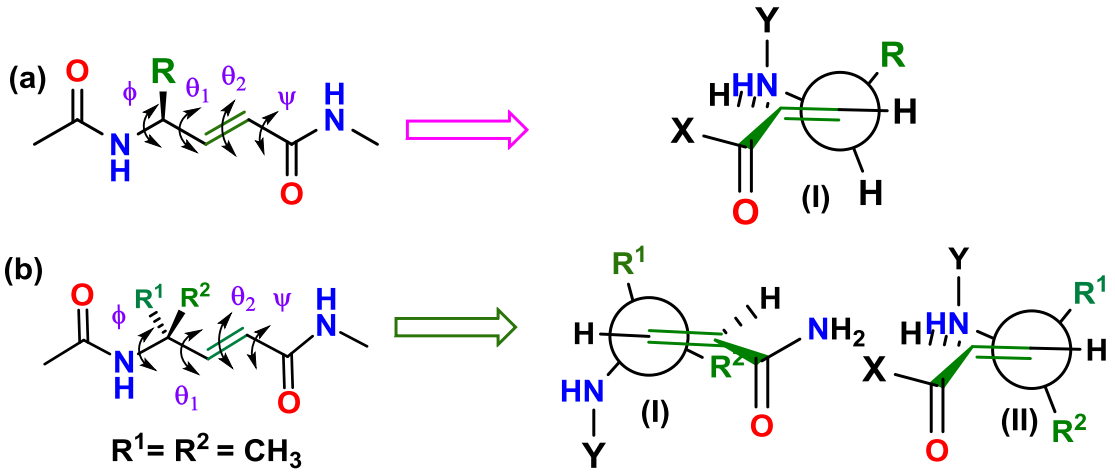

Figure 3 a) H-C$^{\gamma}$-C$^{\beta}$=C$^{\alpha}$ eclipsed conformation (θ_1 = ± 120^{o}) is observed in the vinylogous amides of β-sheet promoting residue.[16] b) The N-C$^{\gamma}$-C$^{\beta}$=C$^{\alpha}$ eclipsed conformation **I** (θ_1 = 0^{o}) is normally observed for the peptide **P1** and **P2**.

Table 3 Backbone torsion angles (in degree) of α,β-unsaturated γ-residues involved in the β-double helix conformation of **P1** and **P2**.[a]

Peptide	Residue	ϕ^{o}	θ_1^{o}	θ_2^{o}	ψ^{o}
P1	dγAic(1)	70±4	12±6	170±1	-168±0
	dγAic(2)	68±5	19±6	172±4	-167±3
	dγAic(3)	69±3	21±6	174±2	±175±3
P2	dγAic(1)	70±1	15±1	169±1	-173±1
	dγAic(2)	73±7	16±8	173±3	-169±5
	dγAic(3)	70±12	23±10	171±1	-173±5
	dγAic(4)	66±4	22±8	174±0	-172±5

[a]C-terminal residues are not included in the list because they are not participated in the double helix.

This is in sharp contrast with the β-sheet type structures displayed by the (*E*)-vinylogous residues, where θ_1 preferred to adopt extended conformation with value 120±20.[14-17] The ϕ values observed in the β-double helices are equivalent to that of α-helix (-60±20).[19] Being achiral, these γ-peptides also displayed β-double helical structures with opposite handedness in the asymmetric unit. To gain insight into the structural similarities between the γ- and L, D-α-peptide double helices, we analyzed the backbone torsion angles of various L, D-peptides.[4b] The average torsion angles of L and D-α-residues (ϕ_L, ψ_L and ϕ_D, ψ_D) in the β-double helix structures were found to be -123±15, +137±30 and +135±20, -121±30, respectively. In contrast to the –, + and +, – alternating sign of torsion angles observed in the L, D-peptide β-double helices, the γ-peptide double helices displayed +,+,+ and - (or -, -, - and +) for ϕ, θ_1, θ_2 and ψ, respectively however with few exceptions at the C-terminal residues.

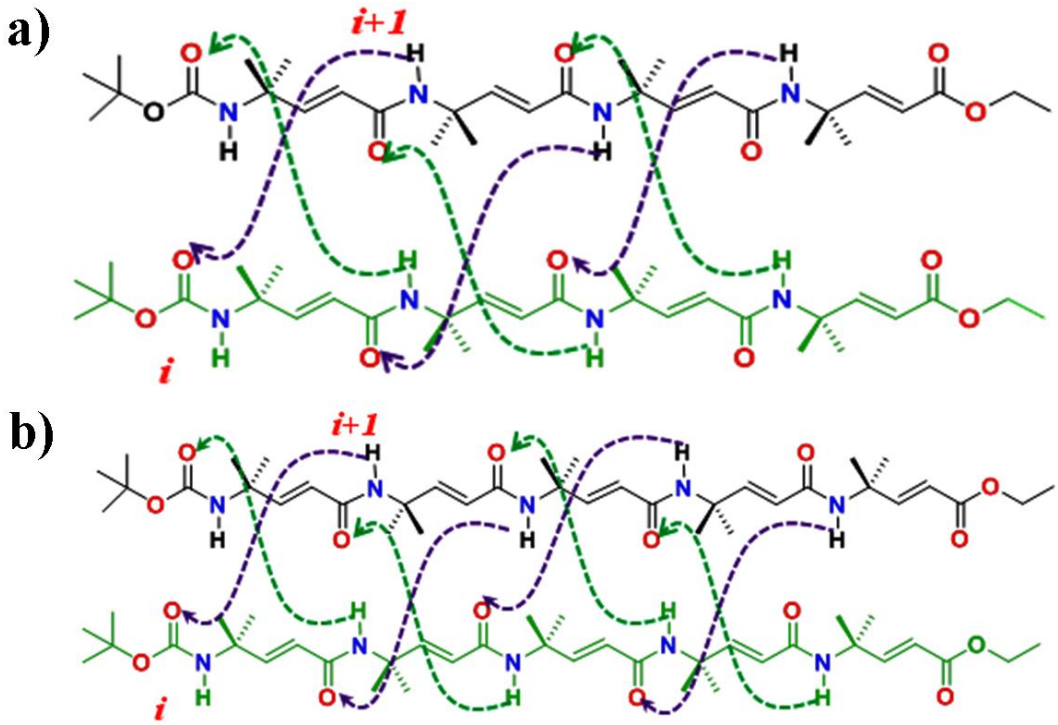

Figure 4: H-bonding patterns of peptide a) **P1** and (b) **P2.**

2.3.3 Solution conformation of peptide P1 and P2

^{1}H NMR analyses of both **P1** and **P2** in $CDCl_3$ gave well-resolved spectra corresponding to the one set of protons. To understand the double helix conformation of **P1** and **P2** in solution, DMSO-d_6 titration, concentration and temperature dependent ^{1}H NMR experiments were undertaken. DMSO-d_6 titration experiment revelled that except urethane NH at 4.7 ppm, all other amide NH protons showed insignificant change in their chemical shifts with increasing concentration of DMSO-d_6 (Fig. 5a and Fig. 5b), indicating their involvement in the intermolecular H-bonds between the γ-peptide-strands. However, Boc-NH urethane protons both **P1** and **P2** showed downfield shift upon increasing concentration of DMSO-d_6, indicating their exposure to the solvent for H-bonding.

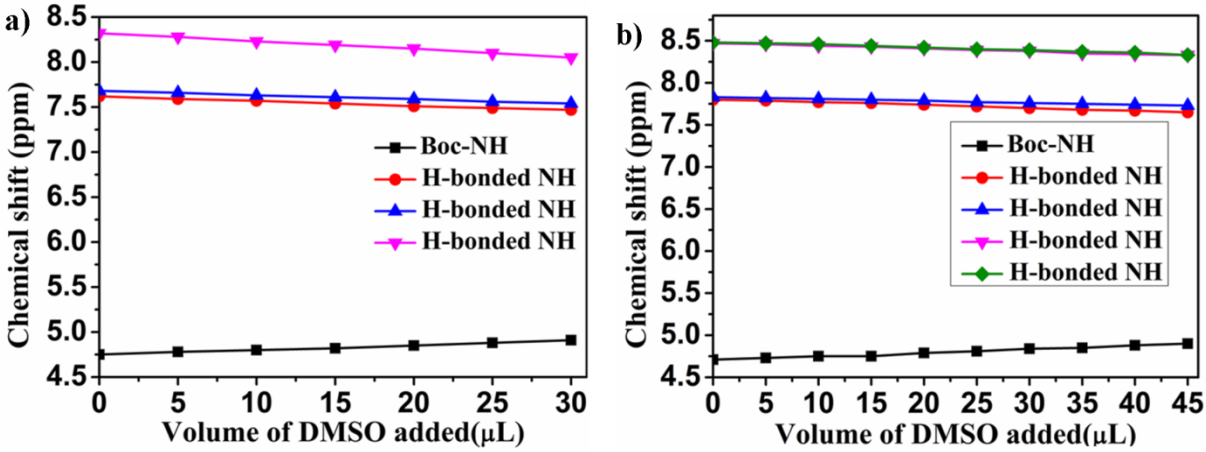

Figure 5: DMSO-d6 titration plots of a) **P1** and b) **P2** in $CDCl_3$ solution. Both peptides showing negligible change in the NH chemical shifts except BocNH urethane protons (block squares).

Concentration dependent ^{1}H NMR spectra for the peptide **P1** in $CDCl_3$ showing slight downfield shift for all the amide NH proton expect Boc-NH urethane proton, indicating the involvement of amide NH protons in H-bonding expect Boc-NH urethane proton (Figure 6a). However, for the peptide **P2** with increasing the concentration of peptide **P2** in $CDCl_3$ no pronounced chemical shift amide, NH proton was observed suggesting the stability of double helix even in very low concentration (Figure 6b).

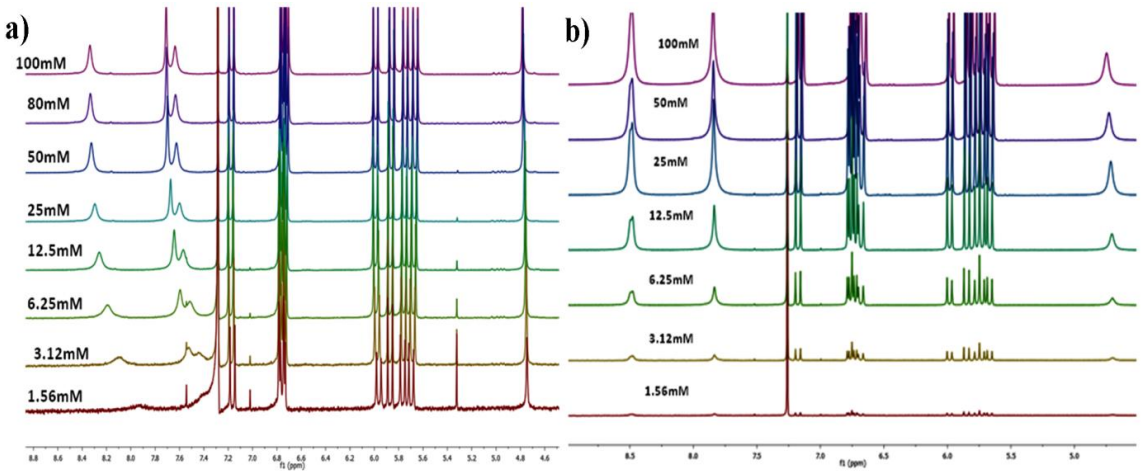

Figure 6: a) Concentration dependent partial (amide region) ^{1}H NMR spectra of **P1** in $CDCl_3$, b) of peptide **P2**

The temperature dependent ^{1}H NMR in $CDCl_3$ showed the gradual upfield NH chemical shifts with increasing temperature for the peptide **P1** suggesting the breaking of H-bonds and possible dissociation of double helix into individual γ-peptide strands upon increasing temperature. Similar results were also observed for the peptide **P2** where the temperature dependent ^{1}H NMR spectra in $C_2D_2Cl_4$ showed the sharpening the amide NH signal and as well as upfield shifting of amide NH protons indicating the dissociation of double helix structure into individual strands upon increasing temperature. Partial temperature dependent ^{1}H NMR spectra are shown in Figure 7.

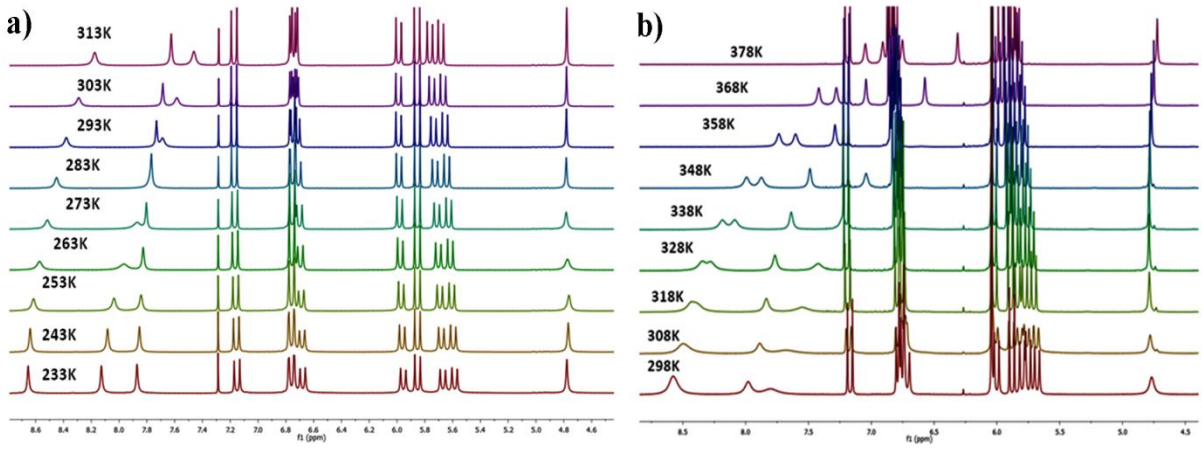

Figure 7: a) Temperature dependent partial (amide region) ^{1}H NMR spectra of **P1** in $CDCl_3$, b) of peptide **P2** in $C_2D_2Cl_4$

Further, Infrared spectroscopy experiments were carried to understand the hydrogen bonding in $CHCl_3$. The IR spectra for the both **P1** and **P2** showing NH stretching vibration band around 3290 cm^{-1} (Figure 8)[20] suggesting the involvement of amide NH protons in the H-bonding. These results further support the double helix conformations of peptides.

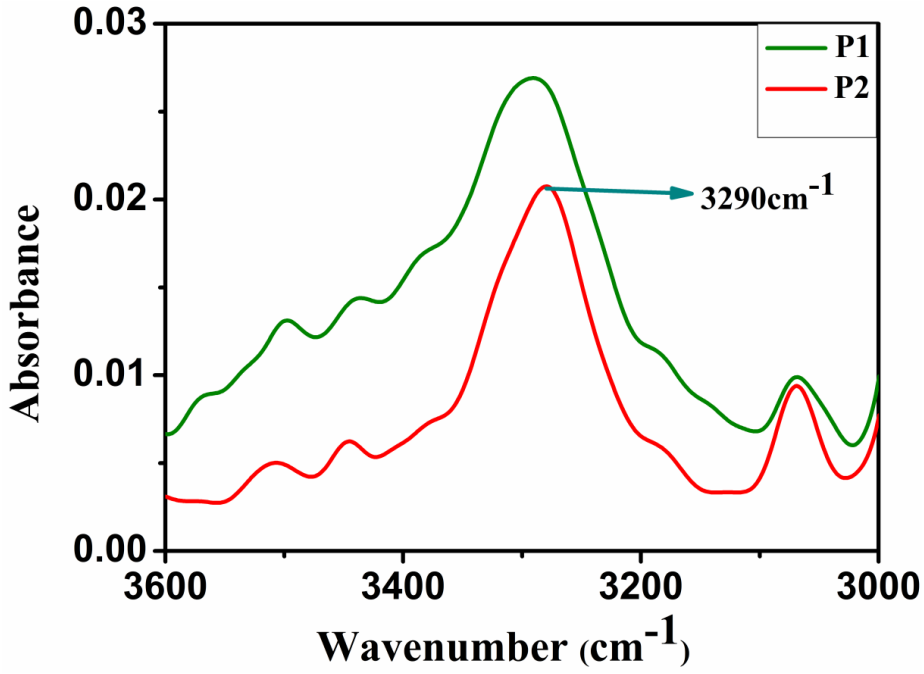

Figure 8: FTIR spectra of peptide a **P1** and **P2** in $CHCl_3$ (1mg/mL)

Due to the lack of NH connectivity, we found difficult to identify the individual amino acids in the sequences of **P1** and **P2**. Though the above NMR experiments signify the double helix conformation in solution, however, parallel or antiparallel orientation of the γ-peptide strands was not clear. We theorized that the fluorescence of pyrene excimers[21] can be used to probe the orientation of γ-peptide strands in the double helix. In this connection, peptide **P3** was synthesized.

2.3.4 Single crystal X-ray analysis of peptide P3

Peptide **P3** gave diffraction-quality single crystals in $CHCl_3$/toluene solution and its X-ray structure is shown in Figure 9a. The parallel β-double helix of **P3** is reminiscent of **P1** and **P2** except the pattern of interstrand H-bonds. The structure is stabilized by ten independent interstrand H-bonds. Instructively, insertion of bulky pyrenyl moiety did not disturb the overall double helix conformation. To accommodate pyrenyl moieties, one γ-peptide strand is lagging behind the other. The spatially proximal pyrenyl moieties at the C-terminus of the

double helix are stabilized by the π-π interactions. Accommodation of bulky pyrenyl groups led to the two types of H-bonding patterns in the β-double helix of **P3** (Figure 10). The amide NH (*i*) protons of strand A are involved in the H-bonding with *i'-1* CO groups (NH*i*→CO *i'-1*) of strand B similar to the **P1** and **P2**. Interestingly, the amide NH protons (*i*) of strand B are involved in the H-bonding with *i'-3* CO groups of strand A (NH*i*→CO*i'-3*). Two *N*-terminal amides NH protons of strand B and two C-terminal CO groups of strand A are not involved in the interstrand H-bonds. However, they are involved in the head-to-tail intermolecular H-bonding with other β-double helices (Figure 9b).

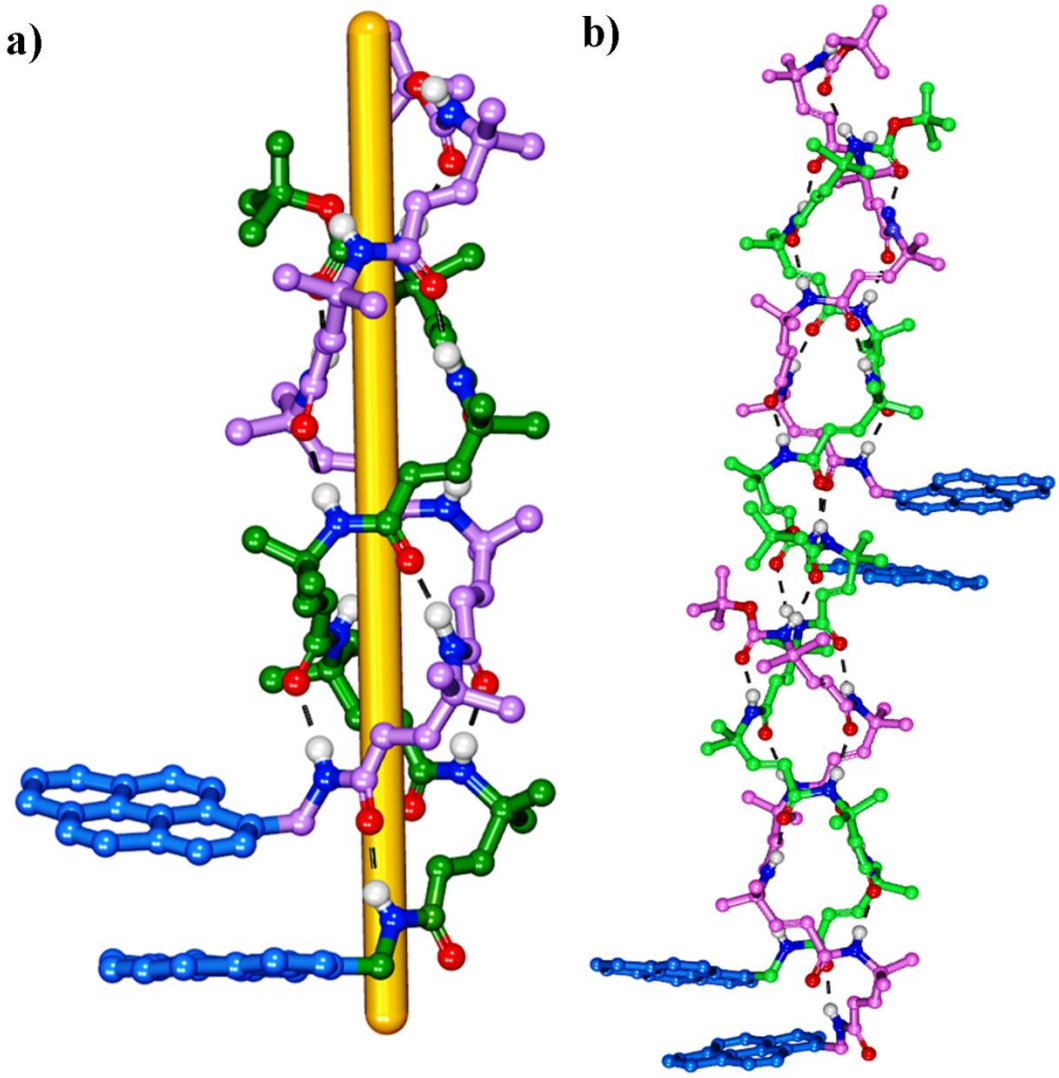

Figure 9: a) X-ray structure of **P3**. To get a better view of parallel β-double helices, pictorially rods are created along the central axis. b) Head-to-tail hydrogen bonding of double helix **P3.**

Analysis of the torsion angles reveals that there is a change in sign of ψ at the residue 1 in strand A and at the residues 3 and 5 in strand B. In addition, opposite sign is also observed for θ_2 of residue 5 in strand B. Except these, other residues follow the same trend as observed in the peptides **P1** and **P2**. The change in the sign of torsion angles can be attributed to the plasticity of γ-peptide strands to accommodate bulky pyrenyl moieties along the double helix. The torsion angles of P3 are tabulated in the Tables 4-7. Being achiral, the double helices with opposite sign of torsion angles are observed. The H-bond parameters of **P3** double helix are tabulated in Tables 8 and 9. Overall, the structure observed in peptide **P3** suggests the sliding of one helical strand along with another in a spiral motion as observed in the aromatic oligoamide[5] double helices as well as in the gramicidin A.

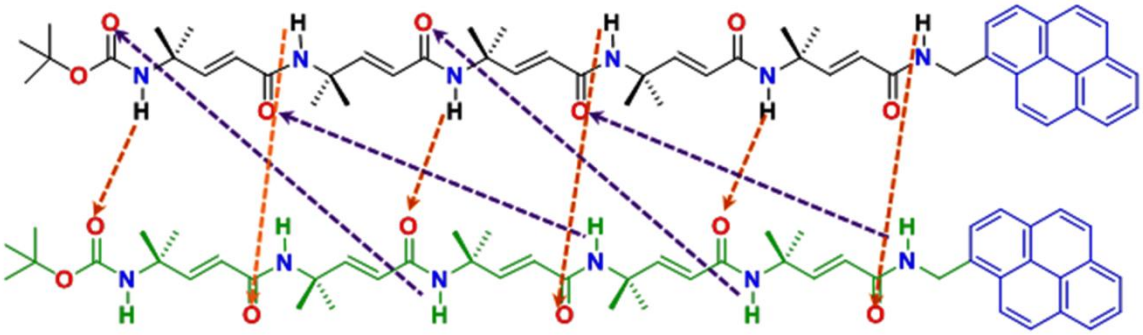

Figure 10: H-bonding patterns of peptide **P3**

Table 4: Torsional Angle (in degree) Parameters of **P3 (Molecule 1, Strand 1)**

Peptide P3 (Strand 1)	ϕ	θ_1	θ_2	ψ
dγAic 1	-75	-38	-168	166
dγAic 2	-70	-21	-171	-178
dγAic 3	-77	-23	-167	178
dγAic 4	-68	-28	-170	171
dγAic 5	-63	-22	178	-169

Table 5: Torsional Angle (in degree) Parameters of **P3 (Molecule 1, Strand 2)**

Peptide P3 (Strand 2)	ϕ	θ_1	θ_2	ψ
dγAic 1	-89	-3	180	-179
dγAic 2	-66	-25	-169	169
dγAic 3	-74	-20	-176	178
dγAic 4	-70	-16	-173	176
dγAic 5	-60	-28	-165	170

Table 6: Torsional Angle (in degree) Parameters of **P3 (Molecule 2, Strand 1)**

Peptide P3 (Strand 1)	ϕ	θ_1	θ_2	ψ
dγAic 1	68	36	168	-164
dγAic 2	70	16	174	-174
dγAic 3	68	25	167	179
dγAic 4	79	20	174	-175
dγAic 5	70	19	-177	166

Table 7: Torsional Angle (in degree) Parameters of **P3 (Molecule 2, Strand 2)**

Peptide P3 (Strand 1)	ϕ	θ_1	θ_2	ψ
dγAic 1	91	12	175	177
dγAic 2	67	25	165	-166

dγAic 3	75	17	170	-178
dγAic 4	73	16	172	-171
dγAic 5	62	16	174	-162

Table 8: Hydrogen Bond Parameters of **P3**

Interstrand H-bonds

Donor (D)	**Acceptor (A)**	**D….A (Å)**	**DH….A (Å)**	**NH….O (deg)**
N7	O2	2.82	1.99	164
N8	O3	2.84	2.02	160
N9	O4	2.79	1.98	161
N11	O6	2.79	1.95	164
N12	O7	2.83	2.05	151
N5	O11	2.85	2.00	178
N4	O10	2.90	2.07	164
N10	O5	2.77	1.92	171
N6	O12	2.84	1.99	171

Intermolecular H-bonds with other double helices

Donor (D)	**Acceptor (A)**	**D….A (Å)**	**DH….A (Å)**	**NH….O (deg)**
N2	O28	3.056	2.31	144
N1	O27	2.90	2.14	146

N14	O14	3.03	2.27	147
N13	O13	2.89	2.08	156

2.3.5 Solution conformation of peptide P3

To understand the solution conformation of peptide **P3** and to understand the orientation of γ-peptide strands in the double helix in solution, fluorescence studies were carried out. The fluorescence spectra of **P3** in $CHCl_3$ are shown Figure 11a. The fluorescence emission at 475 nm indicates the excimer complex of pyrene in solution.[21] The presence of excimer in **P3** was confirmed at the concentration as low as 7 μM, indicating the existence of parallel β-double helix conformation in solution even at very low concentrations. Further Infrared spectroscopy studies showing NH stretching vibration band around at 3290 cm^{-1}, suggesting the involvement of amide NH in H-bonding and support the double helix formation (Figure 11b).

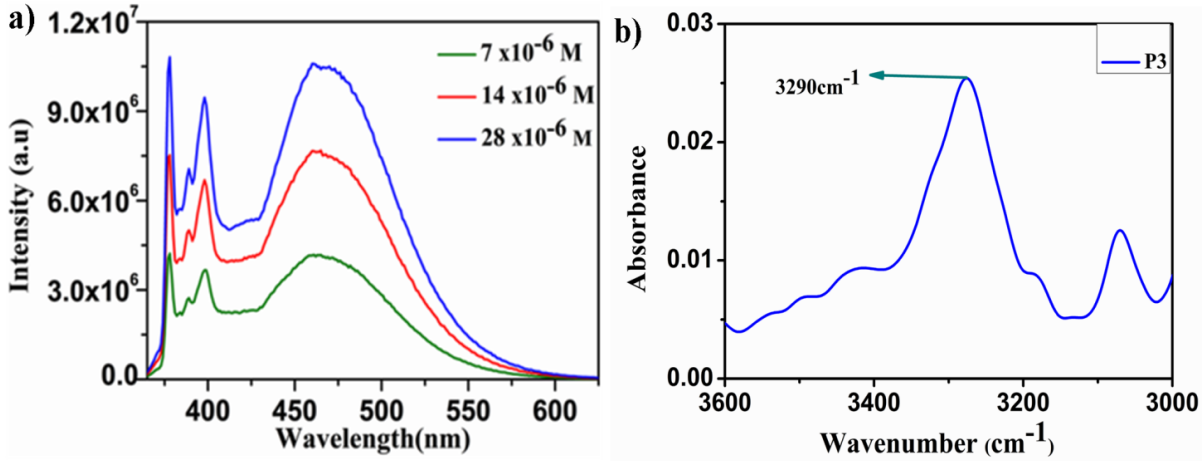

Fig 11: a) Fluorescence of pyrene excimer of **P3** in $CHCl_3$. b) FTIR spectra of peptide **P3** in $CHCl_3$ (1mg/mL).

Furthermore, to understand the stability of double helix at higher temperatures, temperature dependent fluorescence studies were carried out. Upon increasing temperature from 293 to 373 K, we observed a decrease in the fluorescence intensity at 475 nm corresponding to the pyrene excimer (Figure 12). These results advocate that the temperature dependent dissociation of double helix into individual γ-peptide strands and supporting the results observed in the temperature dependent NMR experiments. Instructively, temperature

dependent dissociation of double helices into individual strand has also been observed in the aromatic oligoamide double helices.[5]

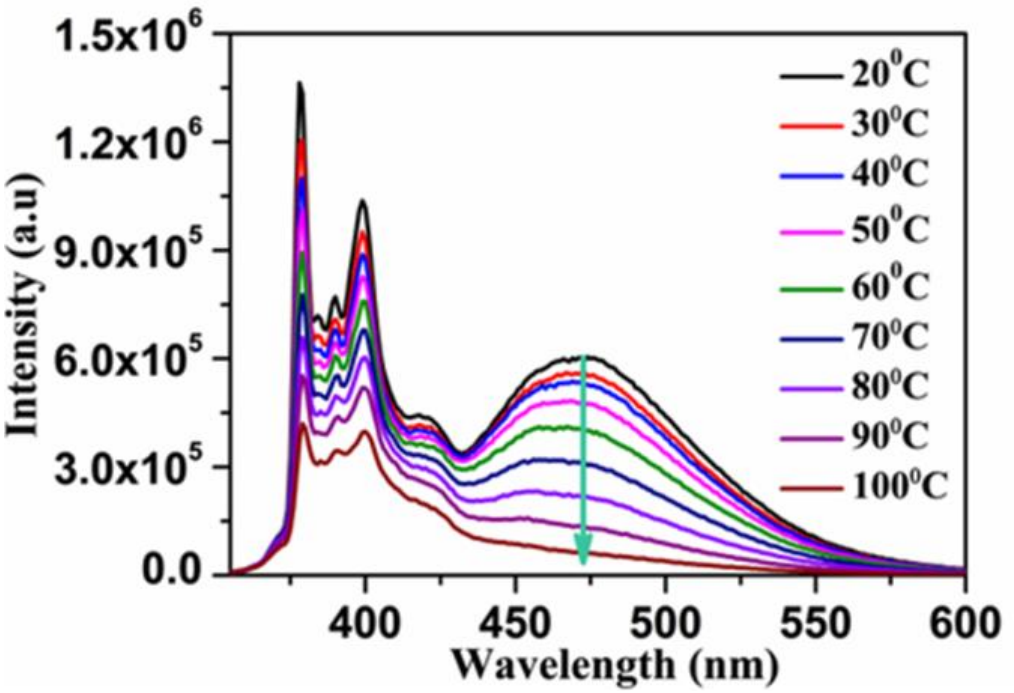

Fig 12: Fluorescence spectra of **P3** in $C_2D_2Cl_4$ with increasing temperature.

2.4 Conclusion

In summary, the short γ-peptides constructed from achiral 4,4-gem-dimethyl α,β-unsaturated γ-amino acids have displayed a high propensity to fold into a β-double helix pattern. Both X-ray and fluorescence studies revealed the parallel orientation of γ-peptide strands in single crystals as well as in solution. The supramolecular β-double helix structures are stabilized by the interstrand H-bonds. Moreover, these γ-peptides are capable of accommodating bulky groups like pyrenyl moieties without deviating overall double helix structure. Thus far, only alternating L, D-peptides have been shown to adopt β-double helix structures, however, our findings show that γ-peptides can also fold into β-double helix structures. The predictable β-double helix property of γ-peptide foldamers can be further explored to design artificial transmembrane ion channels and macromolecular scaffolds for nanobiological applications, and biomaterials sciences.

2.5 Experimental section

2.5.1 Synthesis of monomer and peptides

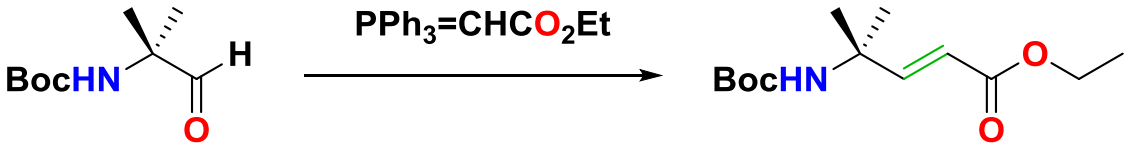

a) Synthesis of (*E*) ethyl -4-((*tert*-butoxycarbonyl) amino)-4-methylpent-2-enoate[Boc-(*E*)-dgU-OEt] (compound 1):

Boc-2-Aminoisobutyric aldehyde [*tert*-butyl (2-methyl-1-oxopropan-2-yl) carbamate] (3.74 g, 20 mmol) was dissolved in 60 mL of dry THF. Then ylide (PPh_3=$CHCO_2Et$) (10.45 g, 30 mmol) was added to this solution at RT. Reaction mixture was stirred for 5 hrs at RT. Completion of the reaction was monitored by TLC. After completion, the reaction mixture was quenched with 2M ammonium chloride solution in water (100 mL). Then product was extracted with EtOAc (3 × 100 mL). Combined organic layer was washed with brine (100 mL) and dried over anhydrous Na_2SO_4. Organic layer was concentrated under reduced pressure to give crude product. The crude product was further purified on silica gel column chromatography using EtOAc/hexane to get pure ethyl ester of *N*-Boc-(*E*)-α, β-unsaturated γ-2-aminoisobutyric acid good yield (3.85 g, 75%)

Synthesis of peptides

Synthesis of Dipeptide, tetrapeptide and pentapeptides were carried out through conventional solution-phase methods using a fragment-condensation strategy. The *tert*-butyloxycarbonyl group was used for *N*-terminus protection and the *C*-terminus was protected as an ethyl ester. Deprotections were performed with trifluoroacetic acid and saponification for the N- and C-termini, respectively. Couplings were mediated by *N*-(3-dimethylaminopropyl)-*N*′-ethylcarbodiimide hydrochloride (EDC.HCl) and 1- hydroxybenzotriazole (HOBt).

Typically, Boc-dγAic-OH (6.55 mmol, 1.5 g) and NH_2-dgγAic-OEt were dissolved together in DMF (4 mL), followed by EDC.HCl (6.55 mmol, 1.25 g) and (6.55 mmol, 884 mg) was added. The reaction mixture and cooled to 0 ^oC for 5 min. Then DiPEA (19.65 mmol, 3.52 mL) was added to the reaction mixture with stirring condition and the reaction mixture was allowed to come to room temperature. The progress of the reaction was monitored by TLC. After completion of the reaction (roughly 24 hrs), reaction mixture was diluted with 300 mL

of ethyl acetate and washed with 5% HCl (5 % by vol. in water, 2 × 80 mL), 10 % sodium carbonate solution in water (2 × 80 mL) and followed by brine (100 mL). The organic layer was dried over Na_2SO_4 and evaporated under reduced pressure to give gummy yellowish product, which was purified on silica gel column chromatography using EtOAc/hexane solvent system to gummy product, which was further crystallized using EtOAc/hexane. Overall yield 60% (3.7 mmol, 1.4 g). The tetrapeptide Boc-dγAic-dγAic-dγAic-dγAic-OEt (**P1**) was prepared by [2 + 2] condensation involving *N*-terminal dipeptide acid Boc-dγAic-dγAic-COOH and H_2N-dγAic-dγAic-OEt. The pentapeptide Boc-dγAic-dγAic-dγAic-dγAic-dγAic-OEt (**P2**) was prepared by [4+1] condensation involving *N*-terminal tetrapeptide acid Boc-dγAic-dγAic-dγAic-dγAic-dγAic-COOH and H_2N-dγAic-OEt. The peptide Boc-dγAic-dγAic-dγAic-dγAic-dγAic-Pyr (**P3**) was prepared by [5 + 1] condensation involving *N*-terminal pentapeptide acid Boc-dγAic-dγAic-dγAic-dγAic-dγAic-COOH and H_2N-CH_2-Pyr. Finally, all peptides were purified through reversed-phase HPLC employing MeOH/H_2O gradient system.

Characterization of monomer and peptides:

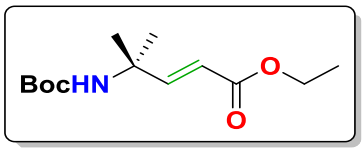

Characterization of Boc-dγAic-OEt(Compound 1)

^{1}H NMR (400 MHz, $CDCl_3$) δ 6.99 (d, *J* = 15.9 Hz, 1H), 5.82 (d, *J* = 15.9 Hz, 1H), 4.74 (s, 1H), 4.17 (q, *J* = 7.2 Hz, 2H), 1.41 (s, 9H), 1.39 (s, 7H), 1.27 (t, *J* = 7.2 Hz, 3H). ^{13}C NMR (101 MHz, $CDCl_3$) δ 166.72, 153.61, 118.43, 60.33, 52.88, 28.23, 27.33, 14.22. MALDI TOF/TOF m/z calculated value for $C_{13}H_{23}NO_4$ $[M+K]^+$ 296.12 and observed 296.12.

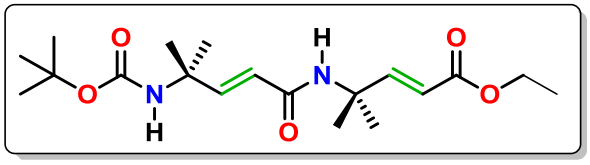

Characterization of Boc-dγAic-dγAic-OEt (Compound 2)

^{1}H NMR (400 MHz, $CDCl_3$) δ 7.03 (d, J = 15.9, 1.0 Hz, 1H), 6.77 (d, J = 15.5 Hz, 1H), 5.84 (dt, J = 15.9, 0.9 Hz, 1H), 5.77 (d, J = 15.5 Hz, 1H), 5.60 (BS, 1H), 4.64 (s, 1H), 4.17 (qt, J = 7.2, 1.0 Hz, 2H), 1.49 – 1.47 (m, 6H), 1.43 – 1.40 (m, 9H), 1.39 (bs, J = 1.4 Hz, 6H), 1.27 (m, 3H). ^{13}C NMR (101 MHz, $CDCl_3$) δ 166.68, 164.93, 152.60, 121.10, 118.78, 60.42, 53.77, 52.76, 28.41, 27.14, 14.24; MALDI TOF/TOF m/z calculated value for $C_{19}H_{32}N_2O_5$ $[M+Na]^+$ 391.22 and observed 391.21.

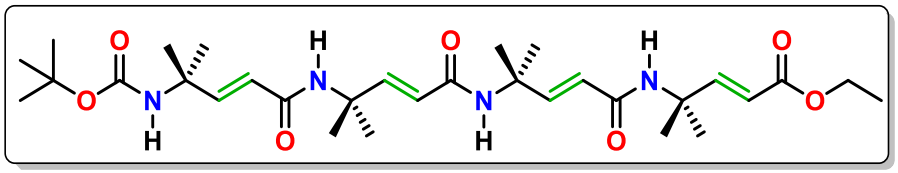

Characterization of peptide P1

^{1}HNMR (400MHz, $CDCl_3$) δ 8.29 (bs, 1H), 7.67 (s, 1H), 7.60 (s, 1H), 7.18 (d, J = 15.9 Hz, 1H), 6.80 – 6.71 (m, 3H), 6.00 (d, J = 15.2 Hz, 1H), 5.87 (d, J = 15.9 Hz, 1H), 5.76 (d, J = 15.3 Hz, 1H), 5.68 (d, J = 15.3 Hz, 1H), 4.76 (s, 1H), 4.18 (q, J = 7.1 Hz, 2H), 1.52(bs, 10H), 1.42 (s, 17H), 1.33-1.28 (t, J = 7.1 Hz, 3H); HR-MS m/z calculated for $C_{31}H_{50}N_4O_7$ is $[M+H]^+$ 591.37 and observed 591.37

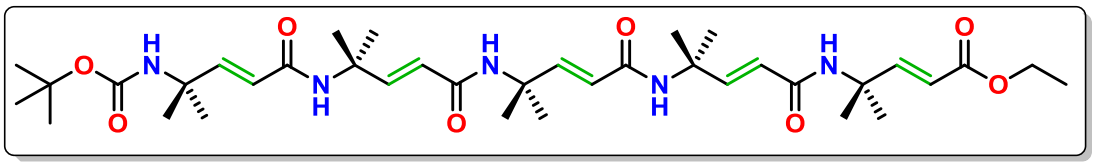

Characterization of peptide P2

^{1}H NMR (400 MHz, $CDCl_3$) δ 8.49 (bs, 2H), 7.85 (bs, 2H), 7.20 (d, J = 15.9 Hz, 1H), 6.83 – 6.67 (m, 4H), 6.01 (bs, 1H), 5.92 – 5.66 (m, 4H), 4.87 – 4.59 (m, 1H), 4.28 – 4.05 (m, 2H), 1.70 – 1.55 (m, 15H), 1.53 (s, 11H), 1.46 – 1.26 (m, 18H); HR-MS m/z calculated for $C_{37}H_{59}N_5O_8$ is $[M+H]^+$ 702.44 and observed 702.44

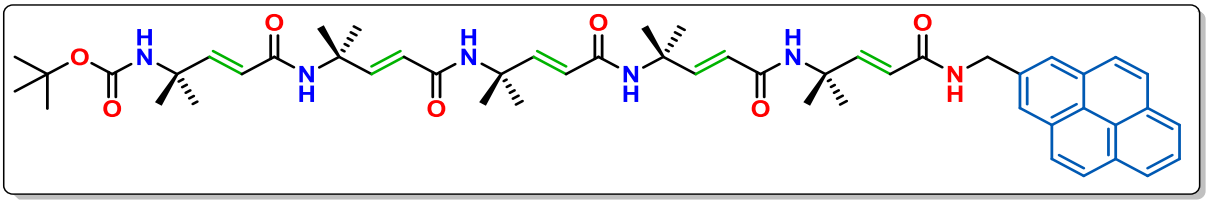

Characterization of peptide P3

^{1}H NMR (400 MHz, 1,1,2,2-tetrachloroethane-d_2,) δ 8.39 (d, *J* = 9.3 Hz, 1H), 8.35 – 8.15 (m, 4H), 8.14 – 8.03 (m, 6H), 8.01 – 7.93 (m, 3H), 7.00 (d, *J* = 15.6 Hz, 1H), 6.83 (d, *J* = 15.4 Hz, 1H), 6.78 (d, *J* = 15.3 Hz, 1H), 6.73 (d, *J* = 7.8 Hz, 1H), 6.69 (d, *J* = 7.7 Hz, 1H), 6.03 – 5.73 (m, 5H), 5.24 – 5.11 (m, 2H), 4.87 (s, 1H), 1.68 (s, 12H), 1.62 – 1.45 (m, 40H), 1.40 (m, *J* = 18.8 Hz, 14H). MALDI TOF/TOF m/z calculated value for $C_{52}H_{66}N_6O_4$ $[M+Na]^+$ 909.48 and observed 909.49.

2.5.2 Crystal Structure Information

General procedure for crystallization of peptides

All crystallization attempts were conducted at room temperature. All oligomers of dγAic were purified carefully before keeping for crystallization. Glass sample vials (2 mL) were washed with acetone and dried under a nitrogen gas stream before use. PARAFILM was used to close the vials. HPLC-grade solvents were used for crystallization.

Crystal structure analysis of P1

Crystals were grown from chloroform/n-heptane solution by slow evaporation. A single crystal (0.22 × 0.08 × 0.11 mm) was mounted on loop with a small amount of the paraffin oil. The X-ray data were collected at 100 K temperature using Mo K_α radiation (λ = 0.71073 Å), *ω*-scans (2*θ* = 57.028), for a total of 21460 independent reflections. Space group P-1, a = 14.593(5), b = 18.778(6), c = 18.850(6), *α* = 100.981(7), *β* = 108.634(7), *γ* = 111.442(7) V = 4270(2) Å^3, triclinic, Z = 4 for chemical formula C_{33} H_{52} C_{l6} N_4 O_7, with one molecule in asymmetric unit; *ρ*calcd = 1.290 gcm^{-3}, *μ* = 0.448 mm^{-1}, F (000) = 19210, The structure was obtained by direct methods using SHELXS-97.[1] The final R value was 0.0800 (wR2 = 0.1850) 4189 observed reflections ($F_0 \geq 4\sigma$ ($|F_0|$)) and 558 variables, S = 1.027.The largest difference peak and hole were 0.954 and -0.669eÅ^3 respectively.CCDC No 1812184

Crystal structure analysis of P2

Crystals were grown from chloroform/**n**-heptane solution by slow evaporation. A single crystal (0.28 × 0.09 × 0.15 mm) was mounted on loop with a small amount of the paraffin oil. The X-ray data were collected at 100 K temperature using Mo K_α radiation (λ = 0.71073 Å), ω-scans (2θ = 56.854), for a total of 23376 independent reflections. Space group P-1, a = 14.655(3), b = 17.312(3), c = 19.369(3), α = 105.130(3), β = 99.564(3), γ = 90.962(4) V = 4668.2(14)Å^3, triclinic, Z = 1 for chemical formula C_{152} H_{238} C_{l12} N_{20} O_{35}, with one molecule in asymmetric unit; ρcalcd = 1.185gcm^{-3}, μ = 0.248mm^{-1}, F (000) = 1952, The structure was obtained by direct methods using SHELXS-97.[1] The final R value was 0.1143 (wR2 = 0.2846) 3599 observed reflections ($F_0 \geq 4\sigma$ (|F_0|)) and 1018 variables, S = 1.314.The largest difference peak and hole were 2.137and -0.891eÅ^3 respectively. CCDC No 1812185

The investigated single crystal was a small-sized and the quality of diffraction was poor. Numerous datasets were collected on single crystals from different batches and one of the highest quality is reported herein.

Crystal structure analysis of P3

Crystals were grown from chloroform/tolune solution by slow evaporation. A single crystal (0.20 × 0.05 × 0.13 mm) was mounted on loop with a small amount of the paraffin oil. The X-ray data were collected at 100K temperature using Mo K_α radiation (λ = 0.71073 Å), ω-scans (2θ = 56.96), for a total of 60013 independent reflections. Space group P 21/c, a = 44.330(14), b = 24.634(8), c = 22.432(7), , β = 90.112(6), V = 24497(13)Å^3, triclinic, Z = 4 for chemical formula C_{208} H_{265} N_{24} O_{28}, with two molecules in asymmetric unit; ρcalcd = 0.962gcm^{-3}, μ = 0.064mm^{-1}, F (000) = 8964, The structure was obtained by direct methods using SHELXS-97.[1] The final R value was 0.1948 (wR2 = 0.4184) 9914 observed reflections ($F_0 \geq 4\sigma$ (|F_0|)) and 2393 variables, S = 1.314.The largest difference peak and hole were 0.418and -0.450Å^3 respectively. CCDC No 1812186

The investigated single crystal was a small and the quality of diffraction was poor. Numerous datasets were collected on single crystals from different batches and the one of the highest quality is reported herein.

There is some partially occupied solvent molecule also present in the asymmetric unit. A significant amount of time was invested in identifying and refining the disordered molecule. Option SQUEEZE of program PLATON[2] was used to correct the diffraction data for diffuse

scattering effects and to identify the solvent molecule. PLATON calculated the upper limit of volume that can be occupied by the solvent to be 6762 $Å^3$ or 27.60% of the unit cell volume. The program calculated 1945 electrons in the unit cell for the diffuse species. No data are given for the diffusely scattering species. Outputs of SQUEEZE report are appended in CIF file **P3**.

2.6 References

1. Watson, J. D.; Crick, F. C. H. *Nature*, **1953**, *171*, 737; b) Alberts, B.; Johnson, A.; Lewis, J.; Morgan, D.; Raff, M.; Roberts, K.; Walter, P. Mol. Biol. Cell, 6th ed.; Garland Science: New York,
2. Saenger, W. Principles of Nucleic Acid Structure; Springer-Verlag: New York, 1984.
3. Langes, D. A. *Science* **1988**, *241*, 188; b) Urry, D. W.; Glickson, J. D.; Mayers, D. F.; Haider, J. *Biochemistry* **1972**, *11*, 487; c) Wallace, B. A.; Ravikumar, K. *Science* **1988**; *241*, 182. d) Sychev, S. V.; Barsukov, L. I.; Ivanov, V. T. *J. Pept. Sci.* **2013**, *19*, 452; e) Kelkar, D. A.; Chattopadhyay, A. *Biochim. Biophys. Acta*. **2007**, *1768*, 2011; f) Sychev, S. V.; Barsukov, L. I.; Ivanov, V. T. *Eur. Biophys. J.* **1993**, *22***,** 279.
4. Benedetti, E.; Di Blasio, B.; Pedone, C.; Lorenzi, G. P.; Tomasic, L.; Gramlich, V. *Nature*, **1979**, *282*, 630; b) Di Blasio, B.; Benedetti, E.; Pavone, V.; Pedone, C.; Gerber, C.; Lorenzi, G. P. *Biopolymers* **1989**, *28*, 203; c) Kulp, J. L.; Clark, T. D. *Chem. Eur. J.* **2009**, *15*, 11867; d) Navarro, E.; Fenude, E.; Celda, B. *Biopolymers* **2004**, *73*, 229; e) Sastry, M.; Brown, C.; Wagner, G.; Clark, T. D. *J. Am. Chem. Soc.* **2006**, *128*, 10650; f) Schramm, P.; Hofmann, H. -J. *J. Pept. Sci.* **2010**, *16*, 276; g) Jadhav, K. B.; Lichtenecker, R. J.; Bullach, A.; Mandal, B.; Arndt, H. -D. *Chem. Eur. J.* **2015**, *21*, 5898.
5. a) Berl, V.; Huc, I.; Khoury, R. G.; Krische, M. J.; Lehn, J. -M. *Nature* **2000**, *407*, 720; b) Gan, Q.; Wang, X.; Kauffmann, B.; Rosu, F.; Ferrand, Y.; Huc. I. *Nature Nanotech*. **2017**, *12*, 447; c) Wang, X.; Wicher, B.; Ferrand, Y.; Huc, I. *J. Am. Chem. Soc*. **2017**, *139*, 9350; d) Li, X.; Markandeya, N.; Jonusauskas, G.; McClenaghan, N. D.; Maurizot, V.; Denisov, S. A.; Huc, I. *J. Am. Chem. Soc.* **2016**, *138*, 13568; e) Denisov, S. A.; Gan, Q.; Wang, X.; Scarpantonio, L.; Ferrand, Y.; Kauffmann, B.; Jonusauskas, G.; Huc, I.; McClenaghan, N. D. *Angew. Chem. Int. Ed.* **2016**, *55*, 1328; f) Shang, J.; Gan, Q.; Dawson, S. J.; Rosu, F.; Jiang, H.;

Ferrand, Y.; Huc I. *Org. Lett*. **2014**, 16, 4992; g) Denisov, S. A.; Gan, Q.; Wang, X.; Scarpantonio, L.; Ferrand, Y.; Kauffmann, B.; Jonusauskas, G.; Huc, I.; McClenaghan, N. D. *Angew. Chem. Int. Ed*. **2016**, *55*, 1328; h) Denisov, S. A.; Gan, Q.; Wang, X.; Scarpantonio, L.; Ferrand, Y.; Kauffmann, B.; Jonusauskas, G.; Huc, I.; McClenaghan, N. D. *Angew. Chem. Int. Ed.* **2016**, *55*, 1328; i) Maurizot, V.; J. Léger, M.; Guionneau, P.; Huc, I. *Russ.Chem.Bull. Int.Ed*., **2004**, *53*, 1572. j) Zhan, C.; Léger, J.-M.; Huc, I. *Angew. Chem. Int. Ed.* **2006**, *45*, 4625; k) Haldar, D.; Jiang, H.; Léger, J.-M.; Huc, I. *Angew. Chem. Int. Ed.* **2006**, *45*, 5483.

6. Yashima, E.; Maeda, K.; Furusho, Y. *Acc. Chem. Res.* **2008**, *41*, 1166.
7. Koert, U.; Harding, M.M.; Lehn, J.-M. *Nature*, **1990**, 346, 339
8. Gabriel, G. J.; Iverson, B. L.; *J. Am. Chem. Soc*., **2002**, *124*, 15174. b) Lokey, R.S.; Iverson, B.L. *Nature*, **1995**, *375*, 303. c) Ikkanda, B. A.; Iverson, B. L. *Chem. Commun.*, **2016**, *52*, 7752.
9. Tanaka, Y.; Katagiri, H.; Furusho, Y. Yashima, E. *Angew. Chem., Int. Ed*., **2005**, *44*, 3867; b) E. Yashima, N. Ousaka, D. Taura, K. Shimomura, T. Ikai, K. Maeda, *Chem. Rev.* **2016**, *116*, 13752; c) Wang, J.; Meersman, F.; Esnouf, R.; Froeyen, M.; Busson, R. Heremans, K.; Herdewijn, P.; *Helv. Chim. Acta*, **2001**, *84*, 2398.
10. Miller, B.; Friedman, A. J.; Choi, H.; Hogan, J.; McCammon, J. A.; Hook. V.; Gerwick, W. H. *J. Nat. Prod*. **2014**, *77*, 92; b) Krahn, D.; Ottmann, C.; Kaiser, M. *Nat. Prod. Rep*. **2011**, *28*, 1854.
11. Baldauf, C.; Günther, R.; Hofmann, H.–J. *J. Org. Chem.* **2005**, *70*, 5351; b) Baldauf, C.; Gunther, R.; Hofmann, H.–J. *Helv. Chim. Acta* **2003**, *86*, 2573.
12. Mathieu, L.; Legrand, B.; Deng, C.; Vezenkov, L.; Wenger, E.; Didierjean, C.; Amblard, M.; Averlant-Petit, M. –C.; Masurier, N.; Lisowski, V.; Martinez, J.; Maillard, L. T. *Angew. Chem. Int. Ed*. **2013**, *52*, 6006.
13. Ganesh Kumar, M.; Thombare, V. J.; Katariya, M. M.; Veeresh, K.; Raja, K. M.P.; Gopi, H. N. *Angew. Chem. Int. Ed*. **2016**, *55*, 7847.
14. Bandyopadhyay, A.; Misra, R.; Gopi, H. N. *Chem. Commun.* **2016**, *52*, 4938
15. Hagihara, M.; Anthony, N. J.; Stout, T. J.; Clardy, J.; Schreiber, S. L.; *J. Am. Chem. Soc.* **1992**, *114*, 6568.
16. Mali, S. M.; Bandyopadhyay, A.; Jadhav, S. V.; Ganesh Kumar, M.; Gopi, H. N. *Org. Biomol. Chem.* **2011**, *9*, 6566.
17. Bandyopadhyay, A.; Gopi, H. N. *Org. Lett*. **2012**, *14*, 2770.

18. Seebach, D. A.; Beck, K.; Bierbaum, D. J. *Chem. Biodiv.* **2004**, *1*, 1111; b) Horne, W. S.; Gellman, S. H. *Acc. Chem. Res*. **2008**, *41*, 173; c) Vasudev, P. G.; Chatterjee, S.; Shamala, N.; Balaram, P. *Chem. Rev.* **2011**, *111*, 657. d) Guichard, G.; Huc, I. *Chem. Commun.* **2011**, *47*, 5933; e) Collie, G. W.; Pulka-Ziach, K.; Lombardo, C. M.; Fremaux, J.; Rosu, F.; Decossas, M.; Mauran, L.; Lambert, O.; Gabelica,V.; Mackeret, C. D.; Guichard, G.; *Nature Chemistry*, **2015, *7***, 871; f) Rudzińska-Szostak, E.; Berlicki, Ł. *Chem. Eur. J.* **2017**, *23*, 14980; g) Fülöp, F.; Martinek, T. A.; Tóth, G. K. *Chem. Soc. Rev.* **2006**, *35*, 323; h) Hecht, S.; Huc, I. (Eds.), *Foldamers: Structure, Properties and Applications*, Wiley-VCH, Weinheim, 2007. i) Goodman, C. M.; Choi, S.; Shandler, S.; DeGrado, W. F. *Nat. Chem. Biol.* **2007**, *3*, 252; j) Bouillère, F.; Thétiot-Laurent, S.; Kouklovsky, C.; Alezra, V. *Amino Acids* **2011**, *41*, 687. k) Pilsl, L. K. A.; Reiser, O. *Amino Acids* **2011**, *41*, 709; l) Saraogi, I.; Hamilton, A. D. *Chem. Soc. Rev.* **2009**, 38, 1726

19. a) Karle, I. L. Balaram, P. *Biochemistry* **1990**, *29*, 6747; b) Toniolo, C.; Crisma, M.; Formaggio, F.; Peggion, C. *Biopolymers* **2001**, *60*, 396; c) Toniolo, C.; Benedetti, E. *Trends Biochem. Sci.* **1991**, *16*, 350. d) Le Baillya, B. A. F.; Clayden, J. *Chem. Commun*. **2016**, *52*, 4852; e) Clayden, J.; Castellanos, A.; Solá, J.; Morris, G. A. *Angew. Chem. Int. Ed.* **2009**, *48*, 5962; f) Solá, J.; Morris, G. A.; Clayden, J. *J. Am. Chem. Soc.* **2011**, 133, g) Crisma, M.; Zotti, M. De.; Formaggio, F.; Peggion, C.; Moretto, A.; Toniolo, C. *J. Pept. Sci*., **2015**, *21*, 148; h) Millhauser, G. L. *Biochemistry* **1995**, *34*, 3873; i) Marshall, G. R.; Hodgkin, E. E.; Langs, D. A., Smith, G. D.; Zabrocki, J.; Leplawy, M. T. *Proc. Natl. Acad. Sci. USA* **1990**, *87*, 487; j) Aravinda, S.; Shamala, N.; Balaram, P. *Chem. Biodiversity*, **2008**, *5*, 1238. k) Bolin, K. A.; Millhauser, G. L. *Acc. Chem. Res.* **1999**, *32*, 1027. l) Crisma, M.; Saviano, M.; Moretto, A.; Broxterman, Q. B.; Kaptein, B.; Toniolo, C. *J. Am. Chem. Soc.* **2007**, *129*, 15471.

20. Fanelli, R.; Berthomieu, D.; Didierjean, C.; Doudouh, A.; Lebrun, A.; Martinez, J.; Cavelier, F.; *Org. Lett.*, **2017**, *19* , 2937.

21. Stevens, E. S.; Sugawara, N.; Bonora, G. M.; Toniolo, C. *J. Am. Chem. Soc*.**1980**, *102*, 7048.

22. Zhu, H.; Lewis, F. D. *Bioconjugate Chem*. **2007**, *18*, 1213

2.7 Appendix I: Mass spectra and ^{1}H NMR spectra for the monomer and peptides P1 to P3

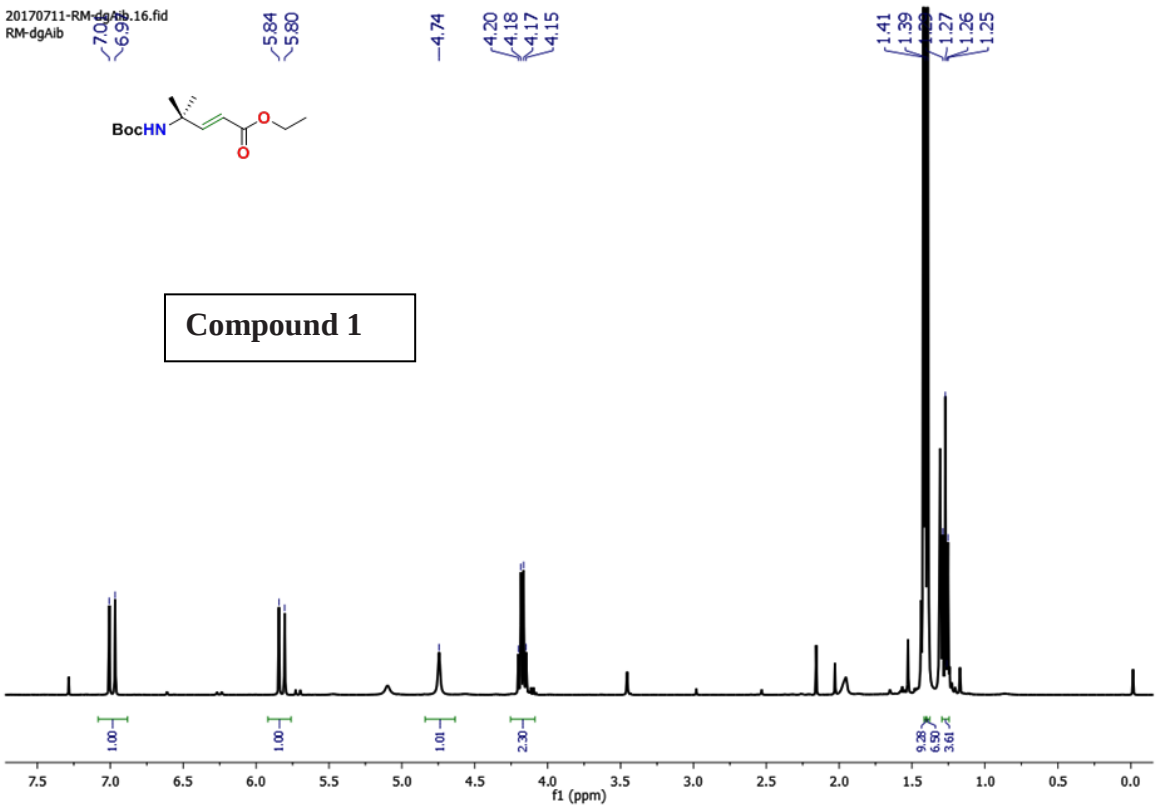

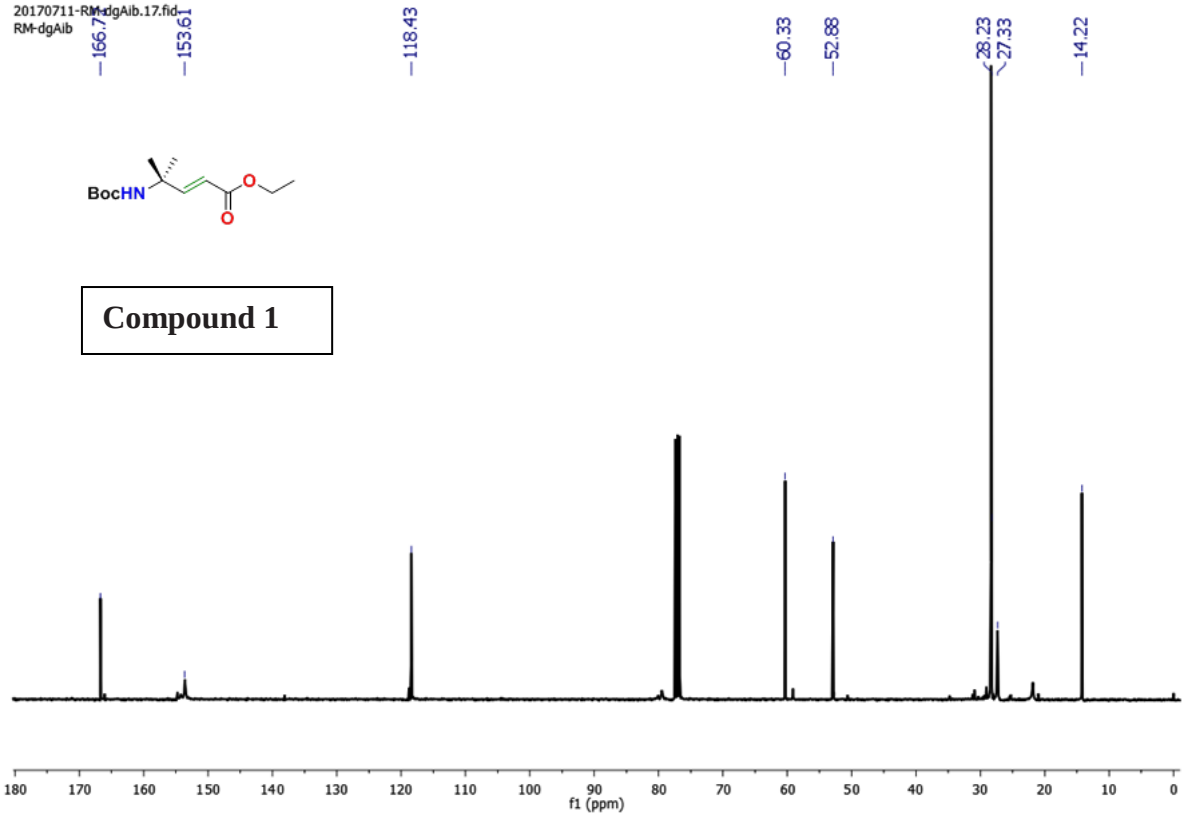
20170711-RM-dgAib.17.fid
RM-dgAib
166.71
153.61
118.43
60.33
52.88
28.23
27.33
14.22
BocHN
O
O
180
170
160
150
140
130
120
110
100
90
80
70
60
50
40
30
20
10
0
f1 (ppm)

Compound 1

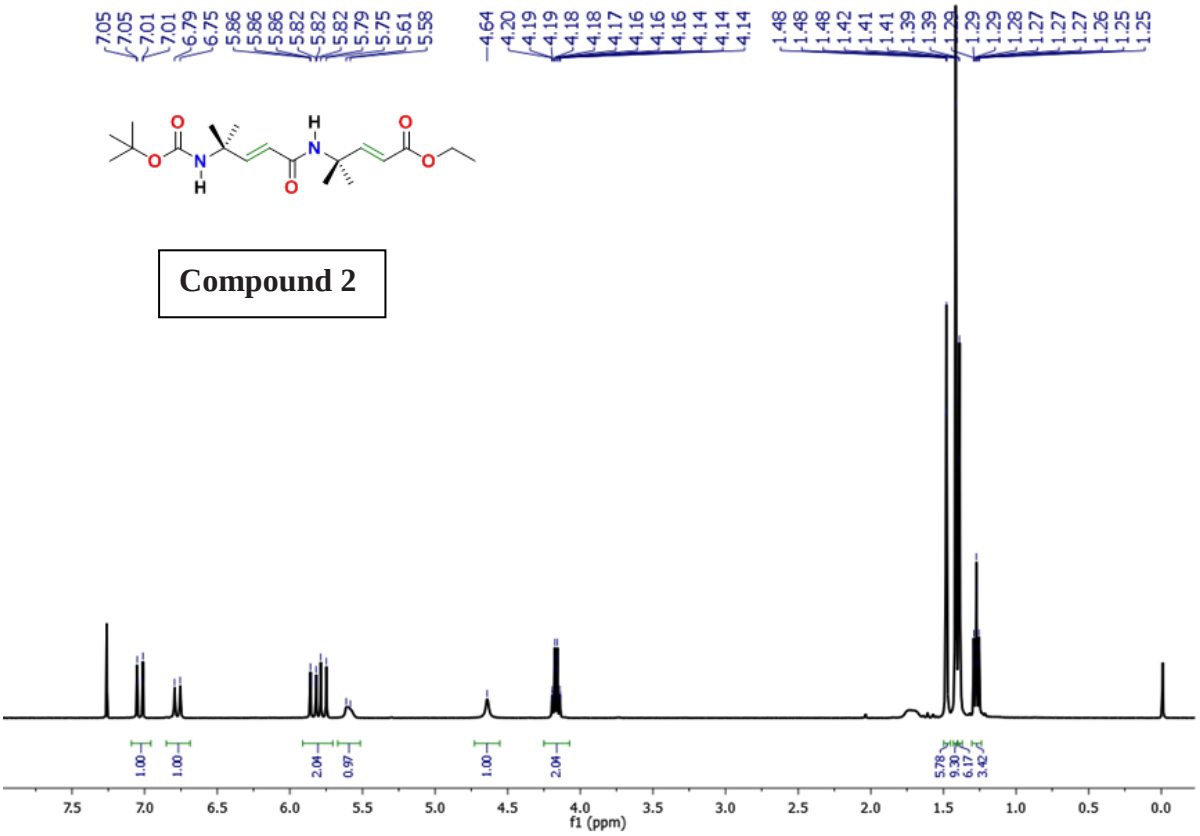
7.05
7.05
7.01
7.01
6.79
6.75
5.86
5.86
5.82
5.82
5.82
5.79
5.75
5.61
5.58
4.64
4.20
4.19
4.19
4.18
4.18
4.17
4.16
4.16
4.14
4.14
4.14
1.48
1.48
1.48
1.42
1.41
1.41
1.39
1.39
1.29
1.29
1.29
1.28
1.27
1.27
1.27
1.26
1.25
1.25
O
O
N
H
H
N
O
O
O
Compound 2
1.00
1.00
2.04
0.97
1.00
2.04
5.78
9.30
6.17
3.42
7.5
7.0
6.5
6.0
5.5
5.0
4.5
4.0
3.5
3.0
2.5
2.0
1.5
1.0
0.5
0.0
f1 (ppm)

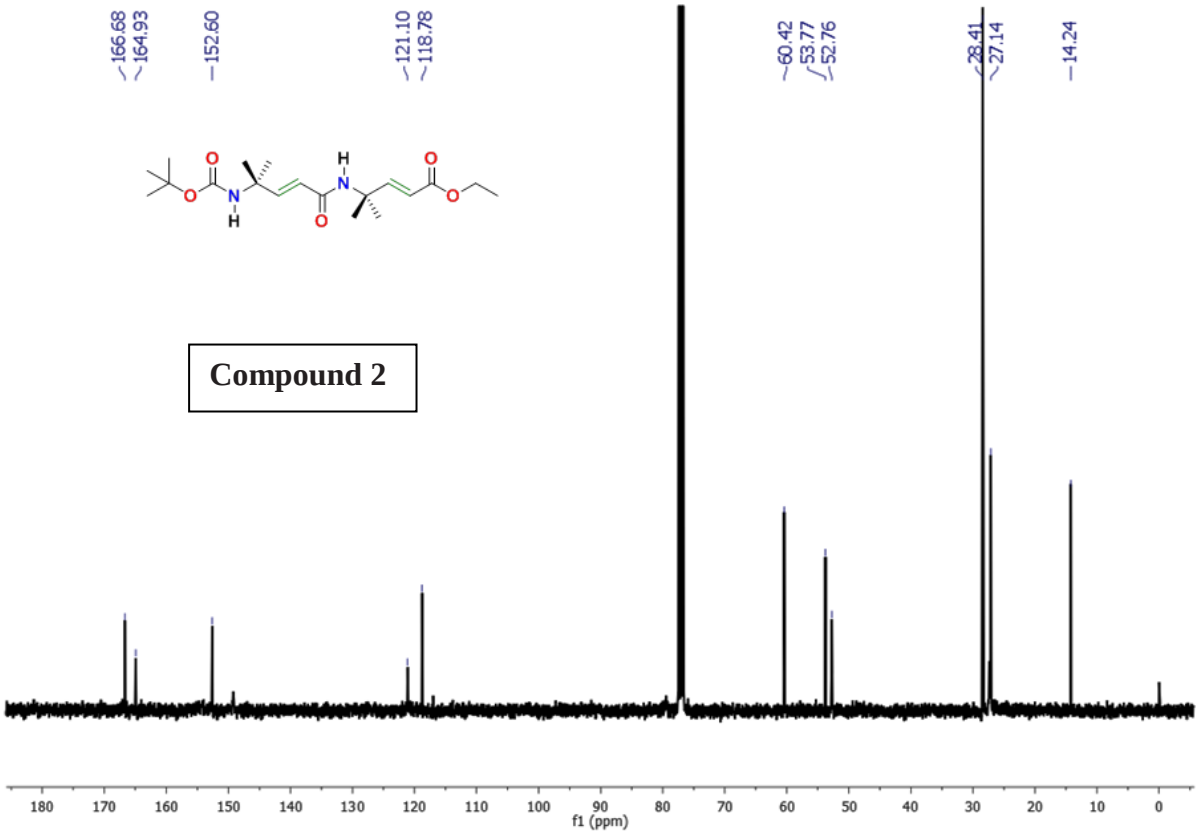
166.68
164.93
152.60
121.10
118.78
60.42
53.77
52.76
28.41
27.14
14.24
Compound 2
180
170
160
150
140
130
120
110
100
90
80
70
60
50
40
30
20
10
0
f1 (ppm)

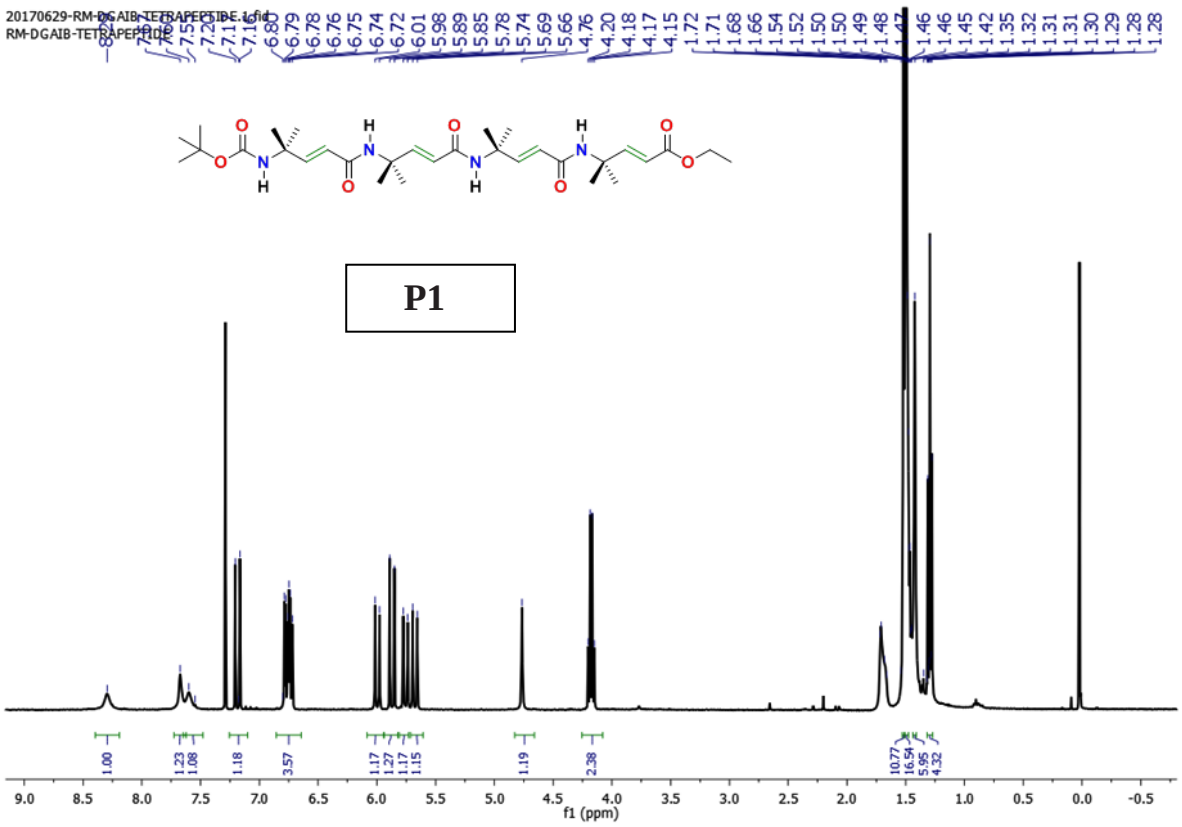
20170629-RM-DGAIB-TETRAPEPTIDE-1.fid
RM-DGAIB-TETRAPEPTIDE
P1
f1 (ppm)

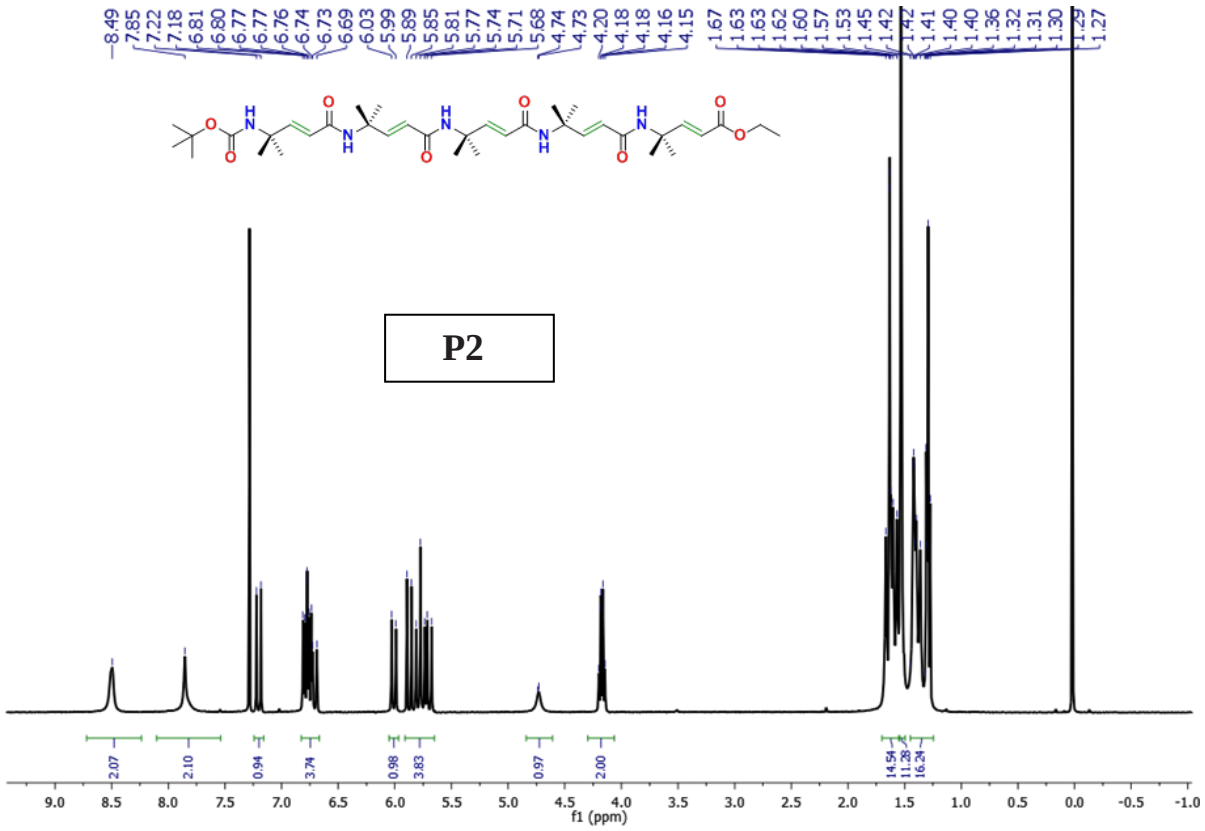
P2
f1 (ppm)

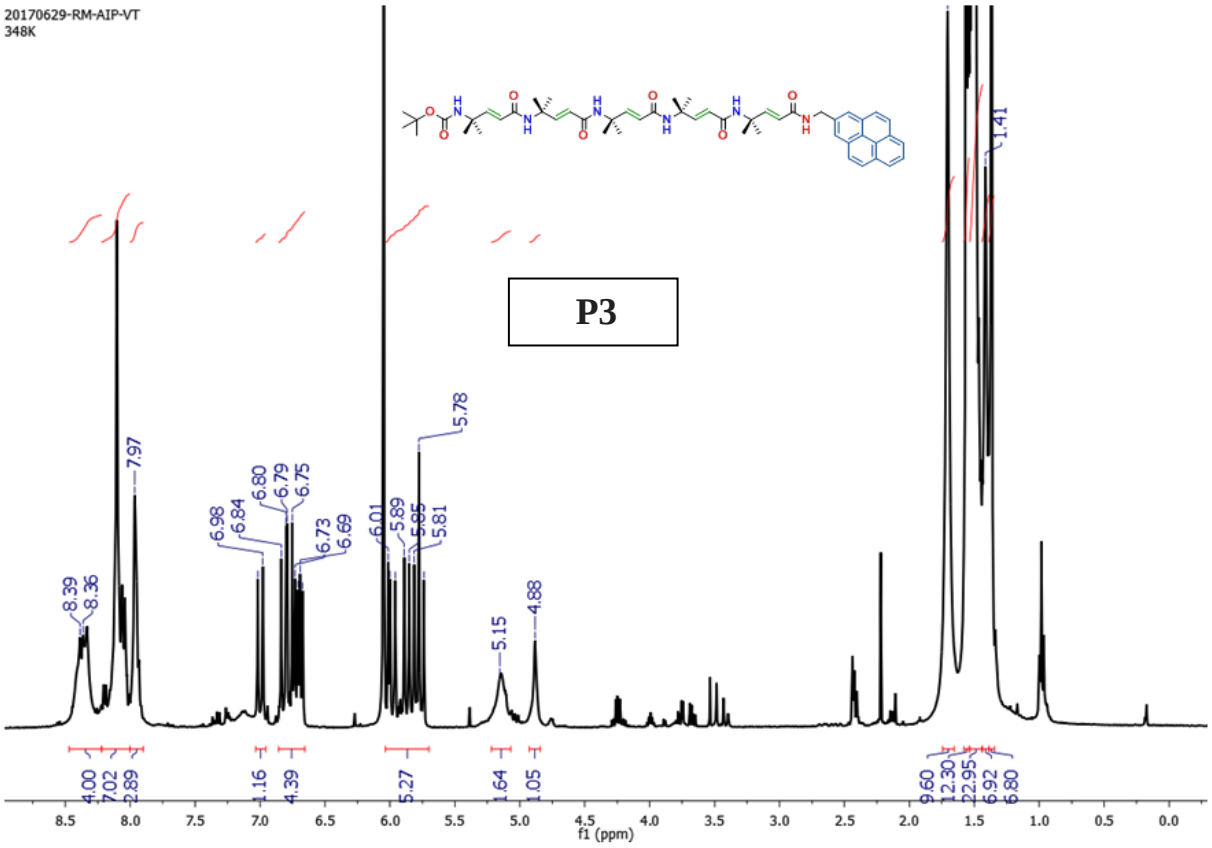
20170629-RM-AIP-VT
348K
P3
8.39
8.36
7.97
6.98
6.84
6.80
6.79
6.75
6.73
6.69
6.01
5.89
5.85
5.81
5.78
5.15
4.88
1.41
4.00
7.02
2.89
1.16
4.39
5.27
1.64
1.05
9.60
12.30
22.95
6.92
6.80
f1 (ppm)

Spectrum Report

Final - Shots 1000 - IISER-96-2-2017; Run #47; Label B5

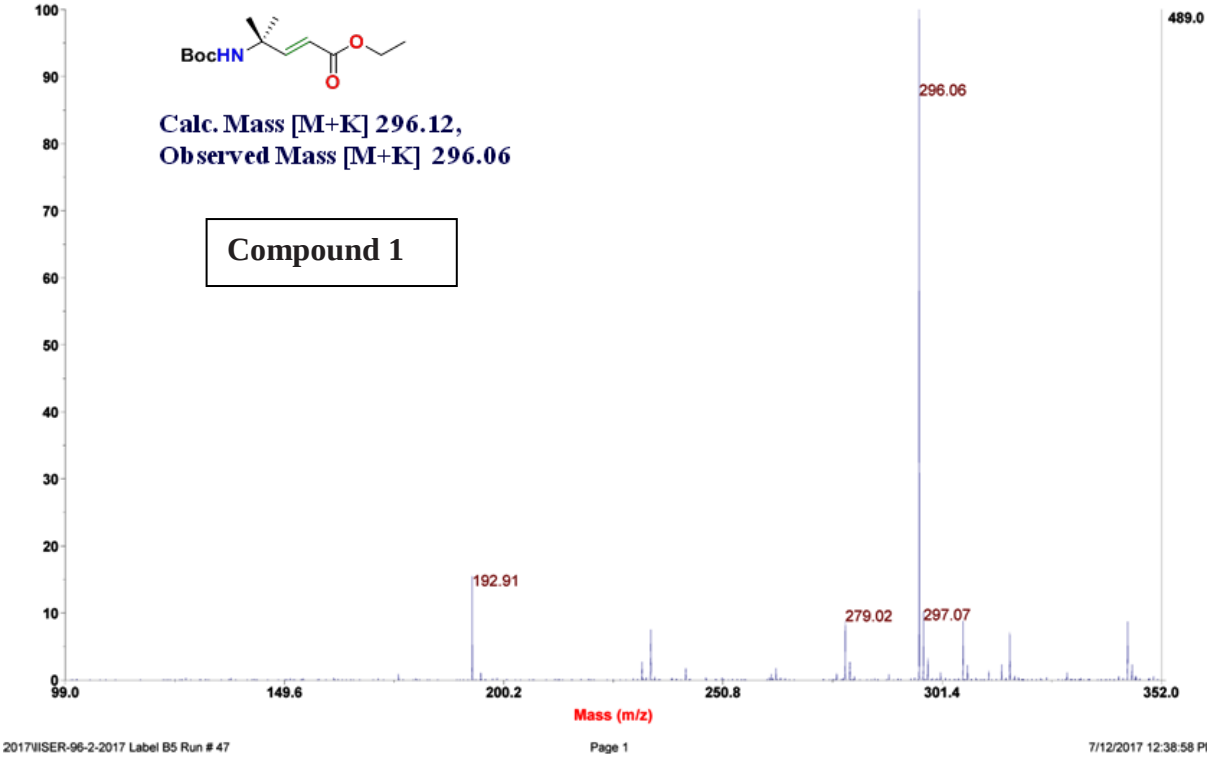

2017\IISER-96-2-2017 Label B5 Run # 47 Page 1 7/12/2017 12:38:58 PI

Spectrum Report

Final - Shots 1000 - IISER-96-1-2017; Run #76; Label E1

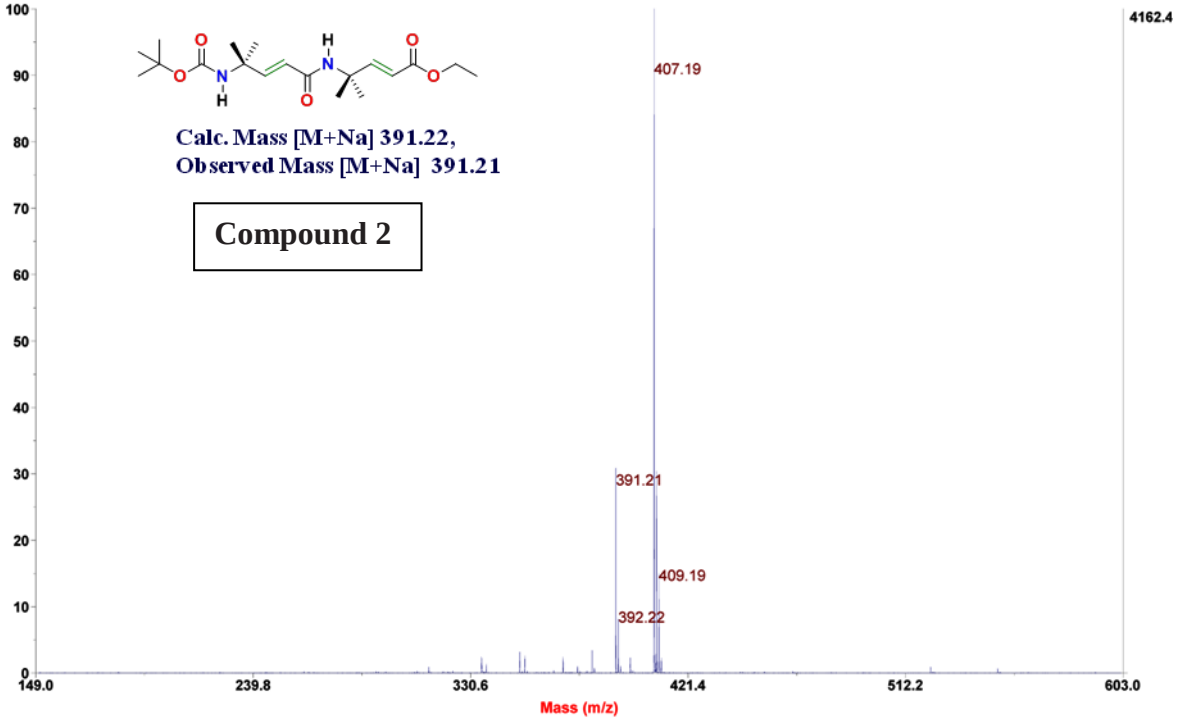

Calc. Mass [M+Na] 391.22,
Observed Mass [M+Na] 391.21

Compound 2

2017\IISER-96-1-2017 Label E1 Run # 76 Page 1 7/11/2017 10:28:14 AM

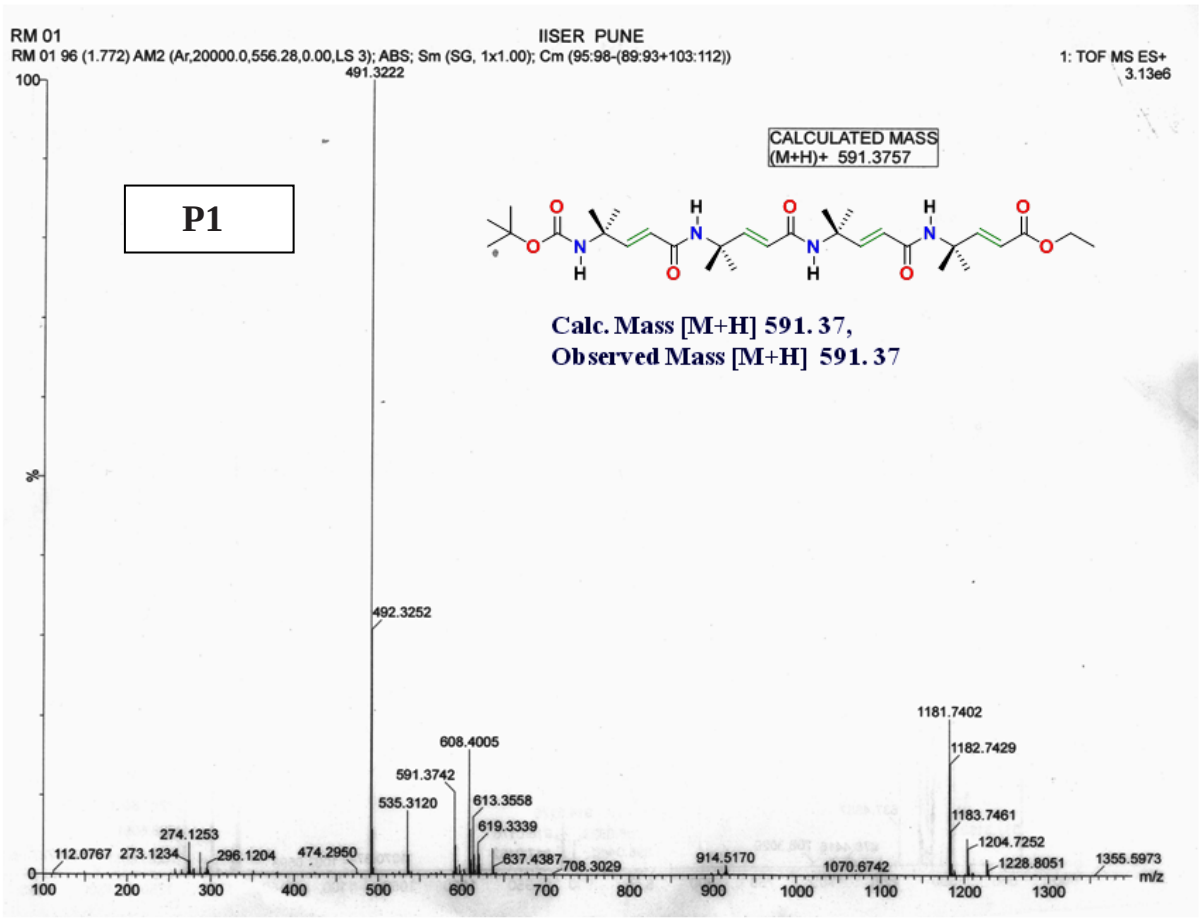
RM 01
IISER PUNE
RM 01 96 (1.772) AM2 (Ar,20000.0,556.28,0.00,LS 3); ABS; Sm (SG, 1x1.00); Cm (95:98-(89:93+103:112))
1: TOF MS ES+
3.13e6
P1
CALCULATED MASS
(M+H)+ 591.3757
Calc. Mass [M+H] 591. 37,
Observed Mass [M+H] 591. 37
491.3222
492.3252
608.4005
591.3742
535.3120
613.3558
619.3339
1181.7402
1182.7429
1183.7461
1204.7252
1228.8051
1355.5973
274.1253
112.0767
273.1234
296.1204
474.2950
637.4387
708.3029
914.5170
1070.6742
m/z

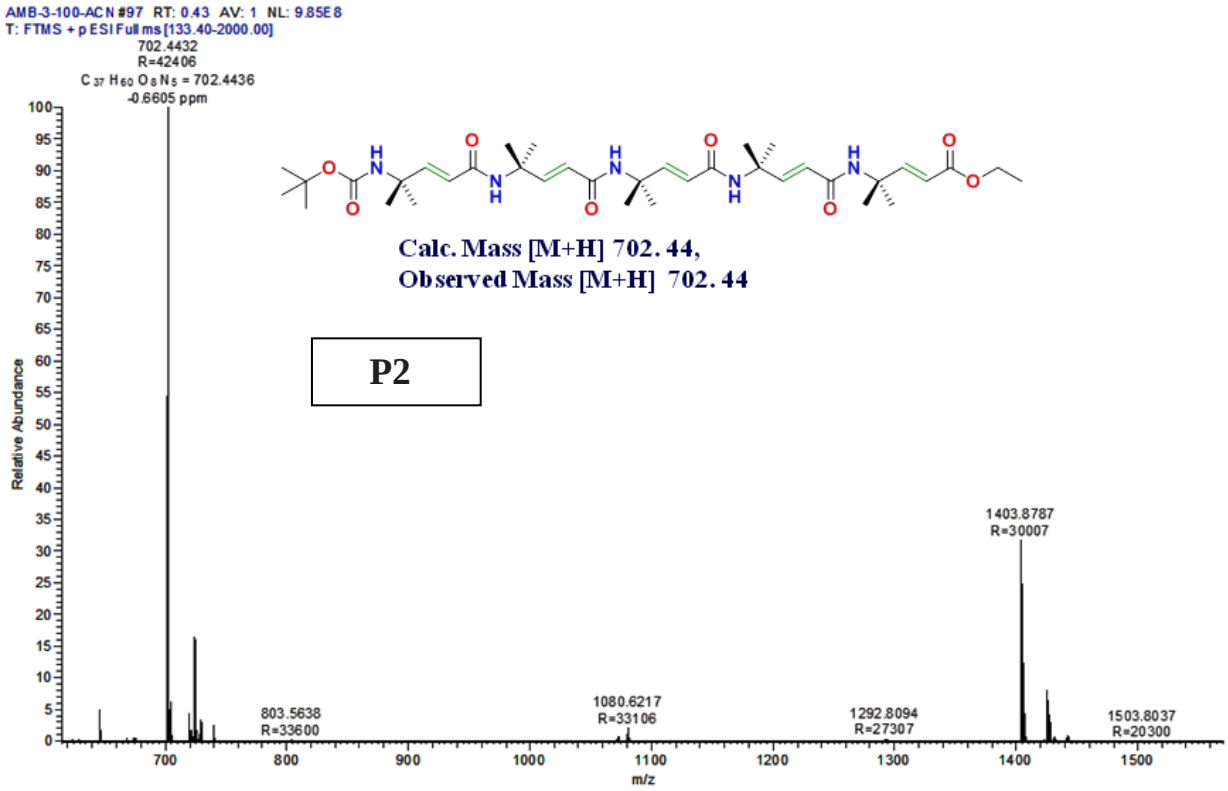
AMB-3-100-ACN #97 RT: 0.43 AV: 1 NL: 9.85E8
T: FTMS + p ESI Full ms [133.40-2000.00]
702.4432
R=42406
C 37 H 60 O 8 N 5 = 702.4436
-0.6605 ppm
Calc. Mass [M+H] 702. 44,
Observed Mass [M+H] 702. 44
P2
Relative Abundance
m/z
803.5638
R=33600
1080.6217
R=33106
1292.8094
R=27307
1403.8787
R=30007
1503.8037
R=20300

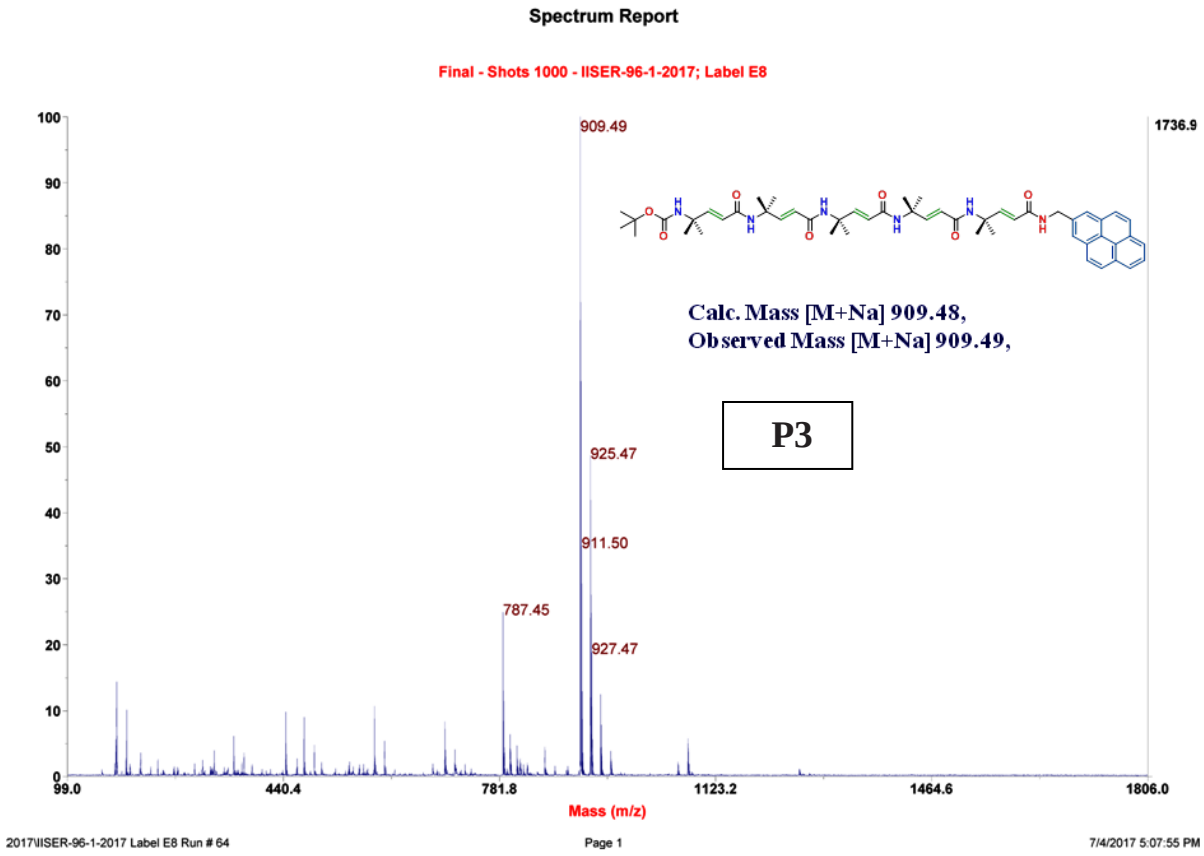
Spectrum Report
Final - Shots 1000 - IISER-96-1-2017; Label E8
909.49
1736.9
Calc. Mass [M+Na] 909.48,
Observed Mass [M+Na] 909.49,
P3
925.47
911.50
787.45
927.47
100
90
80
70
60
50
40
30
20
10
0
99.0
440.4
781.8
1123.2
1464.6
1806.0
Mass (m/z)
2017\IISER-96-1-2017 Label E8 Run # 64
Page 1
7/4/2017 5:07:55 PM

Chapter 3

Structural dimorphism of achiral α,γ-hybrid peptide foldamers: coexistence of 12- and 15/17-helices

3.1 Introduction

Synthetic peptides play a vital role in understanding structure, folding and functions of proteins. Recent progress in the design of definite artificially folded architectures from unnatural amino acids suggested that the folding phenomenon is not limited to natural polypeptides.[1,2] Helices are major secondary structure components of proteins and are mostly classified on the basis of their intramolecular hydrogen bonding patterns. Thus, the main types of naturally occurring protein and peptide helices, the α- and 3_{10}-helices, can be recognized by their 5→1 (*i*←*i+4*) and 4→1 (*i*←*i+3*) intramolecular hydrogen-bonded pseudocycles,[3,4] respectively. Comparatively, 3_{10}-helices are shorter in length (<4 residues) than α-helices and are often observed at the N- and C-termini of α-helices.[4] It has been postulated that 3_{10}-helices may be intermediates in the process of α-helix folding.[5] α-Amino isobutyric acid (Aib) has been extensively utilized in this regard to design α-peptide helical secondary structures. The restriction in the backbone conformational space (ϕ and ψ) of Aib and other gem-dialkyl α-amino acids forced the peptides to adopt stable helical structures.[6] The X-ray structures of some the germinal disubstituted homooligomers of Aib residues are shown in Figure 1. Longer 3_{10}-helices have been designed in homooligomers of the achiral α,α-dimethyl substituted amino acid Aib (α-aminoisobutyric acid).[6] It has been observed that either decreasing the percentage of Aib residues or increasing the sequence length lead to the preference of the α-helix over the 3_{10}-helix.[7] The transition from a 3_{10}- into an α-helix has been investigated both experimentally[8] and theoretically.[9]

The suggestion of peptides completely composed of the higher homologs of α-amino acids, as for instance β- and γ-amino acids, by the groups of Seebach[1a,2a] and Gellman[1b,c,h] and by others[1d,e,f,2h,10] led to the field of "foldamers" and opened a new dimension in the field of protein structure mimetics. The homopeptides of β- and γ-amino acids and hybrid peptides with heterogeneous backbones of the form $(\alpha\beta)_n$,[11] $(\alpha\gamma)_n$,[12] $(\alpha\delta)_n$,[13] $(\alpha\varepsilon)_n$,[14] and $(\beta\gamma)_n$[12a,15] showed remarkable novel helical structures with an expansion of intramolecular H-bonded pseudocycles. As described in the Chapter 1, the majority of helical structures in the foldamer homooligomers and heterooligomers are stabilized by 4→1 intramolecular hydrogen bonding, similar to the 3_{10}-helix of α-peptides. Though the α-helix predominantly occurs in proteins, continuous 5→1 hydrogen-bonded structures are only scarcely found in β- and γ-homopeptides and in hybrid peptides. Nevertheless, Gellman and co-workers reported continuous 5→1 hydrogen bonding inα,β-hybrid peptides,[11b,g,h] incorporating the

stereochemically constrained cyclic β-amino acid ACPC (*trans*-2-aminocyclopentane-carboxylic acid). Numerous foldamer helix types were predicted and suggested by theoretical methods.[11i, 12a, 13, 14, 16]

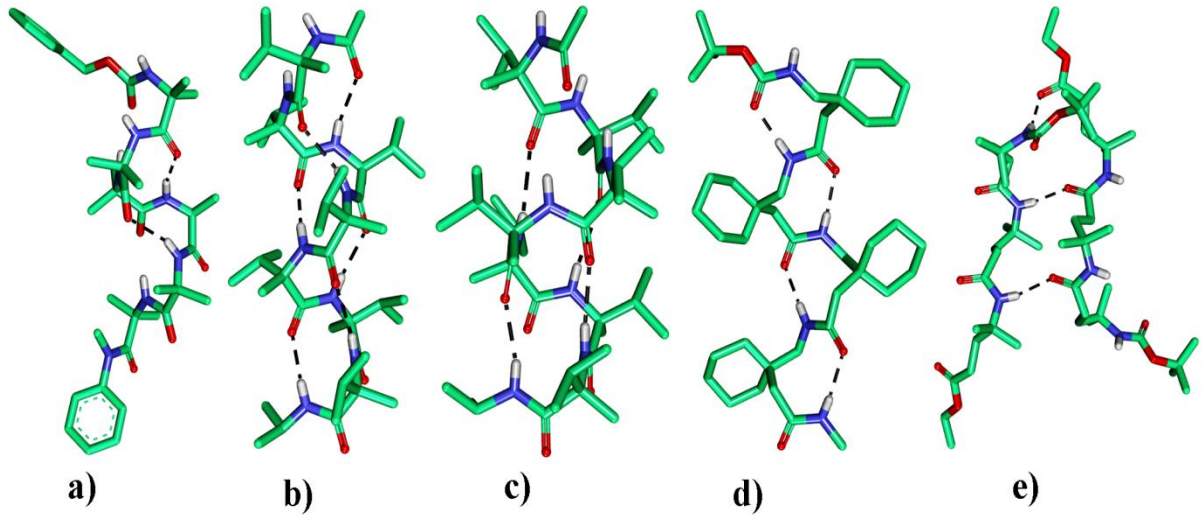

Figure 1 Helical conformation in crystals from geminal di-substituted amino acid containing peptides. a) Poly Aib peptide, Cbz-Aib$_6$-N(Me)Ph.[6h] b) 3_{10} Helical conformation of oligomer of α-methylated L-valine, Ac-[L-(RMe)Val]$_7$-NH*i*Pr and c) α-Helical conformation of oligomer of α-methylated L-valine, Ac-[L-(RMe)Val]$_7$-NH*i*Pr.[8] d) C_9 helical conformation of oligomers Gabapentin, Boc-Gpn-Gpn-Gpn-Gpn-NHMe.[20] e) Extended sheet conformation of oligomer of 4-amino isocaproic acid (Aic), Boc-Aic-Aic-Aic-OEt.[21]

3.2 Aim and rationale of the present Work

The considerable influence of Aib in the design of α-peptide helices[6-9,17] and its recent applications as amyloid fibril breakers[18] and in nanotechnology[19] motivated us to investigate the conformational properties of doubly homologated Aib (4-aminoisocaproic acid, Aic), which is a $\gamma^{4,4}$-amino acid. In their pioneering work, Balaram and colleagues demonstrated the helix-inducing properties of the 3,3-disubstituted γ-amino acid gabapentin (Figure 1d).[20] In contrast to the 9-helical structures of $\gamma^{3,3}$-peptides, homopeptides of Aic showed unusually extended conformations and spontaneously formed self-aggregates in various organic solvents (Figure 1e).[21]

The interesting properties of Aic in its homopeptides inspired us to examine its influence on the secondary structure formation in achiral α,γ-hybrid peptides with Aib in 1:1 alternation by NMR studies in solution, X-ray crystallography and quantum chemical calculations to look

for possible helical folding patterns. Until now, three helix types were found in several chiral α,γ-hybrid peptides: a helix with 12-membered hydrogen-bonded pseudocycles[2d,f,12b,e,f,] and two "mixed" helix alternatives with alternating 12- and 10-membered pseudocycles.[2d,f,12g,i,q]

3.3 Results and discussion

3.3.1 Design and synthesis

The sequences of achiral α,γ-hybrid peptides which were subject of our study are shown in Scheme 1. The γ-amino acid Aic was synthesized starting from Aib, as reported earlier.[21] All hybrid peptides were synthesized in conventional solution phase strategy and isolated in good yields (see Experimental Section). They were subjected to conformational analysis in solution by NMR spectroscopy and as well as in single crystals. Diffraction quality single crystals of the peptides **P1**-**P3** for the X-ray structure determination were grown in various solvent combinations. The systematic quantum chemical conformational analyses were performed on the basis of *ab initio* MO theory employing the B3LYP/6-31G* algorithm of density functional theory in the gas phase and considering solvent influence (see Experimental Section).

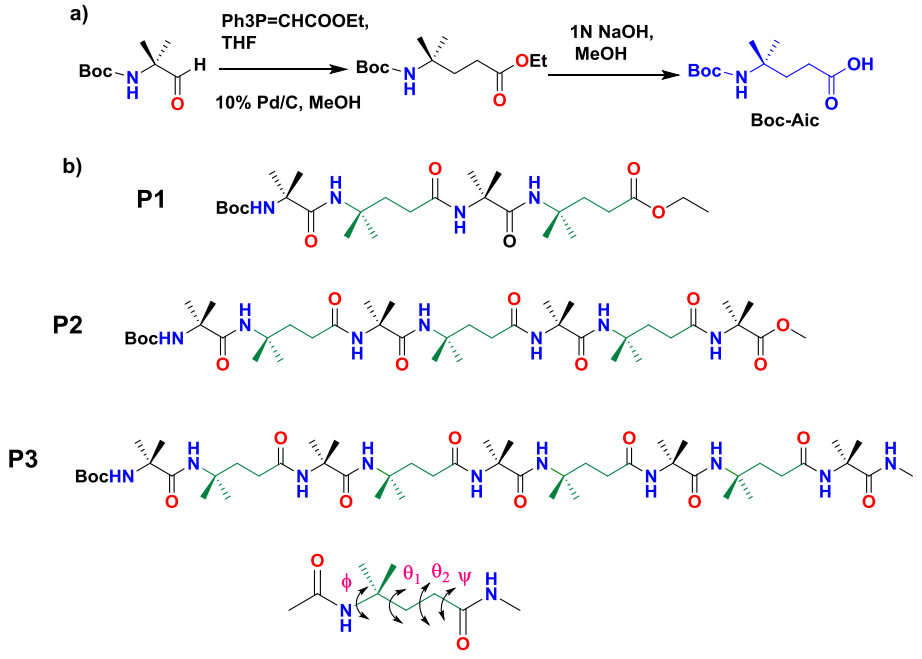

Scheme 3.1 a) Synthesis of *N*-Boc-Aic from *N*-Boc-Aib. b) Chemical structures of Aic homooligomers and local torsional variables of γ-residues.

3.3.2 Single crystal X-ray analysis of peptide P1 and P2

The X-ray structures of **P1** and **P2** are shown in Figure 2. The conformation of the γ-amino acid residues are described by the backbone torsion angles ϕ(N-C^{γ}), θ_1(C^{γ}-C^{β}), θ_2(C^{β}-C^{α}) and ψ(C^{α}- C=O) (Scheme 1). The torsion angles of the γ-amino acid constituents are given in Table 1. The hybrid peptides **P1** and **P2** display helical conformations in their single crystals.

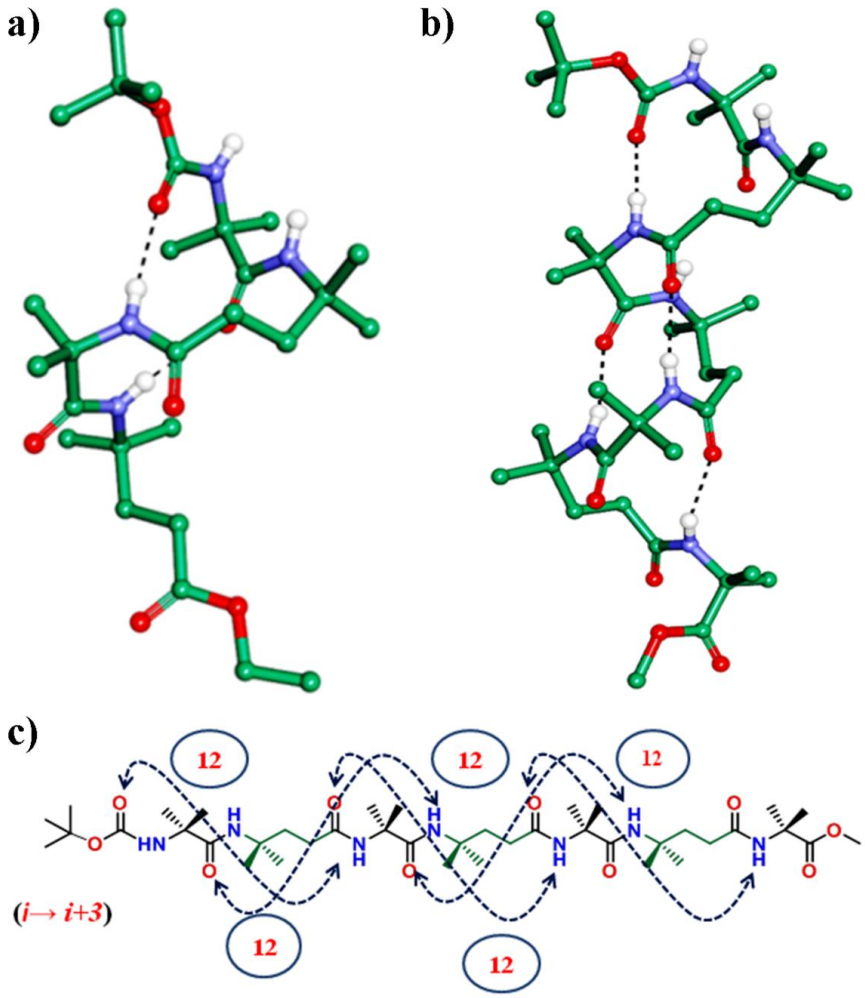

Figure 2 a) X-ray structure of peptides **P1** b) X-ray structure of peptides **P2** c) Hydrogen bonding schemes for the 12-helix **P2**

As expected for achiral molecules, the crystal structure of **P1** reveals two molecules with opposite handedness in the asymmetric unit. The structure is stabilized by two intramolecular hydrogen bonds between BocCO (*i*)←HNAib(3) (*i*+*3*) (H···O distance: 2.11 Å, N···O distance: 2.9 Å) and between Aib(1)CO (*i*)←NHAic(4) (*i*+*3*) (H···O distance: 2.38 Å, N···O distance: 3.2 Å), leading to the formation of two 12-membered hydrogen-bonded

pseudocycles (Figure 2). Due to the lack of an amide NH group, the C-terminal Aic ester is not part of a hydrogen bond. Though the structure is stabilized by the 12-membered pseudocycles, a comparison of the torsion angle values reported in the literature with those of the 12-helix of **P1** shows considerable differences. Table 2 lists the backbone conformations of various γ-amino acid constituents in α,γ-hybrid peptide 12-helices reported in the literature.[12] The dihedral angles θ_1 and θ_2 in **P1** correspond to *gauche* (-53°) and semi-extended (+141°) conformations, respectively. In the 12-helices of the other peptides in Table 2 with γ^4-, $\gamma^{2,3}$-, $\gamma^{3,3}$-, $\gamma^{3,4}$- and $\gamma^{2,3,4}$-amino acid constituents, these two torsion angles (θ_1 and θ_2) have always the same sign and correspond both to a *gauche* conformation (± 60°).

The X-ray structure of **P2** reveals both right- and left-handed 12-helices in the single crystals (Figure 2b). The structure is stabilized by five intramolecular 4→1 hydrogen bonds. The hydrogen bond distances correspond to typical values with exception of the H-bond between Aib(1)CO (*i*) and Aic(4)NH (*i+3*), which seems to be weaker reflected by values of 3.03 Å for the H···O and 3.8 Å for the N···O distances (Table 3). The torsion angle θ_1 of the $\gamma^{4,4}$-residues reflects a *gauche* (-60°±5°) conformation, whereas θ_2 adopts a semi-extended conformation (+147°±8°) with opposite sign. A clear distinction can also be observed for the ϕ and ψ values of the Aic residues with ϕ = -59°±6° and ψ = -95°±7°, respectively. The average torsion angle values of ϕ and ψ of the Aib residues in the distinct 12-helix were found to be -56°±6° and -42°±6°, respectively. These values are consistent with the values of the Aib residues in the α,γ-hybrid peptides containing γ^4-amino acids.[12f]

Table 1. Backbone torsion angles of the Aic residues in the hybrid peptides **P1** and **P2**

Boc-Aib-Aic-Aib-Aic-OEt (**P1**)			
ϕ^a	$\theta_1{}^a$	$\theta_2{}^a$	ψ^a
-59			-46
-45	-53	141	-118
-64			-30
-63	-59	-179	155
Boc-Aib-Aic-Aib-Aic-Aib-Aic-Aib-OMe (**P2**)			
ϕ^a	$\theta_1{}^a$	$\theta_2{}^a$	ψ^a
-61			-48

-64	-60	154	-97
-56			-37
-52	-55	137	-102
-56			-39
-61	-63	149	-86
-51			-47

[a] In degrees. [b]The Aic residue is not part of a helix

Table 2. Backbone torsion angles of γ-amino acid constituents in selected 12-helices of α, γ-hybrid peptides

12-helix	ϕ^a	$\theta_1{}^a$	$\theta_2{}^a$	ψ^a
γ^4-amino acid [12f]	-125±7	51±2	62±3	-118±10
$\gamma^{3,3}$-amino acid [12d]	-124±4	56±6	64±8	-112±10
$\gamma^{2,3,4}$-amino acid[b,12b]	140±10	-56±2	-52±2	111±4
$\gamma^{2,3}$-amino acid[b, 12c]	-129±9	56±2	55±2	-120±9
$\gamma^{3,4}$-amino acids[12o]	-120±2	50±5	64±2	-127±2
ab initio MO theory [12a]	122±2	-52±2	-62±2	125±4
$\gamma^{4,4}$-amino acids[c]	-54±9	-55±5	140±10	-104±18
ab initio MO theory[c]	-52±2	-53±2	141±2	-106±7

[a] In degrees. [b]Cyclic. [c] Present work.

Table 3: Hydrogen bond parameters of peptides **P1 and P2**

Type of H-bond	Acceptor(A)	Donor(D)	D···A (Å)	D-H···A (Å)	∠N-H···O (deg)	∠C=O···H (deg)
Boc-Aib-Aic-Aib-Aic-OEt (**P1**)						
1←4	BocCO	NHAib3	2.97	2.11	175	164
1←4	Aib1CO	NHAic4	3.20	2.38	162	143
Boc-Aib-Aic-Aib-Aic-Aib-Aic-Aib-COOMe (**P2**)						
1←4	BocCO	NHAib3	2.92	2.07	169	142
1←4	Aib1CO	NHAic4	3.82	3.03	153	122
1←4	Aic2CO	NHAib5	2.95	2.10	171	151
1←4	Aib3CO	NHAic6	3.05	2.22	163	143
1←4	Aic4CO	NHAib7	2.93	2.12	156	153

3.3.3 Solution conformations of P2

To gain insight into their solution conformations, we subjected the peptide **P2** to ^{1}H and 2D NMR (TOCSY and ROESY) analysis. The NMR spectra of **P2** were recorded in $CDCl_3$.

The well-dispersed amide NHs of **P2** suggesting ordered structure in solution and also clear distinction between the amide NHs of α- and γ-residues were observed. The weak intramolecular H-bonds observed in the crystal structures of **P2** are reflected in the upfield chemical shifts of the γ-residue NHs. The ROESY spectra reveal a complete set of sequential NH↔NH NOEs between the *i* and (*i+1*) residues, however with an alternating pattern of strong and weak NOEs. The NH↔NH NOEs observed in the ROESY spectrum are shown in Figures 3-5. The NOEs across the Aib resides (1↔2, 3↔4 and 5↔6) are stronger, while the NOEs across the Aic residues (2↔3 and 4↔5) are weaker. Along with sequential NH↔NH interactions, strong NOEs between Aic $C^{\alpha}H(i)$↔HNAib(*i+1*) and weak NOEs between Aic$C^{\beta}H(i)$↔HNAib(*i+1*) residues are observed. The partial ROESY spectrum depicting NH↔$^{\alpha,\beta}CH_2$ NOEs is shown Figure 6. Furthermore, we examined the solvent exposure of the NHs by titration of the peptide with DMSO-d_6 in a $CDCl_3$ solution (Figure 7). Only

Aib(1)NH shows a distinct solvent shift. The other residues show almost no solvent dependence apart from a small effect for Aic(2)NH. On the basis of unambiguous NOEs (listed in the Table 4), the solution structure of **P2** was generated. The superimposition of the ten lowest energy minimized structures is shown in Figure 8a. The peptide adopts a well-folded 12-helix conformation in solution. The overlay of the crystal and solution structures of **P2** is shown in Figure 8b.

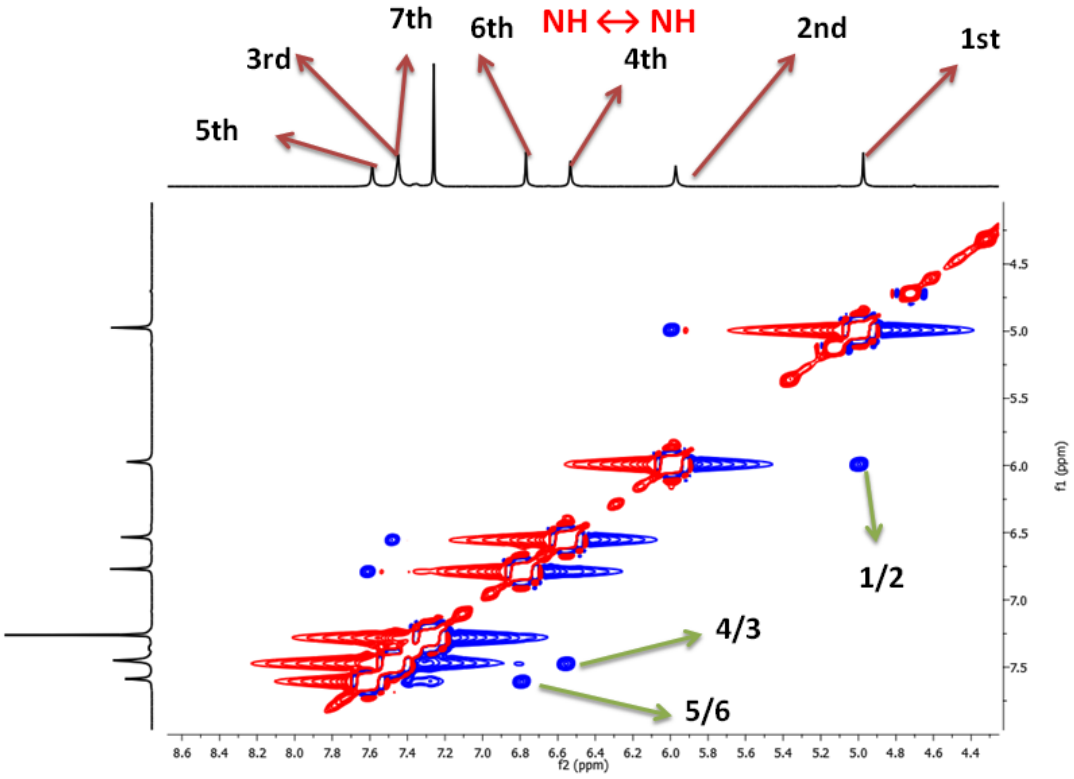

Figure 3 Partial ROESY spectrum of **P2** (4 mM) in $CDCl_3$ showing strong NH↔NH NOEs.

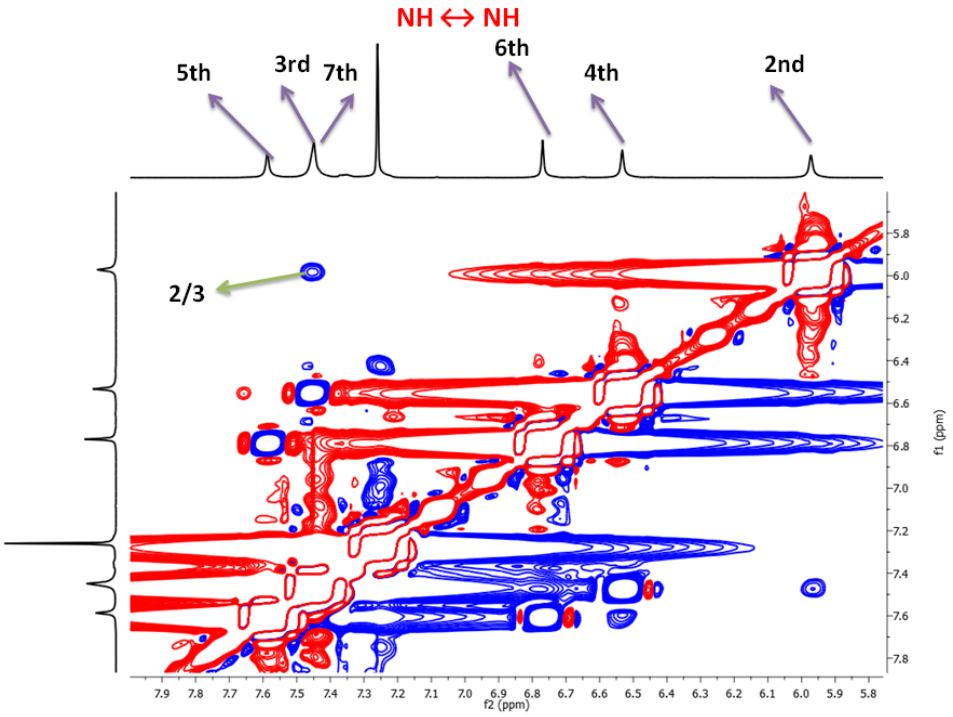

Figure 4 Partial ROESY spectrum of **P2** (4 mM) in $CDCl_3$ showing weak NH↔NH NOEs.

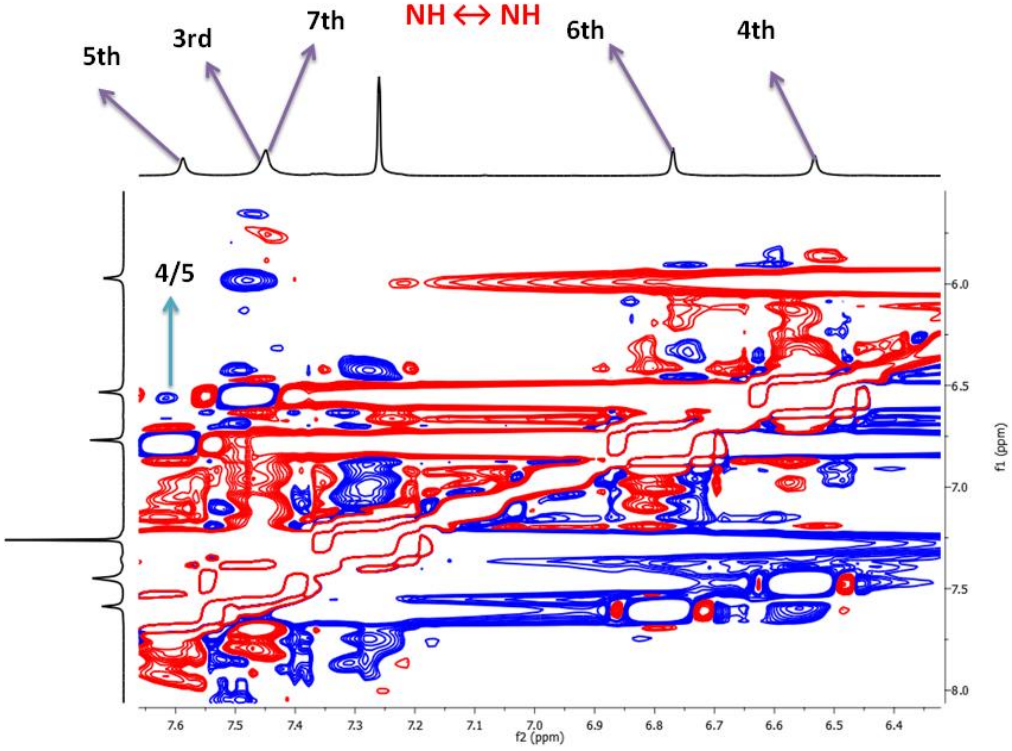

Figure 5 Partial ROESY spectrum of **P2** (4 mM) in $CDCl_3$ showing weak NH↔NH NOEs.

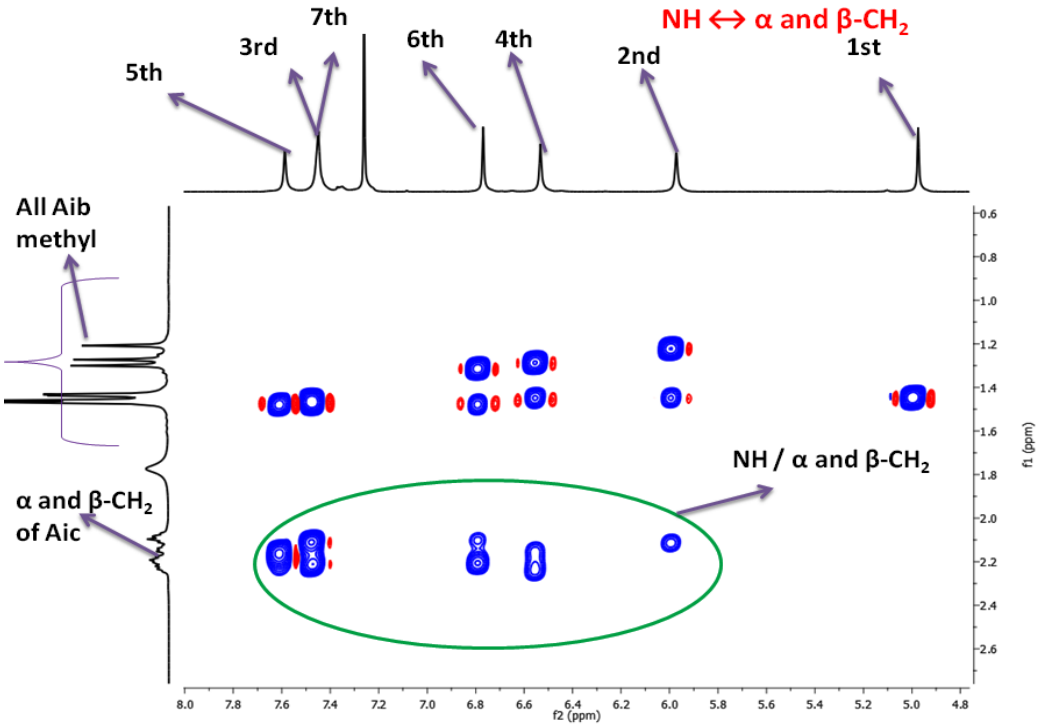

Figure 6 Partial ROESY spectrum of **P2** (4 mM) in $CDCl_3$ showing NH↔$^{\alpha,\beta}CH_2$ NOEs of Aic .

Table 4. List of NOEs used in the NMR structure calculation of peptide **P2**

Residue	H-atom	Residue	H-atom	NOE($CDCl_3$)
Aib(1)	NH	Aic(2)	NH	Strong
Aib(1)	NH	Aic(2)	$C^{\alpha}H_2$(backbone)	Weak
Aic(2)	NH	Aib(3)	NH	Weak
Aic(2)	NH	Aic(2)	$C^{\beta}H_2$(backbone)	Medium(self)
Aic(2)	NH	Aic(2)	$C^{\alpha}H_2$(backbone)	Strong(self)
Aib(3)	NH	Aic(4)	NH	Strong
Aib(3)	NH	Aic(2)	$C^{\alpha}H_2$(backbone)	Strong
Aib(3)	NH	Aic(2)	$C^{\beta}H_2$(backbone)	Medium
Aic(4)	NH	Aic(4)	$C^{\alpha}H_2$(backbone)	Strong(self)

Aic(4)	NH	Aic(4)	$C^{\beta}H_2$(backbone)	Medium(self)
Aic(4)	NH	Aib(5)	NH	Weak
Aib(5)	NH	Aic(6)	NH	Strong
Aib(5)	NH	Aic(4)	$C^{\alpha}H_2$(backbone)	Strong
Aib(5)	NH	Aic(4)	$C^{\beta}H_2$(backbone)	Medium
Aic(6)	NH	Aic(6)	$C^{\alpha}H_2$(backbone)	Strong(self)
Aic(6)	NH	Aic(6)	$C^{\beta}H_2$(backbone)	Medium(self)
Aic(6)	NH	Aib(7)	NH	Weak
Aib(7)	NH	Aic(6)	$C^{\alpha}H_2$(backbone	Strong
Aic(7)	NH	Aic(6)	$C^{\beta}H_2$(backbone)	Medium

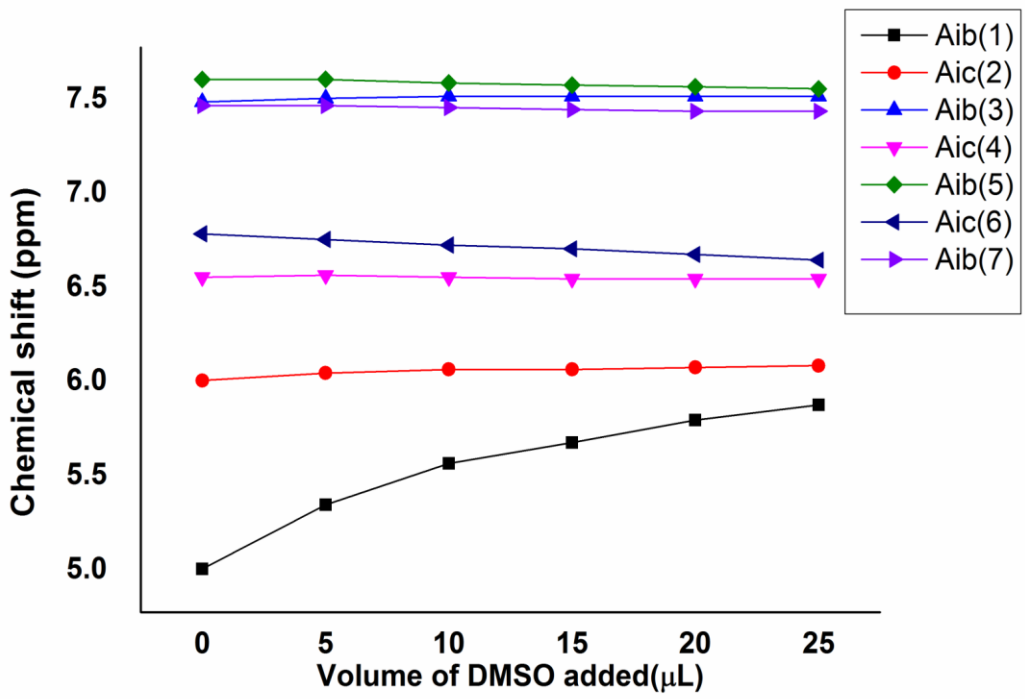

Figure 7 Solvent dependence of NH chemical shifts of the peptide **P2** at varying concentrations of $(CD_3)_2SO$.

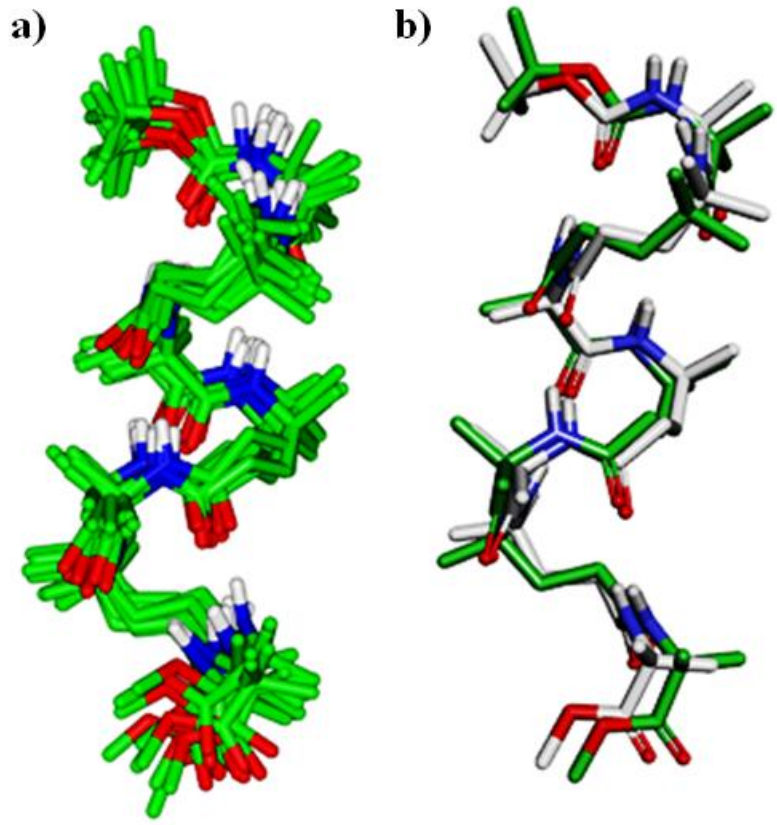

Figure 8 a) Solution structure of peptide **P2**. **b**) Overlay of crystal and solution structures of **P2**.

3.3.4 Single crystal X-ray analysis of peptide P3

The results obtained for the peptides **P1** and **P2** motivated us to synthesize the nonapeptide **P3** in solution phase with the C-terminus capped by an *N*-methyl group to be involved in the intramolecular hydrogen bonding network. In contrast to **P1** and **P2**, **P3** did not give X-ray quality single crystals by crystallization in methanol/water, however diffraction quality crystals were obtained in ethylacetate/methanol and methyl acetate/methanol/water combinations. The X-ray structures of **P3** are shown in Figure 9. Single crystals obtained in ethyl acetate adopted a well-folded 12-helix conformation (**P3A** in Figure 9), corresponding to that of the peptides **P1** and **P2**. The 12-helix conformation in **P3A** is stabilized by eight intramolecular 4→1 H-bonds (Figure 9a). Similar to **P2,** the hydrogen bonds of the type Aib(*i*) CO···HNAic(*i*+*3*) show longer distances compared to those between the Aic(*i*)CO···HNAib(*i*+*3*) residues, which makes them weaker. In addition, smaller C=O···H bond angles have been found in these weaker H-bonds. The H-bond parameters of the **P3** 12-helix are tabulated in the Table 5. The torsion angle values of the Aib and Aic residues are

tabulated in Table 6. All γ-residues in **P3A** adopt similar backbone conformations as in peptide **P2**.

Surprisingly, the crystals of **P3** obtained from the methyl acetate/methanol/water mixture provided a very unusual helical structure (**P3B** in Figure 9b). After two consecutive 12-membered hydrogen-bonded pseudocycles, as in **P3A**, the CO group of Aic(2) (*i*) is involved in a 15-membered hydrogen-bonded pseudocycle closed by the NH group of Aic(6) (*i+4*). Similarly, the CO group of Aib(3) (*i*) is partner in a hydrogen bond of the NH group of Aib(7) (*i+4*), thus forming a 17-membered pseudocycle (Figure 2b). The pattern of alternating 15- and 17-membered pseudocycles continues along the rest of the sequence. A 15/17-helix of this type was not found in α,γ-hybrid peptides so far. Only a structure with one single 17-membered hydrogen-bonded pseudocycle was observed in a hybrid tetrapeptide of the type ααγα with gabapentin as the γ-amino acid constituent.[12m] Inspecting the structure of the novel helix type in more detail shows the 15-membered rings always formed between γ-amino acid constituents by 5→1 interaction, while the 17-membered rings are observed between the α-amino acid constituents again formed by 5→1 interaction. Thus, the 15/17-helix in α,γ-hybrid peptides represents a backbone-expanded analog to the native α-helix. The fact of the occurrence of two hydrogen-bonded 12-rings at the N-terminus of the nonapeptide is an analogy to the frequent finding of 3_{10}-helical turns at the termini of many native α-helices. Obviously, the two novel helices in α,γ-hybrid peptides are in a comparable relationship with each other as the native 3_{10}- and α-helices.[5,8,9] The hydrogen bonds of the 17-membered rings are rather perfectly formed. Those of the narrower 15-membered rings show the correct hydrogen bond directions, however their distances are longer than usual. The comparison of the backbone torsion angles of the Aic residues involved in the 15/17- and 12-helical hydrogen bonding demonstrates a remarkable agreement of the angles ϕ, θ_1 and θ_2 (Table 6). The most decisive difference concerns the angle ψ, which tends clearly to an extended conformation with a value near ±180° in the 15/17-helical structure. Figure 10 provides a clear distinction of the backbone ϕ,ψ angles of various side-chain substituted γ-residues in 12-helices and the novel 15/17-helix.

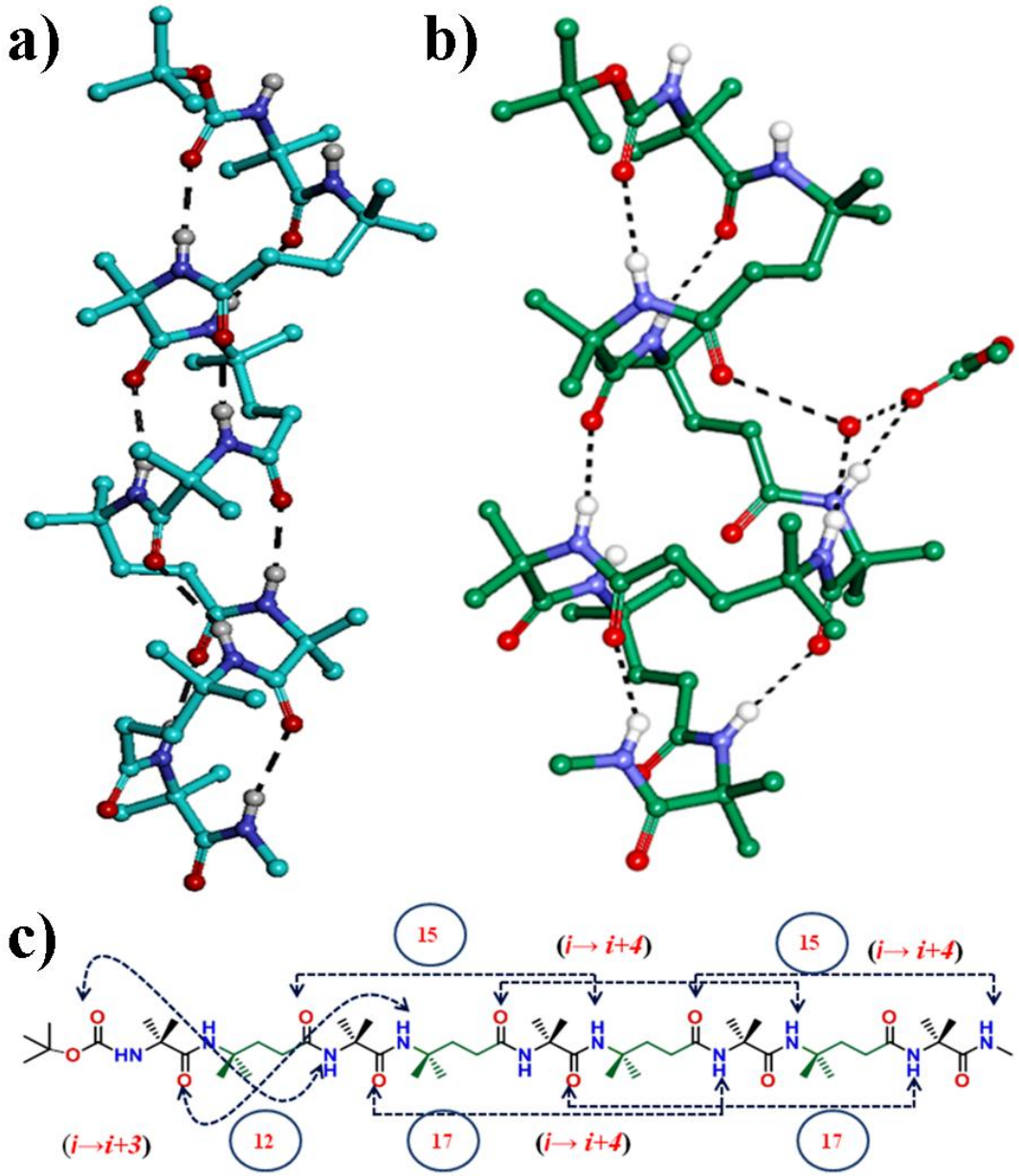

Figure 9 X-ray structures of **P3:** a) 12-helix (**P3A**); b) 15/17-helix (**P3B**); c) Hydrogen bonding schemes for the 15/17-helix **P3B** beginning with two 4→1 turns at the N-terminus, but then continuing with alternating 15- and 17-membered pseudocycles stabilized by 5→1 interactions as in the native α-helix**.**

The close backbone relationship between the two novel helical patterns contributes to an understanding of the possible transition of the 12-helix into the 15/17-hydrogen-bonded network and *vice versa*. A similar behavior is already known for native 3_{10}- and α-helices.[8,9] A comparable phenomenon has also been observed in α,β-hybrid peptides,[11] where an 11-

helix, predominating in shorter sequences, changes into a 14/15-helix in longer peptide sequences.[11b, g, h]

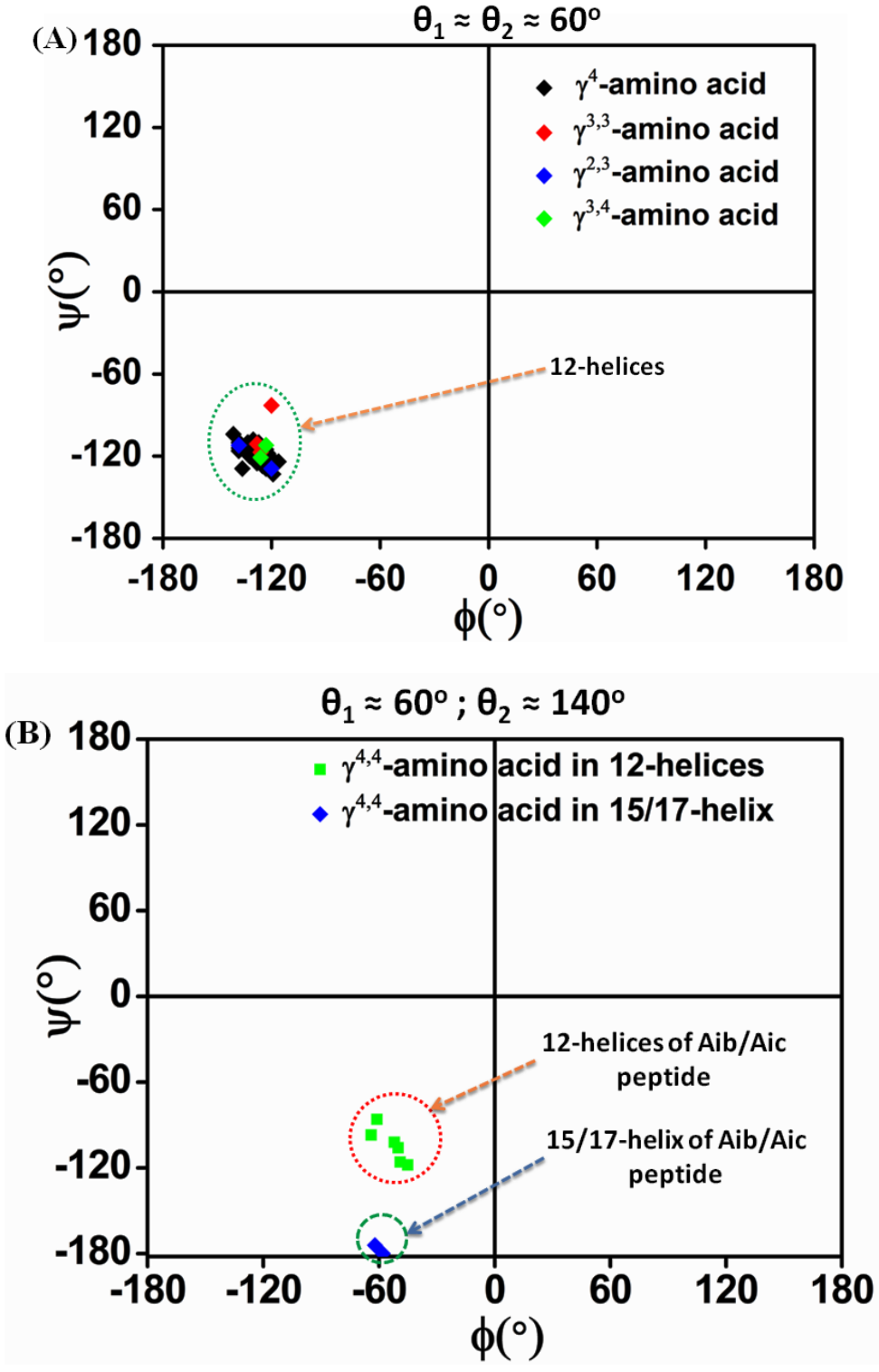

Figure 10 Two-dimensional ϕ,ψ maps of various γ-residues from literature (A) and the $\gamma^{4,4}$-residues from the present work in 12- and 15/17-helices (B).

Table 5 Intramolecular H-bond parameters of peptides **P3**

Type of H-bond	Acceptor(A)	Donor(D)	D⋯A (Å)	D-H⋯A (Å)	∠N-H⋯O (deg)	∠C=O⋯H (deg)
Boc-Aib-Aic-Aib-Aic-Aib-Aic-Aib-Aic-Aib-NHMe (**P3A**, 12-Helix)						
1←4	BocCO	NHAib3	2.95	2.09	177	158
1←4	Aib1CO	NHAic4	3.06	2.22	165	146
1←4	Aic2CO	NHAib5	2.88	2.02	169	155
1←4	Aib3CO	NHAic6	3.15	2.32	161	139
1←4	Aic4CO	NHAib7	2.90	2.05	170	162
1←4	Aib5CO	NHAic8	3.15	2.34	158	135
1←4	Aic6CO	NHAib9	2.92	2.06	177	159
1←4	Aib7CO	C-NH_2	3.20	2.38	161	132
Boc-Aib-Aic-Aib-Aic-Aib-Aic-Aib-Aic-Aib-NHMe (**P3B**, 15/17-Helix)						
1←4	BocCO	NHAib3	2.89	2.03	168	160
1←4	Aib1CO	NHAic4	2.99	2.18	161	145
1←5	Aic2CO	NHAic6	4.56	4.00	125	159
1←5	Aib3CO	NHAib7	2.84	2.00	157	142
1←5	Aic4CO	NHAic8	3.30	2.62	136	140
1←5	Aib5CO	NHAib9	2.98	2.12	176	147
1←5	Aic6CO	C-NH_2	2.84	2.14	144	145

Table 6. Backbone torsion angles of the Aic residues in the hybrid peptides **P3**

Boc-Aib-Aic-Aib-Aic-Aib-Aic-Aib-Aic-Aib-NHMe (**P3A**)				
Residue	ϕ^a	$\theta_1{}^a$	$\theta_2{}^a$	ψ^a
Aib(1)	-56			-39
Aic(2)	-47	- 53	137	-112
Aib(3)	-55			-40
Aic(4)	-60	-53	140	-92
Aib(5)	-51			-43
Aic(6)	-42	-50	135	-129
Aib(7)	-59			-35
Aic(8)	-62	-58	147	-174
Aib(9)	-52			-42
Boc-Aib-Aic-Aib-Aic-Aib-Aic-Aib-Aic-Aib-NHMe (**P3B**)				
Residue	ϕ^a	$\theta_1{}^a$	$\theta_2{}^a$	ψ^a
Aib(1)	-58			-47
Aic(2)[c]	-49	-50	141	- 116
Aib(3)[c]	-60			-36
Aic(4)[c]	-55	-51	170	145
Aib(5)[c]	-51			-43
Aic(6)[c]	-58	-61	156	-180
Aib(7)[c]	-62			-38
Aic(8)[c]	-62	-58	147	-174
Aib(9)[c]	-57			-40

3.3.5 Solution conformations of P3

To gain insight into the solution conformations, we subjected the peptide **P3** to ^{1}H and 2D NMR (TOCSY and ROESY) analysis in CD_3OH. The ^{1}H NMR spectra of peptide **P3** revels a pronounced distinction between the α- and γ-amide NHs. The well-dispersed amide NH groups of **P3** are shown in Figure 11. A clear distinction between the amide NH groups of α- and γ-residues can be observed in ^{1}H NMR. The same trend was also observed in the peptide **P2** in $CDCl_3$. The weak intramolecular hydrogen bonds observed in the crystal structures of **P2** and **P3A** are reflected in the upfield chemical shifts of the γ-residue NH groups. The chemical shifts of all amine NH protons and change in the chemical shifts with increasing temperature (dδ/dt) are tabulated in the Table 7. Upon increasing temperature all amide NHs showed the upfield chemical shifts (Figure 12). The ROESY spectrum depicting the sequential NH↔NH NOEs is shown in Figure 13. Similar to **P2**, we observed strong sequential NH↔NH NOEs between the residues 1↔3, 3↔4, 5↔6, 7↔8 and 9↔NH_2 (C-terminal) and weak NH↔NH interactions between the residues 2↔3, 4↔5, 6↔7 and 8↔9. The partial ROESY spectrum depicting the NH(*i*) ↔C^{α}H(*i-1*) and NH(*i*)↔C^{β}H(*i-1*) NOEs is shown Figure 14. Strong NOEs are also observed between Aic C^{α}H(*i*)↔HNAib(*i+1*) and weak NOEs between AicC^{β}H(*i*)↔HNAib(*i+1*) residues. Except a weak NOE between Aib(1)NH and Aib(3)NH, no other long-range NOEs are observed. List of the NOEs are tabulated in Table 8. Using the distance restraints from ROESY data, the solution conformation of **P3** was generated. The ensemble of NMR structures resulting from the restrained MD simulations on the basis of the NOE and H-bond data is shown in Figure 15a. The correlation of the solution structure with the X-ray structure (**P3A**) is demonstrated in Figure 15b. These results suggest that the nonapeptide adopts a 12-helix conformation in solution, whereas both this 12-helix and the 15/17-helix could be observed in the crystal structures.

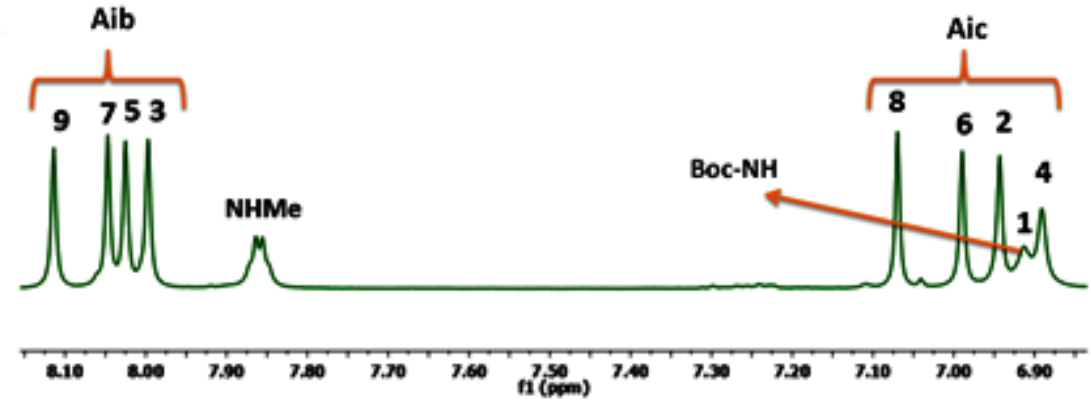

Figure 11 1H NMR spectrum (amide NH region) depicting the distinction between Aib and Aic NH chemical shifts.

Table 7 Chemical shifts and dδ/dT values of amide NHs of **P3** with respect to the temperature.

Residue	**Temperature**							**dδ/dT PPBK**
	278K	283K	288K	293K	298K	303K	308K	
Aib(1)	7.044	6.975	6.943	6.911	6.883	6.853	6.826	-6.8
Aic(2)	7.094	7..013	6.976	6.942	6.912	6.881	6.853	-7.5
Aib(3)	8.121	8.054	8.025	7.996	7.965	7.936	7.905	-6.8
Aic(4)	7.020	6.949	6.917	6.888	6.859	6.832	6.805	-6.6
Aib(5)	8.125	8.068	8.045	8.021	7.995	7.971	7.944	-5.6
Aic(6)	7.135	7.058	7.023	6.989	6.957	6.928	6.897	-7.4
Aib(7)	8.164	8.100	8.072	8.044	8.016	7.989	7.916	-6.3
Aic(8)	7.231	7.146	7.108	7.071	7.037	7.004	6.972	-8.0
Aib(9)	8.287	8.201	8.159	8.118	8.078	8.039	7.999	-9.0
NHMe	8.042	7.952	7.908	7.886	7.824	7.784	7.74	-9.4

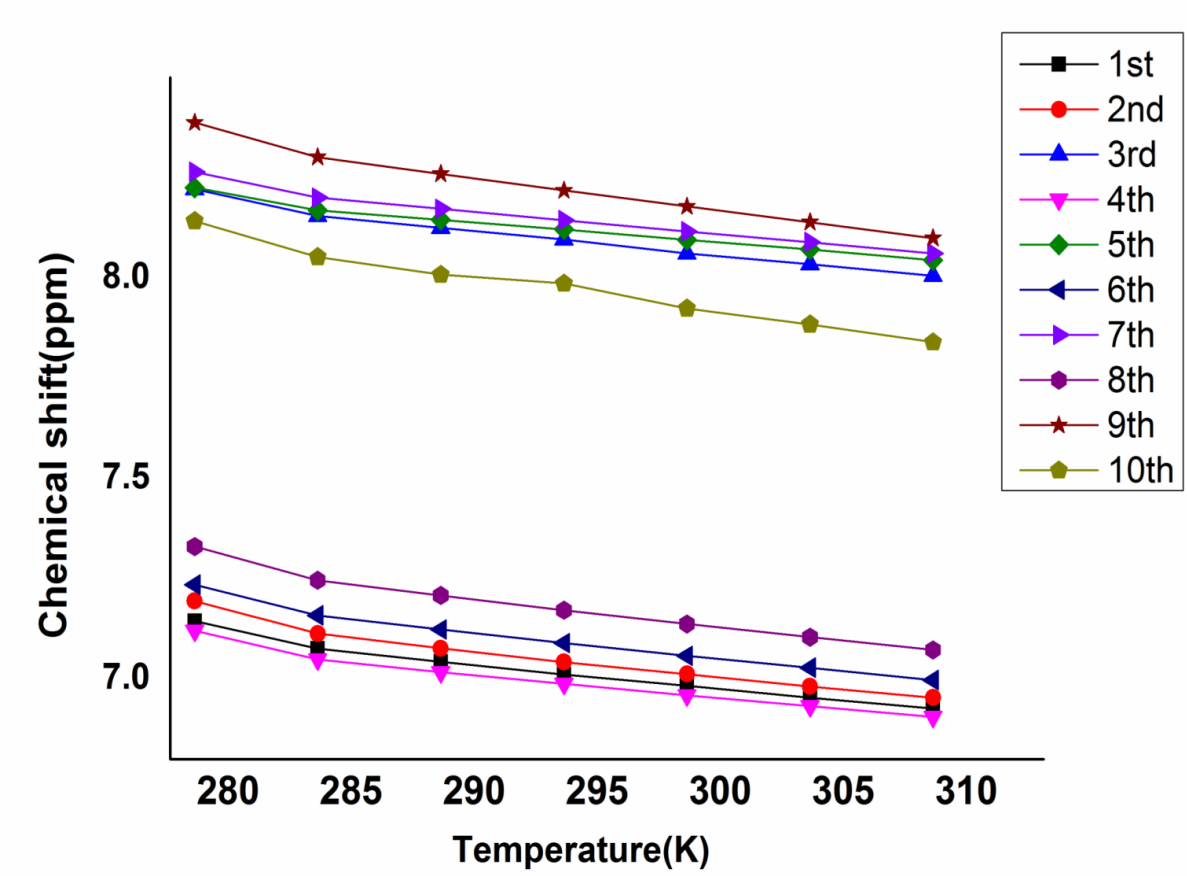

Figure 12. Plot of amide chemical shifts versus temperature

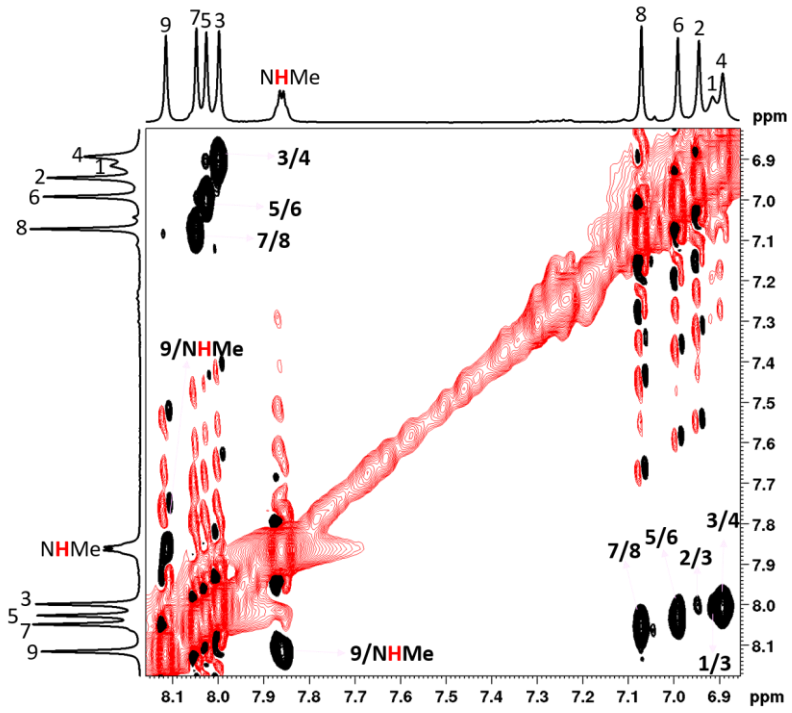

Figure 13 Partial ROESY spectrum of **P3** (5 mM) in CD_3OH showing sequentially strong and weak NH↔NH NOEs.

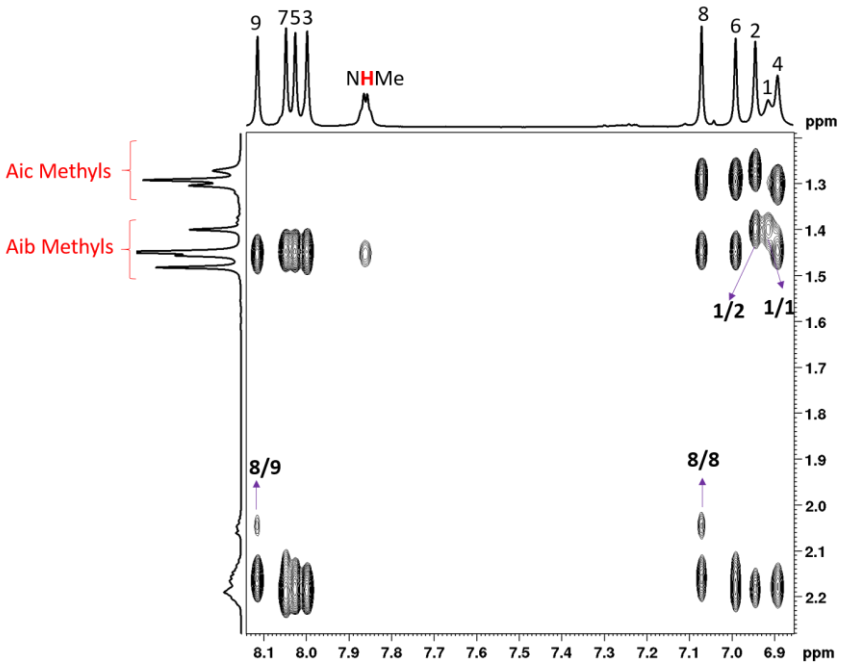

Figure 14 Partial ROESY spectrum of **P3** (4 mM) in CD_3OH showing NH(*i*) ↔$C^{\alpha}H$(*i-1*) and NH(*i*)↔$C^{\beta}H$(*i-1*) NOEs.

Table 8 List of NOEs used in the MD calculation of peptide **P3**

Residue	H-atom	Residue	H-atom	NOE(CD_3OH)
Aib(1)	NH	Aic(3)	NH	Strong
Aic(2)	NH	Aib(3)	NH	Weak
Aic(2)	NH	Aic(2)	$C^{\beta}H_2$(backbone)	Medium(self)
Aic(2)	NH	Aic(2)	$C^{\alpha}H_2$(backbone)	Strong(self)
Aib(3)	NH	Aic(4)	NH	Strong
Aib(3)	NH	Aic(2)	$C^{\alpha}H_2$(backbone)	Strong
Aib(3)	NH	Aic(2)	$C^{\beta}H_2$(backbone)	Medium
Aic(4)	NH	Aic(4)	$C^{\alpha}H_2$(backbone)	Strong(self)
Aic(4)	NH	Aic(4)	$C^{\beta}H_2$(backbone)	Medium(self)
Aic(4)	NH	Aib(5)	NH	Weak
Aib(5)	NH	Aic(6)	NH	Strong
Aib(5)	NH	Aic(4)	$C^{\alpha}H_2$(backbone)	Strong
Aib(5)	NH	Aic(4)	$C^{\beta}H_2$(backbone)	Medium
Aic(6)	NH	Aic(6)	$C^{\beta}H_2$(backbone)	Medium(self)
Aic(6)	NH	Aib(7)	NH	Weak
Aib(7)	NH	Aic(6)	$C^{\alpha}H_2$(backbone	Strong
Aib(7)	NH	Aic(6)	$C^{\beta}H_2$(backbone)	Medium
Aib(7)	NH	Aic(8)	NH	Strong
Aic(8)	NH	Aic(8)	$C^{\alpha}H_2$(backbone)	Strong(self)

Aic(8)	NH	Aic(8)	$C^{\beta}H_2$(backbone)	Medium(self)
Aic(8)	NH	Aib(9)	NH	Weak
Aib(9)	NH	-NHMe	NH	Strong
Aib(9)	NH	Aic(8)	$C^{\alpha}H_2$(backbone	Strong
Aic(9)	NH	Aic(8)	$C^{\beta}H_2$(backbone)	Medium

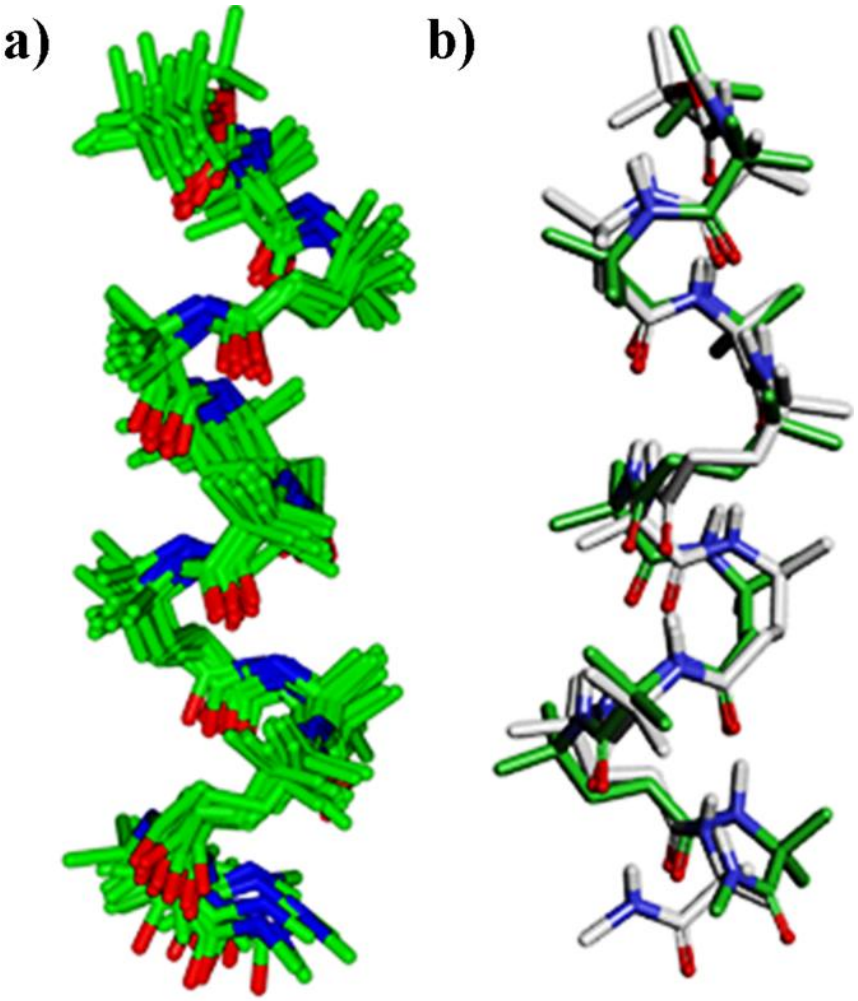

Figure 15 a) Solution structure of peptide **P3**, b) and overlay of crystal (12-helix, **P3A**) and solution structures of **P3**.

3.3.6 Quantum chemical calculations

The coexistence of the novel 12- and the unprecedented 15/17-helix in single crystals of **P3** motivated us to systematically investigate the folding propensities of achiral α,γ-hybrid peptides employing *ab initio* MO theory. Therefore, we performed systematic quantum chemical calculations at the B3LYP/6-31G* level of *ab initio* MO theory, considering also the influence of solvents on the basis of the SMD solvation model, which is a special algorithm of a Polarizable Continuum Model (PCM).[22] For this purpose, the geometry of the 12- and 15/17-helices was optimized for Aib/Aic oligomers in the gas phase and in solution, beginning with tripeptides and going up to undecapeptides. All helices could be localized as minimum conformations and show the typical hydrogen bonding patterns (Figure 16). It is worth noting that the hydrogen bonds of the 17-membered rings in 15/17-helices are rather perfectly realized. The hydrogen bonds of some, but not all 15-membered rings, although in the right direction, are lengthened beyond typical values for hydrogen bonds, which is also observed in the X-ray structure. The energy differences between both helix alternatives are given in Table 9. It can be seen that the 12-helix is distinctly favored over the 15/17-helix in the gas phase independent of the sequence length. This situation changes in the solvent methanol. Here, the 12-helix predominates in shorter sequences (n=3-5), but the 15/17-helix becomes more stable than the 12-helix in the longer sequences (n = 8-11). In fact, both helix

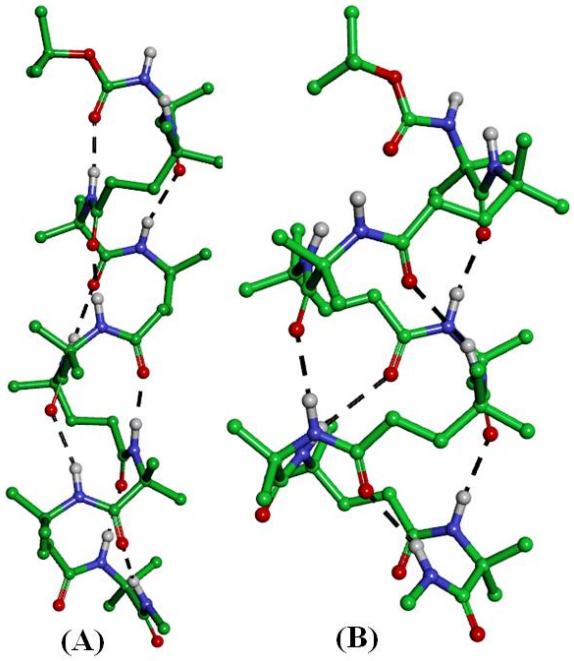

Figure 16 12-helix (A) and 15/17-helix (B) of peptide **P3** according to *ab initio* MO theory.

Table 9 Energy differences between the 12- and 15/17-helices of oligomers of Aib/Aic hybrid peptides according to *ab initio* MO theory.

Oligomer	$\Delta E(H_{12}\text{-}H_{15/17})^{a,b}$	$\Delta E(H_{12}\text{-}H_{15/17})^{a,c}$
n = 3	-17.9	-8.8
n = 4	-20.7	-2.6
n = 5	-21.8	-2.9
n = 6	-26.9	+1.4
n = 7	-27.4	-0.3
n = 8	-30.8	+4.7
n = 9	-31.1	+2.2
n = 10	-33.4	+7.8
n = 11	-34.6	+4.9
[a]Energy values in kJ/mol. [b] B3LYP/6-31G* data for the gas phase. [c]SMD/B3LYP/6-31G* data for the solvent methanol.		

types are of comparable energy within a definite range of the sequence length. This makes understandable that small changes of external factors may shift the equilibrium from one conformer to the other or may even favor the co-existence of two helix types.

3.4 Conclusions

Solution and X-ray studies on achiral α,γ-hybrid peptides composed of Aib and Aic constituents in 1:1 alternation provide two novel helical patterns. In short sequences of 4-7 amino acid residues, a helix with 12-membered hydrogen-bonded pseudocycles is formed both in solution and in the solid state. The longer nonapeptide exhibits the same helix in solution. However, single crystals of the nonapeptide obtained from crystallization in different solvent mixtures provide either the 12-helix or an unprecedented 15/17-helix. Both

helix types are representatives of backbone-expanded 3_{10}- and α-helices characterized by 4→1 and 5→1 hydrogen bonding interactions, respectively. Foldamer helices with the 5→1 interaction of the α-helix are relatively rare. Quantum chemical studies support the experimental results and show that the novel 12-helix with this side chain pattern is more stable than a 12-helix alternative found in several former studies on chiral α,γ-hybrid peptides. The theoretical studies also confirm the tendency to stabilize helices with larger hydrogen-bonded rings with increasing length of the sequence and suggest the possibility of a split-personality between the two novel helix types for special sequence lengths. Comparing with secondary structures of peptides containing other γ-amino acid constituents, it is demonstrated that relatively minor structure variations, as they are realized in the $\gamma^{4,4}$-amino acid constituents, may lead to distinct changes of secondary structure formation. This opens further possibilities for a rational peptide and foldamers design.

3.5 Experimental section

General experimental details

All amino acids, triphenylphosphine, TFA, Ethyl bromoacetate, DCC, HOBt and LAH were commercially available. DCM, DMF, ethyl acetate and pet-ether (60-80 ^{o}C) have used after distillation. THF was dried over sodium and distilled immediately prior to use. Column chromatography was performed on silica gel (120-200 mesh). Final peptides were purified on reverse phase HPLC (C18 column, MeOH/H_2O 60:40-95:5 as gradient with flow rate 1.00 mL/min). ^{1}H spectra were recorded on 500 MHz (or ^{13}C on 125 MHz) and 400 MHz (or ^{13}C on 100 MHz) using residual solvents as internal standards ($CDCl_3$ δ_H 7.26 ppm, δ_C77.3 ppm). Chemical shifts (δ) reported in *ppm* and coupling constants (*J*) reported in Hz.

NMR spectroscopy

All NMR studies were carried out by using either 400 or 600 MHz spectrometer. Resonance assignments were obtained by TOCSY and ROESY analysis. All two-dimensional data were collected in phase-sensitive mode by using the time-proportional phase incrementation (TPPI) method. Sets of 1024 and 512 data points were used in the t_2 and t_1 dimensions, respectively. For TOCSY and ROESY analysis, 32 and 72 transients, respectively, were collected. A spectral width of 6007 Hz was used in both dimensions. Spin-lock times of 200 and 250 ms were used to obtain ROESY spectra. Zero-filling was carried out to finally yield a data set of 2 K × 1 K. A shifted square-sine-bell window was used before processing.

Molecular Dynamics (MD)

Model building and molecular dynamics simulation of **P2** and **P3** was carried out using the Insight II (97.0)/ Discover program. The cvff force field with default parameters was used throughout the simulations. Minimizations were done first with steepest descent, followed by conjugate gradient methods for a maximum of 1000 iterations each or RMS deviation of 0.001 kcal/mol, whichever was earlier. The energy-minimized structures were then subjected to MD simulations. A number of interatomic distance constraints obtained from NMR data was used as restraints in the minimization as well as MD runs. For MD runs, a temperature of 300 K was selected. The molecules were initially equilibrated for 50 ps and subsequently subjected to an 1 ns dynamics with a step size of 1 fs, sampling the trajectory at equal intervals of 10 ps. Within the trajectory 50 samples were generated and the best structures were again energy minimized with the protocol given above and superimposed then

3.5.1 Crystallographic information for peptides

Crystals for the peptides **P1-P2** were grown by slow evaporation of a methanol/water solution, for peptide **P3** by slow evaporation of methyl acetate/methanol/water and ethyl acetate/methanol solutions. Single crystals were mounted on loop with a small amount of parafin oil. The X-ray data were collected at 100 K. The structures were obtained by direct methods using SHELXS-97.

Crystal Data for Peptide P1

Crystal size: 0.26 x 0.1 x 0.12 mm^3; CuK_α radiation $\lambda = 1.54$ Å, ω-scans ($2\theta = 133.476$) for a total of 5655 independent reflections; space group: P21/n, a = 9.22(2) Å, b = 20.37(5) Å, c = 17.14(5) Å; $\alpha = 90$, $\beta = 96.5690(13)$, $\gamma = 90$, V = 3199.98(14) $Å^3$, Monoclinic, Z = 4 for chemical formula $C_{27}H_{50}N_4O_7$; $\rho_{calcd} = 1.127$ g cm^{-3} , $\mu = 0.660$ mm^{-1}, F(000) = 1408; final R value = 0.0435 (wR2 = 0.1390), 5655 measured reflections ($F0 \geq 4\sigma(|F0|)$) and 355 variables, S = 1.153. The largest difference peak and hole were 0.493 and -0.464 e$Å^3$, respectively. CCDC No 1470559

Crystal Data for P2

Crystal size: 0.15 × 0.08 × 0.10 mm^3; MoK_α radiation: $\lambda = 0.71073$ Å; ω-scans ($2\theta = 57.244$) for a total of 11723 independent reflections; space group P21/n, a = 17.471(8) Å, b = 16.185(7) Å, c = 17.571(8) Å; $\alpha = 90$, $\beta = 109.960(8)$, $\gamma = 90$, V = 4670(4) $Å^3$, Monoclinic, Z = 4 for chemical formula ($C_{40}H_{73}N_7O_{10,}$ O); $\rho_{calcd} = 1.178$ g cm^{-3}, $\mu = 0.086$ mm^{-1}, F(000) = 2046; final R value = 0.0872 (wR2 = 0.1770); 11723 measured reflections ($F0 \geq 4\sigma(|F0|)$)

and 542 variables, S = 0.941. The largest difference peak and hole were 0.836 and -0.468 eÅ^{3}, respectively. CCDC No 1470560

Crystal Data for Peptide P3A

Crystal size: 0.33 × 0.25 × 0.25 mm^{3}; MoK$_{\alpha}$ radiation: λ = 0.71073 Å; ω-scans (2θ = 56.746) for a total of 98417 independent reflections; space group P21/n, a = 20.285(3) Å, b = 8.7974(12) Å, c = 35.553(5) Å; α = 90, β = 98.303(5), γ = 90, V = 6278(14) Å^{3}, Monoclinic, Z = 4 for chemical formula $C_{50}H_{92}N_{10}O_{11}$, $C_3H_6O_2$ (ethyl acetate); ρ_{calcd} = 1.162g cm^{-3}, μ =0.083mm^{-1}, F(000) = 2490; final R value = 0.0869 (wR2 =0.1960); 15657 measured reflections (F0 ≥ 4σ(|F0|)) and 718 variables, S = 1.139. The largest difference peak and hole were 0.592 and -0.5474 eÅ^{3}, respectively

Crystal Data for Peptide P3B

Crystal size: 0.36 × 0.31 × 0.29 mm^{3}; MoK$_{\alpha}$ radiation: λ = 0.71073 Å; ω-scans (2θ = 57.024) for a total of 17282 independent reflections; space group P21/n, a = 12.342(3) Å, b = 30.432(8) Å, c = 18.376(5) Å; α = 90, β = 96.450(5), γ = 90, V = 6858(3) Å^{3}, Monoclinic, Z = 4 for chemical formula $C_{50}H_{92}N_{10}O_{11}$; $C_3H_6O_2$ (methyl acetate); O (water); ρ_{calcd} = 1.065 g cm^{-3}, μ = 0.077 mm^{-1}, F(000) = 3014; final R value = 0.0602 (wR2 =0.1580); 17282 measured reflections (F0 ≥ 4σ(|F0|)) and 718 variables, S = 1.020. The largest difference peak and hole were 0.632 and -0.646 eÅ^{3}, respectively. There is a partially occupied solvent molecule present in the asymmetric unit. Considerable time was invested for the identification and refinement of the disordered molecule. Option SQUEEZE of program PLATON2 was used to correct the diffraction data for diffusely scattering effects and to identify the solvent molecule. PLATON calculated the upper limit of volume occupied by the solvent molecule to be 976.6 Å^{3}. The program calculated 215 electrons in the unit cell for the diffuse species. No data are given for the diffusely scattering species. Outputs of SQUEEZE report are appended in the cif-file of **P3**. CCDC No 1470560

3.5.2 Quantum chemical calculations

Geometry optimizations at the B3LYP/6-31G* level were performed on the two 12-helix alternatives and the 15/17-helix for all oligomers of Aib/Aic peptides beginning with the tripeptides and going until the undecapeptides. The influence of the solvent methanol was estimated employing the SMD solvation model as it is implemented in the Gaussian09 program package.[1] Geometries were also optimized in the SMD calculations. For the most stable 12-helix and the 15/17-helix of the nonapeptides the backbone torsion angles are given

in the Tables S8 and S9. These geometries correspond well to those of the other oligomer helices.

Table 10. Backbone torsion angles for the most stable 12-helix of the Aib/Aic nonapeptide **P3** at the B3LYP/6-31G* level of *ab initio* MO theory

Residue	ϕ	θ_1	θ_2	ψ
Aib(1)	-65.9			-36.4
Aic(2)	-53.2	-54.5	141.4	- 103.0
Aib(3)	-57.3			-39.8
Aic(4)	-52.8	-53.4	141.5	-104.0
Aib(5)	-57.9			-38.6
Aic(6)	-53.0	-53.3	141.3	-104.5
Aib(7)	-59.0			-36.9
Aic(8)	-52.1	-53.2	142.7	-117.1
Aib(9)	-65.5			-26.8

Table 11: Backbone torsion angles for the 15/17-helix of the Aib, Aic nonapeptide **P3** at the B3LYP/6-31G* level of *ab initio* MO theory

Residue	ϕ	θ_1	θ_2	ψ
Aib(1)	-68.3			-30.3
Aic(2)	-56.6	-56.7	161.0	- 162.6
Aib(3)	-57.9			-39.8
Aic(4)	-59.6	-60.7	158.1	179.5
Aib(5)	-58.9			-42.1
Aic(6)	-61.3	-59.3	158.6	-179.9
Aib(7)	-63.3			-37.0

Aic(8)	-66.0	-62.8	158.3	-174.0
Aib(9)	-64.9			-24.4

3.5.3 Synthesis of the ethyl ester of *N*-Boc-protected Aic (*N*-Boc-4-aminoisocaproic ethyl ester) and peptides

The synthesis of the Boc-Aic ethyl ester was reported earlier.[21] Therefore, only a short description is given here.

Activated Pd/C (20% by weight) and (*E*)-ethyl 4-((*tert*-butoxycarbonyl)amino)-4-methylpent-2-enoate (1.3 g, 5 mmol) was dissolved in MeOH (25 mL), and stirred at room temperature in the presence of hydrogen. After completion of the reaction (TLC, ~5 h), Pd/C was filtered through the bed of celite and the filtrate was evaporated to dryness under vacuum to get gummy *N*-Boc protected Aic. The pure product was obtained after silica gel column chromatography with 6% ethyl acetate in hexane in good yield (1.43 g, 90%).

Synthesis of peptides P1-P3

The tetrapeptide, heptapeptide and nonapeptide were prepared by solution-phase fragment condensation strategy. Deprotections were performed with trifloroacetic acid and saponification for the N- and C-termini, respectively. Couplings were carried out using *N*-Ethyl-*N′*-(3-dimethylaminopropyl)carbodiimide hydrochloride (EDC) or *N,N,N′,N′*-Tetramethyl-O-(*1*H-benzotriazol-1-yl)uronium hexafluorophosphate, O-(Benzotriazol-1-yl)-*N,N,N′,N′*-tetramethyluronium hexafluorophosphate (HBTU) and 1-hydroxybenzotriazole (HOBt). The dipeptide was synthesized by 1+1 condensation strategy involving Boc-Aib-OH and NH_2-Aic-OEt employing EDC/HOBt as coupling reagents and DCM as a solvent. For converting C-terminal esters into NHMe, peptide esters were dissolved in MeOH and bubbled with methyl amine gas under cold condition until there was an increase in 5 mL of total volume. Then the flask was stored under N_2 atmosphere for one day at room temperature. After completion of the reaction, methanol was evaporated and the product was diluted with EtOAc (50 mL). The organic layer was washed with dil. HCl (3 × 25 mL), 25 mL of brine solution, dried over anhydrous Na_2SO_4 and concentrated under reduced pressure. The tetrapeptide was synthesized by 2+2 condensation strategy involving Boc-Aib-Aic-COOH and NH_2-Aib-Aic-OEt. The heptapeptide was synthesized by 4+3 condensation

strategy involving Boc-Aib-Aic-Aib-Aic-COOH and NH_2-Aib-Aic-Aib-OMe and the nonapeptide was synthesized by 4+5 condensation strategy involving Boc-Aib-Aic-Aib-Aic-COOH and NH_2-Aib-Aic-Aib-Aic-Aib-NHMe. All peptides were purified using RP-HPLC employing the MeOH/H_2O gradient system.

Structural characterization of monomer and hybrid peptides.

Characterization of 4-((*tert*-butoxycarbonyl)amino)-4-methylpentanoic acid (Aic):

^{1}H NMR (400 MHz, 25 °C, $CDCl_3$) δ: 4.5 (bs, 1H), 2.36 (m, 2H), 2.01 (m, 2H), 1.44 (s, 9H), 1.27 (s, 6H); ^{13}C NMR (100 MHz, $CDCl_3$) δ: 179.12, 154.23, 78.82, 51.94, 34.66, 30.92, 29.41, 28.38, 27.19; MALDI-TOF m/z: calcd for $C_{11}H_{21}N_1O_4$ $[M+Na]^+$ 254.1368, found: 254.11

Characterization of peptide P1

^{1}H NMR (400 MHz, $CDCl_3$, 25 °C, TMS) δ: 1.22-1.25 (m, 9H), 1.31-1.32 (bs, 7H), 1.43-1.44 (bs, 16H), 1.47 (s, 6H), 2.04-2.07 (m, 2H), 2.13 (bs, 4H), 2.30-2.33 (m, 2H), 4.08-4.13 (m, 2H) 5.02-5.03 (bs, 1H), 6.22 (bs, 1H), 6.70 (s, 1H), 6.94 (bs, 1H) ppm ; MALDI-TOF m/z: calcd for $C_{27}H_{50}N_4O_7$ $[M+Na]^+$ 565.35, found: 565.33

Characterization of peptide P2

^{1}H NMR (600 MHz, $CDCl_3$, 25 °C, TMS) δ: 1.23 (bs, 4H), 1.29 (bs, 4H), 1.32 (bS, 4H), 1.45-1.47 (m, 9H), 1.48-1.50 (m, 13H), 2.08-2.28 (m, 12H),3.71(s,3H), 5.0 (s, 1H), 6.0 (s, 1H), 6.55 (s, 1H), 6.81 (s, 1H), 7.47 (bs, 2H), 7.61 (s, 1H); MALDI-TOF m/z: calcd for $C_{40}H_{73}N_7O_{10}$ $[M+Na]^+$ 834.53, found: 834.52

Characterization of peptide P3

^{1}H NMR (600 MHz, CD_3OH, 25 °C, TMS) δ: 1.27 (bs, 6H), 1.29 (bs, 12H), 1.30 (bs, 8H) 1.40 (bs, 7H), 1.44-1.46 (m, 24H), 1.48 (bs, 10H), 2.02-2.06 (m, 3H), 2.11-2.23 (m, 15H), 2.73 (d,3H), 6.89 (s, 1H), 6.91 (s, 1H), 6.95 (s, 1H), 6.99 (s, 1H), 7.06 (s, 2H), 7.86 (q, 1H) 8.00 (s, 1H) 8.02 (s, 1H) 8.04 (s, 1H) 8.12 (s, 1H); MALDI-TOF m/z: calcd for $C_{50}H_{92}N_{10}O_{11}$ $[M+Na]^+$ 1031.68, found: 1031.71.

3.6 References

1. a) Seebach, D.; Beck, A. K.; Bierbaum, D. J. *Chem. Biodiversity* **2004**, *1*, 1111; b) Gellman, S. H. *Acc. Chem. Res.* **1998**, *31*, 173; c) Cheng, R. P.; Gellman, S. H.; De Grado, W. F. *Chem. Rev.* **2001**, *101*, 3219; d) Venkatraman, J.; Shankaramma, S. C.; Balaram, P. *Chem. Rev.* **2001**, *101*, 3131; (e) Fülöp, F.; Martinek, T. A.; Tóth, G. K. *Chem. Soc. Rev.* **2006**, *35*, 323; f) Goodman, C. M.; Choi, S.; Shandler, S.;

DeGrado, W. F. *Nat. Chem. Biol.* **2007**, *3*, 252; g) Hecht, S.; Huc, I. (Eds.), *Foldamers: Structure, Properties and Applications*, Wiley-VCH, Weinheim, 2007. h) Horne, W. S.; Gellman, S. H. *Acc. Chem. Res.* **2008**, *41*, 1399.

2. a) Seebach, D.; Gardiner, J. *Acc. Chem. Res.* **2008**, *41*, 1366; b) Saraogi, I.; Hamilton, A. D. *Chem. Soc. Rev.* **2009**, 38, 1726; c) Guichard, G.; Huc, I. *Chem. Commun.* **2011**, *47*, 5933; d) Bouillère, F.; Thétiot-Laurent, S.; Kouklovsky, C.; Alezra, V. *Amino Acids* **2011**, *41*, 687; e) Pilsl, L. K. A.; Reiser, O. *Amino Acids* **2011**, *41*, 709. f) Vasudev, P. G.; Chatterjee, S.; Shamala, N.; Balaram, P. *Chem. Rev.* 2**011**, *111*, 657; g) Martinek, T. A.; Fülöp, F. *Chem. Soc. Rev.* **2012**, *41*, 687.
3. Pauling, L.; Corey, R.; Branson, H. R. *Proc. Nat. Acad. Sci. USA* **1951**, *37*, 235.
4. a) Toniolo, C.; Benedetti, E. *Trends Biochem. Sci.* **1991**, *16*, 350. b) Leader, D. P.; Milner-White, E. J. *Proteins* **2010**, *79*, 1010.
5. a) Millhauser, G. L. *Biochemistry* **1995**, *34*, 3873; b) Shea, J. E.; Brooks, C. L. *Annu. Rev. Phys. Chem.* **2001**, *52*, 499; c) Bolin, K. A.; Millhauser, G. L. *Acc. Chem. Res.* **1999**, *32*, 1027.
6. a) Pavone, V.; Blasio, B.; Santini, A.; Benedetti, E.; Pedone, C.; Toniolo, C.; Crisma, M. J. *J. Mol. Biol.* **1990**, *214*, 633; b) Gessman, R.; Brückner, H.; Petratos, K. *J. Pept. Sci*. **2003**, *9*, 753; c) Karle, I. L.; Balaram, P. *Biochemistry* **1990**, *29*, 6747; d) Aravinda, S.; Shamala, N.; Balaram, P. *Chem. Biodiversity* **2008**, *5*, 1238; e) Toniolo, C.; Crisma, M.; Formaggio, F.; Peggion, C. *Biopolymers* **2001**, *60*, 396; f) Marshall, G. R.; Hodgkin, E. E.; Langs, D. A., Smith, G. D.; Zabrocki, J.; Leplawy, M. T. *Proc. Natl. Acad. Sci. USA* **1990**, *87*, 487; g) Solà, J.; Helliwell, M.; Clayden, J. *Biopolymers* **2011**, *95*, 62; h) Dannecker-Doring, I.; Linden, A.; Heimgartner, H. *Helv. Chim. Acta.* **2011**, *94*, 993.
7. Karle, I. L.; Flippen-Anderson, J. L.; Gurunath, R.; Balaram, P. *Protein Science* **1994**, *3*, 1547.
8. Crisma, M.; Saviano, M.; Moretto, A.; Broxterman, Q. B.; Kaptein, B.; Toniolo, C. *J. Am. Chem. Soc.* **2007**, *129*, 15471.
9. Pengo, P.; Pasquato, L.; Moro, S.; Brigo, A.; Fogolari, F.; Broxterman, Q. B.; Kaptein, B.; Scrimin, P. *Angew. Chem. Int. Ed*. **2003**, *42*, 3388.
10. a) Hanessian, S.; Luo, X.; Schaum, R.; Michnik, S. *J. Am. Chem. Soc.* **1998**, *120*, 8569; b) Fremaux, J.; Mauran, L.; Pulka-Ziach, K.; Kauffmann, B.; Odaert, B.; Guichard. G. *Angew. Chem. Int. Ed.* **2015**, *54*, 9816; c) Shin, S.; Lee, M.; Guzei, I. A.; Kang, Y. K.; Choi, S. H. *J. Am. Chem. Soc.* **2016**, *138* , 13390.

11. a) De Pol, S.; Zorn, C.; Klein, C. D.; Zerbe, O.; Reiser, O. *Angew. Chem. Int. Ed.* **2004**, *43*, 511; b) Hayen, A.; Schmitt, M. A.; Ngassa, F. N.; Thomasson, K. A.; Gellman, S. H. *Angew. Chem. Int. Ed.* **2004**, *43*, 505; c) Sharma, G. V. M.; Nagendar, P.; Jayaprakash, P.; Krishna, P. R.; Ramakrishna, K. V. S.; Kunwar, A. C. *Angew. Chem. Int. Ed.* **2005**, *44*, 5878; d) Schmitt, M. A.; Choi, S. H.; Guzei, I. A.; Gellman, S. H. *J. Am. Chem. Soc.* **2005**, *127*, 13130; e) Schmitt, M. A.; Choi, S. H.; Guzei, I. A.; Gellman, S. H. *J. Am. Chem. Soc.* **2006**, *128*, 4538; f) Horne, W. S.; Price, J. L.; Keck, J. L.; Gellman, S. H. *J. Am. Chem. Soc.* **2007**, *129*, 4178; g) Choi, S. H.; Guzei, I. A.; Gellman, S. H. *J. Am. Chem. Soc.* **2007**, *129*, 13780; h) Choi, S. H.; Guzei, I. A.; Spencer, L. C.; Gellman, S. H. *J. Am. Chem. Soc.* **2008**, *130*, 6544; i) Baldauf, C.; Günther, R.; Hofmann, H.-J. *Biopolymers* **2006**, *84*, 408.

12. a) Baldauf, C.; Günther, R.; Hofmann, H.-J. *J. Org. Chem.* **2006**, *71*, 1200; b) Guo, L.; Chi, Y. G.; Almeida, A. M.; Guzei, I. A.; Parker, B. K.; Gellman, S. H. *J. Am. Chem. Soc*. **2009**, *131*, 16018; c) Guo, L.; Zhang, W.; Guzei, I. A.; Spencer, L. C.; Gellman, S. H. *Org. Lett*. **2012**, *14*, 2582; d) Vasudev, P. G.; Ananda, K.; Chatterjee, S.; Aravinda, S.; Shamala, N.; Balaram, P. *J. Am. Chem. Soc.* **2007**, *129*, 4039*;* e) Sonti, R.; Dinesh, B.; Basuroy, K.; Raghothama, S.; Shamala, N.; Balaram, P.; *Org. Lett*. **2014**, *16*, 1656; f) Jadhav, S. V.; Bandyopadhyay, A.; Gopi, H. N. *Org. Biomol. Chem*. **2013**, *11*, 509; g) Sharma, G. V. M.; Chandramouli, N.; Choudhary, M.; Nagendar, P.; Ramakrishna, K. V. S.; Kunwar, A. C.; Schramm, P.; Hofmann, H.-J. *J. Am. Chem. Soc*. **2009**, *131*, 17335; h) Vasudev, P. G.; Chatterjee, S.; Ananda, K.; Shamala, N.; Balaram, P. *Angew. Chem. Int. Ed*. **2008**, *47*, 6430; i) Fisher, B. F.; Guo, L.; Dolinar, B. S.; Guzei, I. A.; Gellman, S. H. *J. Am. Chem. Soc*. **2015**, *137*, 6484; j) Basuroy, K.; Dinesh, B.; Shamala, N.; Balaram, P. *Angew. Chem. Int. Ed*. **2012**, *51*, 8736; k) Chatterjee, S.; Vasudev, P. G.; Ragothama, S.; Ramakrishna, C.; Shamala, N.; Balaram, P. *J. Am. Chem. Soc.* **2009**, *131*, 5956; l) Bandyopadhyay, A.; Jadhav, S. V.; Gopi, H. N. *Chem. Commun.* **2012**, *48*, 7170; m) Chatterjee, S.; Vasudev, P. G.; Ananda, K.; Raghothama, S.; Shamala, N.; Balaram, P. *J. Org. Chem.* **2008**, *73*, 6595; n) Fisher, B. F.; Gellman, S. H. *J. Am. Chem. Soc.*, **2016**, *138*, 10766. (o) Bandyopadhyay, A.; Malik, A.; Ganesh Kumar, M.; Gopi, H. N. *Org. Lett*. **2014**, *16*, 294; p) Ganesh Kumar, M.; Gopi, H. N. *Org. Lett*. **2015**, *17*, 4738; q) Sharma, G. V. M.; Jadhav, V. B.; Ramakrishna, K. V. S.; Jayaprakash, P.; Narsimulu, K.; Subash, V.; Kunwar, A. C. *J. Am. Chem. Soc.* **2006**, *128*, 14657.

13. Sharma, G. V. M.; Babu, B. S.; Ramakrishna, K. V. S.; Nagendar, P.; Kunwar, A. C.; Schramm, P.; Baldauf, C.; Hofmann, H.-J. *Chem. Eur. J.* **2009**, *15*, 5552.
14. Sharma, G. V. M.; Babu, B. S.; Chatterjee, D.; Ramakrishna, K. V. S.; Kunwar, A. C.; Schramm, P.; Hofmann, H.-J. *J. Org. Chem.* **2009**, *74*, 6703.
15. a) Guo, L.; Almeida, A. M.; Zhang, W.; Reidenbach, A. G.; Choi, S. H.; Guzei, I. A.; Gellman, S. H. *J. Am. Chem. Soc*. **2010**, *132*, 7868; b) Araghi, R. R.; Jäckel, C.; Cölfen, H.; Salwiczek, M.; Völkel, A.; Wagner, S. C.; Wieczorek, S.; Baldauf, C.; Koksch, B. *ChemBioChem* **2010**, *11*, 335; c) C. M. Grison, S. Robin, D. J. Aitken, *Chem. Commun.* **2016**, *52*, 7802.
16. a) Baldauf, C.; Hofmann, H.-J. *Helv. Chim. Acta* **2012**, *95*, 2348; b) Wu, Y. -D.; Han, W.; Wang, D. P.; Gao, Y.; Zhao, Y. -L. *Acc. Chem. Res.* **2008**, *41*, 1418; c) Baldauf, C.; Günther, R.; Hofmann, H.-J. *Angew. Chem. Int. Ed.* **2004**, *43*, 1594; d) Baldauf, C.; Günther, R.; Hofmann, H.-J. *Biopolymers* **2005**, *80*, 675; e) Schramm, P.; Hofmann, H.-J *J. Mol. Struct. (Theochem)* **2009**, *907*, 109; f) Baldauf, C.; Günther, R.; Hofmann, H.-J. *J. Org. Chem*. **2005**, *70*, 5351.
17. a) Jones, E.; Diemer, V.; Adam, C.; Raftery, J.; Ruscoe, R. E.; Sengel, J. T.; Wallace, M. I.; Bader, A.; Cockroft, S. L.; Clayden, J.; Webb, S. *J. Am. Chem. Soc*. **2016**, *138*, 688; b) Le Baillya, B. A. F.; Clayden, J. *Chem. Commun.* **2016**, 52, 4852; c) Mazzier, D.; Crisma, M.; De Poli, M.; Marafon, G.; Peggion, C.; Clayden, J.; Moretto, A. *J. Am. Chem. Soc.* **2016**, *138*, 8007; d) Bryden, A. F. L.; Byrne, L.; Diemer, V.; Foroozandeh, M.; Morris, G. A.; Clayden, J. *Chem*. *Sci*. **2015**, *6*, 2313.
18. Gilead, S.; Gazit, E. *Angew. Chem. Int. Ed.* **2004**, *43*, 4041.
19. a) Gatto, E.; Quatela, A.; Caruso, M.; Tagliaferro, R.; De Zotti, M.; Formaggio, F.; Toniolo, C.; Carlo, A. D.; Venanzi, M. *ChemPhysChem* **2014**, *15*, 64; b) Mondal, S.; Adler-Abramovich, L.; Lampel, A.; Bram, Y.; Lipstman, S.; Gazit, E. *Nat. Commun*. **2015**, *6*, 8615.
20. Vasudev, P. G.; Chatterjee, S.; Shamala, N.; Balaram, P. *Acc. Chem. Res*. **2009**, *42*, 1628.
21. Jadhav, S. V.; Gopi, H. N. *Chem. Commun*. **2013**, *49*, 9179.
22. Marenich, A. V.; Cramer, C. J.; Truhlar, D. G. *J. Phys. Chem. B* **2009**, *113*, 6378.
23. Frisch, M. J.; Trucks, G. W.; Schlegel H. B.; Scuseria, G. E.; Robb, M. A.; Cheeseman, J. R.; Scalmani, G.; Barone, V.; Mennucci, B.; Petersson, G. A.; Nakatsuji, H.; Caricato, M.; Li, X.; Hratchian, H. P.; Izmaylov, A. F.; Bloino, J.; Zheng, G.; Sonnenberg, J. L.; Hada, M.; Ehara, M.; Toyota, K.; Fukuda, R.;

Hasegawa, J.; Ishida, M.; Nakajima, T.; Honda, Y.; Kitao, O.; Nakai, T.; Vreven, J.; Montgomery, J. A.; Peralta, J. E.; Ogliaro, F.; Bearpark, M.; Heyd, J. J.; Brothers, E.; Kudin, K. N.; Staroverov, V. N.; Kobayashi, R.; Normand, J.; Rhaghavachari, K.; Rendell, A.; Burant, J. C.; Iyengar, S. S.; Tomasi, J.; Cossi, M.; Rega, N.; Millam, J. M.; Klene, M.; Knox, J. E.; Cross, J. B.; Bakken, V.; Adamo, C.; Jaramillo, J.; Gomperts, R.; Stratmann, R. E.; Yazyev, O.; Austin, A. J.; Cammi, R.; Pomelli, C.; Ochterski, J. W.; Martin, R. L.; Morokuma, K.; Zakrzewski, V. G.; Voth, G. A.; Salvador, P.; Dannenberg, J. J.; Dapprich, S.; Daniels, A. D.; Farkas, O.; Foresman, J. B.; Ortiz, J. V.; Cioslowski, J.; Fox, D. J. Gaussian09, Revision D.01, Gaussian Inc, Wallingford, CT, **2013**

3.7 Appendix I: Mass spectra and ^{1}H NMR, ^{13}C NMR spectra for the Aic and peptides P1 to P3

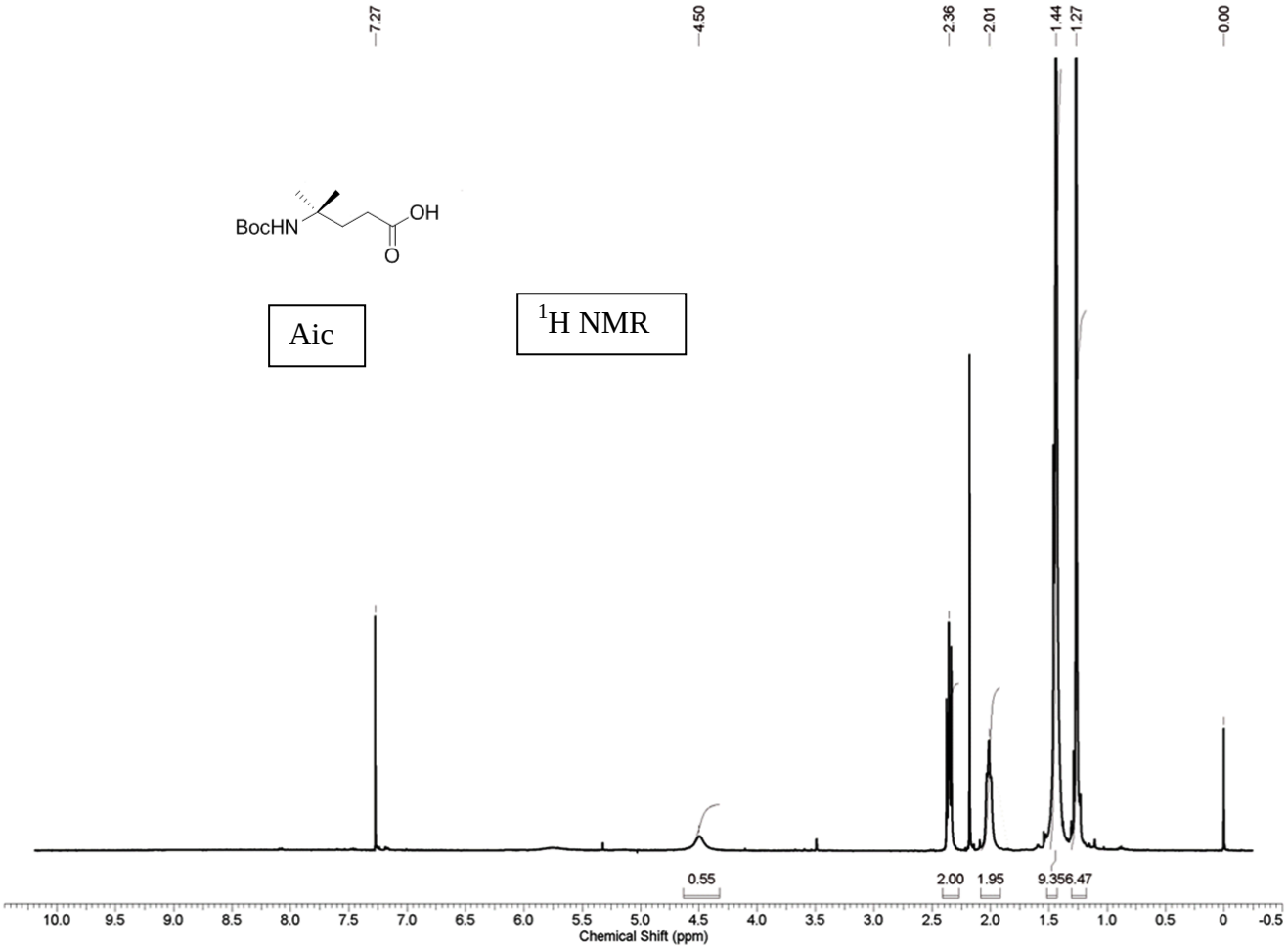

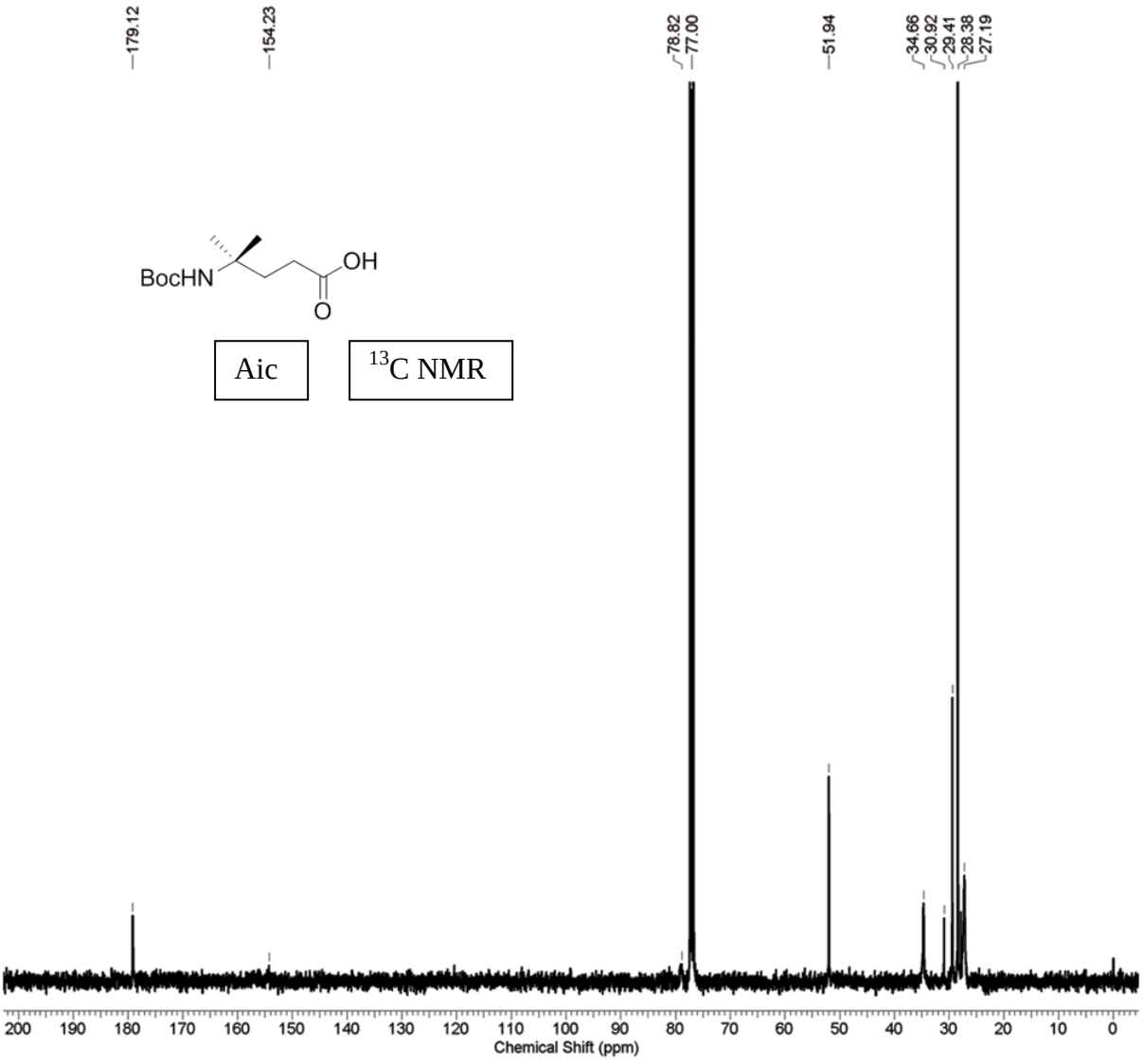
179.12
154.23
78.82
77.00
51.94
34.66
30.92
29.41
28.38
27.19
BocHN
OH
O
Aic
13C NMR
200 190 180 170 160 150 140 130 120 110 100 90 80 70 60 50 40 30 20 10 0
Chemical Shift (ppm)

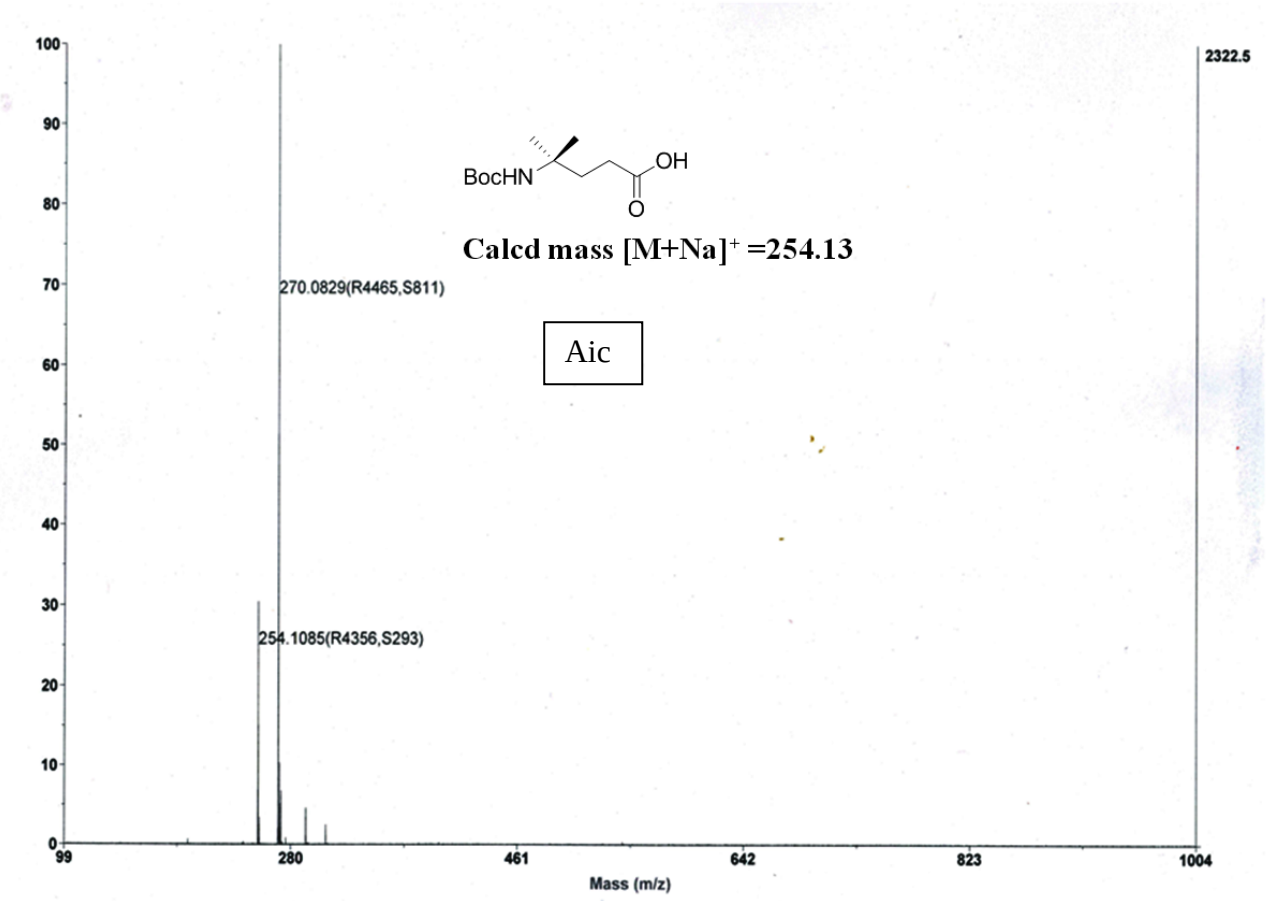
BocHN
OH
O
Calcd mass [M+Na]+ =254.13
270.0829(R4465,S811)
Aic
254.1085(R4356,S293)
2322.5
100
90
80
70
60
50
40
30
20
10
0
99
280
461
642
823
1004
Mass (m/z)

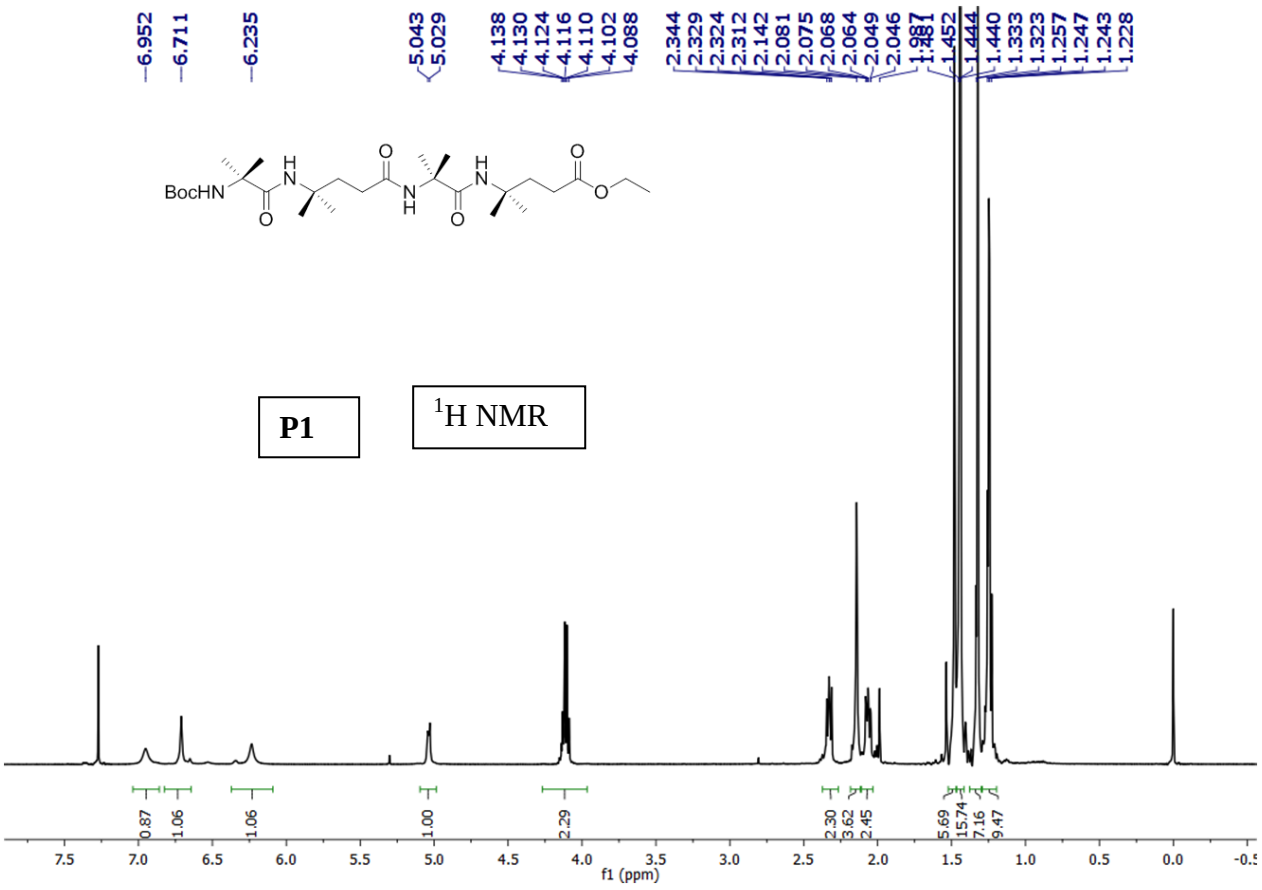
6.952
6.711
6.235
5.043
5.029
4.138
4.130
4.124
4.116
4.110
4.102
4.088
2.344
2.329
2.324
2.312
2.142
2.081
2.075
2.068
2.064
2.049
2.046
1.452
1.444
1.440
1.333
1.323
1.257
1.247
1.243
1.228
BocHN
O
H
N
O
N
H
O
H
N
O
O
P1
1H NMR
0.87
1.06
1.06
1.00
2.29
2.30
3.62
2.45
5.69
15.74
7.16
9.47
7.5
7.0
6.5
6.0
5.5
5.0
4.5
4.0
3.5
3.0
2.5
2.0
1.5
1.0
0.5
0.0
f1 (ppm)

Spectrum Report

Final - Shots 500 - IISER-96-3; Run #77; Label A5

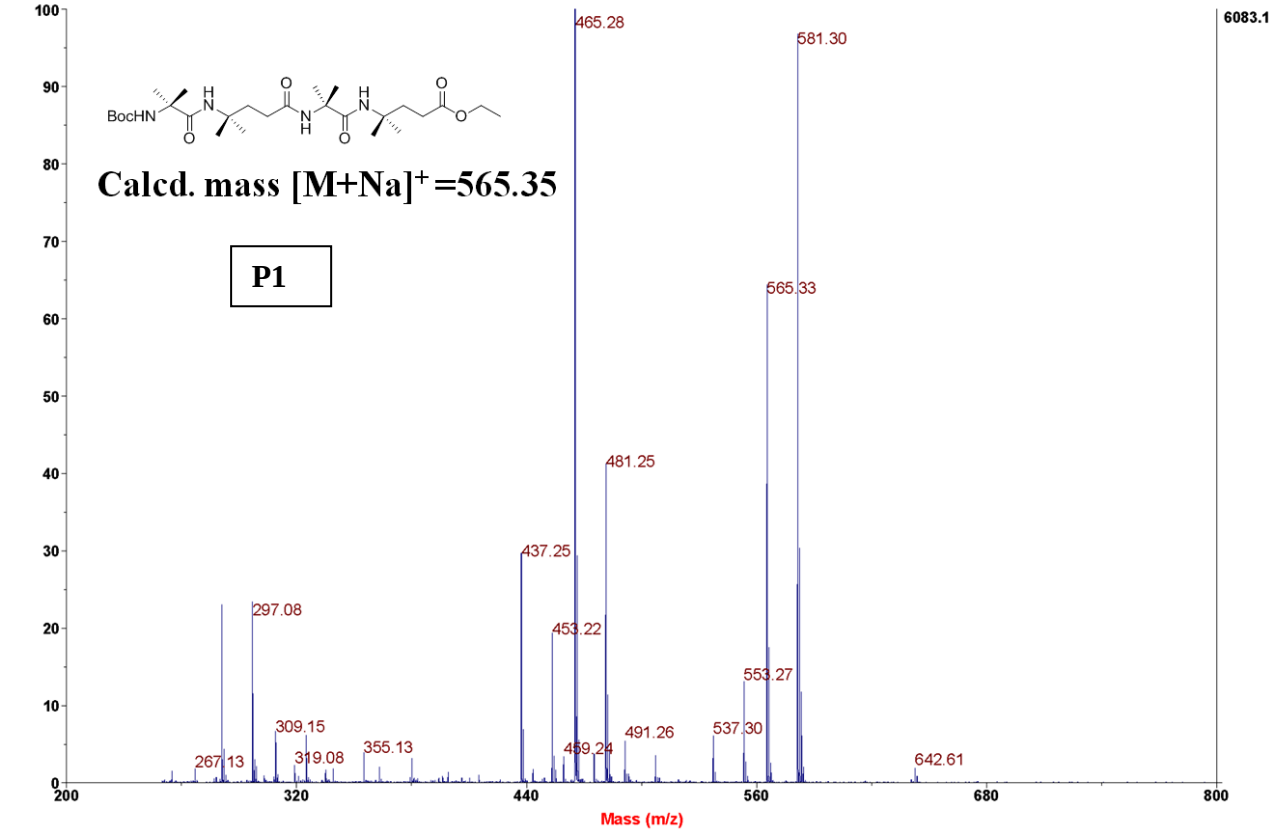

IISER New\IISER-96-3 Label A5 Run # 77 Page 1 2/15/2016 3:32:20 PM

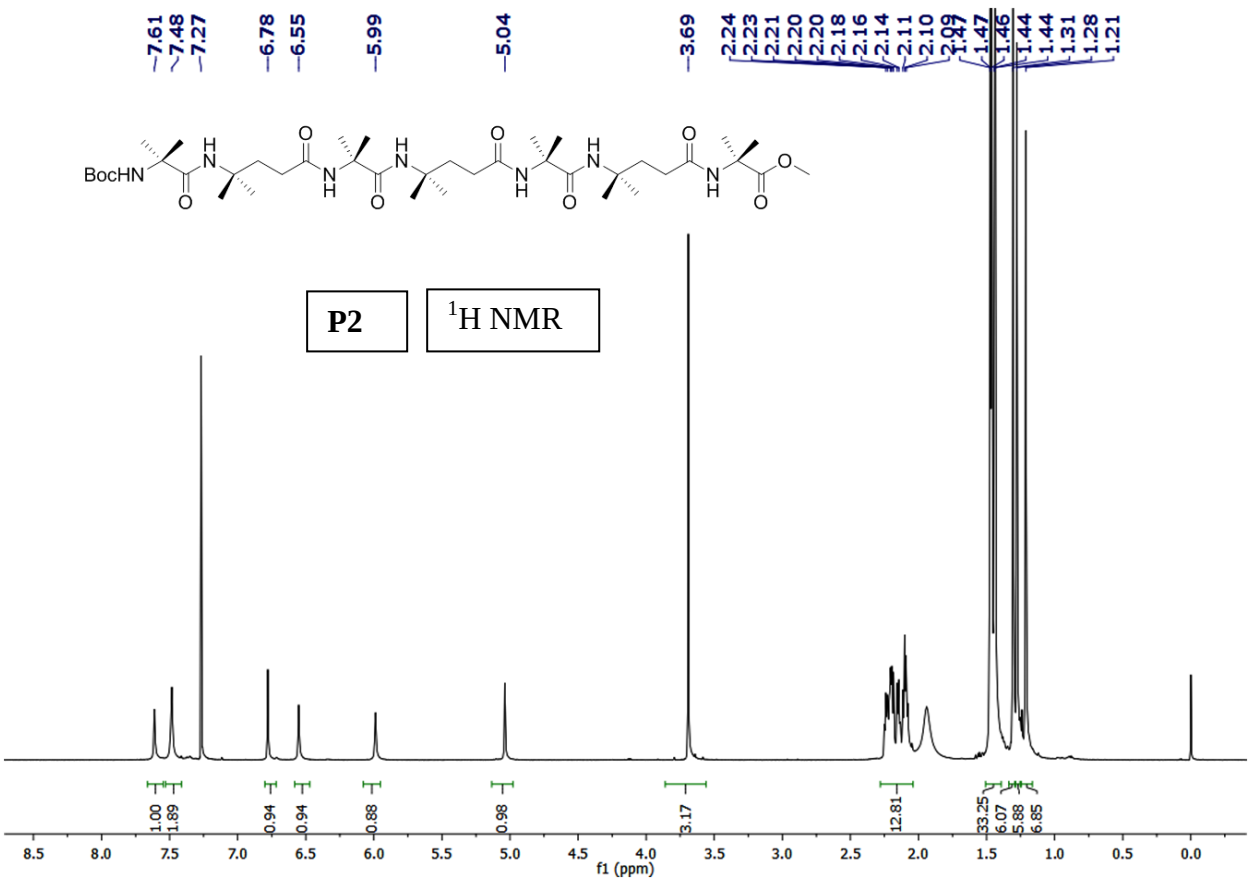
7.61
7.48
7.27
6.78
6.55
5.99
5.04
3.69
2.24
2.23
2.21
2.20
2.20
2.18
2.16
2.14
2.11
2.10
2.09
1.47
1.46
1.44
1.44
1.31
1.28
1.21
BocHN
P2
1H NMR
1.00
1.89
0.94
0.94
0.88
0.98
3.17
12.81
33.25
6.07
5.88
6.85
f1 (ppm)

Spectrum Report

Final - Shots 500 - IISER-96-3; Run #77; Label A6

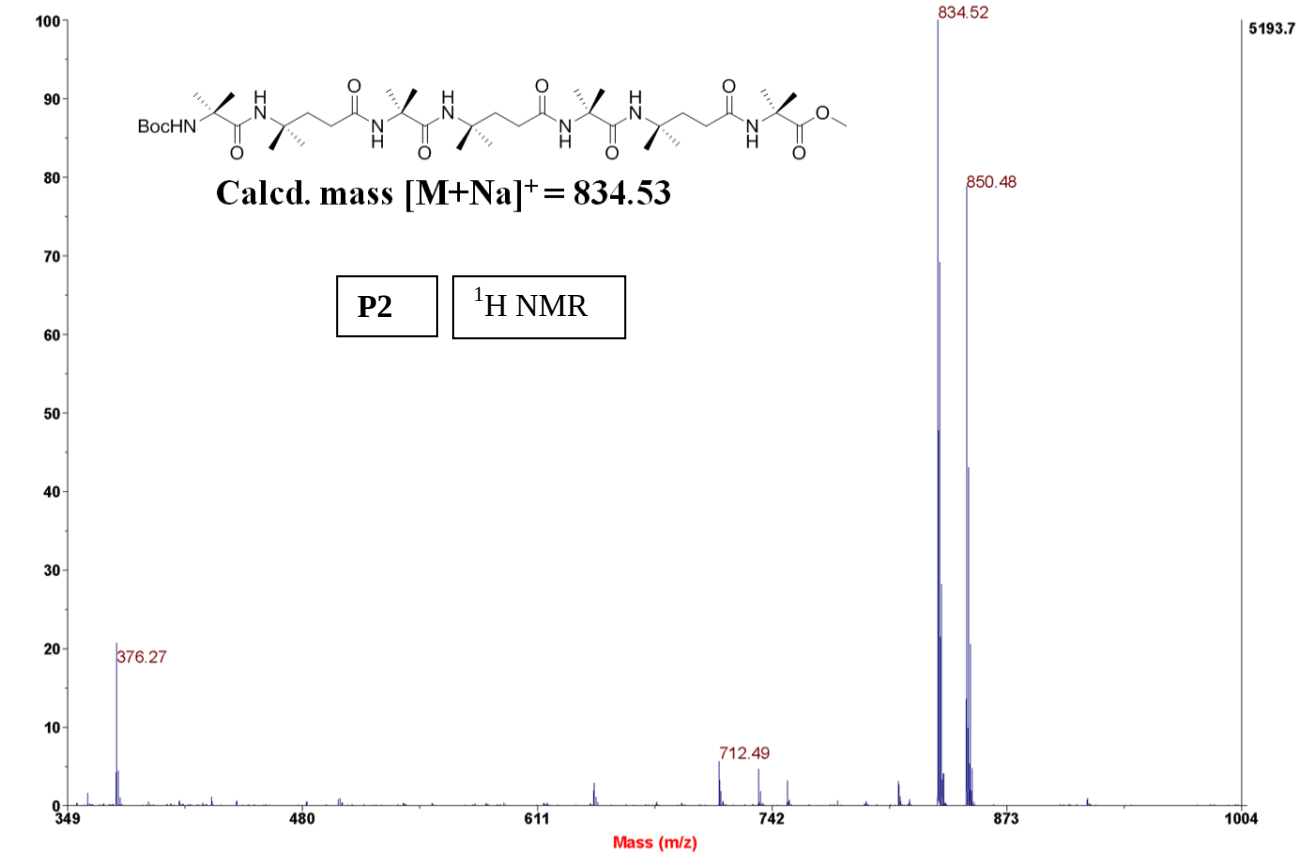

Calcd. mass $[M+Na]^+ = 834.53$

P2	^{1}H NMR

IISER New\IISER-96-3 Label A6 Run # 77 Page 1 2/15/2016 3:38:53 PM

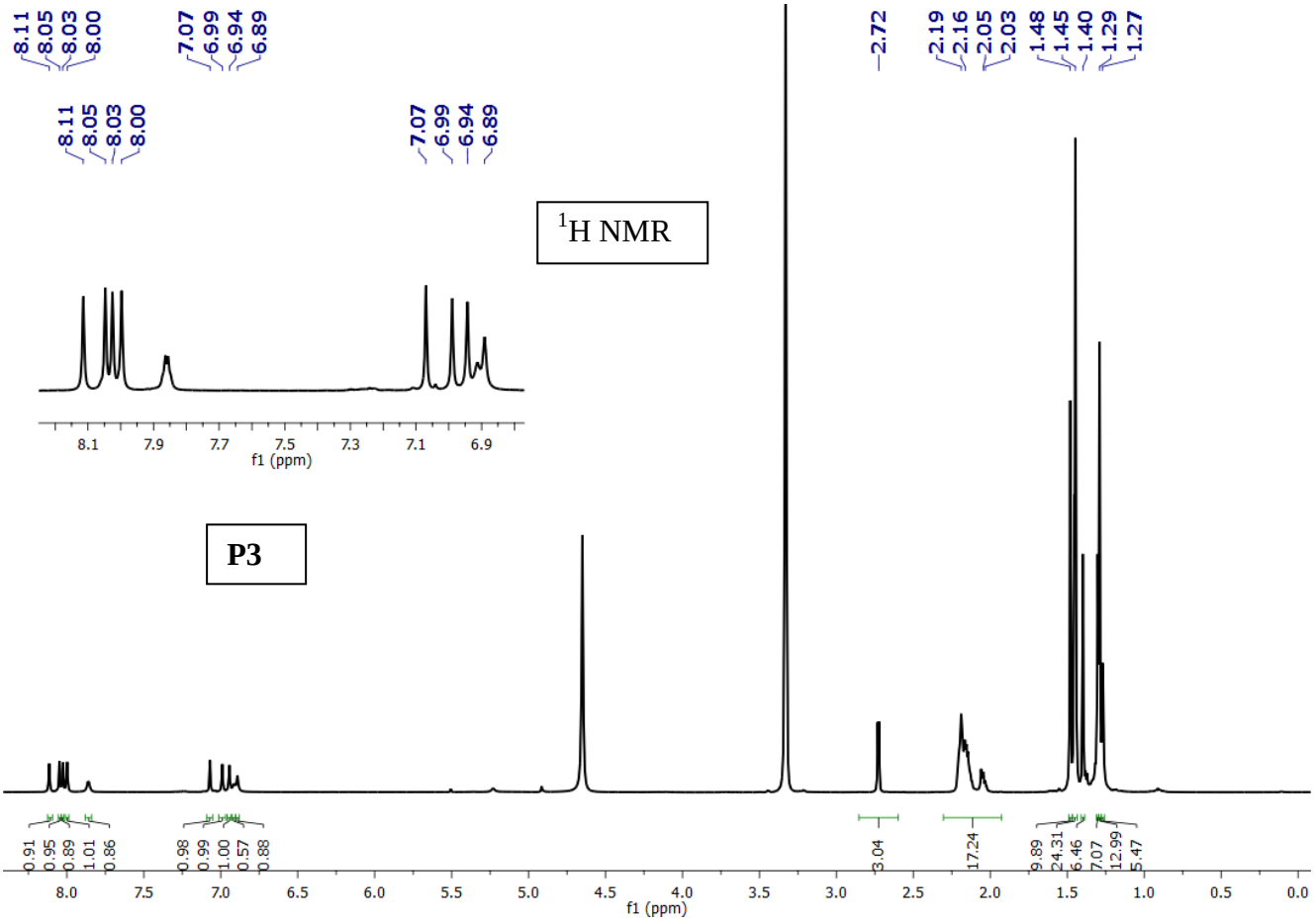
8.11
8.05
8.03
8.00
7.07
6.99
6.94
6.89
2.72
2.19
2.16
2.05
2.03
1.48
1.45
1.40
1.29
1.27
1H NMR
P3
f1 (ppm)

Spectrum Report

Final - Shots 500 - IISER-96-3; Run #73; Label G4

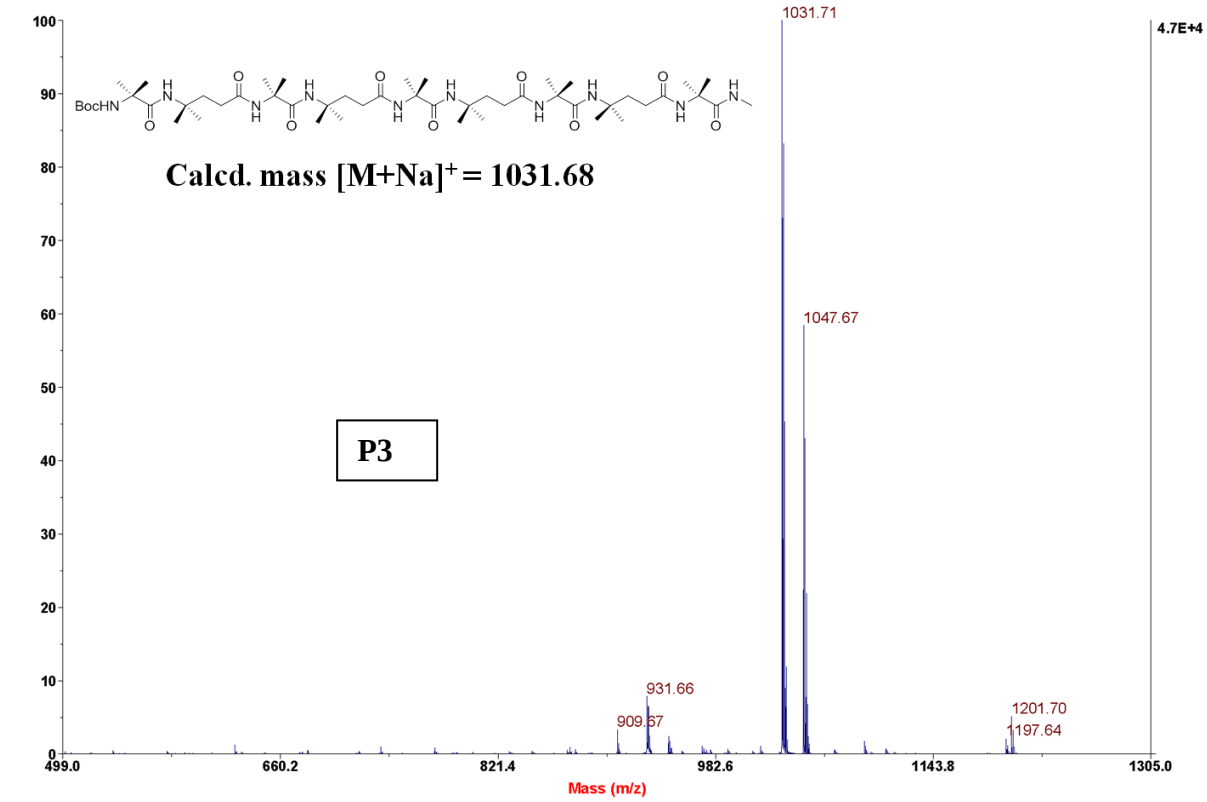

IISER New\IISER-96-3 Label G4 Run # 73 Page 1 2/16/2016 5:01:17 PM

Chapter 4

Modulating the structural properties of α,γ-hybrid peptides by α-amino acid residues: Uniform 12-helix *versus* "mixed" 12/10-helix

4.1 Introduction

The folding abilities of β- and γ-amino acid oligomers (foldamers) provide the opportunity to design architectures beyond the classical protein secondary structures.[1] As described in the Chapters 1 and 3, one of the most intriguing strategies in foldamer research is the combination of α-amino acids with their higher homologous amino acids. Dependent on the nature and periodicity of the amino acids in the heterogeneous (hybrid) peptide sequence, different helix types can be generated. Thus, extensive efforts have been made to understand the conformational properties of α,β-[1,2] and α,γ-hybrid[1,3] peptides with the two amino acid constituents in 1:1 alternation. Moreover, Gellman and coworkers explored this strategy to design various biologically active α,β-hybrid peptides.[4] In case of α,γ-hybrid peptides the formation of stable uniform 12-helical conformations was often found in analogy to the 3_{10}-helix in α-peptides.[3g,h,i,k,l,m,n,r] A very interesting observation was that α,β-[2d-g] and α,γ-hybrid peptides[3a,b,f,o,q] are able to form helices with alternately changing H-bond directionality,[5] as they were found at first in β-peptide sequences composed of alternating β^3-and β^2-amino acids by Seebach and coworkers[6a,b] and later by further authors[6c-f]. Such "mixed" helices are very scarcely realized in α-peptides and proteins. The available literature data suggest that the stereochemistry of the β- and γ-amino acid constituents plays a crucial role in dictating the direction of the helical hydrogen bonds. Until now only few examples of an alternate change of the H-bond directionality are available for α,γ-hybrid peptides. Thus, Sharma and Kunwar reported mixed 12/10-helices for α,γ-hybrid peptides with γ-carboamino acid (γ-Caa) constituents.[3b] The same helix type was later found by Gellman et al.[3q] An alternative 12/10-helix type was obtained by Balaram and coworkers in short αγαα tetrapeptide sequences with gabapentin as γ-amino constituent[3f] and later confirmed by Gellman et al. in peptides with trisubstituted cyclic γ-amino acids.[3o] A selection of γ-amino acids that have been proved to induce an alternating change of hydrogen bond directionality in α,γ-hybrid peptides is shown in Figure 1. Typical backbone torsion angle values of the two alternative 12/10-helix types are given in Table 1.

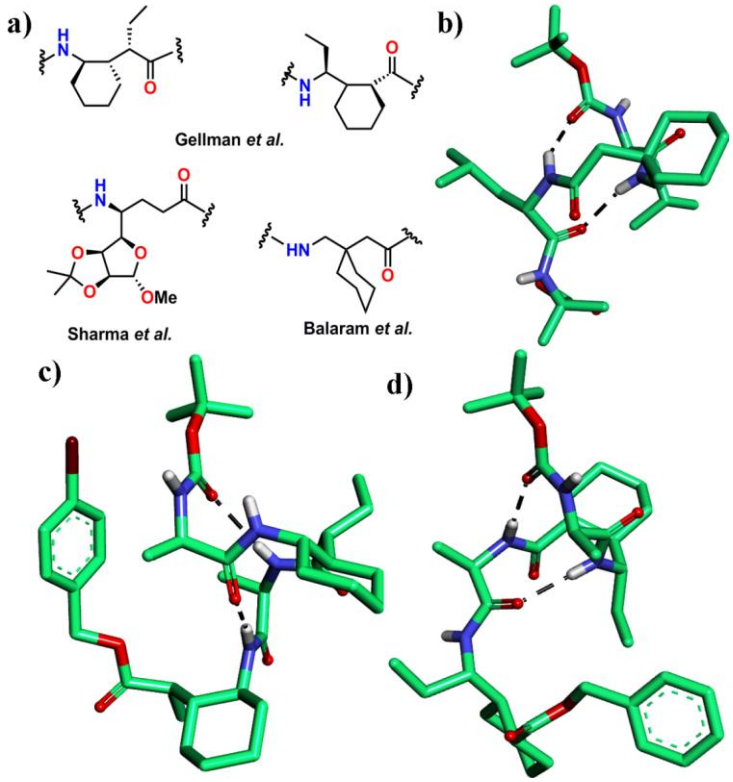

Figure 1. Chemical structures of γ-amino acid constituents in 12/10-helices of α,γ-hybrid peptides. b) X-ray structure of 12/10 for the peptides Boc-Leu-Gpn-Leu-Aib-OMe.[3f] c) X-ray structure of 12/10 for the peptides Boc-Ala-*trans*-EtACHA-Ala- *trans*-EtACHA- OBn(Br).[3q] d) X-ray structure of 12/10 for the peptides Boc-^{D}Ala-APCH-^{D}Ala-APCH- OBn.[3o]

Table 1. Backbone torsion angles[a] of γ-amino acid constituents in various α,γ-hybrid 12/10-helices from literature.

Constituent	ϕ	θ_1	θ_2[	ψ
APCH[b, 3o]	-84.2	-20.5	-56.1	130.2
Gpn[c, 3f]	87	37	45	-129
γ-Caa amino acid[d, 3b]	139±3	-52±5	101±3	-104±3
trans-EtACH[b, 3q]	119.9	-55.2	146.1	-109.4
ab initio MO theory[f, 3a]	-64	-32	-48	132
ab initio MO theory[g, 3a]	129	-51	96	120

[a] In degrees. [b](1*R*,2*R*,3*S*)-2-(1-aminopropyl)-cyclohexanecarboxylic acid (APCH),[3g] cyclic $\gamma^{2,3,4}$-amino acid, see Figure 1. [c]Gpn = Gabapentin = (1-aminomethyl)-cyclohexaneacetic acid, $\gamma^{3,3}$-amino acid, see Figure 1. [d] γ-Caa = C-linked carbo-γ-amino acid from D-mannose, see Figure 1. [e] ACHA = cyclic $\gamma^{2,3,4}$-amino acid with (*S*,*S*,*R*)-configuration. [f]Most stable 12/10-helix for the unsubstituted backbone. [g]Second most stable 12/10-helix for the unsubstituted backbone.

4.2 Aim and rationale of the present Work

We have been interested in the design of folded architectures constructed from sterically constrained γ-amino acids. Along with our studies on stable 12-helices in α,γ^4-hybrid peptides without steric constraints,[3l,m] in the previous chapter we have demonstrated the co-existence of uniform 12- and 15/17-helical conformations in achiral α,$\gamma^{4,4}$-hybrid peptides composed of the sterically constrained α-amino acid Aib and its doubly backbone homologated amino acid Aic in 1:1 alternation.[3r] The serendipitous 15/17-helix in achiral α,$\gamma^{4,4}$-hybrid peptides motivated us to investigate the structural behavior of α,γ-hybrid peptide sequences composed of chiral proteinogenic α-amino acids in combination with Aic residues in 1:1 alternation. In this chapter, we are describing the crystal and solution conformations of a series of novel α,$\gamma^{4,4}$-hybrid peptides composed of the natural aliphatic α-amino acids alanine and leucine, respectively, and the γ-amino acid constituent Aic.

4.3 Results and discussion

4.3.1 Synthesis of the peptides.

To investigate the structural properties of the new α,$\gamma^{4,4}$-hybrid peptides, monomer Aic was synthesized reported protocol describe in the previous Chapter (Scheme 1) and the peptides **P1**-**P6** (Scheme 1) by solution phase method using EDC/HOBt as coupling agents and purified them by reverse phase HPLC.

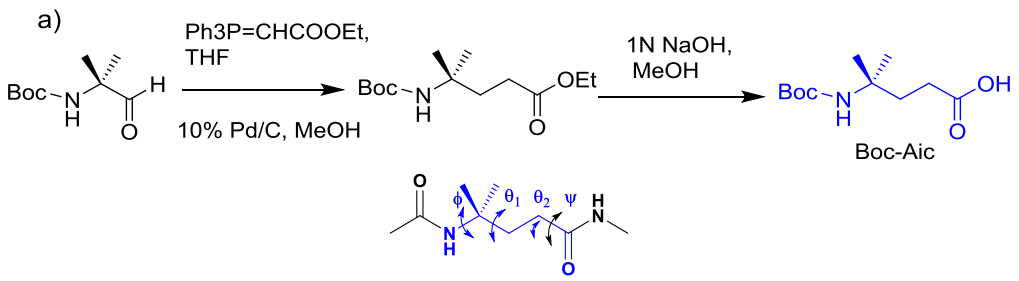

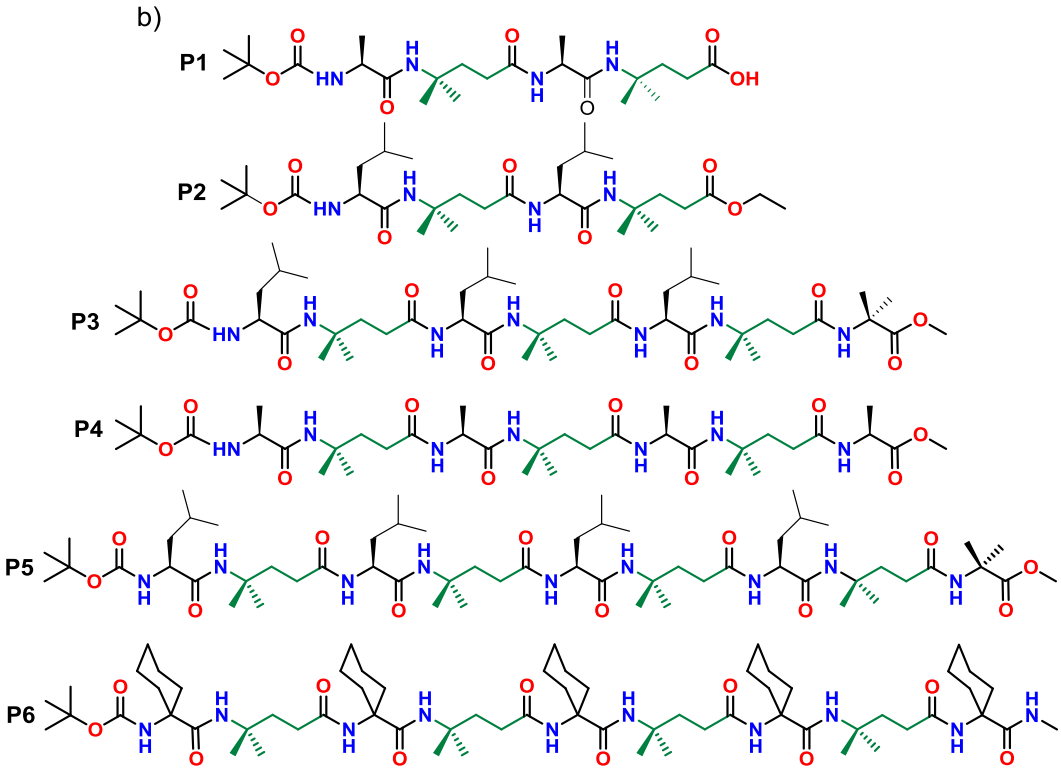

Scheme 1. Sequence of α,γ^{4,4}-hybrid peptides composed of the α-amino acids Ala, Leu, Aib, Ac_6c and the γ-amino acid Aic.

4.3.2 Single crystal conformational analysis of peptides P1 and P2

In the process of synthesizing longer sequences of α,γ^{4,4}-hybrid peptides, we obtained single crystals of the tetrapeptide acid **P1** composed of Ala and Aic in $CHCl_3$ solution. The structure of **P1** is shown in Figure 2. The peptide folds into a 12/10-helical conformation stabilized by two intramolecular 12- and 10-membered H-bonds with opposite directionality. The 12-membered H-bond is observed between BocCO and NH of Ala(3) ($i \rightarrow i+3$, 4→1), whereas the 10-membered H-bond is realized between NH of Aic(2) and CO of Ala(3) ($i \rightarrow i-1$, 2→3). The 10-membered ring H-bond is longer compared to the 12-membered hydrogen-bonded rings. This suggests a higher stability of the hydrogen bonds in 12-rings than in 10-rings, which may be explained by better steric conditions for the formation of hydrogen bonds in larger rings. The C-terminus Aic(4) is not involved in hydrogen bonding. The values for the backbone torsion angles are given in Table 2. The H-bond parameters are tabulated in the Table 3. Interestingly, the two α-amino acid residues Ala(1) and Ala (2) adopted a polyproline II (PP_{II})-like helical conformation.

The serendipitous finding of the 12/10-helical structure of the α,γ-hybrid tetrapeptide **P1** motivated us to extend our studies to other natural amino acids and to longer peptide sequences. Thus, the tetrapeptide **P2** with the α-amino acid Leu instead of Ala, the heptapeptides **P3** and **P4** with Leu and Ala and finally the nonapeptide **P5** again with Leu were synthesized. Tetrapeptide **P2** with Leu residues provided X-ray quality single crystals from the solvent $CHCl_3$. Its structure (Figure 2) is fully compatible with that of **P1**. The backbone torsion angle values are given in Table 2. The H-bond parameters are tabulated in the Table 4. The 12/10-helical structures observed in the crystal structures of peptides **P1** and **P2** are in agreement with those reported for other α,γ-hybrid peptides by the Balaram[3f] and Gellman[3o] groups (Table1), but differ from the 12/10-helical alternatives found by Sharma et al.[3b] and Gellman et al[3q] (Table 1).

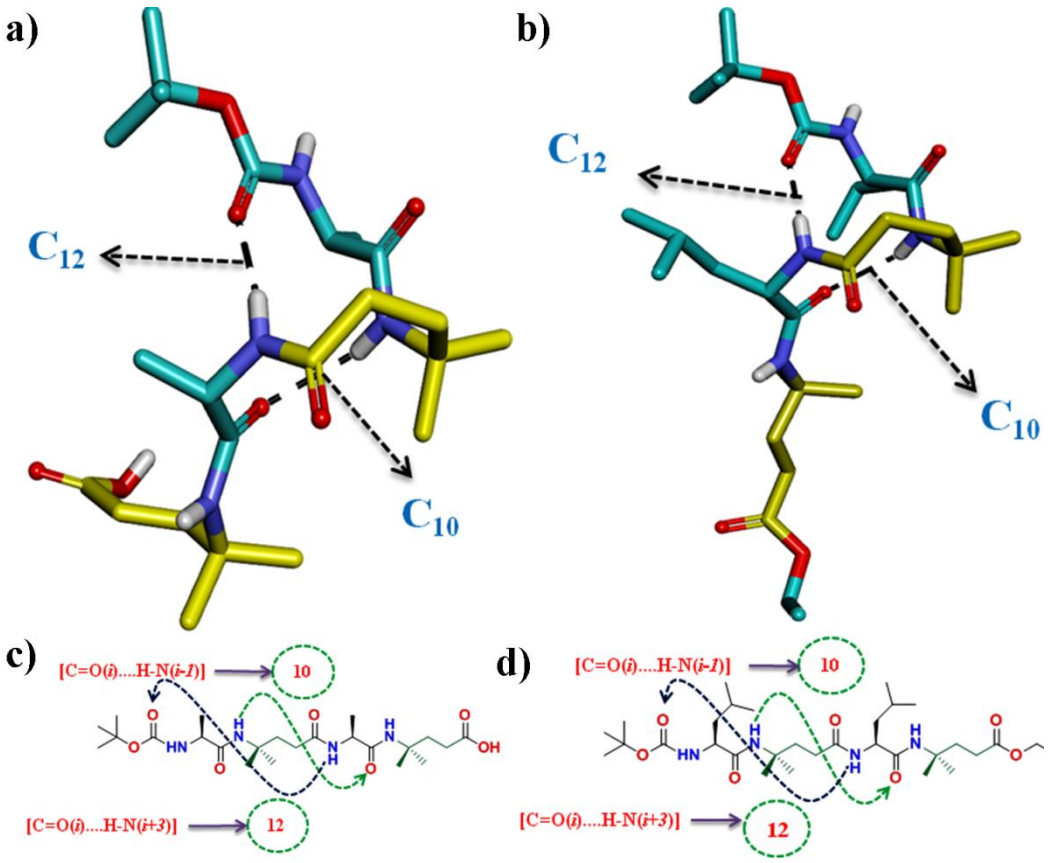

Figure 2 X-ray structures of **P1** a) and **P2** b)**.** Both peptides adopt a 12/10-helical conformation in single crystals. The alternate H-bonding directionality in **P1** and **P2** is depicted in c) and d), respectively.

Table 2 Backbone torsion angles[a] of the α-amino acid residues Ala and Leu and the γ-amino acid Aic in the hybrid peptides **P1-P2** compared with quantum chemical data.[b]

Peptide	Residue	φ	θ_1	θ_2	ψ
P1	Ala(1)	-81			146
	Aic(2)	59	34	50	-121
	Ala(3)	-84			147
	Aic(4)[b]	-64	-58	177	-176
P2	Leu(1)	-74			144
	Aic(2)	60	33	53	-124
	Leu(3)	-86			147
	Aic(4)[b]	-179	-176	175	159

[a] In degrees. [b]The Aic residue is not part of a helix.

Table 3: Hydrogen bond parameters of peptide **P1**

Donor (D)	**Acceptor (A)**	**D….A (Å)**	**DH….A (Å)**	**NH….O (deg)**
N3	O2	2.88	2.02	165
N2	O5	3.11	2.32	149

Table 4: Hydrogen Bond Parameters of **P2**

Intramolecular H-bonds

Donor (D)	**Acceptor (A)**	**D….A (Å)**	**DH….A (Å)**	**NH….O (deg)**

N3	O2	2.94	2.10	163
N2	O5	2.95	2.11	158

4.3.3. Conformational analysis of peptide P3 in solution.

Unfortunately, the longer peptides **P3**, **P4** and **P5** did not give X-ray quality single crystals. Therefore, the structure of these was investigated by 2D NMR (TOCSY and ROESY) analysis. The well-dispersed ^{1}H NMR spectrum of heptapeptide **P3** in $CDCl_3$ suggested an ordered structure in solution. The TOCSY spectrum depicting the amide NH region is shown Figure 3. The NH↔NH and NH↔C$^{\alpha}$H NOEs observed in the ROESY spectrum are shown the Figures 4 and 5, respectively. The analysis of the ROESY spectrum revealed strong NH↔NH NOEs between α-NH(*i*) and γ-NH(*i+1)* and weak NOEs between γ-NH(*i)* and α-NH(*i+1)*. Along with sequential NH↔NH NOEs, a weak Leu(1)NH↔Leu(3)NH interaction was also observed. In addition to the strong C$^{\alpha}$H(*i*)↔NH(*i*+1) interactions, long range NOEs between the residues Leu(1)C$^{\alpha}$H↔Leu(3)NH and Leu(5)C$^{\alpha}$H↔ Aib(7)NH were found. The list of NOEs observed in the 2D NMR is given in the Table 5. Furthermore, DMSO titration experiments revealed that all amide NHs (except the *N*-terminal BocNH) displayed negligible changes in their chemical shifts, thus suggesting their involvement in intramolecular H-bonding (Figure 6). The superimposition of the ten lowest energy structures derived from the NOEs is shown in Figure 7 and torsional angles are tabulated in Table 6.

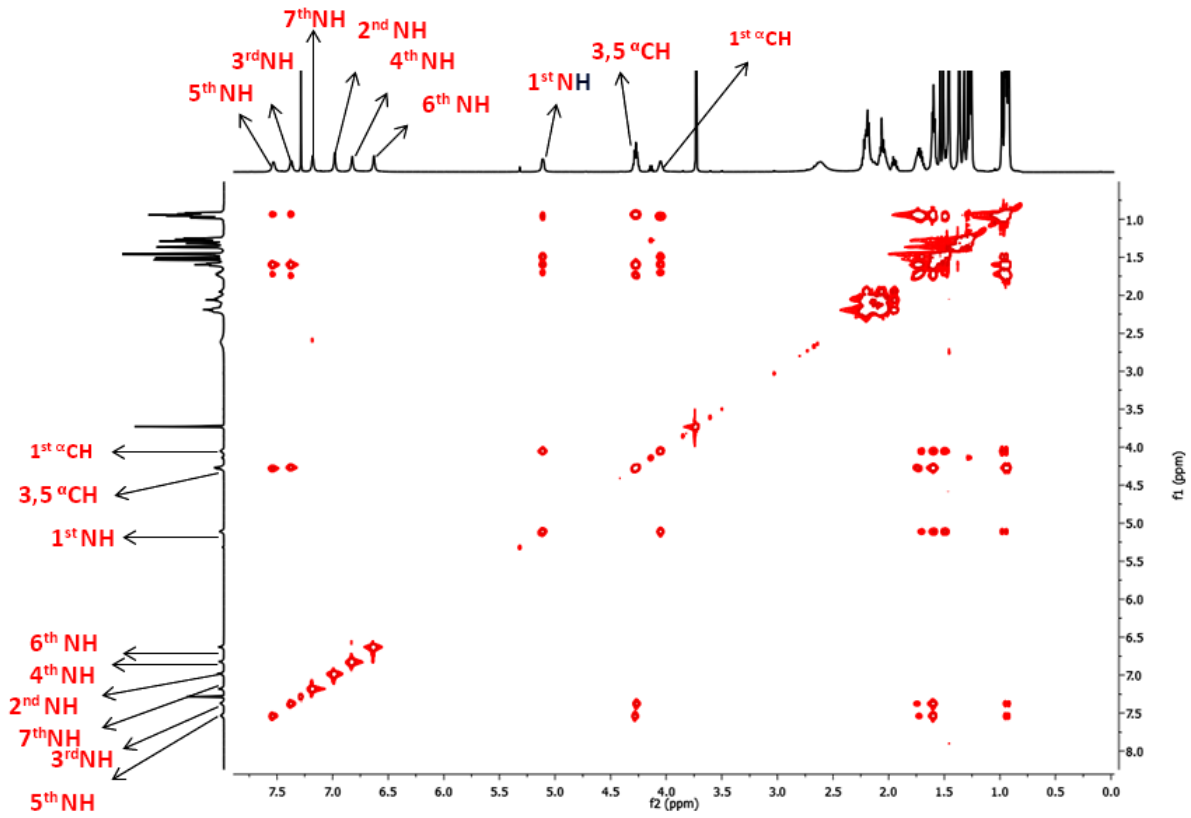

Figure 3: TOCSY spectrum of peptide **P3** (5 mM) in $CDCl_3$.

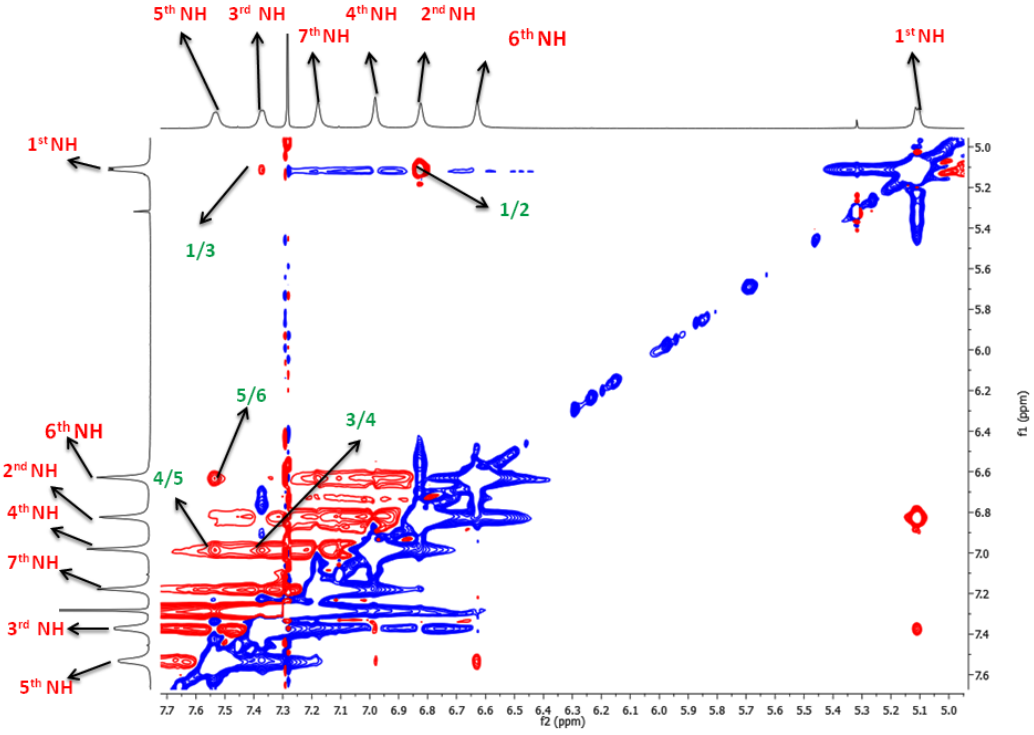

Figure 4: Partial ROESY spectrum of **P3** (5 mM) in $CDCl_3$ showing NH↔NH NOEs.

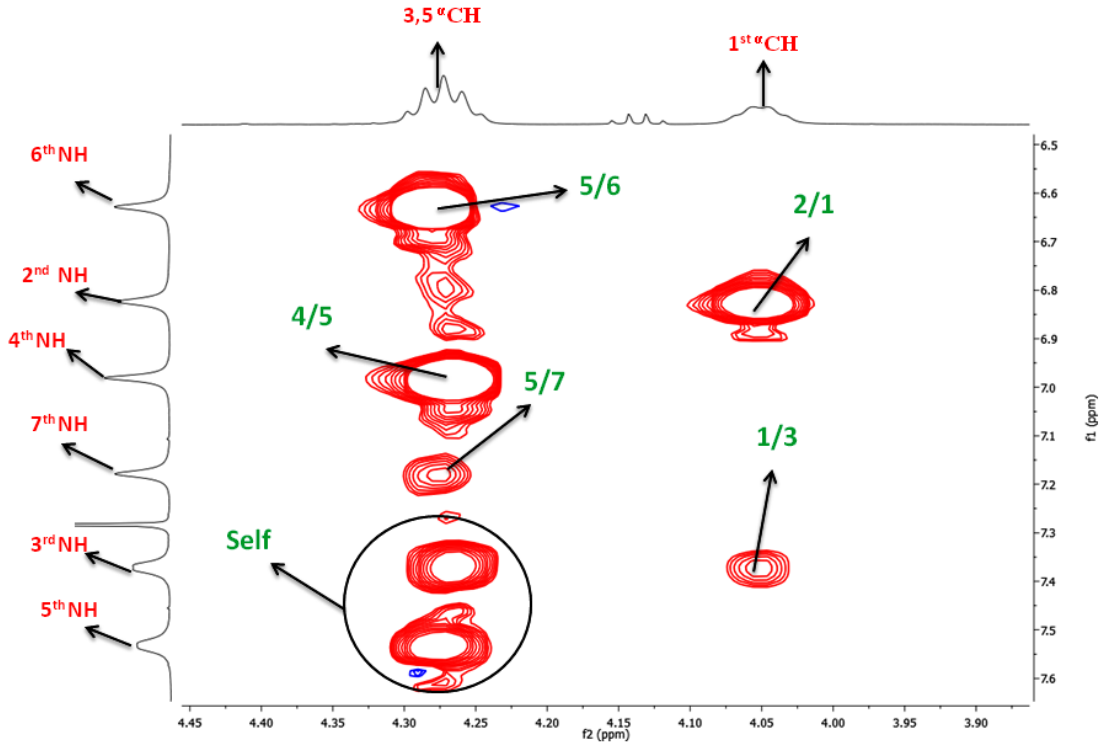

Figure 5: Partial ROESY spectrum of **P3** showing sequential NOEs of NH↔$C^{\alpha}H$.

Table 5: List of NOEs used in the MD calculations on peptide **P3**

Residue	H-atom	Residue	H-atom	NOE($CDCl_3$)
Leu(1)	NH	Aic(2)	NH	Strong
Leu(1)	NH	Leu(3)	NH	Medium
Leu(1)	$C^{\alpha}H$	Aic(3)	NH	Medium
Leu(1)	$C^{\alpha}H$	Aic(2)	NH	Strong
Leu(1)	NH	Aic(2)	$C^{\alpha}H_2$(backbone)	Medium
Leu(3)	NH	Aic(4)	NH	Weak
Leu(3)	NH	Aic(2)	$C^{\alpha}H_2$(backbone)	Strong

Leu(3)	NH	Aic(2)	$C^{\beta}H2$(backbone)	Medium
Leu(3)	$C^{\alpha}H$	Aic(4)	NH	Strong
Aic(4)	NH	Leu(5)	NH	Weak
Leu(5)	$C^{\alpha}H$	Aic(7)	NH	Medium
Leu(5)	NH	Aic(4)	$C^{\alpha}H_2$(backbone)	Strong
Leu(5)	NH	Aic(4)	$C^{\beta}H_2$(backbone)	Medium

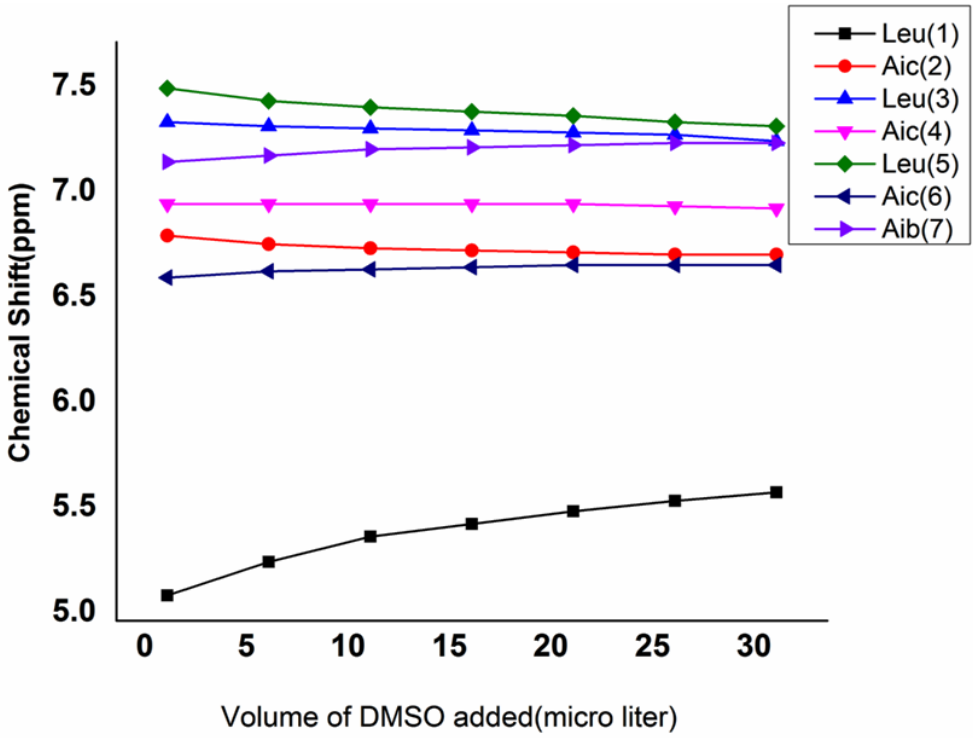

Figure 6: Solvent dependence of NH chemical shifts of peptide **P3** at varying concentrations of $(CD_3)_2SO$.

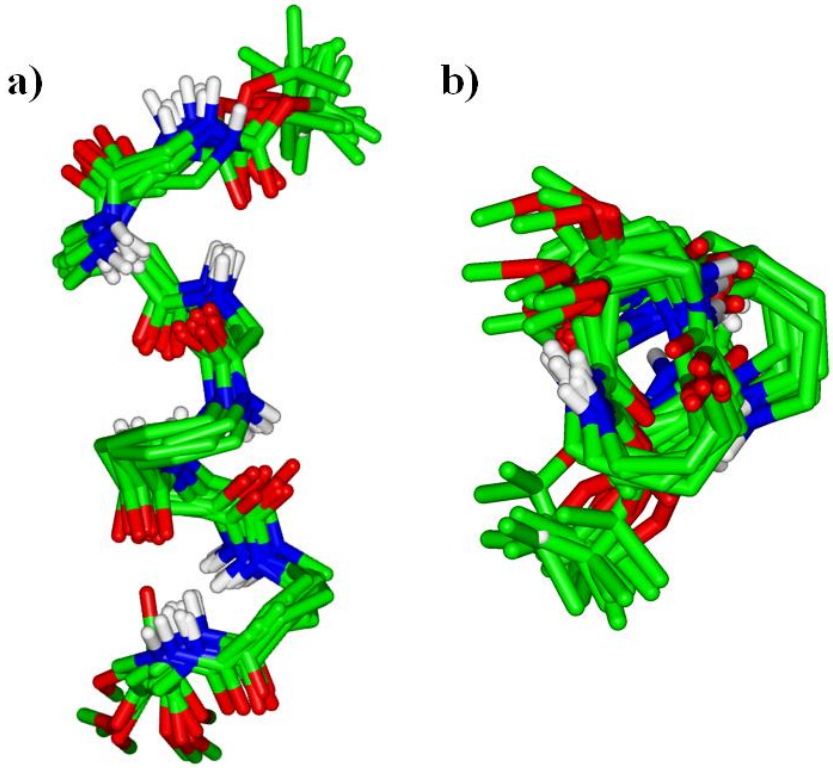

Figure 7. Solution conformations of peptides **P3**

Table 6. Average backbone torsional angles[a] in peptides **P3** NMR solution structure ensembles

Peptide	Residue	φ	θ_1	θ_2	ψ
P3	Leu(1)	-110±24			139±22
	Aic(2)	58±5	37±18	6±15	-113±14
	Leu(3)	-78±11			153±14
	Aic(4)	73±13	25±18	49±13	-110±18
	Leu(5)	-74±16			150±18
	Aic(6)	67±15	27±20	48±17	-114±18
	Aib(7)	-86.±48			132±40

[a] In degrees

4.3.4 Solution conformation of peptide P4

The heptapeptide **P4** displayed a similar pattern of NOEs. The TOCSY spectrum of peptide (amide portion) is shown in Figure 8. We observed sequential NH↔NH NOEs between the

residues 1 and 2, 2 and 3, 3 and 4, and 5 and 6 in the ROESY spectrum (Figure 9 and 10). The NOEs between γ-NH(*i*) and α-NH(*i+1*) were found to be weaker than the NOEs between α-NH(*i*) and γ-NH(*i+1*). In addition to the sequential $C^{\alpha}H(i)\leftrightarrow NH(i+1)$ interactions, we also observed medium NOEs Ala(1)$C^{\alpha}H\leftrightarrow$Ala(3)NH and Ala(5)$C^{\alpha}H\leftrightarrow$Ala(7)NH (Figure 11). The observed NOEs of **P4** are also tabulated in Table 7. The superimposition of the ten lowest energy-minimized structures of **P4** derived from the observed NOEs is shown in Figure 12. The solution structures of **P3** and **P4** revealed a continuous 12/10-helix conformation, in close correspondence to the 12/10-helices of peptides **P1** and **P2**. The backbone torsion angles of the **P4** are given in Table 8. They are in good agreement with the values observed in the crystal structures of **P1** and **P2**.

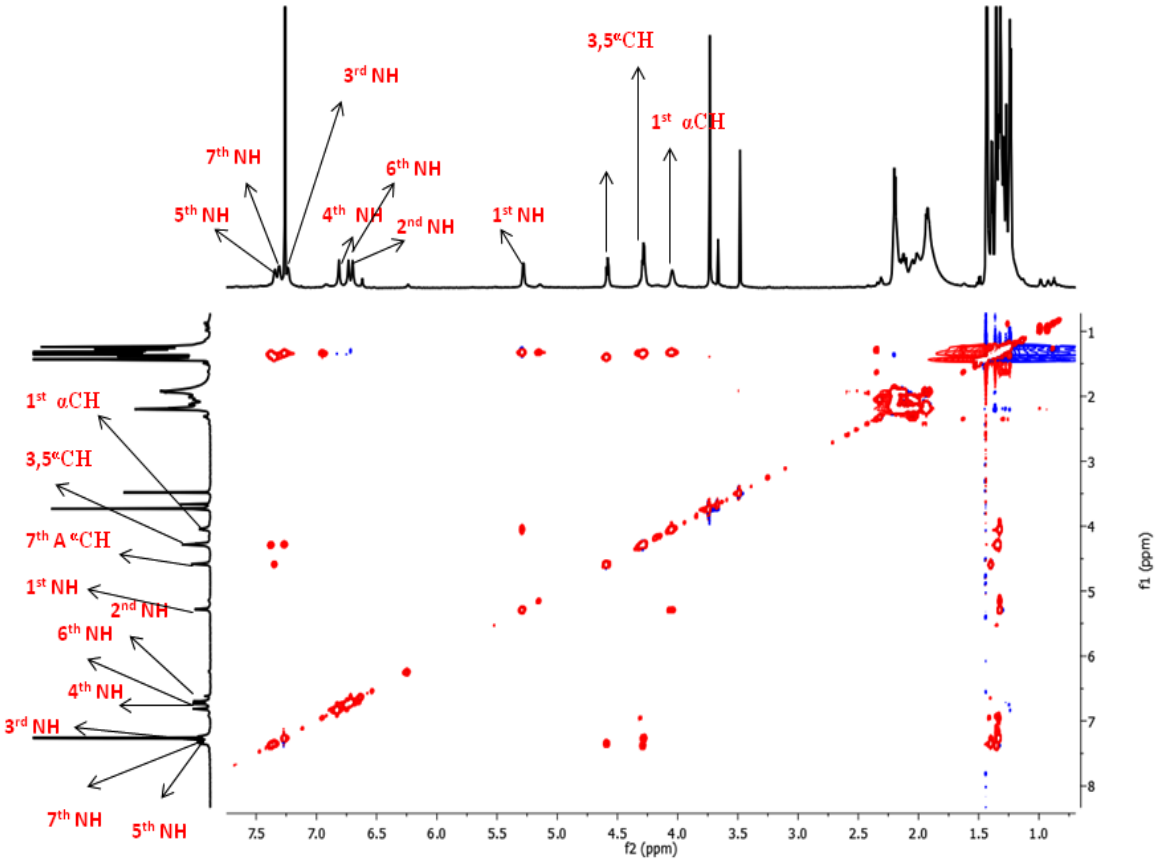

Figure 8: TOCSY spectrum of peptide **P4** (5 mM) in $CDCl_3$.

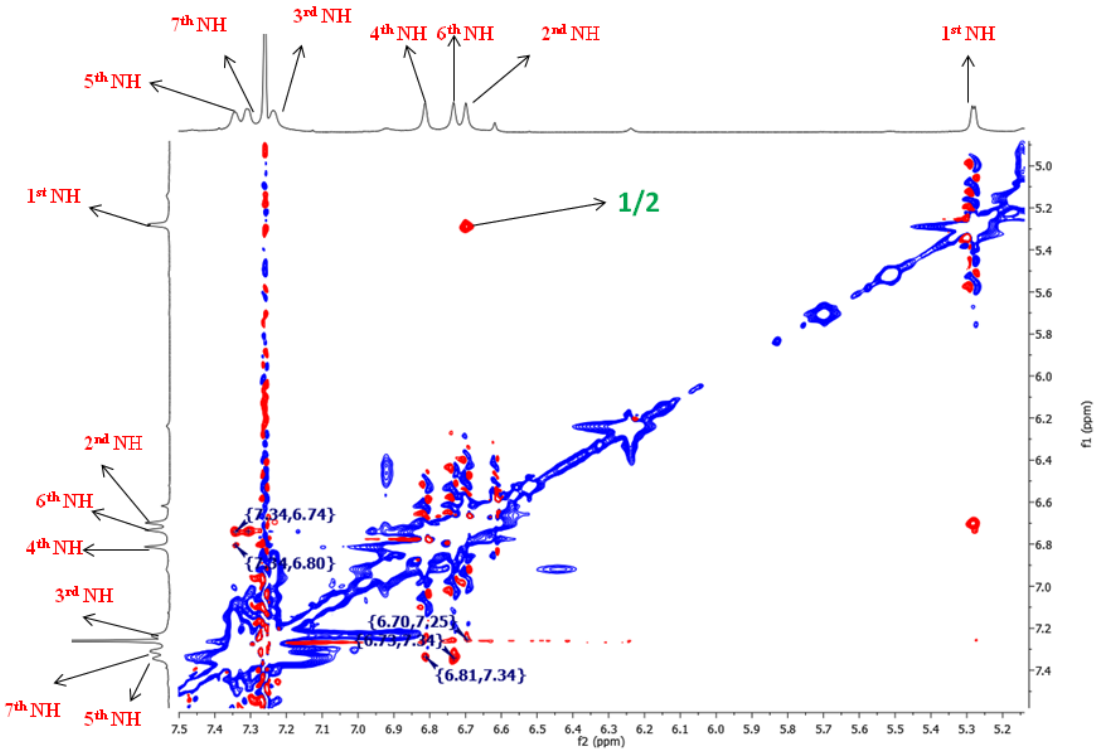

Figure 9: Partial ROESY spectrum of **P4** (5 mM) in $CDCl_3$ showing NH↔NH NOEs.

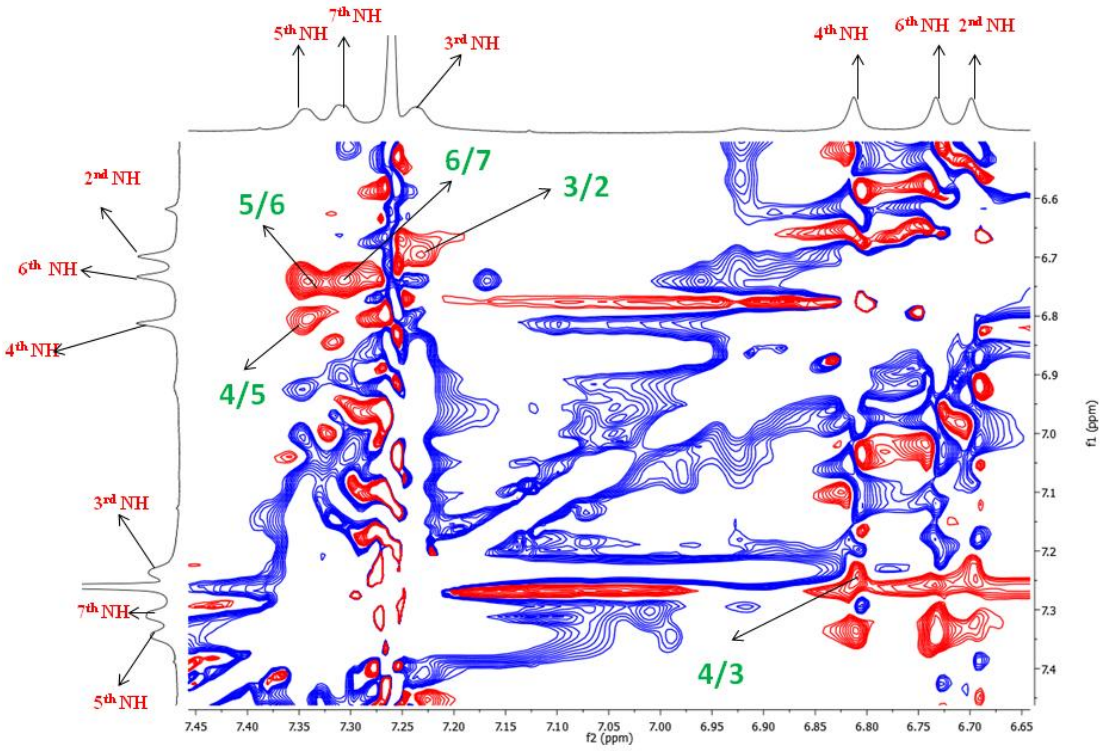

Figure10: Partial ROESY spectrum of **P4** (5 mM) in $CDCl_3$ showing NH↔NH NOEs.

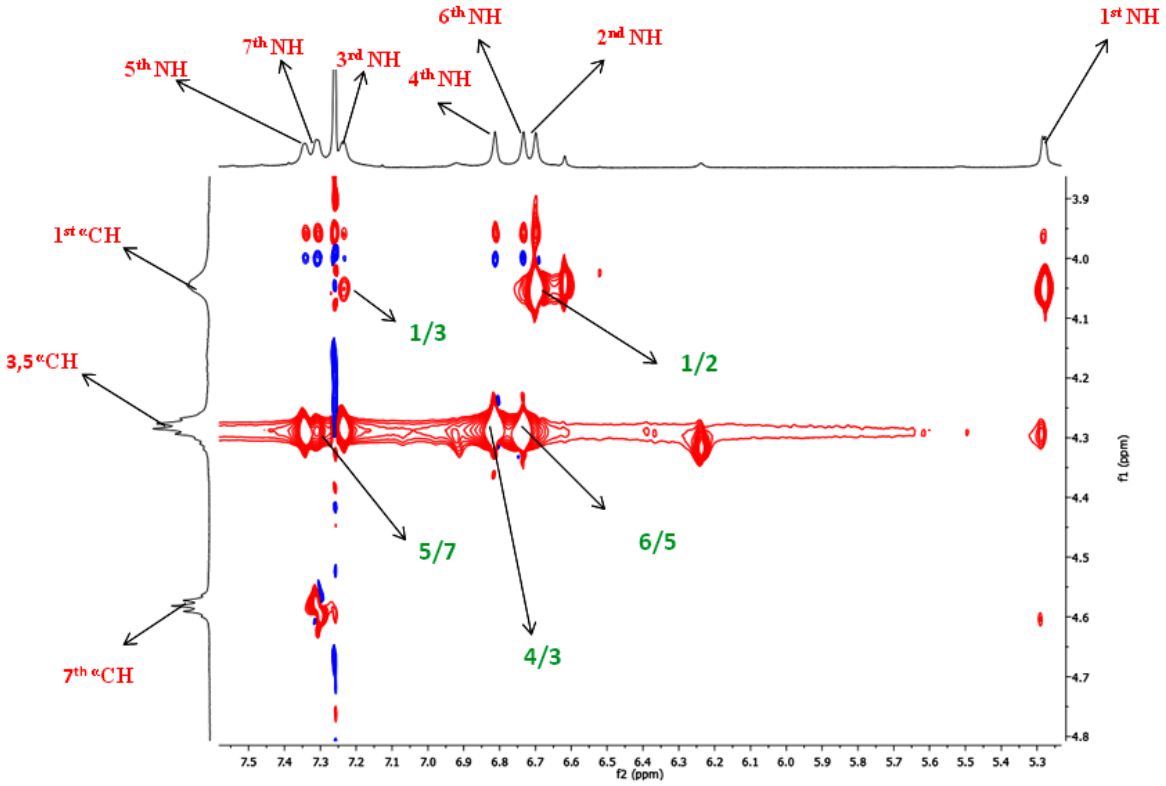

Figure 11: Partial ROESY spectrum of **P4** (5 mM) in $CDCl_3$ showing $C^{\alpha}H\leftrightarrow$ NH NOEs.

Table 7: List of NOEs used in the MD calculations on peptide **P4**

Residue	H-atom	Residue	H-atom	NOE($CDCl_3$)
Ala(1)	NH	Aic(2)	NH	Strong
Ala(1)	$C^{\alpha}H$	Aic(3)	NH	Medium
Ala(1)	$C^{\alpha}H$	Aic(2)	NH	Strong
Ala(3)	NH	Aic(4)	NH	Weak
Ala(3)	NH	Aic(2)	$^{\alpha}CH_2$(backbone)	Strong
Ala(3)	NH	Aic(2)	$^{\beta}CH_2$(backbone)	Medium
Ala(3)	$C^{\alpha}H$	Aic(4)	NH	Strong
Aic(4)	NH	Ala(5)	NH	Weak

Ala(5)	$C^{\alpha}H$	Aic(7)	NH	Medium
Ala(5)	NH	Aic(4)	$^{\alpha}CH_2$(backbone)	Strong
Ala(5)	NH	Aic(4)	$^{\beta}CH_2$(backbone)	Medium
Ala(5)	$C^{\alpha}H$	Aic(6)	NH	Strong
Ala(5)	NH	Aic(6)	NH	Strong
Aic(6)	NH	Ala(7)	Medium	Medium
Ala(7)	NH	Aic(6)	$C^{\alpha}H_2$(backbone	Strong
Ala(7)	NH	Aic(6)	$C^{\beta}H_2$(backbone)	Medium

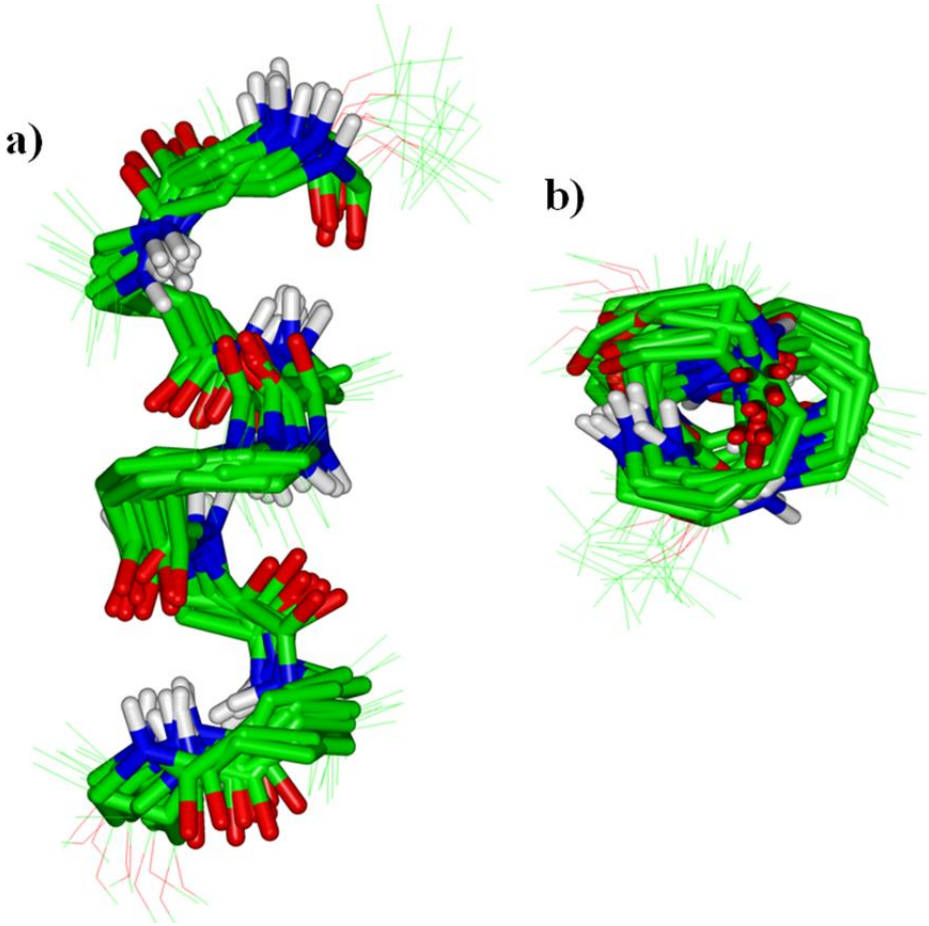

Figure 12. Solution conformations of peptides **P4**

Table 8. Backbone torsion angles (in degrees) of **P4** NMR solution structure ensembles generated from the best 10 models using NOEs and H-bonding constraints.

P4	ϕ	θ_1	θ_2	ψ
Ala1	-79.8±22.1			139.7±17.15
Aic 2	69.9±13.6	31.6±16.6	56.6±13.5	-119.8±25.8
Ala 3	-67.9±22.36			140.1±14.9
Aic 4	65.6±19.5	29.1±20.0	54.6±6.3	-123.9±29.7
Ala 5	-75.8±29.1			141.6±14.3
Aic 6	69.2±30.5	29.4±14.6	53.5±8.7	-115.8±11.8
Ala 7	-79.8±22.5			150.4±23.6

4.3.5 Solution NMR structure of peptide P5

To understand whether still longer sequences of α,γ[4,4]-hybrid peptides adopt a 12/10-helix conformation in solution, the nonapeptide **P5** was subjected to 2D NMR analysis in $CDCl_3$. Peptide **P5** also displayed a well-dispersed ^1H NMR spectrum in $CDCl_3$, indicating an ordered structure in solution. Partial TOCSY spectrum (amide region) of **P5** is shown in Figure 13. In addition to the strong NH↔NH NOEs between α-NH(*i*)↔γ-NH(*i+1*), weak NH↔NH NOEs were observed between the γ-NH(*i*)↔α-NH(*i+1*) residues along the peptide sequence (Figure 14). Medium long range $C^{\alpha}H$↔NH (Figure 15) interactions appeared between the residues Leu(1)$C^{\alpha}H$↔Leu(3)NH and Leu(7)$C^{\alpha}H$↔Aib(9)NH, respectively. A list of the NOEs observed in the ROESY spectrum is in the Table 9. Similar to the other peptides (**P3** and **P4**), no pronounced changes of the chemical shifts were observed for the amide NHs in DMSO-d_6 titrations (again except Boc-NH), indicating that all NHs are involved in intramolecular H-bonding (Figure 16). The overlay of the ten lowest energy minimized structures of **P5** derived from the observed NOEs is shown in Figure 17. The torsion angles of **P5** were found to be very similar to those of **P3** and **P4**. They are given in the Table 10.

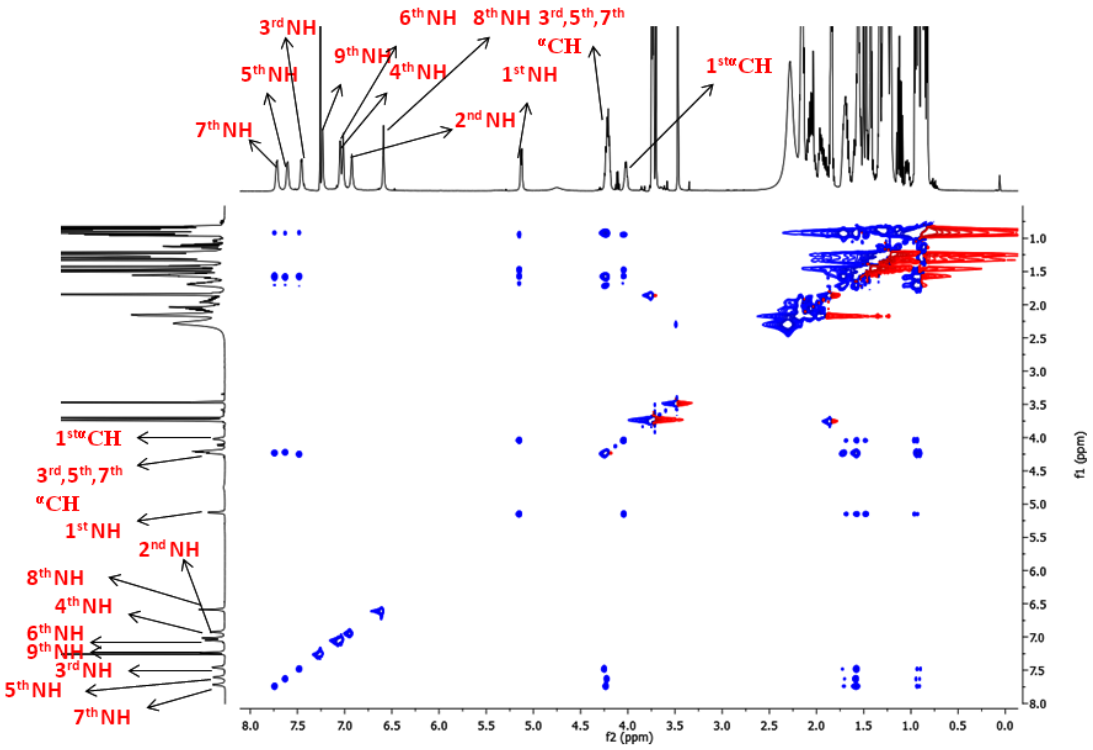

Figure 13: TOCSY spectrum of peptide **P5** (5 mM) in $CDCl_3$.

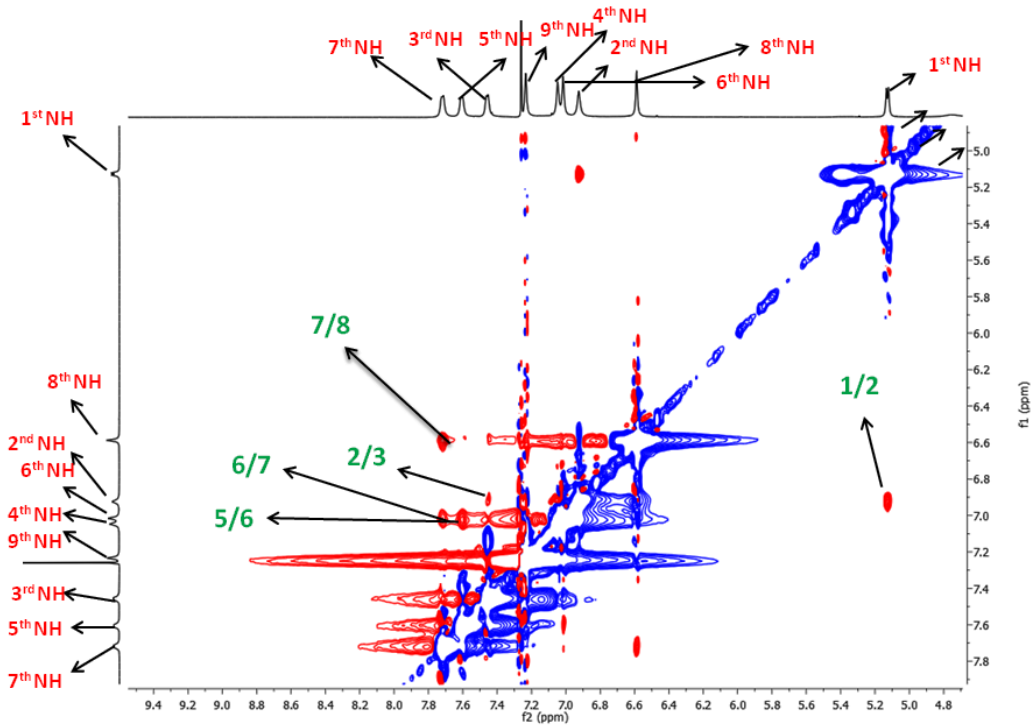

Figure 14: Partial ROESY spectrum of **P5** (5 mM) in $CDCl_3$ showing NH↔NH NOEs.

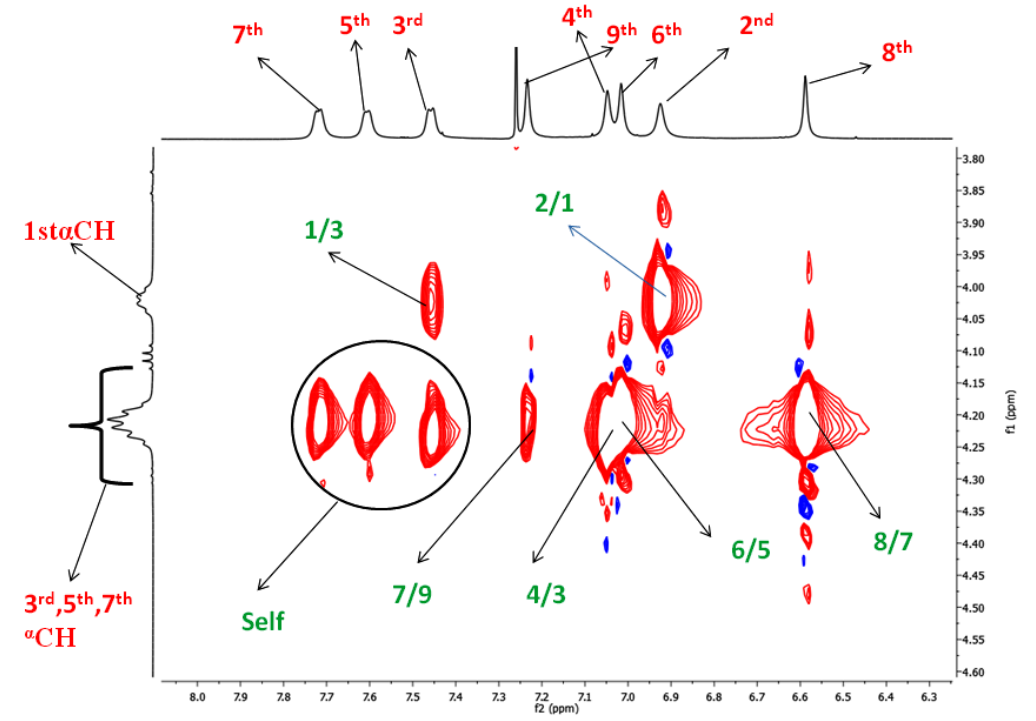

Figure 15: Partial ROESY spectrum of **P5** (5 mM) in $CDCl_3$ showing $C^{\alpha}H$↔ NH NOEs.

Table 9: List of NOEs used in the MD calculations on peptide **P5**

Residue	H-atom	Residue	H-atom	NOE($CDCl_3$)
Leu(1)	NH	Aic(2)	NH	Strong
Leu(1)	$C^{\alpha}H$	Leu(3)	NH	Medium
Leu(1)	$C^{\alpha}H$	Aic(2)	NH	Strong
Leu(1)	NH	Aic(2)	$C^{\alpha}H_2$(backbone)	Medium
Leu(1)	NH	Aic(2)	$C^{\beta}H_2$(backbone)	Medium
Aic(2)	NH	Leu(3)	NH	Weak
Leu(3)	NH	Aic(2)	$C^{\alpha}H_2$(backbone)	Strong
Leu(3)	NH	Aic(2)	$C^{\beta}H_2$(backbone)	Strong
Leu(3)	$C^{\alpha}H$	Aic(4)	NH	Strong
Leu(5)	NH	Aic(4)	$C^{\alpha}H_2$(backbone)	Strong
Leu(5)	NH	Aic(4)	$C^{\beta}H_2$(backbone)	Strong
Leu(5)	$C^{\alpha}H$	Aic(6)	NH	Strong
Leu(5)	NH	Aic(6)	NH	Strong
Aic(6)	NH	Leu(7)	NH	Weak
Leu(7)	NH	Aic(6)	$C^{\alpha}H_2$(backbone	Strong
Leu(7)	NH	Aic(6)	$C^{\beta}H_2$(backbone)	Strong
Leu(7)	$C^{\alpha}H$	Aib(9)	NH	Medium
Leu(7)	$C^{\alpha}H$	Aic(8)	NH	Strong

Leu(7)	NH	Aic(8)	NH	Strong
Aic(8)	NH	Aib(9)	NH	Weak
Aib(9)	NH	Aic(8)	$C^{\alpha}H_2$(backbone	Strong
Aib(9)	NH	Aic(8)	$C^{\beta}H_2$(backbone)	Strong

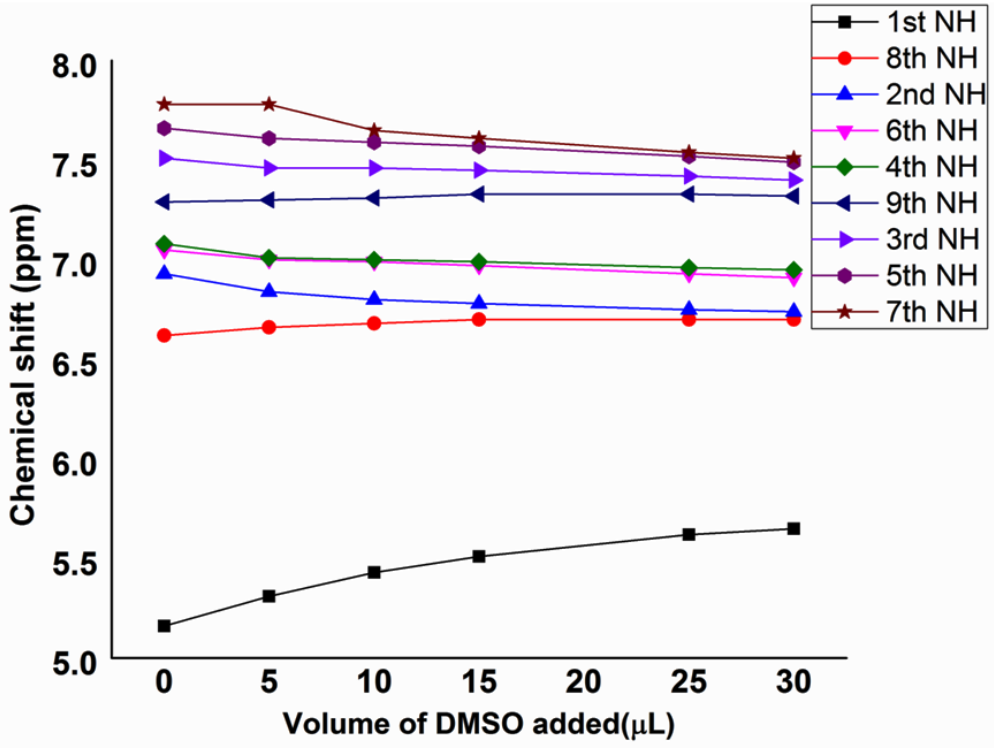

Figure 16 Solvent dependence of NH chemical shifts of the peptide **P5** at varying concentrations of $(CD_3)_2SO$.

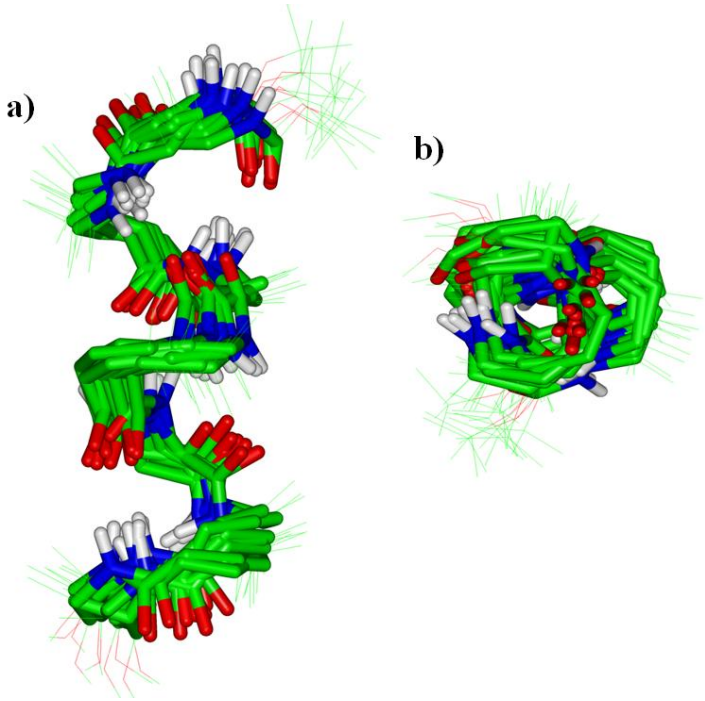

Figure 17 a) Solution conformations of peptides **P5.** B) Top of **P5** 12/10-hybrid helix.

Table 10 Backbone torsion angles (in degrees) of **P5** NMR solution structure ensembles generated from the 10 best models using NOEs and H-bonding constraints.

P5	ϕ	θ_1	θ_2	ψ
Leu 1	-89.2±22.6			137.7±1.2
Aic 2	77.7±13.3	28.6±15.17	48.8±15.1	-113.4±18.2
Leu 3	-80.5±13.0			148.7±20.8
Aic 4	53.1±13.4	38.8±7.7	41.3±11.3	-115.8±15.5
Leu 5	-84.2±14.5			150.8±19.9
Aic 6	67.6±14.1	31.8±12.3	45.8±13.6	-114.6±17.7
Leu 7	-85.0±13.5			148.2±23.5
Aic 8	76.3±25.9	19.4±13.2	49.1±13.1	-113.6±16.6
Aib 9	-96.3±31.5			133.3±42.6

4.3.6 Single crystal X-ray analysis of peptide P6.

The structural data for peptides **P1**-**P5** show that the combination of various chiral natural amino acids with the achiral $\gamma^{4,4}$-amino acid Aic in 1:1 alternation leads to 12/10-helices with alternately changing H-bond directionality both in the solid state and in the solvent chloroform. This is completely different from the folding behaviour of $\alpha,\gamma^{4,4}$-hybrid peptides composed of achiral α-amino acid constituents, as for instance Aib, and the γ-amino acid constituent Aic in our former studies[3r]. As already mentioned in the previous chapter unidirectional hydrogen bonding has been observed in both 12- and 15/17-helices of Aib/Aic-hybrid peptides.

The obviously different folding behavior of α,γ-hybrid peptides dependent on the stereochemistry of the α-amino acid constituent motivated us to investigate the structure of another achiral $\alpha,\gamma^{4,4}$-hybrid peptide composed of the sterically constrained dialkyl substituted α-amino acid, Ac_6c, instead of Aib employed in the former studies. The

corresponding nonapeptide **P6** (Scheme 1) provided single crystals in ethyl acetate/methanol solution. Its X-ray structure is shown in Figure 18. In contrast to peptides **P1**-**P5**, peptide **P6** adopted the same novel unidirectional 12-helix in single crystals as it has recently been found in the Aib/Aic-hybrid peptides for the first time.[3r] This 12-helix is stabilized by eight 4→1 intramolecular H-bonds (Figure 18b). The distances of the H-bonds $Ac_6cCO(i)\cdots HNAic(i+3)$ are longer in comparison to the $AicCO(i)\cdots NHAc_6c(i+3)$ distances (Table 11). Thus, a pattern of alternately changing stronger and weaker H-bonds can be observed in this helix type. The backbone conformations of Ac_6c and Aic residues in this 12-helix are completely different from those in the 12/10-helices. The torsion angles of **P6** are tabulated in the Table 12. The average torsion angles for the Ac_6c residues are ϕ = -56°±5° and ψ = -42°±6°, corresponding to an α-helix, whereas the PP_{II} conformation of the α-amino acid constituent was preferred in the 12/10-helix (Figure 18c, d). The torsion angle values for the Aic residues are ϕ = -56±6°, θ_1 = -56±6, θ_2 = 143°±16°, ψ = -115°±8°. These torsion angle values also differ from those in the corresponding 12-helix alternatives.[1n,3g,h,i,k,l,m,n,r] The torsion angle θ_2 of the Aic residues corresponds to an extended conformation, whereas gauche conformations occur in the 12/10-helix and the 12-helix alternative. The structure analysis of peptides **P1**-**P6** reveals that the α-amino acid residues obviously dictate the conformational behavior of the Aic residues in α,γ-hybrid peptides.

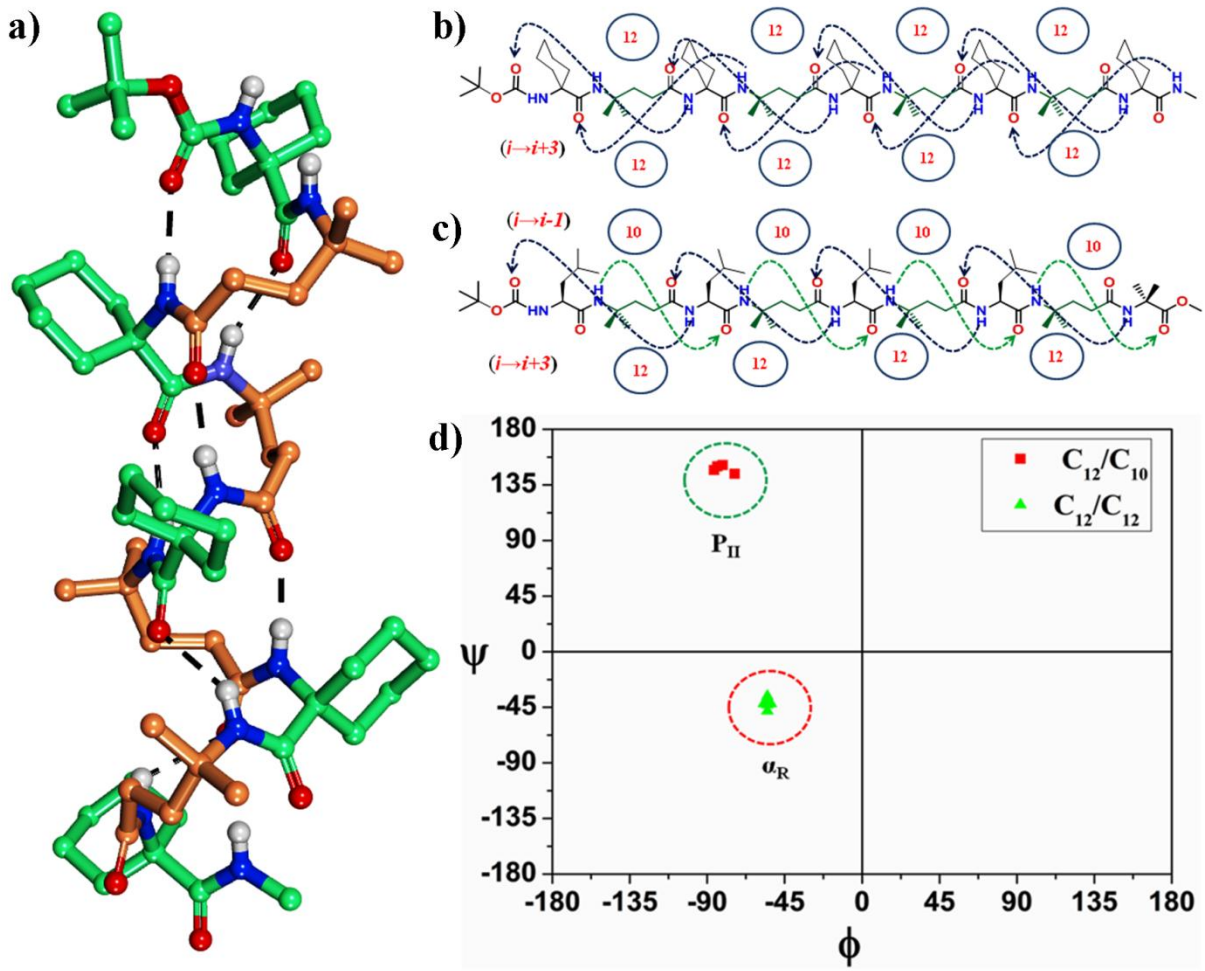

Figure 18. a) X-ray structure peptide **P6**. (a) Intramolecular hydrogen bonding in the 12/10-helix of **P5**. c) 12-helix in **P6**. d) Ramachandran plot for the α residues in the 12/10- (**P1** and **P2**) and 12-helices **P6**.

Table 11: Intramolecular hydrogen bond parameters of **P6**

Donor (D)	Acceptor (A)	D···A (Å)	DH···A (Å)	NH···O (deg)
N3	O2	2.91	2.02	170
N4	O3	3.06	2.21	163
N5	O4	2.86	1.99	170
N6	O5	3.15	2.32	158
N7	O6	2.85	1.98	171
N8	O7	3.09	2.34	143
N10	O8	3.27	2.41	168

Table 12: Backbone torsion angles (in degrees) of peptide **P6**

Residue	ϕ	θ_1	θ_2	ψ
Ac_6c 1	-59	-	-	-43
Aic 2	-49	34	50	-107
Ac_6c 3	-55	-	-	-44
Aic 4	-54	-49	143	-103
Ac_6c 5	-55			-36
Aic 6	-45	-49	127	-125
Ac_6c 7	-57			-42
Aic 8	-63	-64	156	-123

Ac_6c 9	-54			-42

4.3.7 Theoretical studies

It is not really possible to estimate a priori the stability relationships between mixed helices and their unidirectional helix alternatives for a given backbone by intuition. From the very beginning of foldamer research, the competition of mixed and uniform helices in folding was subject of theoretical studies on a wide variety of foldamer backbones[1n,2e,3a,5,7] In numerous cases, mixed helices were predicted to be more stable than their unidirectional counterparts in the gas phase and in apolar media. A very impressive example from nature is the gramicidin A channel passing apolar membrane regions realized by mixed 20/22-helices of α-peptides. The energetic advantages of mixed helices may disappear in polar environments. Since all local dipoles of unidirectional helices point into the same direction, their addition leads to higher total dipole moments than in the mixed helix alternatives with alternately changing H-bond directions, where the local dipole moments compensate each other. Therefore, unidirectional helices could be preferred in polar media due to their better electrostatic interactions with polar solvent molecules. This is well confirmed by our recent results, demonstrating that 12/10-helices lose their stability in polar solvents and are even transformed into unfolded structures by introducing aromatic α-amino acids.[8]

Our quantum chemical calculations on the helix formation in achiral Aib/Aic-foldamers[3r] of different sequence length showed that the unidirectional 12- and 15/17-helices are distinctly preferred over the mixed 12/10-helix even in the gas phase and in apolar media (Table 13). As expected, this effect is strengthened in polar solvents. Obviously, 12/10-helices cannot be realized in these backbones. We have repeated these calculations for Ala/Aic oligomers of different sequence length at the same B3LYP/6-31G* approximation level of ab initio MO theory and obtained different results (Table 13). In good agreement with the X-ray and NMR data, the mixed 12/10-helices are distinctly favored now over the unidirectional 12-helices in the gas phase. The right-handed 12/10-helix type is preferred over the left-handed 12/10-helix alternative. The values for the backbone torsion angles are given in Tables 2 and 3. The calculations provide longer hydrogen bonds in the 10-membered hydrogen-bonded rings than in the 12-membered pseudocycles, as was also found in the NMR and X-ray studies. Obviously, hydrogen bonds can better be realized in larger 12-rings than in smaller 10-rings

and are, therefore, more stable in 12-rings. The rough estimation of the influence of solvent $CHCl_3$ on the helix stabilities based on the quantum chemical SMD continuum solvation model[9] predicts comparable stability for both helix types (Table 13) with a slight preference of the 12/10-helix in shorter and a slight preference of the 12-helix in longer sequences. This agrees quite well with the NMR data, which still indicate the 12/10-helix in chloroform.

Table 13. Energy differences between the 12/10- and 12-helices of Ala/Aic-hybrid and Aib/Aic-hybrid peptides of different sequence length calculated at the B3LYP/6-31G* level of ab initio MO theory in the gas phase and in solution.

Oligomer	ΔE[a]		
	Ala/Aic		Aib/Aic
	H_{12}-$H_{12/10}$[b]	H_{12}-$H_{12/10}$[c]	H_{12}-$H_{12/10}$[b]
n = 4	20.0	0.5	-4.6
n = 5	26.2	0.3	-4.2
n = 6	31.4	1.0	-11.3
n = 7	34.9	0.0	-14.2
n = 8	37.7	-0.8	-23.8
n = 9	40.4	-1.0	-27.4
n = 10	41.5	-2.1	-36.5
n = 11	43.4	-3.0	-41.5

[a] In kJ/mol; data for blocked Ala/Aic- and Aib/Aic-oligomers in 1:1 alternation at the B3LYP/6-31G* level of ab initio MO theory; for total energies, see Supporting information and ref. 3r. [b] Gas phase. [c]Solvent $CHCl_3$ based on the SMD/B3LYP/6-31G* continuum model.[9]

At first sight, it may be astonishing that relatively small structural modifications as the change from the α-dimethyl substituted amino acids Aib and Ac_6c to the α-monosubstituted native amino acids Ala or Leu can so enormously influence the folding behavior. A very interesting observation by Martinek and Fülöp and their coworkers denoted as "stereochemical patterning" may be helpful for an explanation.[10] These authors correlated in their work the H-bond directionality of foldamer helices with the signs of the backbone

torsion angles ϕ and ψ of the constituents flanking the peptide bonds in the sequence. If all four ϕ,ψ angles of the adjacent residues *i* and (*i*+1) have the same sign (all-plus or all-minus), structures with unidirectional hydrogen bonds should be formed. If the signs of the four torsion angles are alternating (residue *i*: +,–; residue (*i*+1): –,+ or residue *i*: –,–; residue (*i*+1): +,+ and vice versa), the H-bond directionality alternately changes. Meanwhile, a rather complete overview on the helical folding alternatives and their structures was obtained for a wide variety of foldamer backbones (β-, γ-, δ-, ε-, α,β-, α,γ-, α,δ-, α,ε-peptides) employing systematic quantum chemical calculations.[1n,2e,3a,5,7] The backbone torsion angles from these studies convincingly confirm the hypothesis of Martinek and Fülöp and also the backbone torsion angles of the 12/10- and 12-helices in the present study fit into this concept.

Of course, the stereochemical patterning concept can only a posteriori be confirmed for achiral or sterically unconstrained backbones and has no predictive power for a rational design of unidirectional helices or mixed helices for such backbones. However, this situation changes if stereochemically defined or backbone-constrained constituents with fixed or at least clearly preferred backbone torsion angles are employed in peptide design. Combination of such constituents following the rules of Martinek and Fülöp can lead then to a desired helix type. This was recently shown by Gellman and coworkers for α,γ-peptides consisting of the α-amino acid Phe and γ-amino acid constituents with a stereochemically defined backbone.[3q] It was demonstrated that a transition of a uniform 12-helix into a mixed 12/10-helix occurs by only changing the configuration of the backbone γ-carbon atom in their γ-amino acid constituents. This leads to a change of the sign of backbone torsion angle φ, excluding the formation of the 12-helix, when following Martinek and Fülöp´s hypothesis. Now, the formation of a 12/10-helix becomes possible, provided that the α-amino acid constituents Phe follow the dictation of the γ-amino acid residues and adopt their torsion angles accordingly. This is obviously the case.

An opposite situation seems to exist in the Ala/Aic-, Leu/Aic-, Aib/Aic, and Ac_6c/Aic-hybrid peptides of our studies. Here, the α-amino acid constituents determine the folding behavior of the γ-amino acid constituents, inducing 12-helices for Aib/Aic- and Ac_6c/Aic-hybrid peptides, but 12/10-helices for Ala/Aic- and Leu/Aic-peptides. However, we have to consider that the α- and γ-amino acid constituents can principally adopt both helix alternatives in our cases because there are neither essentially steric nor stereochemical backbone restrictions. Therefore, it is not a priori clear which constituents determine folding. It is well-known that α-disubstituted amino acids like Aib or Ac_6c distinctly prefer the

formation of 3_{10}-helices with minus signs of the backbone torsion angles.[11] Obviously, this tendency is decisive and the unconstrained backbones of the γ-amino acid constituents also fold into a conformation with minus signs of the ϕ and ψ backbone torsion angles, enabling the 12-helices in Aib/Aic- and Ac_6c-hybrid peptides. The situation is not so clear for the native α-amino acids Ala and Leu, above all when remembering the behavior of the native amino acid Phe in the examples discussed above, which adopts both 12/10- and 12-helix conformations, depending on the backbone stereochemistry of the γ-amino acid constituents. In the Ala/Aic- and Leu/Aic-peptides without essential backbone restrictions, both folding alternatives, i.e. both sign sequences according to the stereochemical patterning hypothesis, are principally possible and it remains open at first which of them will be realized. We know from very precise quantum chemical calculations on blocked α-amino acid and dipeptide models in the gas phase and in solution, that the conformational range of the poly-proline helix (P_{II}) and the right-handed α- or 3_{10}-helices (α_R) are distinctly favored in solution over all other conformation alternatives[1n,12] In apolar media, the P_{II} conformation, required in mixed 12/10-helices, is more favored, in more polar solvents the stability changes in favor of α- or 3_{10}-helical conformations. These general findings are well reflected by the experimental and theoretical results obtained for our hybrid peptides showing the preference of the 12/10-helices with P_{II} conformation of the α-amino acid constituents in single crystals and in the solvent chloroform. As in the case of the 12-helix of the Aib/Aic- and Ac_6c/Aic-hybrid peptides, the γ-amino acid constituents adopt the helix conformation dictated by the α-amino acid constituents. However, the discussion of our results shows that the folding behavior is determined by a delicate balance of various structural and environmental effects.

4.4 Conclusions

The structural analysis of $\alpha,\gamma^{4,4}$-hybrid peptides composed of natural aliphatic α-amino acids and the 4,4-dialkyl substituted γ-amino acid Aic revealed 12/10-helices with alternating H-bond directionality. The helical structure is stabilized by 12-membered ($i \rightarrow i+3$) H-bonds in forward direction and 10-membered ($i \rightarrow i-1$) in backward direction. Both solution and X-ray structures suggest that the 10-membered H-bonds are weaker than the 12-membered H-bonds. Alternately changing intramolecular H-bond directions occur seldom in natural peptides, but occur more frequently in foldamers of different type. Replacing the chiral aliphatic α-amino acid constituents in the $\alpha,\gamma^{4,4}$-hybrid peptides by achiral dialkyl α-amino acids leads to stable 12-helical conformations. Obviously, the various helix types in $\alpha,\gamma^{4,4}$-

hybrid peptides are dictated by the nature of the α-residues in the sequence. In contrast to the helix-promoting amino acid Aib, its doubly homologated analogue Aic is a highly flexible and can adopt 12/10-, 12-, and 15/17-helical conformations in α,$\gamma^{4,4}$-hybrid peptides dependent on the nature of the α-amino acid residues. The reported results open new possibilities to design different helix types by careful selection of the α-amino acid components in α,γ-hybrid peptide foldamers.

4.5 Experimental Section

NMR spectroscopy

All NMR studies were carried out by using either 400, 600, and 800 MHz spectrometers. Resonance assignments were obtained by TOCSY and ROESY analysis. All two-dimensional data were collected in phase-sensitive mode by using the time-proportional phase incrementation (TPPI) method. Sets of 1024 and 512 data points were used in the t2 and t1 dimensions, respectively. For TOCSY and ROESY analysis, 32 and 72 transients were collected, respectively. A spectral width of 6007 Hz was used in both dimensions. Spin-lock times of 200 and 250 ms were used to obtain ROESY spectra. Zero-filling was carried out to finally yield a data set of 2 K × 1 K. A shifted square-sine-bell window was used before processing.

NMR structure calculations

Solution structures of **P2** and **P3** were derived by molecular modeling and subsequent restrained molecular dynamics simulations using Discover Studio/Insight II (Accelaries Int.). Initial conformations were generated from their fully extended structures by applying NOE and H-bond restraints. Minimizations were done first with steepest descent, followed by conjugate gradient methods for a maximum of 10000 iterations each or RMS deviation of 0.001 kcal/mol, whichever was earlier. The cvff force field with default parameters was used throughout the simulations. A number of interatomic distance constraints obtained from NMR data was used as restraints in the minimization as well as MD runs. The energy-minimized structures were then subjected to MD simulations. For MD runs, a temperature of 300 K was selected. The molecules were initially equilibrated for 50 ps and subsequently subjected to an 1 ns dynamics with a step size of 1 fs, sampling the trajectory at equal

intervals of 10 ps. Within the trajectory 100 structures were generated and the best ten structures having lower energies and compatible NMR data were selected to superimpose.

4.5.1 Crystal structure analysis of peptide P1, P2 and P6

Crystal structure analysis of P1

Crystals of peptide **P1** were grown by slow evaporation from chloroform/n-heptane solution. A single crystal (0.22 × 0.08 × 0.12 mm) was mounted on loop with a small amount of paraffin oil. The X-ray data were collected at 100 K on a Bruker APEX(II) DUO CCD diffractometer using CuK_α radiation (λ = 1.54178 Å), ω-scans (2θ = 135.358), for a total of 10727 independent reflections. Space group P21, a = 11.3016(14), b = 16.4062(17), c = 16.946(2), α = 90, β = 90.027(8), γ = 90, V = 3142.1(7)Å^3, monoclinic, Z = 2 for chemical formula $C_{46}H_{83}N_8O_{14}$, with two molecules in an asymmetric unit; ρ_{calcd} = 1.028 g·cm^{-3}, μ = 0.626 mm^{-1}, F (000) = 1054. The structure was obtained by direct methods using SHELXS-97.[13] The final R value was 0.1038 (wR2 = 0.2252), 4341 observed reflections ($F_0 \geq 4\sigma$ ($|F_0|$)) and 633 variables, S = 0.918. The largest difference peak and hole were 0.283 and -0.322eÅ^3, respectively. CCDC No 1581664

There is also some partially occupied solvent molecule present in the asymmetric unit. A significant amount of time was invested in identifying and refining the disordered molecule. Option SQUEEZE of program PLATON was used to correct the diffraction data for diffuse scattering effects and to identify the solvent molecule. PLATON calculated the upper limit of volume that can be occupied by the solvent to be 526.3 Å^3 or 16.75% of the unit cell volume. The program calculated 154 electrons in the unit cell for the diffuse species. No data are given for the diffusely scattering species. Outputs of SQUEEZE report are appended in the CIF file **P1**.

Crystal structure analysis of P2

Crystals of peptide **P2** were grown by slow evaporation from mixture chloroform/n-heptane solution. A single crystal (0.30 × 0.06 × 0.14 mm) was mounted on loop with a small amount of paraffin oil. The X-ray data were collected at 100 K on a Bruker APEX(II) DUO CCD diffractometer using CuK_α radiation (λ = 1.54178 Å), ω-scans (2θ = 135.358), for a total of 7397 independent reflections. Space group P21, a = 13.932(10), b = 16.950(3), c = 19.208(3), α = 90, β = 105.824(9), γ = 90,V = 3633.9(9) Å^3, triclinic, Z = 2 for chemical formula $C_{62}H_{115}N_8O_{14}$ with two molecules in an asymmetric unit; ρ_{calcd} = 1.094g·cm^{-3}, μ = 0.621mm^{-1}, F (000) = 1606. The structure was obtained by direct methods using SHELXS-97.[17] The final

R value was 0.0941 (wR2 = 0.2065), 7397 observed reflections ($F_0 \geq 4\sigma$ ($|F_0|$)) and 789 variables, S = 1.114. The largest difference peak and hole were 0.501 and - 0.373 Å^3, respectively. CCDC No 1581665

The investigated single crystal was small-sized and poorly diffracting. Numerous data sets were collected on single crystals from different batches and that of highest quality is reported here.

Crystal structure analysis of P6

Crystals of peptide **P6** were grown by slow evaporation from a solution of aqueous methanol. A single crystal (0.33 × 0.08 × 0.14 mm) was mounted on loop with a small amount of paraffin oil. The X-ray data were collected at 100 K on a Bruker APEX(II) DUO CCD diffractometer using MoK_α radiation (λ = 0.71073 Å), ω-scans (2θ = 56.674), for a total of 17192 independent reflections. Space group P b c a, a = 21.016(2), b = 15.6295(14), c = 42.166(4), α = 90, β = 90, γ = 90, V = 13850(2)Å^3, triclinic, Z = 8 for chemical formula $C_{65}H_{112}N_{10}O_{11}$, with two molecules in an asymmetric unit; ρ_{calcd} = 1.160 g·cm^{-3}, μ = 0.079 mm^{-1}, F (000) = 6094. The structure was obtained by direct methods using SHELXS-97.[17] The final R value was 0.0741 (wR2 = 0.1870), 9934 observed reflections ($F_0 \geq 4\sigma$ ($|F_0|$)) and 787 variables, S = 1.241. The largest difference peak and hole were 0.417 and -0.409Å^3, respectively. CCDC No 1581666

4.5.2. Quantum chemical calculations

Complete geometry optimizations were performed on the right-handed and left-handed 12/10- and 12-helices for oligomers of Ala/Aic peptides in 1:1 alternation beginning with tetrapeptides and going until the undecapeptides. The influence of the solvent chloroform was estimated employing the SMD solvation model[S2] as it is implemented in the Gaussian09 program package.[S3] The geometries were also optimized in the SMD calculations. The right-handed helices are distinctly more stable than the left-handed helices. Therefore, only the data for the right-handed helices are given here.

Table 14: Total energies for the right-handed 12/10-helices of Ala/Aic oligomers in the gas phase and in the solvent chloroform at the B3LYP/6-31G* and SMD/B3LYP/6-31G* levels of ab initio MO theory

Oligomer	E_T[a]	E_T[b]
n = 4	-1666.908130	-1666.938326
n = 5	-1914.245801	-1914.278600
n = 6	-2279.519498	-2279.557185
n = 7	-2526.856993	-2526.897279
n = 8	-2892.130636	-2892.175680
n = 9	-3139.468343	-3139.516123
n = 10	-3504.741736	-3504.794499
n = 11	-3752.079525	-3752.134841

[a] Gas phase data for blocked Ala/Aic-oligomers in 1:1 alternation. [b] Data for solvent $CHCl_3$ based on the SMD/B3LYP/6-31G* continuum model.[S2]

Table 15: Hydrogen bond distances DH···A in Å for the Ala/Aic-heptapeptide

H-Brücke[a]	Ring size	Distance
1	12	1.931
2	10	2.041
3	12	1.926
4	10	2.017
5	12	1.937
6	10	2.021

4.5.3 General procedure for the syntheses of peptides P1-P5

The γ-amino acid Aic (4-aminoisocaproic acid) was synthesized by previously described procedures.[S1] Peptide synthesis was carried out using conventional solution-phase procedures. The *tert*-butyloxycarbonyl (Boc) group was used for the N terminal protection and the C terminus was protected using a methyl/ethyl ester groups. Protecting groups were removed with trifluoroacetic acid and saponification for the N- and C-termini, respectively. Couplings were carried out by using *N*-ethyl-*N*'-(3-dimethylaminopropyl)carbodiimide hydrochloride (EDC) and 1-hydroxybenzotriazole(HOBt). The dipeptides were synthesized by a condensation strategy involving Boc-Leu-OH or Boc-Ala-OH and NH_2-Aic-OEt, employing EDC/HOBt as coupling reagents and DMF as solvent. The obtained dipeptides were used further without purification. The tetra-, hepta- and nonapeptides were synthesized using a similar protocol. Finally, all peptides were purified by RP-HPLC using MeOH/H_2O system.

4.5.6 NMR details for peptides P1-P5

Peptide P1

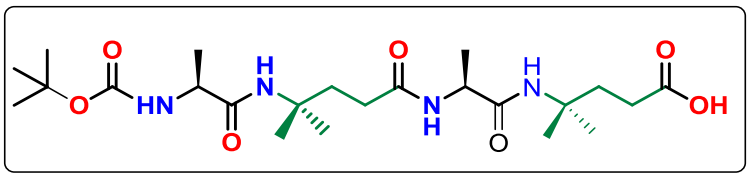

^{1}H NMR (400 MHz, DMSO-d_6) δ 12.03 (s, 1H), 7.74 (d, J = 8 Hz, 1H), 7.31 (s, 1H), 6.65 – (d, J = 8 Hz, 1H), 4.22 – 4.11 (m, 1H), 3.89 – 3.84 (m, 1H), 2.11 – 2.0 (m, 4H), 1.85 – 1.77 (m, 4H), 1.33 (bs, 12H), 1.15-1.08 (m, 24H), MALDI TOF/TOF- *m/z* calcd. for $C_{23}H_{42}N_4O_7$ $[M+Na]^+$ 509.29, obsvd. 509.30

Peptide P2

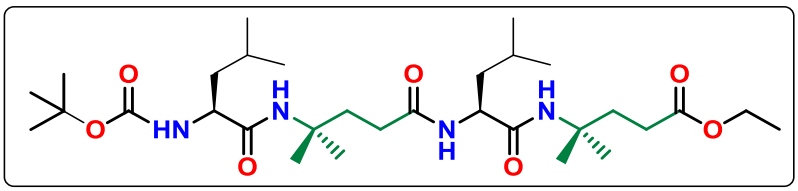

^{1}H NMR (600 MHz, Chloroform-*d*) δ 7.26 (d, J = 6 Hz, 1H), 6.91 (s, 1H), 6.09 (s, 1H), 5.02 (d, J = 6 Hz, 1H), 4.36-4.32 (m, 1H), 4.14 (q, J = 7.1 Hz, 2H), 4.11 – 4.07 (m, 1H), 2.09 – 1.96 (m, 3H), 1.70 (m, J = 13.3, 6.7 Hz, 2H), 1.66 – 1.57 (m, 2H), 1.45 (s, 12H), 1.37 (s, 3H),

1.33 (d, *J* = 4.8 Hz, 6H), 1.27 (t, *J* = 7.1 Hz, 4H), 1.18 (s, 3H), 1.02 – 0.92 (m, 15H), MALDI TOF/TOF- *m/z* calcd. for $C_{35}H_{55}N_4O_7$ $[M+Na]^+$ 621.42, obsvd. 621.44

Peptide P3

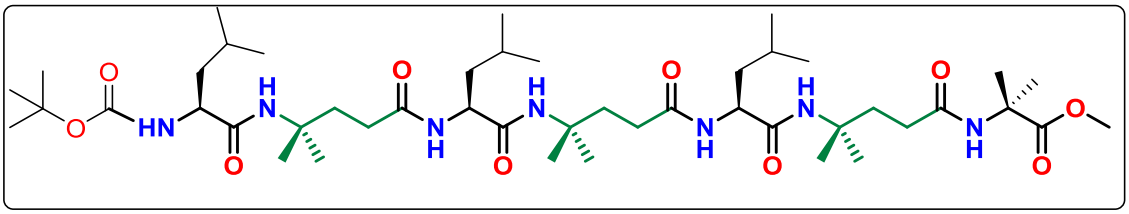

^{1}H NMR (600 MHz, Chloroform-*d*) *δ* 7.53 (m, 1H), 7.37 (m, 1H), 7.18 (s, 1H), 6.98 (s, 1H), 6.82 (s, 1H), 6.63 (s, 1H), 5.11 (d, *J* = 6 Hz, 1H), 4.30-4.25 (m, 2H), 4.08 – 4.02 (m, 1H), 3.73 (s, 3H), 2.25 – 2.21 (m, 7H), 2.08 – 2.01 (m, 4H), 1.97 – 1.92 (m, 4H), 1.77 – 1.72 (m, 4H), 1.54 (s, 3H), 1.51 (s, 3H), 1.46 (s, 9H), 1.36 (d, *J* = 4.6 Hz, 6H), 1.32 (s, 3H), 1.29 (s, 3H), 1.26 (d, *J* = 8.7 Hz, 7H), 0.98 (d, *J* = 6.6 Hz, 4H), 0.96-0.91 (m, 15H), MALDI TOF/TOF- *m/z* calcd. for $C_{46}H_{85}N_7O_{10}$ $[M+Na]^+$ 918.62, obsvd. 918.68

Peptide P4

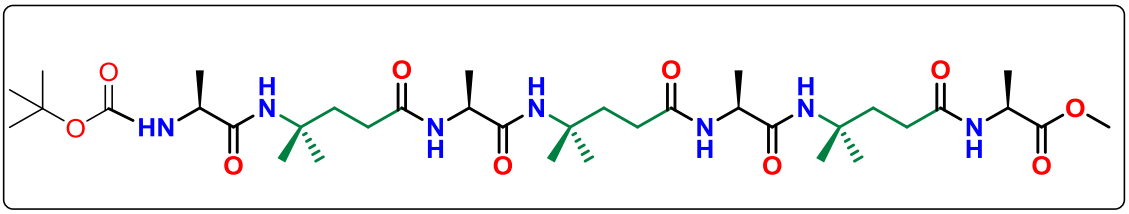

^{1}H NMR (700 MHz, Chloroform-*d*) *δ* 7.35 (d, *J* = 7Hz, 1H), 7.31 (d, *J* = 7Hz, 1H), 7.24 (d, *J* = 7Hz, 1H), 6. 81(s, 1H), 6.73 (s, 1H), 6.70 (s, 1H), 5.28 (d, *J* = 7Hz, 1H), 4.60 – 4.54 (m, 1H), 4.31 – 4.27 (m, 2H), 4.05 (m, 1H), 2.21 – 2.02 (m, 12H), 1.43 (s, 9H), 1.39 – 1.23 (m, 40H), MALDI TOF/TOF- *m/z* calcd. for $C_{36}H_{65}N_7O_{10}$ $[M+Na]^+$ 778.46, obsvd. 778.49

Peptide P5

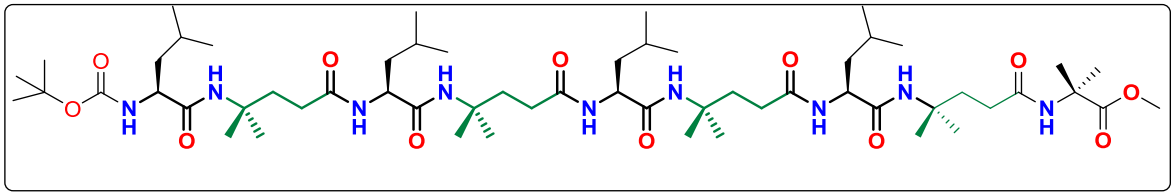

^{1}H NMR (600 MHz, Chloroform-*d*) δ 7.72 (d, *J* = 6 Hz, 1H), 7.61 (d, *J* = 6 Hz, 1H), 7.46 (d, *J* = 4 Hz, 1H), 7.23 (s, 1H), 7.05 (s, 1H), 7.02 (s, 1H), 6.92 (s, 1H), 6.59 (s, 1H), 5.13 (d, *J* = 6 Hz, 1H), 4.21 (m, 3H), 4.02 (m, 1H), 3.70 (s, 3H), 2.20 – 1.86 (m, 20H), 1.75 – 1.63 (m, 6H), 1.55 (m, 7H), 1.43 (s, 10H), 1.34 – 1.18 (m, 49H), 0.97 – 0.80 (m, 58H), MALDI TOF/TOF- *m/z* calcd. for $C_{58}H_{107}N_9O_{12}$ $[M+Na]^+$ 1144.79, obsvd. 1144.96

4.6 References

1. a) Gellman, S. H. *Acc. Chem. Res*. **1998**, *31*, 173; b) Cheng, R. P.; Gellman, S. H.; DeGrado, W. F. *Chem. Rev.* **2001**, *101*, 3219; c) Seebach, D.; Beck, A. K.; Bierbaum, D. J. *Chem. Biodiversity* **2004**, *1*, 1111. d) *Foldamers: Structure, Properties and Applications (Eds.: S. Hecht, I. Huc)*, Wiley-VCH, Weinheim, **2007**; e) Goodman, C. M.; Choi, S.; Shandler, S.; DeGrado, W. F.; *Nat. Chem. Biol*. **2007**, *3*, 252; f) Seebach, D.; Gardiner, J.; *Acc. Chem. Res*. **2008**, *41*, 1366; g) Horne, W. S.; Gellman, S. H. *Acc. Chem. Res*. **2008**, *41*, 1399; h) Vasudev, P. G.; Chatterjee, S.; Shamala, N.; Balaram, P. *Acc. Chem. Res*. **2009**, *42*, 1628; i) Vasudev, P. G.; Chatterjee, S.; Shamala, N.; Balaram, P. *Chem. Rev*. **2011**, *111*, 657. j) Guichard, G.; Huc, I. *Chem. Commun*. **2011**, *47*, 5933; k) Pilsl, L. K. A.; Reiser, O. *Amino Acids* **2011**, *41*, 709. l) Martinek, T. A.; Fülöp, F. *Chem. Soc. Rev*. **2012**, *41*, 687; m) Bouillère, F.; Thétiot-Laurent, S.; Kouklovsky, C.; Alezra, V. *Amino Acids* **2011**, *41*, 687. n) Baldauf, C. ; Hofmann, H.-J.; *Helv. Chim. Acta* **2012**, *95*, 2348.
2. a) De Pol, S.; Zorn, C.; Klein, C. D.; Zerbe, O.; Reiser, O. *Angew. Chem., Int. Ed.* **2004**, *43*, 511; b) Hayen, A.; Schmitt, M. A.; Ngassa, F. N.; Thomasson, K. A.; Gellman, S. H. *Angew. Chem., Int. Ed.* **2004**, *43*, 505; c) Schmitt, M. A.; Choi, S. H.; Guzei, I. A.; Gellman, S. H. *J. Am. Chem. Soc.* **2005**, *127*, 13310; d) Sharma, G. V. M.; Nagendar, P.; Jayaprakash, P.; Krishna, P. R.; Ramakrishna, K. V. S.; Kunwar, A. C. *Angew. Chem., Int. Ed.*, **2005**, *44*, 5878; e) Baldauf, C.; Günther, R.; Hofmann, H.-J. *Biopolymers* **2006**, *84*, 408; f) Srinivasulu, G.; Kumar, S. K.; Sharma, G. V. M.; Kunwar, A. C. *J. Org. Chem.* **2006**, *71*, 8395; g) Angelici, G.; Luppi, G.; Kaptein, B.; Broxtermann, Q. B.; Hofmann, H.-J.; Tomasini, C. *Eur. J.*

Org. Chem. **2007**, *16*, 2713; h) Choi, S. H.; Guzei, I. A.; Gellman, S. H. *J. Am. Chem. Soc.* **2007**, *129*, 13780; i) Jagadeesh, B.; Prabakhar, A.; Sharma, G. D.; Chandrasekhar, S.; Reddy, M. S.; Jagannadh, B. *Chem. Commun.* **2007**, 371; j) Choi, S. H.; Guzei, I. A.; Spencer, L. C.; Gellman, S. H. *J. Am. Chem. Soc.* **2008**, *130*, 6544; k) Lee, M.; Shim, J.; Kang, P.; Guzei, I. A.; Choi, S. H.; *Angew. Chem., Int. Ed*. **2013**, *52*, 12564; l) Legrand, B.; André, C.; Moulat, L.; Wenger, E.; Didierjean, C.; Aubert, E.; Averlant-Petit, M. C.; Martinez, J.; Calmes, M.; Amblard, M.; *Angew. Chem., Int. Ed*. **2014**, *53*, 13131; m) Balamurugan, D.; Muraleedharan, K. M. *Chem. Eur. J.* **2015**, 21, 9332; n) Wani, N. A.; Raghothama, S.; Singh, U. P.; Rai, R.; *Chem. Eur. J.* **2017**, DOI: 10.1002/chem.201700265.

3. a) Baldauf, C.; Günther, R.; Hofmann, H.-J. *J. Org. Chem.* **2006**, *71*, 1200; b) Sharma, G. V. M.; Jadhav, V. B.; Ramakrishna, K. V. S.; Jayaprakash, P.; Narsimulu, K.; Subash,V.; Kunwar, A. C.; *J. Am. Chem. Soc.* **2006**, *128*, 14657; c) Vasudev, P. G.; Ananda, K.; Chatterjee, S.; Aravinda, S.; Shamala, N.; Balaram, P. *J. Am. Chem. Soc.* **2007**, *129*, 4039; d) Chatterjee, S.; Vasudev, P. G.; Ragothama, S.; Shamala, N. Balaram, P. *Biopolymers* **2008**, *90*, 759; e) Chatterjee, S.; Vasudev, P. G.; Ananda, K.; Raghothama, S.; Shamala, N.; Balaram, P. *J. Org. Chem.* **2008**, *73*, 6595. f) Vasudev, P. G.; Chatterjee, S.; Ananda, K.; Shamala, N.; Balaram, P. *Angew. Chem., Int. Ed*. **2008**, *47*, 6430; g) Guo, L.; Chi, Y. G.; Almeida, A. M.; Guzei, I. A.; Parker, B. K.; Gellman, S. H. *J. Am. Chem. Soc*. **2009**, *131*, 16018; h) Chatterjee, S.; Vasudev, P. G.; Ragothama, S.; Ramakrishna, C.; Shamala, N.; Balaram, P. *J. Am. Chem. Soc.* **2009**, *131*, 5956; i) Guo, L.; Almeida, A. M.; Zhang, W.; Reidenbach, A. G.; Choi, S. H.; Guzei, I. A;. Gellman, S. H. *J. Am. Chem. Soc.* **2010**, *132*, 7868; j) Guo, L.; Zhang, W.; Guzei, I. A.; Spencer, L. C.; Gellman, S. H. *Org. Lett*. **2012**, *14*, 2582; k) Basuroy, K.; Dinesh, B.; Shamala, N.; Balaram, P. *Angew. Chem., Int. Ed*. **2012**, *51*, 8736. l) Bandyopadhyay, A.; Jadhav, S. V.; Gopi, H. N. *Chem. Commun.* **2012**, *48*, 7170. m) Jadhav, S. V.; Bandyopadhyay, A.; Gopi, H. N. *Org. Biomol. Chem*. **2013**, *11*, 509; n) Basuroy, K.; Dinesh, B.; Shamala, N.; Balaram, P. *Angew. Chem., Int. Ed.* **2013**, *52*, 3136; o) Giuliano, M. W.; Maynard, S. J.; Almeida, A. M.; Guo, L.; Guzei, I. A.; Spencer, L. C.; Gellman, S. H.; *J. Am. Chem. Soc*. **2014**, *136*, 15046; p) Sonti, R.; Dinesh, B.; Basuroy, K.; Raghothama, S.; Shamala, N.; Balaram, P. *Org. Lett*. **2014**, *16*, 1656; q) Fisher, B. F.; Guo, L.; Dolinar, B. S.; Guzei, I. A.; Gellman, S. H. *J. Am. Chem.*

Soc. **2015**, *137*, 6484; r) Misra, R.; Saseendran, A.; George, G.; Veeresh, K.; Raja, K. M. P.; Raghothama, S.; Hofmann, H.-J; Gopi, H. N. *Chem. Eur. J*. **201**7, *23*, 3764.

4. a) Horne, W. S.; Johnson, L. M.; Ketas, T. J.; Klasse, P. J.; Lu, M.; Moore, J. P.; Gellman, S. H. *Proc. Natl. Acad. Sci. USA* **2009**, *106*, 14751; b) Lee, E. F.; Sadowsky, J. D.; Smith, B. J.; Czabotar, P. E.; Peterson-Kaufman, K. J.; Colman, P. M.; Gellman, S. H.; Fairlie, W. D.; *Angew. Chem., Int. Ed*. **2009**, *48*, 4318; c) Horne, W. S.; Boersman, M. D.; Windsor, M. A.; Gellman, S. H. *Angew. Chem. Int. Ed*. **2008**, *47*, 2853; d) Haase, H. S.; Peterson-Kaufman, K. J.; Lan Levengood, S. K.; Checco, J. W.; Murphy, W. L.; Gellman, S. H. *J. Am. Chem. Soc*. **2012**, *134*, 7652; e) Werner, M.; Horne,W. S. *Curr. Opin. Chem. Biol*. **2015**, *28*, 75.
5. Baldauf, C.; Günther, R.; Hofmann, H.-J. *Angew. Chem., Int. Ed.* **2004**, *43*, 1594.
6. a) Seebach, D.; Gademann, K.; Schreiber, J. V.; Matthews, J. L.; Hintermann, T.; Jaun, B.; Oberer, L.; Hommel, U.; Widmer, H. *Helv. Chim. Acta* **1997**, *80*, 2033; b) Arvidsson, P. I.; Ryder, N. S.; Weiss, H. M.; Gross, G.; Kretz, O.; Woessner, R.; Seebach, D. *ChemBioChem* **2003**, *4*, 1345; c) Martinek, T. A.; Fülöp, F.; *Eur. J. Biochem*. **2003**, *270*, 3657; d) Sharma, G. V. M.; Reddy, K. R.; Krishna, P. R.; Sankar, A. R.; Jayaprakash, P.; Jagannadh, B.; Kunwar, A. C. *Angew. Chem., Int. Ed*. **2004**, *43*, 3961; e) Mandity, I. M.; Fülöp, L.; Vass, E.; Toth, G. K.; Martinek, T. A. F. Fülöp, *Org. Lett*. **2010**, *12*, 5584; f) Shin, S.; Lee, M.; Guzei, I. A.; Kang,Y. K. Choi, S. H. *J. Am. Chem. Soc.* **2016**, *138*, 13390; g) Thodupunuri, P.; S. Katukuri, K. Ramakrishna,V. S.; Sharma, G. V. M.; Kunwar, A. C.; Sarma, A. V. S.; Hofmann, H.-J *J. Org. Chem*. **2017**, *82*, 2018.
7. a) Wu,Y.-D.; Wang, D.-P.; *J. Am. Chem. Soc.* **1998**, *120*, 13485; b) Möhle, K.; Günther, R.; Thormann, M.; Sewald, N.; Hofmann, H.-J. *Biopolymers*, **1999**, *50*, 167; c) Wu,Y.-D.; Wang, D.-P. *J. Am. Chem. Soc.* **1999**, *121*, 9352; d) Baldauf, C.; Günther, R.; Hofmann, H.-J.; *Helv. Chim. Acta*, **2003**, *86*, 2573; e) Baldauf, C.; Günther, R.; Hofmann, H.-J. *J. Org. Chem.* **2004**, *69*, 6214; f) Baldauf, C.; Günther, R.; Hofmann, H.-J. *Biopolymers* **2005**, *80*, 675; g) Wu, Y.-D.; Han, W.; Wang, D.-P. Gao, Y.; Zhao, Y.-L- *Acc. Chem. Res.* **2008**, *41*, 1418; h) Baldauf, C.; Günther, R. Hofmann, H.-J. *J. Mol. Struct. (Theochem)* **2009**, *907*, 109; i) Sharma, G. V. M.; Babu, B. S.; Ramakrishna, K. V. S.; Nagendar, P.; Kunwar, A. C.; Schramm, P.; Baldauf, C.; Hofmann, H.-J. *Chem. Eur. J.* **2009**, *15*, 5552; j) Sharma,G. V. M.; Babu, B. S.; Chatterjee, D.; Ramakrishna, K. V. S.; Kunwar, A. C.; Schramm, P.;

Hofmann, H.-J. *J. Org. Chem.* **2009**, *74*, 6703; k) Schramm, P.; Sharma, G. V. M.; Hofmann, H.-J. *Biopolymers* **2010**, *94*, 279.

8. Misra, R.; Reja, R. M.; Narendra, L. V.; George, G.; Raghothama, S.; Gopi, H. N. *Chem. Commun*., **2016**, *52*, 9597.
9. Marenich, A. V.; Cramer, C. J.; Truhlar, D. G. *J. Phys. Chem. B* **2009**, *113*, 6378.
10. Mandity, I. M.; Weber, E.; Martinek, T. A.; Olajos, G.; Tóth,G. K.; Vass, E.; Fülöp, F. *Angew. Chem. Int. Ed.* **2009**, *48*, 2171.
11. a) Pavone,V.; Blasio, B.; Santini, A.; Benedetti, E.; Pedone, C.; Toniolo, C,; Crisma,. M. J. *J. Mol. Biol.* **1990**, *214*, 633; b) Karle, I. L.; Balaram, P. *Biochemistry* **1990**, *29*, 6747. c) Marshall, G. R.; Hodgkin, E. E.; Langs, D. A.; Smith,G. D.; Zabrocki, J.; Leplawy, M. T. *Proc. Natl. Acad. Sci. USA* **1990**, *87*, 487; d) Toniolo, C.; Crisma, M.; Formaggio, F.; Peggion, C.; *Biopolymers* **2001**, *60*, 396; e) Gessmann, R.; Breckner, H.; Petratos, K.; *J. Pept. Sci.* **2003**, *9*, 753; f) Aravinda, S.; Shamala, N.; Balaram, P. *Chem. Biodiversity* **2008**, *5*, 1238; g) Sola, J.; Helliwell, M. Clayden, J.; *Biopolymers* **2011**, *95*, 62.
12. Hudáky, I.; Hudáky, P.; Perczel, A.; *J. Comput. Chem.* **2004**, *25*, 1522; [13] G. M. Sheldrick, *Acta Crystallogr. Sec A*. **1990**, *46*, 467.
13. Frisch, M. J.; Trucks, G. W.; Schlegel H.B.; Scuseria, G. E.; Robb, M.A.; Cheeseman, J. R.; Scalmani, G.; Barone, V.; Mennucci, B.; Petersson, G. A.; Nakatsuji, H.; Caricato, M.; Li, X.; Hratchian, Izmaylov, A.F.; Bloino, J.; Zheng, K.; Sonnenberg, J. L.; Hada, M.; Ehara, M.; Toyota, K.; Fukuda, R.; Hasegawa, J.; Ishida, M.; Nakajima, T.; Honda, Y.; Kitao, O.; Nakai, T.; Vreven, J.; Montgomery, J. A.; Peralta, J. E.; Ogliaro, F.; Bearpark, M.; Heyd, J. J.; Brothers, E.; Kudin, K. N.; Staroverov, V. N.; Kobayashi, R.; Normand, J.; Rhaghavachari, K.; Rendell, K.; Burant, J. C.; Iyengar, S. S.; Tomasi, J.; Cossi, M.; Rega, N.; Millam, J. M.; Klene, M.; Knox, J. E.; Cross, J. B.; Bakken, V.; Adamo, C.; Jaramillo, J.; Gomperts, R.; Stratmann, R. E.; Yazyev, O.; Austin, A. J.; Cammi, R.; Pomelli, C.; Ochterski, J. W.; Martin, R. L.; Morokuma, K.; Zakrzewski, V. G.; Voth, G. A.; Salvador, P.; Dannenberg, J. J.; Dapprich, S.; Daniels, A. D.; Farkas, O.; Foresman, J. B.; Ortiz, J. V.; Cioslowski, J.; Fox, D. J. Gaussian09, Revision A.1, Gaussian Inc, Wallingford, CT, **2009**.

4.7 Appendix I: Mass spectra and ^{1}H NMR spectra for the peptides P1 to P5

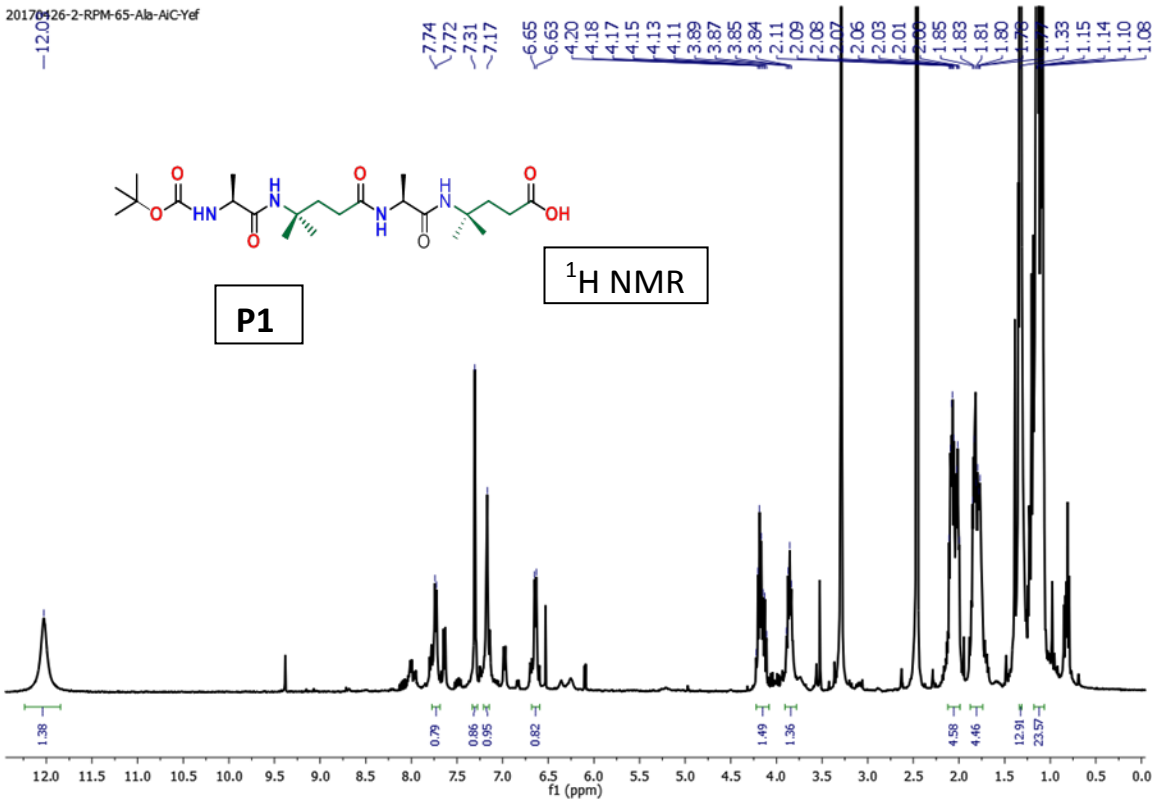

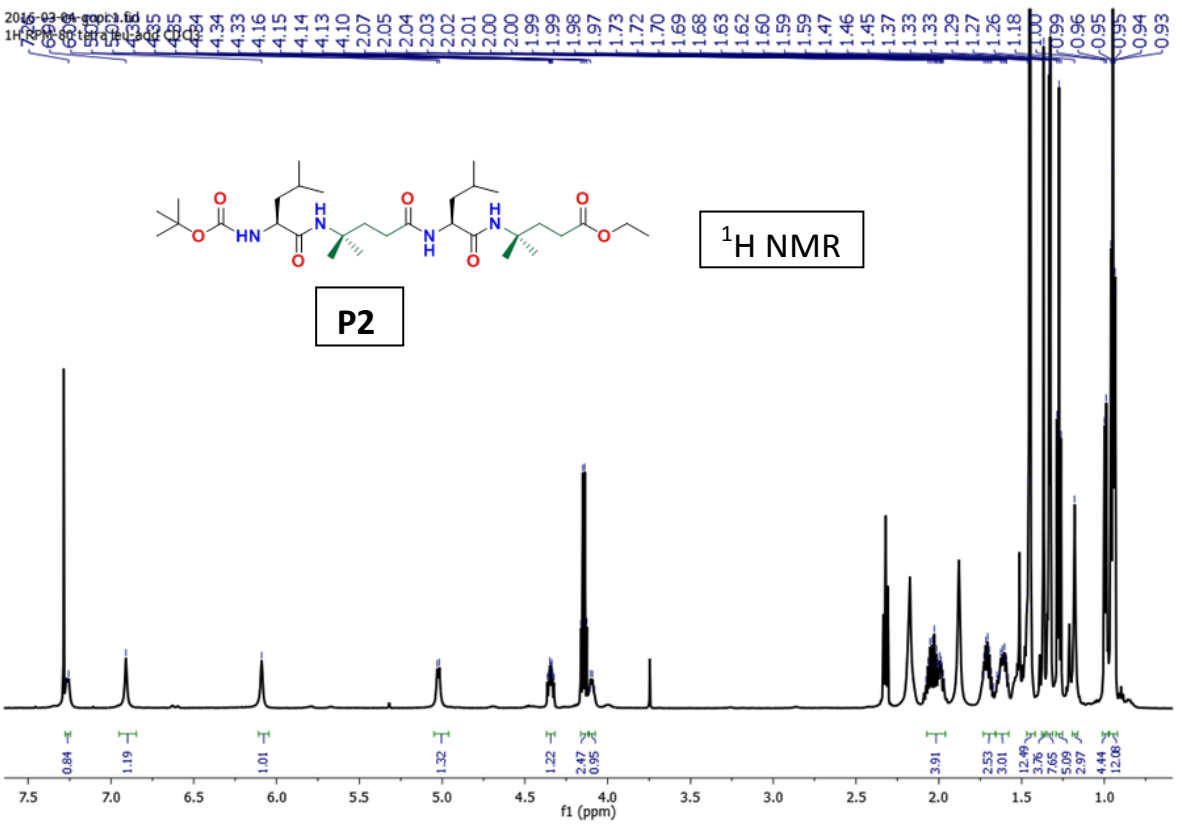
P2
1H NMR
f1 (ppm)

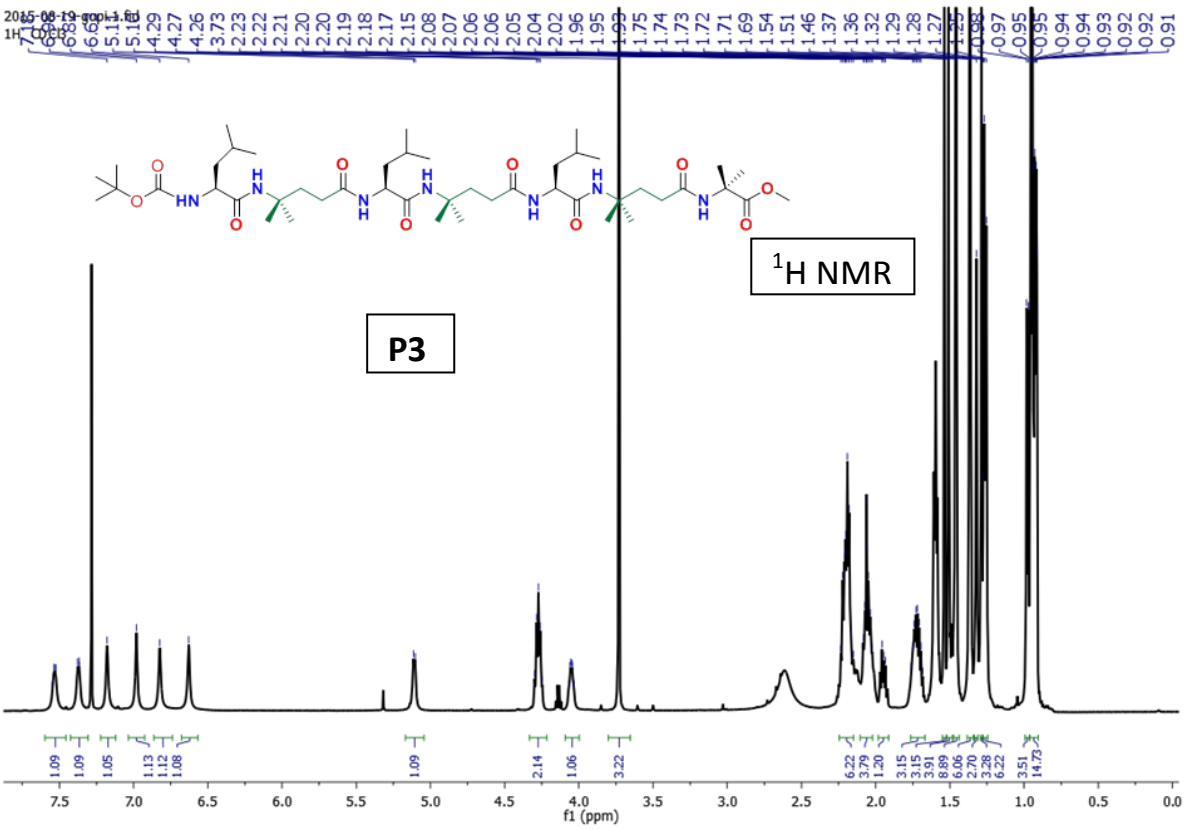
P3
^{1}H NMR
f1 (ppm)

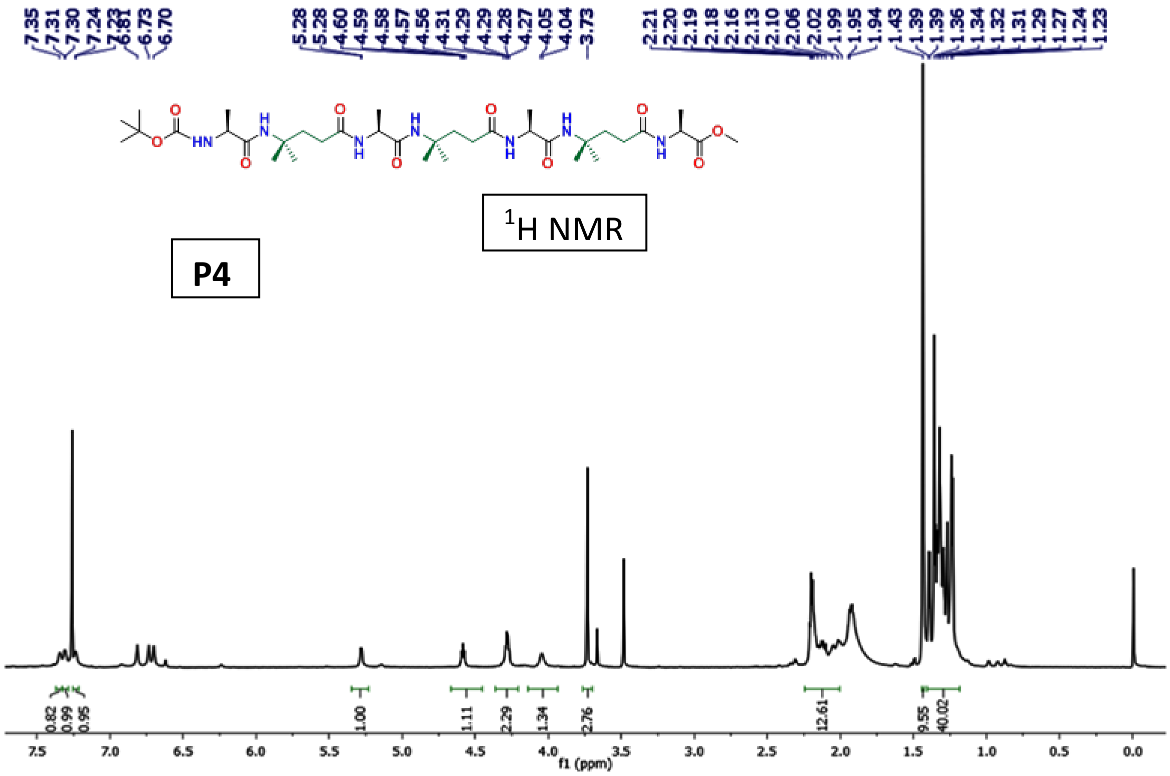

P4
^{1}H NMR
f1 (ppm)

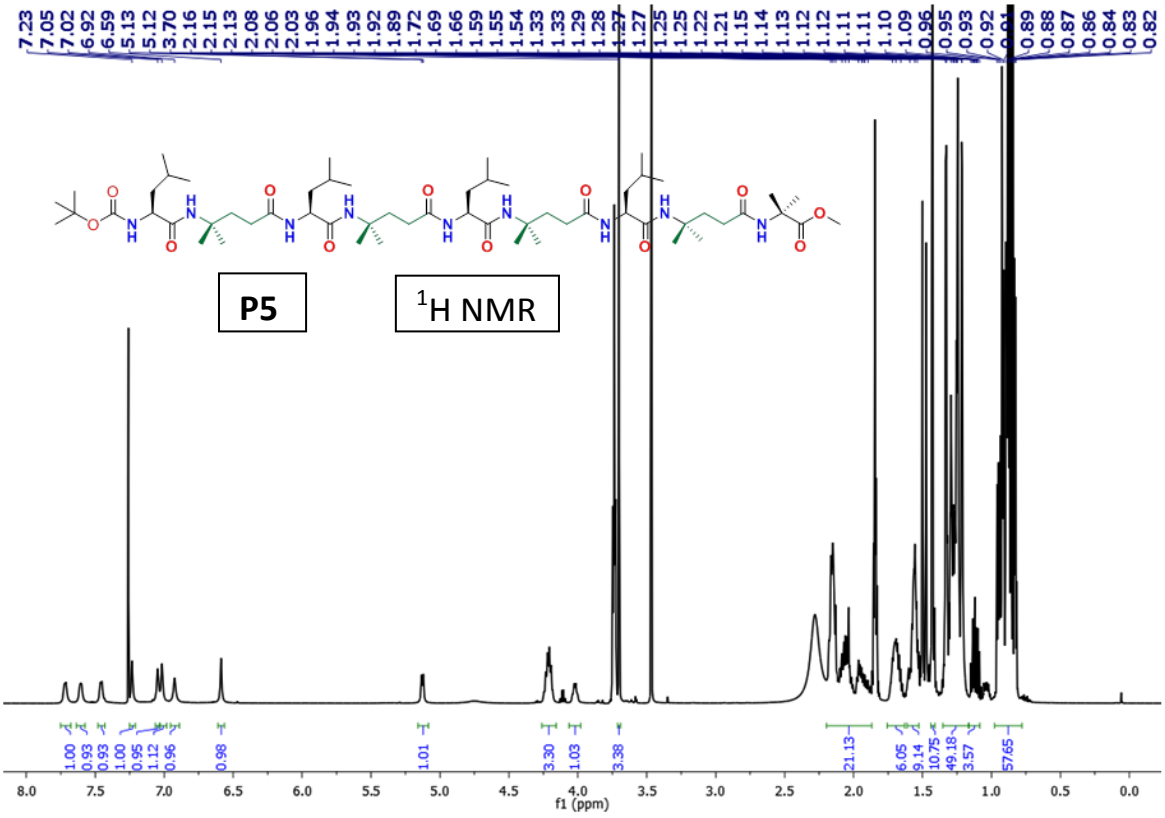
P5
1H NMR
f1 (ppm)

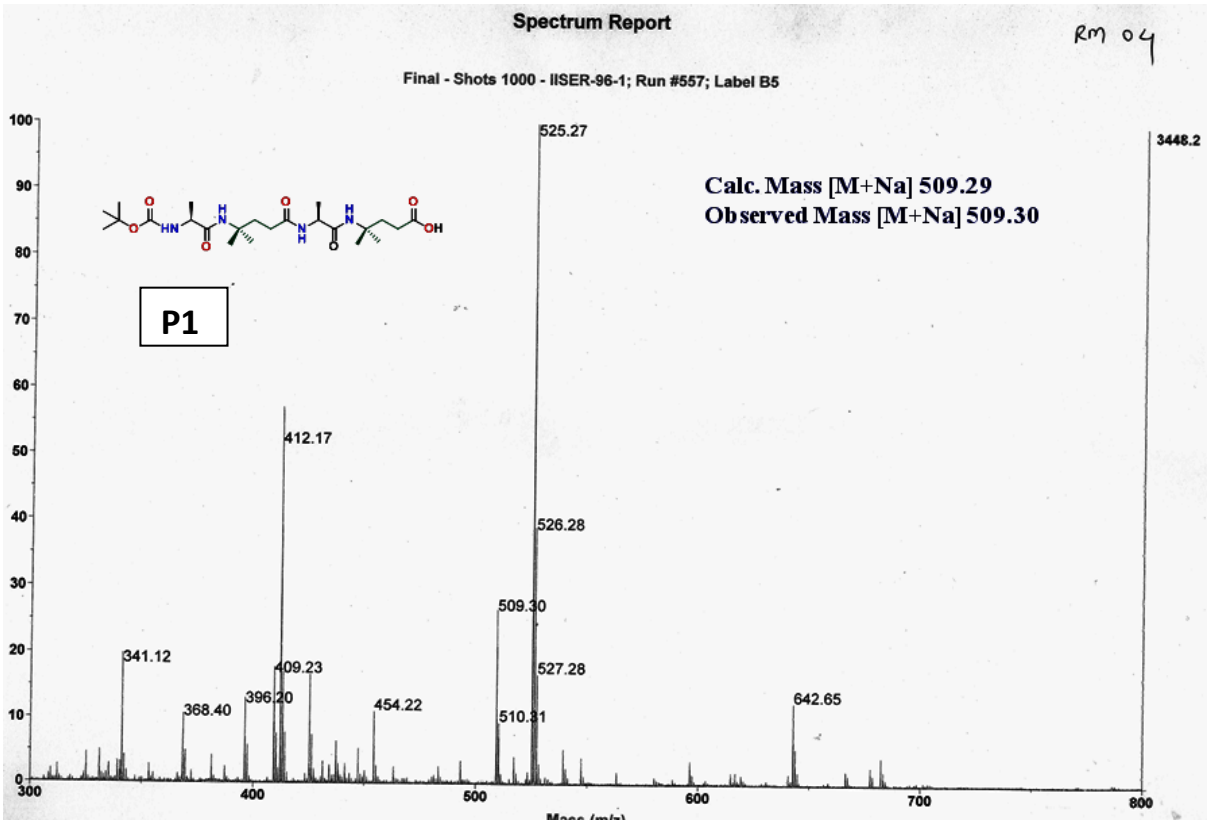
Spectrum Report
RM 04
Final - Shots 1000 - IISER-96-1; Run #557; Label B5
P1
Calc. Mass [M+Na] 509.29
Observed Mass [M+Na] 509.30
525.27
3448.2
412.17
526.28
509.30
341.12
409.23
527.28
396.20
368.40
454.22
510.31
642.65
100
90
80
70
60
50
40
30
20
10
0
300
400
500
600
700
800

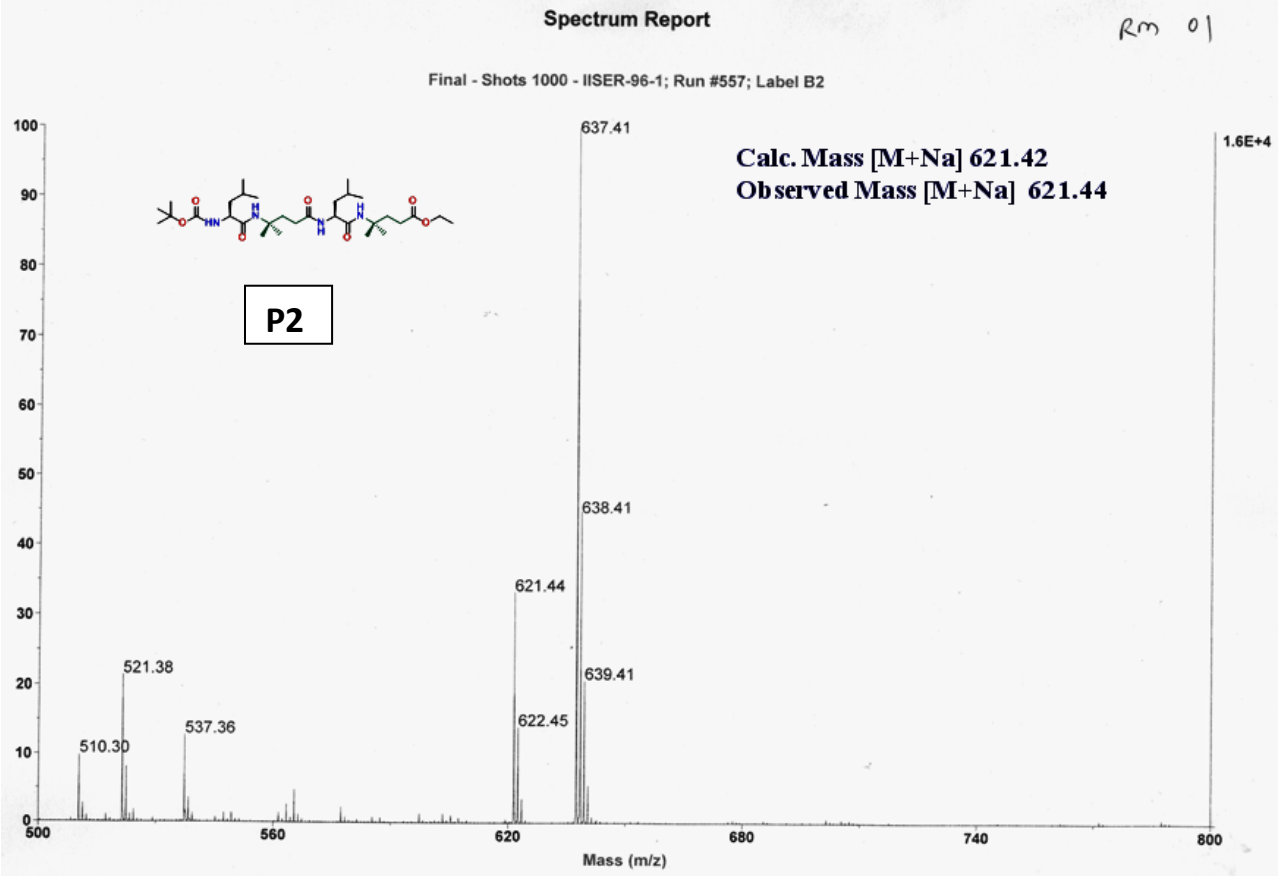
Spectrum Report
Rm 01
Final - Shots 1000 - IISER-96-1; Run #557; Label B2
P2
Calc. Mass [M+Na] 621.42
Observed Mass [M+Na] 621.44
637.41
638.41
621.44
639.41
622.45
521.38
537.36
510.30
1.6E+4
Mass (m/z)

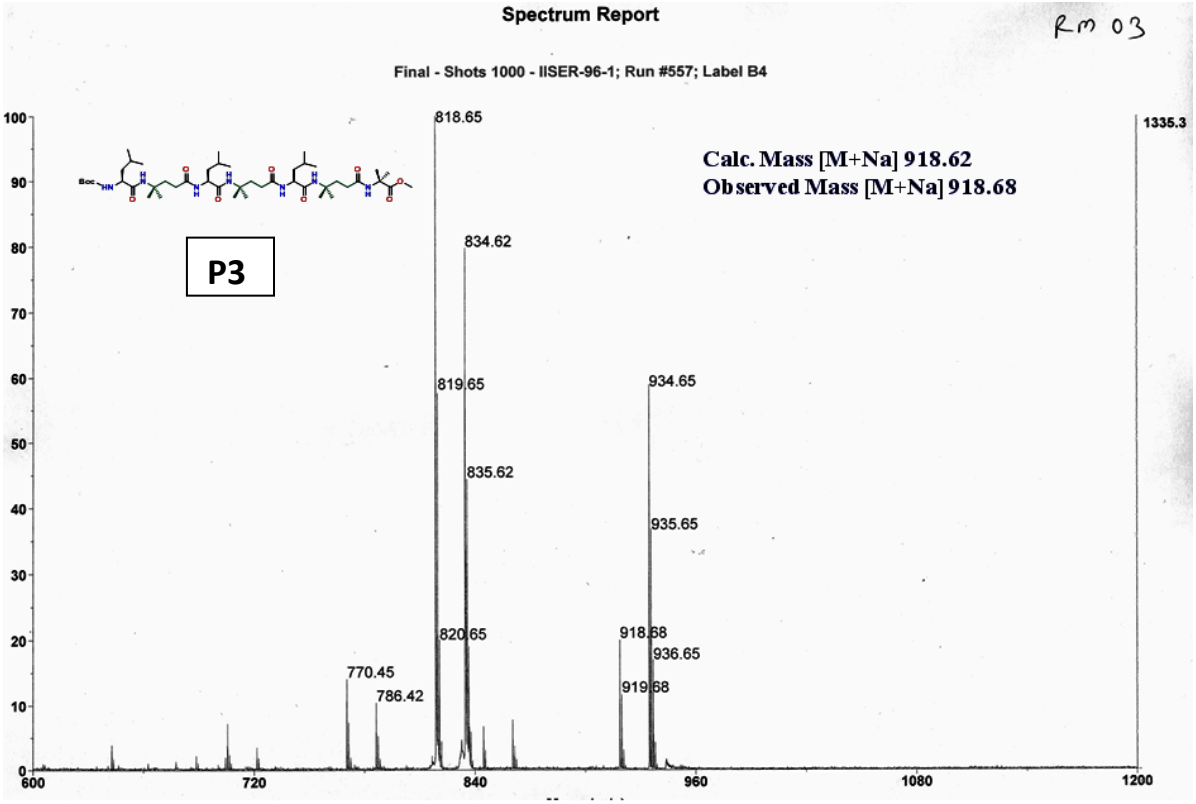
Spectrum Report
Rm 03
Final - Shots 1000 - IISER-96-1; Run #557; Label B4
P3
Calc. Mass [M+Na] 918.62
Observed Mass [M+Na] 918.68
818.65
1335.3
834.62
819.65
934.65
835.62
935.65
820.65
918.68
936.65
770.45
786.42
919.68
100
90
80
70
60
50
40
30
20
10
0
600
720
840
960
1080
1200

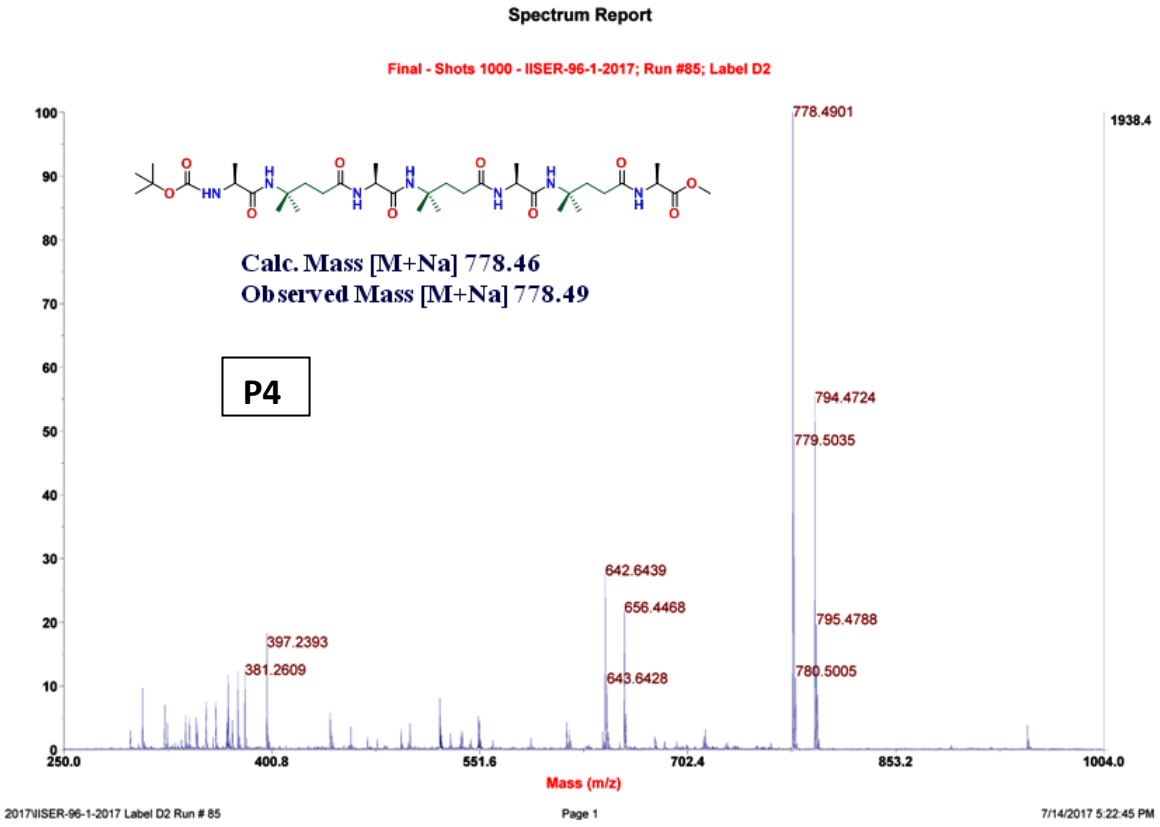
Spectrum Report
Final - Shots 1000 - IISER-96-1-2017; Run #85; Label D2
Calc. Mass [M+Na] 778.46
Observed Mass [M+Na] 778.49
P4
778.4901
1938.4
794.4724
779.5035
642.6439
656.4468
795.4788
397.2393
381.2609
643.6428
780.5005
Mass (m/z)
2017\IISER-96-1-2017 Label D2 Run # 85
Page 1
7/14/2017 5:22:45 PM

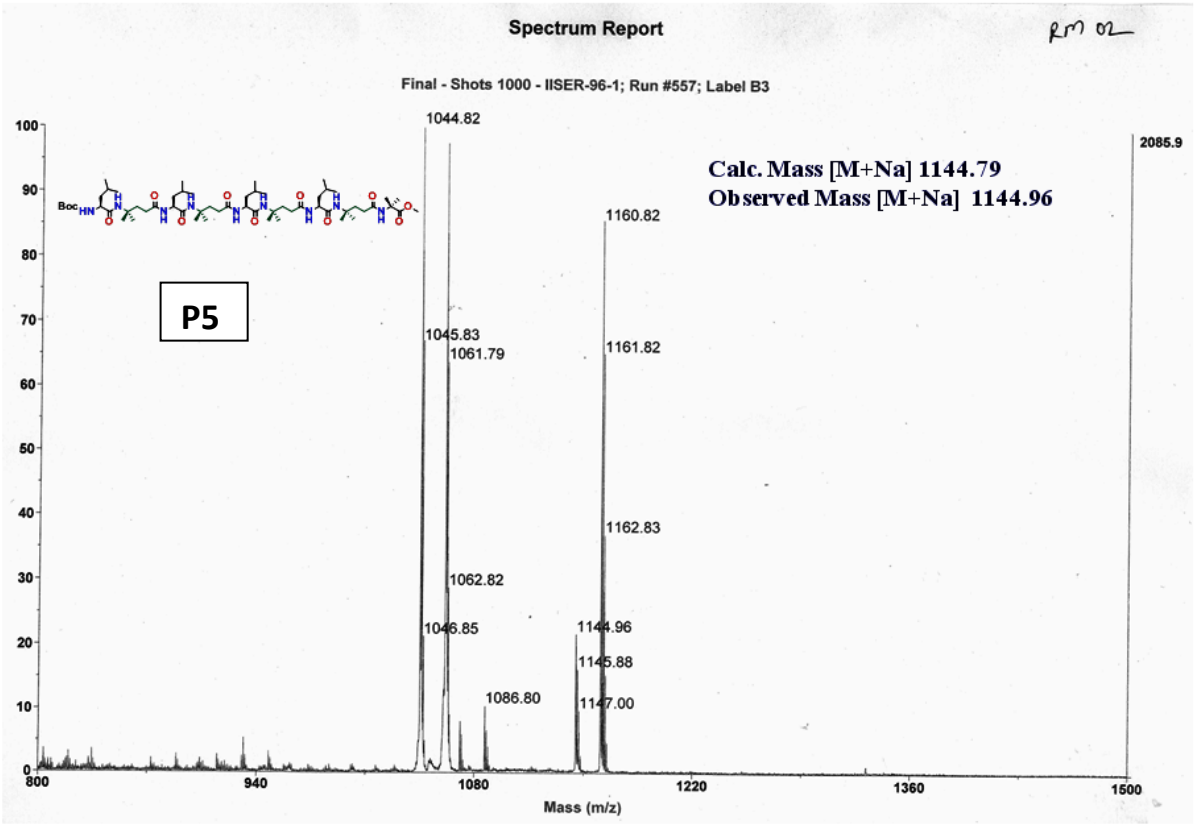
Spectrum Report
Final - Shots 1000 - IISER-96-1; Run #557; Label B3
Calc. Mass [M+Na] 1144.79
Observed Mass [M+Na] 1144.96
P5
1044.82
1160.82
2085.9
1045.83
1061.79
1161.82
1162.83
1062.82
1046.85
1144.96
1145.88
1086.80
1147.00
Mass (m/z)

Chapter 5

Exploring structural features of folded peptide architectures in the construction of nanomaterials

5.1 Introduction

Supramolecular self-assembly of peptides and proteins have gained interest in recent years due to their utility in the design and fabrication of nano-structures with tunable physical and chemical properties.[1] The biomaterials derived from α-peptides have been finding applications in various fields including tissue engineering, drug delivery, biomineralization, regenerative medicine, wound healing and molecular electronics. In comparison to the α-peptides, backbone bone homologated β- and γ-peptide which are well known to form well defined secondary structures[2] have been less explored towards the design of self-assembled biomaterials. Moreover, the influence of structure on the supramolecular assembly of peptides is not fully understood. Nevertheless, in their pioneering work Gellman and colleagues reported the ordered self-assembly of 14-helical β-peptides.[3] Further, Schepartz and coworkers[4] reported the tetrameric bundles and octameric bundles through the lateral assembly of β-peptides 14 helices. In continuation, Gellman's group reported the formation of protein like parallel helical quaternary bundles from α/β-peptides in aqueous solution.[5] Ghadiri and coworkers reported tubular channel like architectures from the supramolecular assembly of cyclic β-peptides. The channel-forming ability of these cyclic peptides in lipid bilayer is examined in liposome-based proton transport assay and single-channel conductance experiments.[6] The non-covalent interactions such as hydrophobic, ionic, and dipolar forces have been further exploited in the generation of peptide materials through supramolecular assemblies. In their initial attempt, Fülöp and colleagues reported the ribbon-like fibrils and vesicles through ordered supra molecular assembly of β-hexapeptide 10/12-helices comprised of *cis*-ACPC and *cis*-ACHC residues.[7] In another interesting study, Ortuno *et al*.[8] reported the supramolecular gels from β-peptides comprised of *cis*-ACBC. In continuation, Gellman and co-workers showed the formation of liquid crystals from the ordered assembly of a series of β-peptide 14-helices.[9] Further, Lee and colleagues reported various ordered supramolecular assemblies from the helical β-peptides, Boc-$(ACPC)_4$-OBn, Boc-$(ACPC)_6$-OBn and Boc-$(ACPC)_7$-OBn in an aqueous environment.[10] Additionally, Perlmutter *et al.* reported self-assembled fibers with the length ranging from nanometers to centimetres using N-acetylated β-tri- and hexapeptides.[11] Very recently, our group reported the spontaneous self-aggregation of short homo-oligomers composed of 4-amino-isocaproic acid (Aic) into nanofibers and their ability to form thermoreversible gels in various organic solvents.[12] As

described in the Chapters 3 and 4, Aic has shown very peculiar properties compared any other γ-amino acids in the literature. The short homooligomers of Aic have shown to adopt extended sheet type conformations and these extended sheets spontaneously self-assembled into ordered nanofibers. Further, the α,γ-hybrid peptides with 1:1 alternating Aic and sterically constrained Aib have shown to adopt novel 12-helices in short sequences and displayed remarkable structural dimorphism in longer sequences by adopting both 12 helix and 15/17 helices.[13] In Chapter 4 we have shown the transformation of 12- or 15/17-helices into 12/10-helices with alternately changing H-bond directionality by replacing sterically constrained Aib residues with natural α-amino acids in α,γ-hybrid peptides containing Aic residues.[14] Further, we have shown the fragility of 12/10 mixed helices in polar solvents. Motivated by the diverse structural properties of hybrid peptides composed of Aic residues, we sought to investigate whether the conformationally biased Aic can explored to design smart biomaterials with alternating aromatic α-amino acids. In this chapter, we are demonstrating the conformational analysis of two isomorphic α,γ-hybrid peptides composed of Phe and Aic and their supramolecular assemblies in aqueous environment. Further, to understand the influence of structure on the supramolecular assembly a known isomorphic α,γ-hybrid peptide 12-helix was also examined along with the hybrid peptides composed of conformationally biased Aic residues.

5.2 Aim and rationale of the present work

The stereochemically constrained α,α-dimethyl substituted α-amino acid (Aib) has been widely used to design helices in α-peptides.[15] The steric repulsions of *gem*-methyl groups forced Aib to occupy confined ϕ, ψ space and promote the onset of helices. In a sharp contrast to the helical structures of Aib monopeptides, we have recently reported the extended conformations of Aic (double backbone homologated Aib, Scheme 1) monopeptides. Instructively, these Aic γ-peptide oligomers spontaneously self-assembled into nanofibers and displayed remarkable thermoreversible gelation properties in various organic solvents.[12]. We anticipate that the remarkable self-assembling properties of conformationally biased Aic peptides can be exploited to design smart nanostructures through the insertion of alternating aromatic α-amino acids. In this context, we have designed three isomorphic peptides and studied their conformations and ordered supramolecular assemblies. The sequences of peptides are shown in the Scheme 1.

5.3 Results and Discussion

5.3.1 Design and synthesis

As a part of our investigation and to test our hypothesis, we have designed two hybrid peptides composed of α-Phe and Aic, **P1** (γ,α), **P2** (α,γ) and a control peptide **P3** which is known to adopt C_{12}-helix are shown in Scheme 1. The γ-amino acid (Aic) and γ^4-Phenylalanine were synthesized using Wittig reaction followed by catalytic hydrogenation as reported earlier.[12] All peptides were synthesized by solid phase method using standard Fmoc-chemistry and purified through reverse phase HPLC using C_{18} columns.

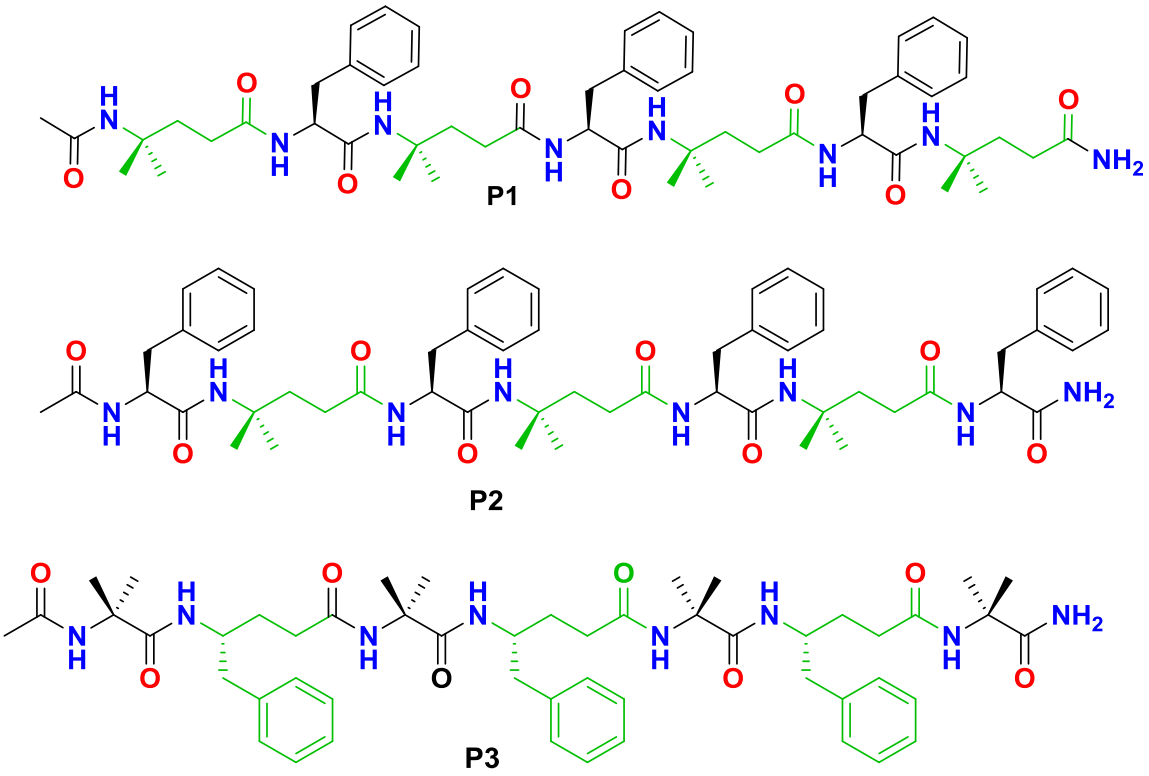

Scheme 1 Chemical structures of peptide **P1**, **P2** and **P3**

5.3.2 Solution conformation of peptide P1 and P2

After purification through reverse phases HPLC, we subjected peptides **P1** and **P2** to 2D NMR analysis in order to understand their solution conformations. Unambiguous peak assignments were performed using TOCSY, COSY and ROESY spectra. The chemical shifts along with $^3J_{NHC^{\alpha}H}$ scalar couplings and amide temperature coefficients (dδ/dT) for peptides **P1** and **P2** are tabulated in the Table 1 and Table 2, respectively. Partial ROESY spectra

depicting the NH↔NH and $C^{\alpha}H$↔NH NOEs of peptides **P1** and **P2** are shown in Figure 1 and Figure 2, respectively. The very weak NH↔NH and no long range NH↔CH NOEs were observed in both the peptides, however, a strong $C^{\alpha}H$↔NH NOEs were observed between *i* to *i+1* residues suggesting the extended type of planar structures. Further, to understand the intramolecular nature of H-bonding in **P1** and **P2**, the temperature dependent ^{1}H NMR experiment was undertaken. The solution of **P1** and **P2** in CD_3OH was gradually heated from 5 °C to 35 °C and chemical shifts for all NHs were acquired after each 10 °C interval. Results of the experiments are shown in Figure 3. It has been observed a clear upfield shift of NHs with increasing temperature suggesting the involvement of amide NHs in intermolecular H-bonding. Based on the NOE constraints, computer molecular models were built and energy minimized structures of **P1** and **P2** are shown in Figure 4. To get clear clarity of the solution conformation of **P1** and **P2** we are showing single structures than the superimposed models. Both peptides adopted extended type structures in solution.

Table 1 Tabulation of chemical shifts along with $^{3}J_{NHC^{\alpha}H}$ scalar couplings and amide temperature coefficients (dδ/dT) for peptide **P1**.

Residue	Chemical shifts (ppm)						$^{3}J_{NHC^{\alpha}H}$ (Hz)	dδ/dT (ppb)
	NH	$C^{\alpha}H$	$C^{\beta}H$	$C^{\gamma}H$	$C^{\delta}H$	Others		
Acetyl						1.86(CH_3)		
Aic($^{\gamma}$U1)	7.63	2.18	1.94		1.25 /1.22			6.6
Phe (F2)	8.22	4.46	2.95/2.91	-	-	Aromatics 7.26-7.18	7.0	8.6
Aic($^{\gamma}$U3)	7.59	2.05	1.94/1.72		1.17/1.05	-	-	7.3
Phe (F4)	8.23	4.47	2.96/2.90	-	-	Aromatics 7.26-7.18	7.2	8.8
Aic($^{\gamma}$U5)	7.56	2.04	1.98/1.73		1.16/1.02	-	-	7.0
Phe (F6)	8.20	4.43	2.96/2.88	-	-	Aromatics 7.26-7.18	7.2	8.7
Aic($^{\gamma}$U7)	7.64	2.09	2.04/1.78	-	1.23/1.12	-	-	7.3
C-ter. NH_2	7.61/6.89	-	-	-	-	-	-	6.8

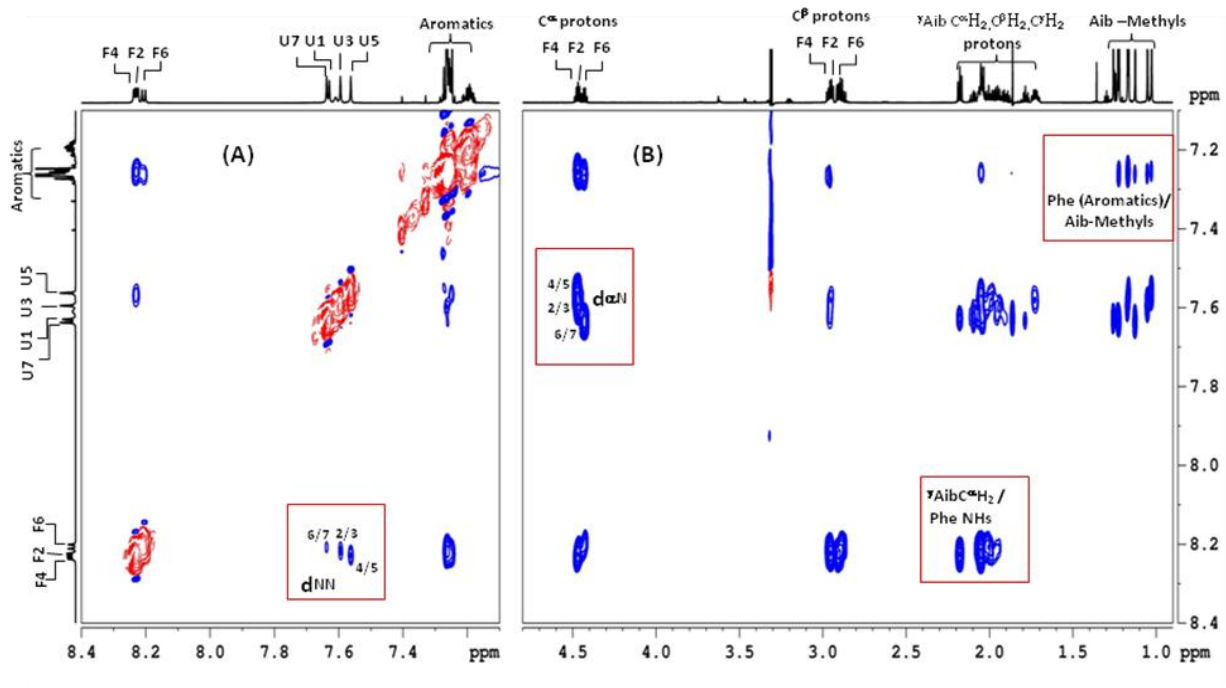

Figure 1 Partial ROESY spectra of **P1**. (A) Amide/aromatic region, (B) Amide/Aromatic-Aliphatic region. d_{NN} and $d_{\alpha N}$ with differential intensities are boxed. So also Aromatics NOEs to Aic methyl's. Most of these NOEs were considered in making a computer energy minimized model of the peptide molecule.

Table 2: Tabulation of chemical shifts along with $^{3}J_{NHC}{}^{\alpha}{}_{H}$ scalar couplings and amide temperature coefficients (dδ/dT) for peptide (**P2**) : Ac-[Phe-Aic]$_3$-Phe-NH_2.

Residue	Chemical shifts (ppm)						$^{3}J_{NHC}{}^{\alpha}{}_{H}$ (Hz)	dδ/dT (ppb)
	NH	$C^{\alpha}H$	$C^{\beta}H$	$C^{\gamma}H$	$C^{\delta}H$	Others		
Acetyl						1.92(CH_3)		
Phe (F1)	8.30	4.45	2.92	-	-	Aromatics 7.24-7.18	7.0	8.3
Aic($^{\gamma}$U2)	7.57	2.04	1.96/1.71	-	1.16/1.02	-	-	7.3
Phe (F3)	8.17	4.46	2.94/2.89	-	-	Aromatics 7.24-7.18	7.4	8.3
Aic($^{\gamma}$U4)	7.56	2.05	1.97/1.72	-	1.17/1.04	-	-	7.3
Phe (F5)	8.19	4.41	2.95/2.88	-	-	Aromatics 7.24-7.18	7.3	8.6
Aic($^{\gamma}$U6)	7.55	2.01	1.86/1.63	-	1.16/1.04	-	-	7.2
Phe (F7)	8.15	4.59	3.12/2.83	-	-	Aromatics 7.24-7.18	8.3	8.1
C-ter. NH_2	7.76/7.19	-	-	-	-	-	-	7.2

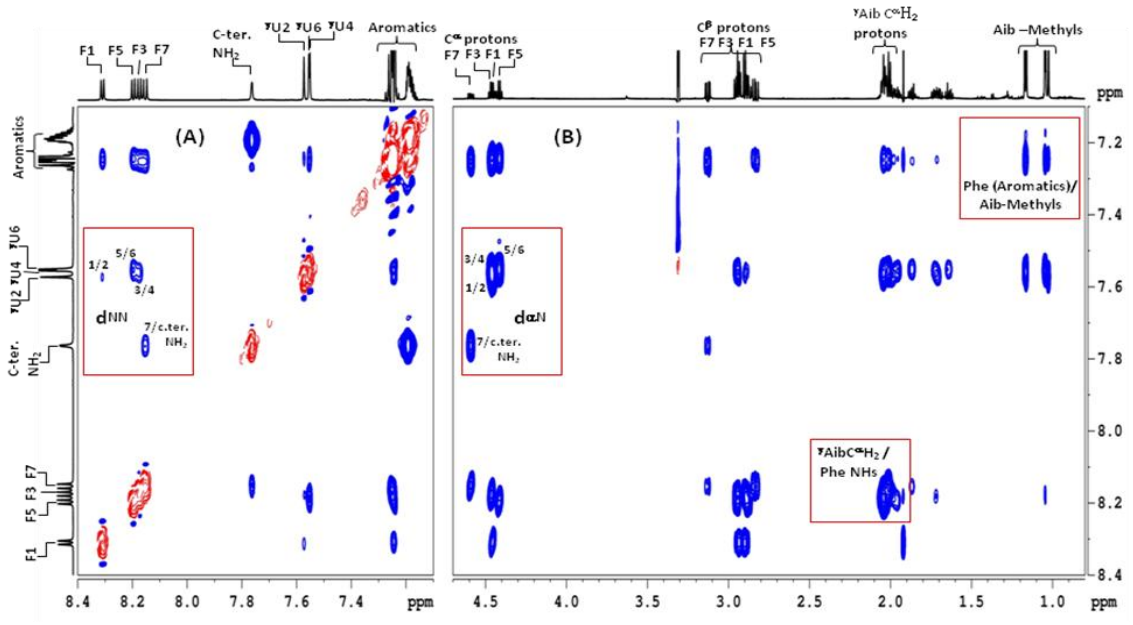

Figure 2: Partial ROESY spectra of **P2**. (A) Amide/aromatic region, (B) Amide/Aromatic-Aliphatic region. d_{NN} and $d_{\alpha N}$ with differential intensities are boxed. So also Aromatics NOEs to Aic methyl's. Most of these NOEs were considered in making a computer energy minimized model of the peptide molecule.

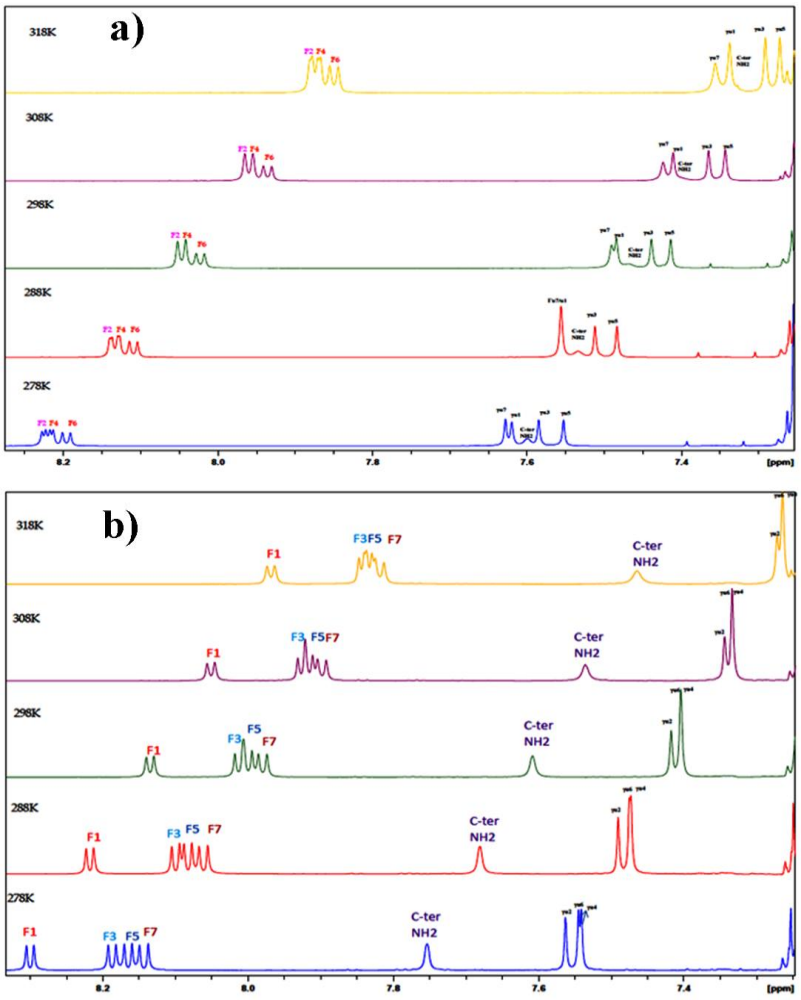

Figure 3 Up field chemical shifts of all amide protons with increasing temperature from 278 K to 308 K. a) Temperature dependent ^{1}H NMR spectra of peptide **P1.** b) Temperature dependent ^{1}H NMR spectra of peptide **P1.** Spectra were recorded in 700 MHz spectrometer in CD_3OH.

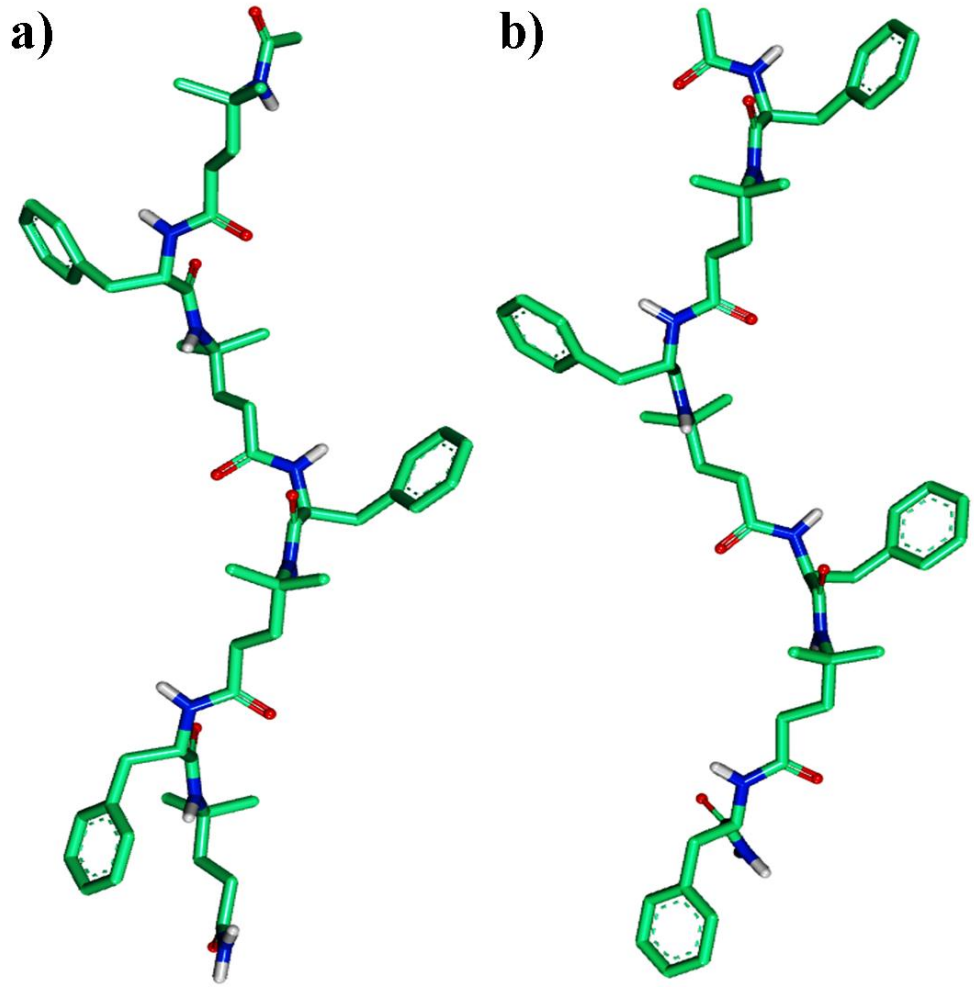

Figure 4 Energy minimized structures of **P1** and **P2** deduced from the NOEs in 2D NMR.

5.3.3 FT-IR supports extended structures in P1and P2

We further probed the characteristic signature of NH---O=C of **P1** and **P2** to understand the H-bond mediated aggregation using FT-IR. The IR spectra of **P1**and **P2** in MeOH are shown in experimental section. Peptides **P1** and **P2** displayed a sharp NH stretching vibration (ν_{NH}) at 3285 cm^{-1} and 3283 cm^{-1}, respectively. These results support the involvement of amide NHs in the intermolecular H-bonding. Further, the amide I and amide II bands, which are directly related to the backbone conformations, were found to be 1637 cm^{-1} and 1546 cm^{-1}, respectively in **P1** (Figure15). Similarly, **P2** also displayed amide I and amide II bands at 1642 cm^{-1} and 1547 cm^{-1}, respectively (Figure 16). The FT-IR values observed for **P1** and **P2** are in close agreement with the values observed in the poly(Ala) infinite β-sheets.[16] All these experimental evidences support the extended conformations of the two peptide.

5.3.4 Single crystal analysis of peptide P3

The X-ray structure of the control peptide **P3** was previously reported from our group[17b] is shown in the Figure 5. The peptide adopted right-handed helical conformations with consecutive 12-membered H-bonds [C=O (*i*)···H–N (*i+3*), 12-atom ring H-bonds. The 12-helical conformation of peptide **P3** is stabilized by six consecutive 1←4 [C=O (*i*)···H–N (*i+3*)] intramolecular H-bonds. Both C-terminal amide and N-terminal Ac-group are involved in the intramolecular H-bonds. Additionally, the crystal packing revealed that each helical peptide is interconnected with the other helical peptides in a head-to-tail fashion through four intermolecular H-bonds. Inspection of the crystal structure of **P3** reveals that Aib residues adopted right handed helical conformations by having average ϕ and ψ values −58 ± 3° and −40 ± 5°, respectively. The dihedral angles of γ^4-Phe residues were measured by introducing two additional variables θ_1 (N–C^{γ}–C^{β}–C^{α}) and θ_2 (C^{γ}–C^{β}–C^{α}–C). In contrast to the Aic residues, the stereochemical analysis of γ^4-Phe residues in **P3** reveals that they adopted *gauche*$^+$, *gauche*$^+$ (g^+, g^+, $\theta_1 \approx \theta_2 \approx 60°$) local conformations about the C^{β}–C^{γ} and C^{α}–C^{β} bonds.

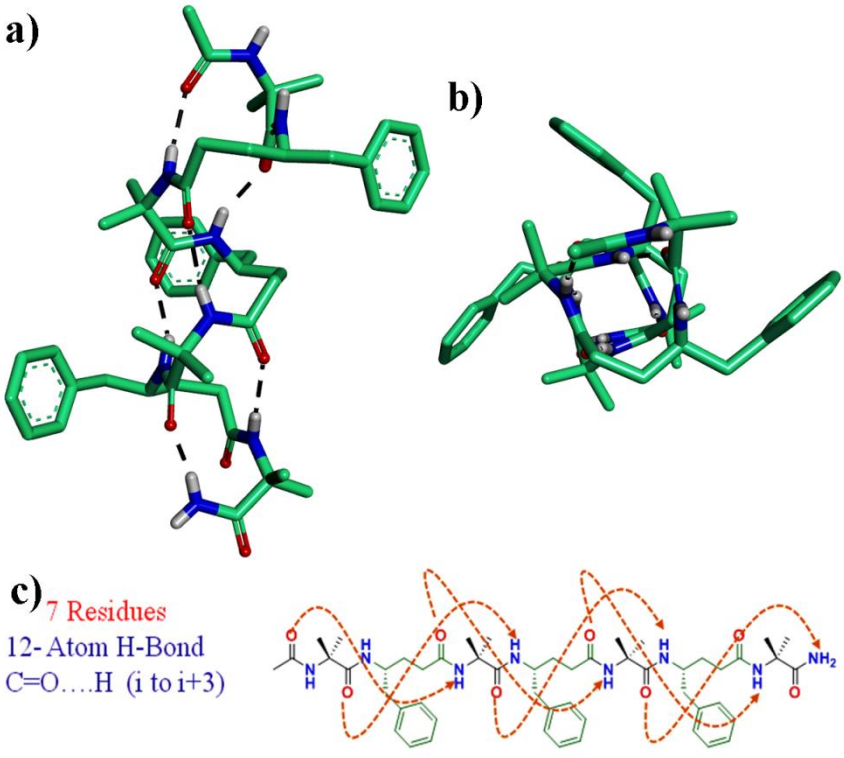

Figure 5 a) Single crystal structure of peptide **P3.** b) Top view of the peptide **P3**. c) Hydrogen bonding pattern observed of peptide in the crystal structure.

5.3.5 Hierarchical Self-Assembly of Peptides P1, P2 and P3

The presence of multiple interactions such as CH-π, π-π and H-bonds between the extended β-sheet structures motivated us to investigate their hierarchical self-assemblies employing scanning electron microscopy (SEM). The SEM samples were prepared by dissolving peptides in methanol/water combination and drop-casted onto a SiO2/Si substrate, dried at room temperature. Remarkable monodispersed capsules were obtained in all methanol/water combinations, however, we found that 60:40 methanol/water best combination to get monodispersed assembled capsules. SEM analysis reveals the remarkable monodispersed vesicles of the peptides as shown in Figure 6a and 7a. Both **P1** and **P2** displayed hollow spheres with the diameter 100-600 nm (Figure 6a and 7a). These results demonstrate that both the peptides, irrespective of the sequential placement of amino acids, spontaneously self-assembled into vesicles. To validate whether the observed vesicles are unique to **P1** and **P2**, we subjected their constitutional isomer α,γ-hybrid peptide12-helix composed of Aib and γPhe (**P3**) to the SEM analysis under identical conditions. The 12-helices displayed various three-dimensional marvelous polyhedrons (Figure 9) as a signature of its crystalline nature.[18]

To gain more information on vesicle superstructures the transmission electron microscopy (TEM) measurements were undertaken. The drop-casted solution of peptides on copper grids was slowly evaporated at room temperature and subjected to TEM analysis. The TEM images of **P1** and **P2** are shown Figure 6c and 7c. The existence of the spherical entities with an average diameter of ~450 nm observed in the TEM are in good agreement with SEM images. It was found that the spherical structures showed a clear contrast between the interior and periphery, which is consistent with the typical characteristic of vesicular structures. The thickness of the vesicle structure was found to be around 66 nm. TEM images of the control **P3** is shown in Figure 9d. We hypothesized that the multiple aromatic-aromatic and intermolecular hydrogen bonding existed between the extended β-sheets are responsible for the formation of multilayer and subsequently this multilayer may transformed into vesicle like nanostructures. Further, we sought to investigate the morphology of the nanostructures of **P1** and **P2** using AFM (atomic force microscopy). The AFM studies reveal that the observed spherical structures of self-assembled peptides (Figure 6d and 7d) are consistent with the structures observed in SEM and TEM analysis. To gain the further insight into the elemental composition of these vesicles, energy dispersive X-ray spectroscope (EDAX) was performed

(Figure 15). Elemental composition of carbon, nitrogen and oxygen found from the vesicles supported that the nanostructures are generated only from the hybrid peptides.

In order to understand the self-aggregation behaviour and the size of the self-aggregate in solution, we carried out DLS (dynamic light scattering) analysis (Figure 8a and 8b). The DLS (1mg/mL) studies reveal that these peptides self-aggregates in solution with size distribution around 200-600 nm which is consistent with the SEM, TEM and AFM studies.

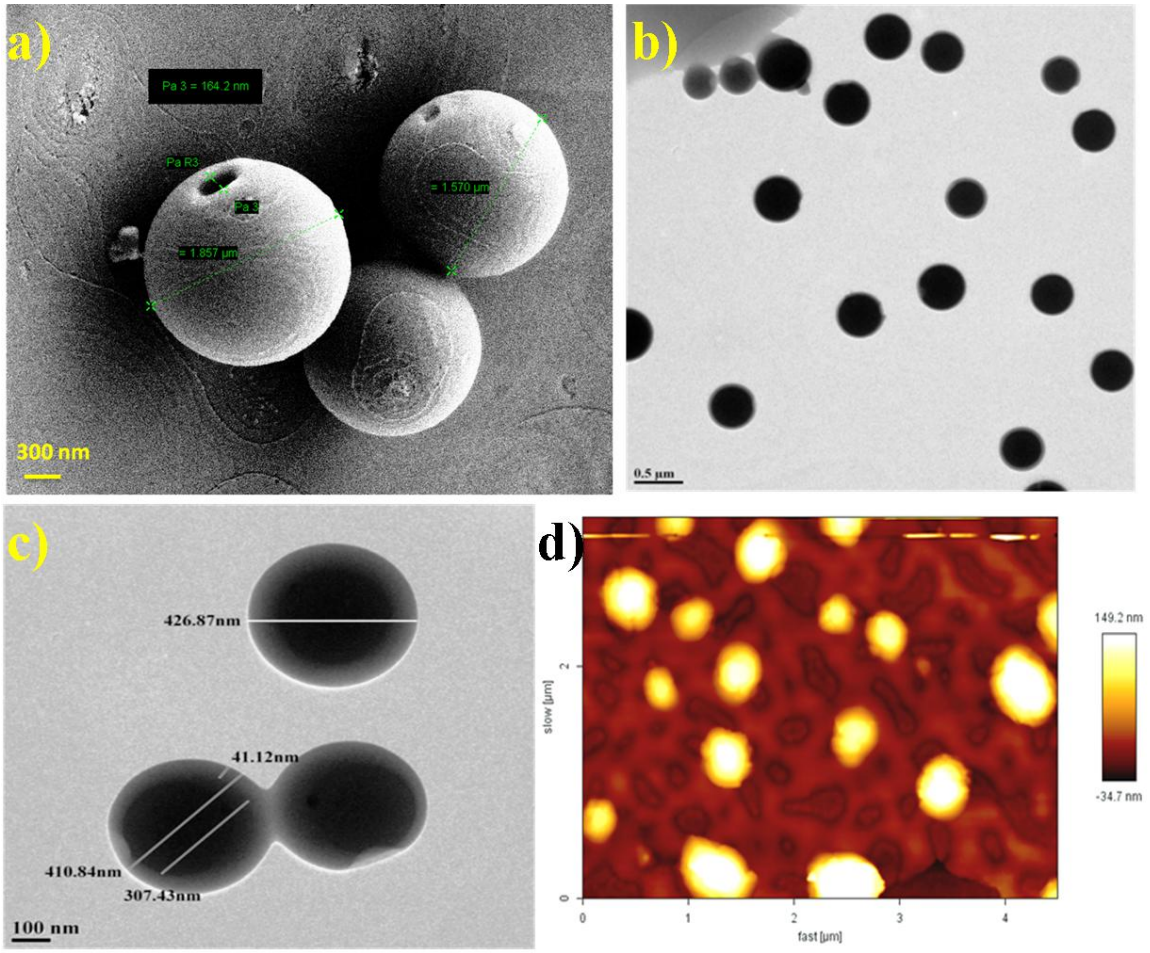

Figure 6 a) SEM, images of vesicles from the hybrid peptides **P1** (b,c) TEM images of peptide vesicles **P1** d) AFM images of peptide vesicles **P1.**

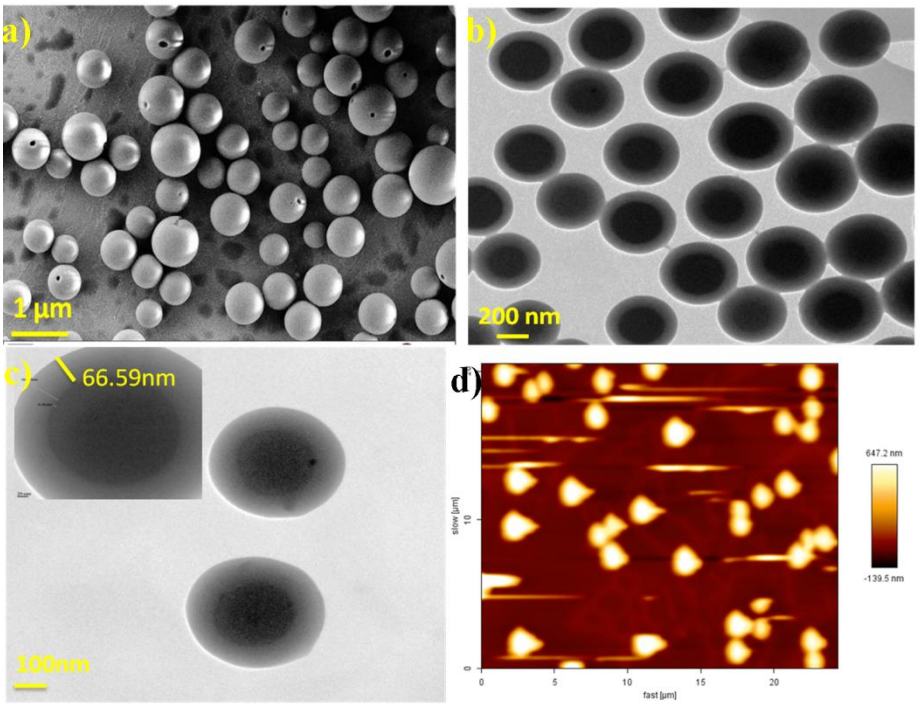

Figure 7: a) SEM, images of vesicles from the hybrid peptides **P2** (b and c) TEM images of peptide vesicles **P1** d) AFM images of peptide vesicles **P2.**

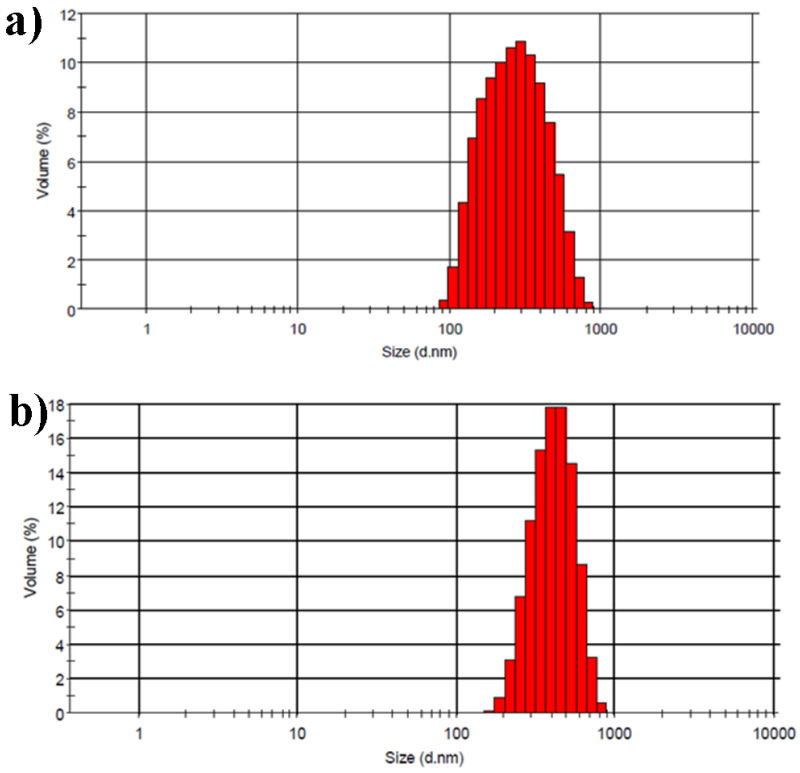

Figure 8 a) DLS data of self-assembled vesicles generated from peptide **P1** b) DLS data of self-assembled vesicles generated from peptide **P2**

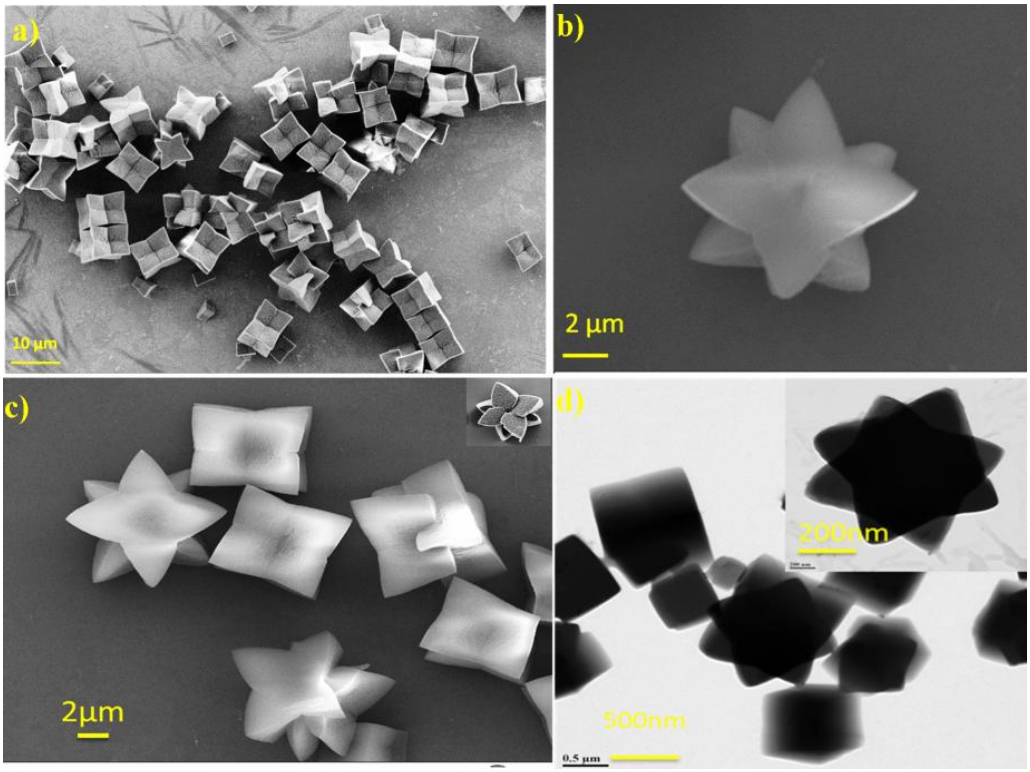

Figure 9 SEM images depicting the polyhedrons of the control α,γ-hybrid peptide 12-helix (a-c). d) TEM images depicting the polyhedrons of the control α,γ-hybrid peptide 12-helix.

5.3.6 Effect of externals stimuli on capsular structure

As both **P1** and **P2** displayed the remarkable monodispersed vesicles, we studied their stability against temperature, acidic and basic pH conditions as well as proteinase K. At acidic conditions (~pH 4) these nanostructures displayed bowl type morphology and at basic condition (~pH 9) these vesicles transformed to disc like morphology (Figure 10). To gain the knowledge regarding their stability against temperature, we drop casted the peptide solution on silicon substrate and heated up to 150 °C and recorded SEM images after cooling it to room temperature. Instructively, SEM analysis reveals that there is no change in the gross morphology of the vesicles, suggesting that they are stable up to 150 °C (Figure 10). In addition, thermogravimetric analysis (TGA) reveals that there is no weight loss of the peptides up to 250 °C (Figure 14). Additionally, we have also studied stability of vesicles against proteinase K, which is used to rupture the Phe-Phe nanotubes.[19] The SEM results reveal that no change in the morphology of vesicles suggesting that they are stable against the protease (Figure 10).

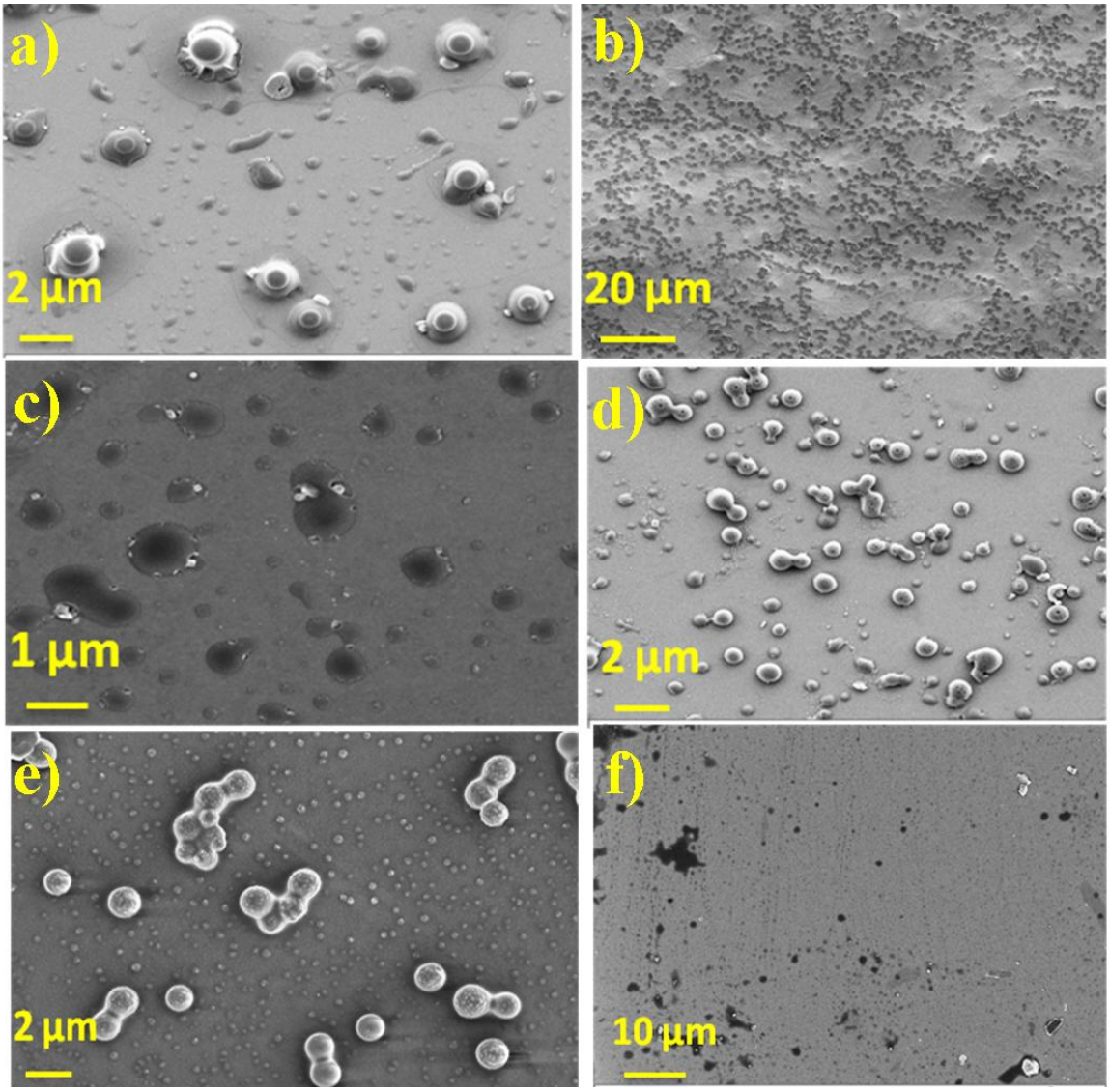

Figure 10 SEM images of peptide vesicles of peptide **P2** with different stimuli. a) At acidic condition; b) Basic condition; c) After heating 100 ^{o}C; d) After heating 150 ^{o}C; e) After treating with Proteinase K; f) After treating with 6 equivalent of Bu_4NBr.

5.3.7 Encapsulation and Control release of small molecules

As hybrid peptides **P1** and **P2** are composed of aromatic amino acids, we envisioned that the capsules formed by the **P1** and **P2** can be disrupted using cationic peptides. It is known that cation-π interactions play a significant role in the protein-folding as well as protein-ligand (protein, peptide, small molecules etc.,) interactions.[20] Instructively, we realized complete disruption of capsules after the interaction with cationic dipeptide Cbz-Lys-Lys-OMe, suggesting that cationic peptides can be used as a stimuli. In addition, these capsules are also susceptible to Bu_4NBr similar to the other vesicles.[21] Stimuli-responsive self-assembled

nanostructures have been attracted considerable attention recently due to their promising applications including as drug delivery agents, biosensors, catalysts, etc.[7,8] We envisioned that the cationic peptide mediated disruption of vesicles may be utilized to encapsulate and delivery of drugs, active substances and small molecules. In this regard, we selected fluorescent carboxyfluorescein as a small molecule model for the investigation. The dye loaded capsules were prepared by mixing 0.1 mM carboxyfluorescein to freshly prepared solution of peptide capsules. After keeping it overnight, the solution was dialyzed. After the dialysis, the solution displayed no green fluorescence, which suggest the absence of free dye in the solution. The laser scanning confocal microscope (LSCM) reveal the green fluorescence emission from the nanostructures suggesting the encapsulation of dye molecules. The confocal microscape (LSCM) image of carboxyfluorescein encapsulated peptide **P2** vesicles is shown in Figure 11a. Further, The SEM (Fig 11b), DLS (Figure 11c) and TEM (Figure 11d) analysis showed that uniform size and morphology of the dye encapsulated peptide capsules.

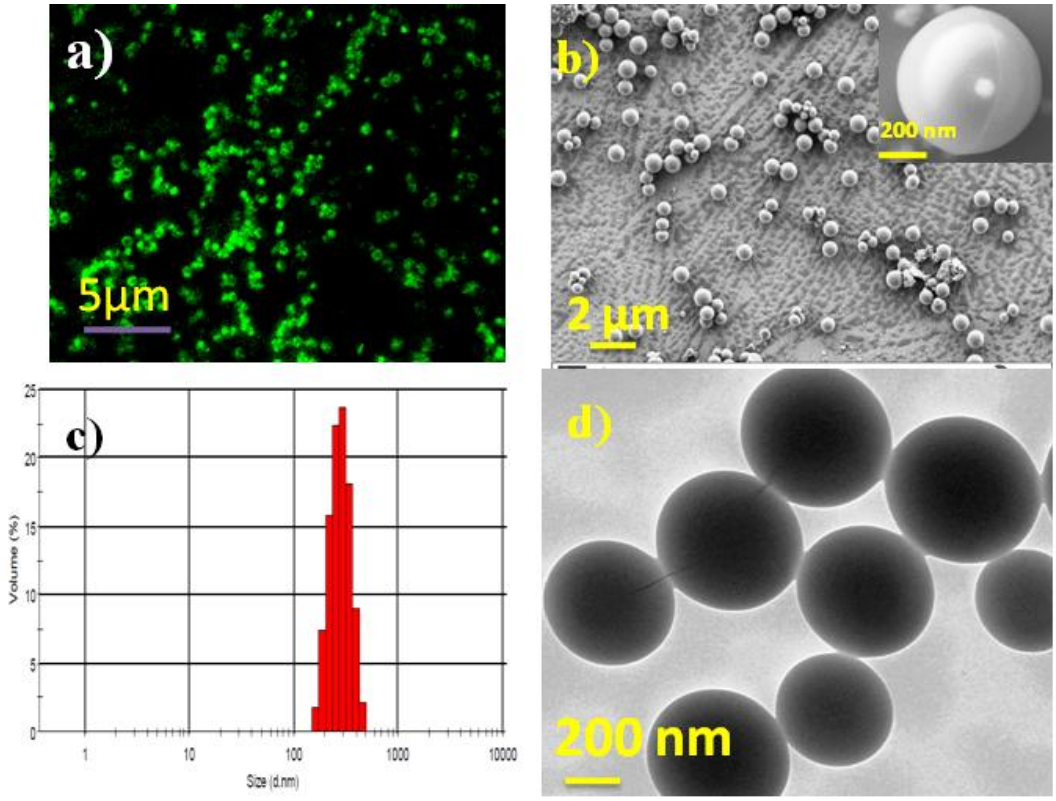

Figure 11 a) Confocal b) SEM, c) DLS data and d) TEM images of carboxyfluorescein encapsulated hybrid peptide **P2** vesicles.

After confirming encapsulation of the fluorescent dye, we subjected capsules for the control release experiment using cationic dipeptide as an external trigger. The controlled release of dye upon addition of the peptide trigger was monitored using increase in the

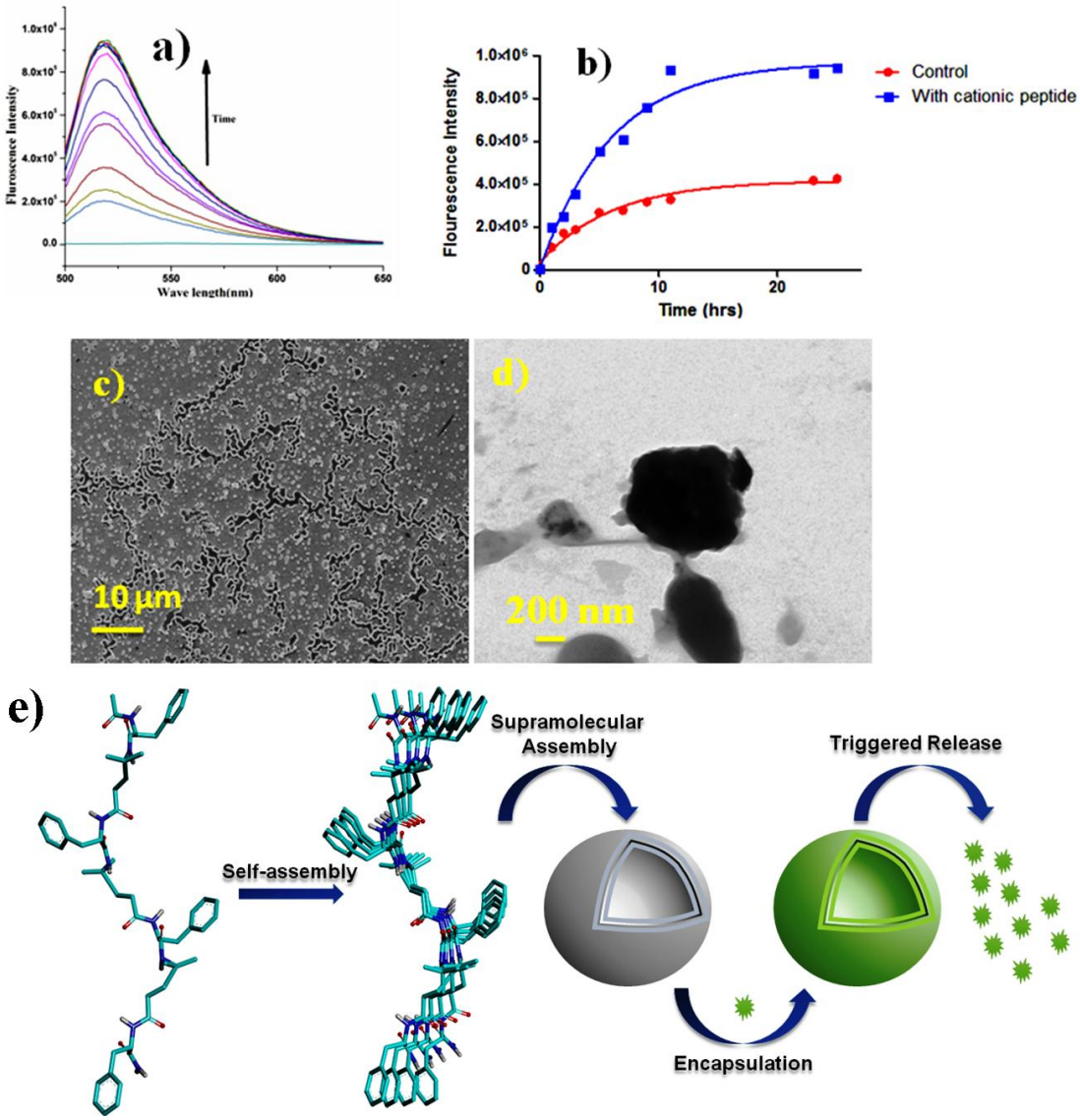

Figure 12 a) Gradual increase in the fluorescent intensity of the solution outside dialysis tube upon addition of 5 equiv of Cbz-Lys-Lys-OMe. b) Change in the emission intensity with increasing time along with the control without peptide stimuli. c) SEM and d) TEM images depicting the drastic change in gross morphology of vesicles after the addition of peptide trigger. e) Schematic representation of the formation of vesicles and cationic peptide triggered control release of fluorescent molecules.

fluorescence of the solution outside the dialysis tube. The control experiment was performed without addition of peptide stimuli. Results are shown in Figure 12a and 12b. Peptide triggered controlled release of fluorescent dye was steadily continued up to 30 hr. Overall, these studies suggested that hybrid peptide vesicles can be used to encapsulate and control release of small molecules. To understand the morphology of vesicles after the release of encapsulated fluorescent molecules through external triggers, we subjected them for SEM and TEM analysis. The SEM and TEM images are shown in Figure 12c and Figure 12d, respectively. The SEM and TEM analysis indicates the complete rupture of vesicles by cationic peptides. The schematic representation of the formation of vesicles and cationic peptide triggered control release of fluorescent molecules is shown in Figure 12e.

5.4 Conclusion

In conclusion, in a sharp contrast to the 12-helical organization adopted by the α,γ-hybrid peptides, α,γ-hybrid peptides composed of alternating Aic and α-Phe displayed extended structures. These conformationally biased α,γ-hybrid peptides spontaneously self-assembled into remarkable capsules due the presences multiple CH-π, π-π and H-bonds between the extended structures. As revealed by the SEM, TEM, AFM and DLS analysis, these peptide vesicles were found to be monodispersed in shape and size. Under identical conditions, analogous α,γ-hybrid peptide 12-helix displayed polyhedron hierarchical assemblies. Thus, the structure, orientation of side-chains play significant role in the supramolecular assemblies. These nanovesicles were found to be susceptible to cationic peptides, organic and inorganic salts. As a proof of concept, we showed the control release of encapsulated fluorescent molecules from peptides capsules using cationic peptide as trigger. The hierarchical assembly of hybrid peptides into monodispersed capsules, their proteolytic and thermal stability, smooth encapsulation of small molecules and the control release reported here may pave way for the generation of new biomaterials for realistic applications.

5.5 Experimental Section

Peptide Synthesis

The N-acetylated peptides were synthesized on a MBHA Knorr amide resin at 0.25 mmol scale by manual synthesis method. The peptide couplings were carried out in NMP by standard Fmoc protocol using HBTU/HOBt as coupling reagents. Fmoc deprotection was accomplished by a solution of 20% piperidine in DMF. N-acetylation of peptides was carried out using acetic anhydride/pyridine (1:9). Peptide cleavage from the resin was achieved by treatment of the resin with a mixture of trifluoroacetic acid (TFA)/ triisopropylsilane/water (90:5:5) for 2 h. The resin was filtered with additional TFA (5 mL) and concentrated. The crude peptide was then precipitated by cold diethyl ether (30 mL) and isolated by centrifugation. The precipitate was re-dissolved in 5 mL of 1:1 mixture of MeOH/H_2O and then lyophilized to give a fine white solid. Then crude peptides were purified by reversed-phase HPLC using C18 column (5 µm, 10 X 250 mm). The gradient applied was from 95% A to 95% B in 30 min; where A was water and B was methanol, at a flow rate of 2 mL/min. Pure fractions of peptide were collected by monitoring UV-Vis at 254 nm. Further, peptides were characterized by MALDI-TOF/TOF.

Circular Dichroism (CD) Spectroscopy

CD spectra were recorded using a JASCO J-815 spectropolarimeter fitted with a Peltier temperature controller. CD spectra were measured by dissolving peptide 1mg/mL in MeOH and then successively diluted to 0.5 mg/mL and 0.25 mg/mL at 20 °C. Temperature dependent experiments were performed from 20 to 80 °C at the rate of 1 °C /min for every 10 °C interval.

Size distribution analysis of peptide vesicles using DLS

Mean diameter of the peptide vesicles in aqueous methanol solution was measured by dynamic light scattering (DLS) experiment using 90° scattering angle. Samples were prepared by dissolving 1mg/mL of peptide in 6:4 MeOH / H_2O.

SEM, TEM, AFM study SEM

sample were prepared by deposing peptide solution (4µL, 1mg/mL in 6:4 MeOH / water) on SiO_2/Si substrate, dried at room temperature and imaged it. Before each and every

experiment, fresh solutions have been made (for P3 immediately drop casted the solution onto a SiO2/Si substrate to avoid the aggregation).

Similarly **TEM** sample were prepared by deposing peptide solution (4µL, 1mg/mL in 6:4 MeOH/water) on cupper grid, dried at room temperature and imaged it. For **AFM**, samples were drop casted on mica, dried at room temperature and imaged.

Effect of physical, chemical and enzyme stability on vesicle morhology

To test pH sensitivity of the vesicles, we made vesicle solution acidic and basic by adding TFA and conc NaOH, respectively and imaged it. For thermal stability we drop casted vesicle solution onto a SiO_2/Si substrate and kept it in the oven at different temperatures and imaged it. The resistance to enzymatic proteolysis of vesicles was investigated by treating them with proteinase K. Proteinase K solution was prepared by dissolving 0.4 mg enzyme in 1 mL 60% methnol/ water and added to the vesicle solution. In order to maintain the proteolytic activity of proteinase K, the solution was incubated for 24 hours at 37 °C. For thermogravimetric analysis (TGA), vesicles solution was lypholized and TGA was carried out on a Perkin Elmer STA 6000 simultaneous thermal analyzer. The sample was heated in an alumina crucible at a rate of 5 °C min^{-1}.

Carboxyfluorescein encapsulation study

1.3 mM carboxyfluorescein solution was added to the peptide vesicles solution to make the final concentration 0.1 mM and then kept it over night and dialyzed .

Procedure for fluorescent leakage study

Peptide vesicles (200 µL) loaded with carboxyfluorescein was sealed in dialysis membrane and then 200µL of 5 mM solution of cationic dipeptide in water was added. This dialysis bag was suspended in agitating methanol /water solution. Further, 300µL aliquot of suspension medium was timely collected and quantification of released carboxyfluorescein was carried out.

Fluorescence measurement

Fluorescent measurement experiments were carried out using FluoroMax-4 HORIBA fluorimeter, with 492 nm excitation and 500-650 nm emission range using 2/2 slit and 1 nm

data interval. The 300 µL aliquots obtained from leakage assay were diluted to 200 µL with methanol.

Laser Scanning Confocal Microscopy Experiments.

Carboxyfluorescein entrapped vesicles solution was drop casted on a glass slide, dried and then imaged using OLYMPUS ZX81 laser scanning microscopy.

NMR

NMR spectra were recorded on 700 MHz spectrometer in CD_3OH solvent. Nearly 3mM peptide concentrations were used. Temperature were maintained at 278K to move away residual water signal away from C^{α} proton signals and the water suppression power had minimal effect on nearby peptide resonances. Resonance assignments were carried by using TOCSY[1] and ROESY[2] spectra. All 2D spectral widths were 12 ppm with 2048 x 512 time domain points in t2 and t1 domains respectively. Data set was zero filled to 4K x 2K before Fourier transformation. A mixing time of 100ms and 250ms were used for TOCSY and ROESY spectrum respectively. All NMR data were processed offline using TOPSPIN version 2.1 software. Scalar coupling (J) values were directly measured from high resolution 1D recording. Amide proton temperature coefficients ($d\delta/dT$) were measured by recording 1D experiment at definite intervals of 10 degrees (K) in the temperature range of 278-318K. Conc dependent NMR spectra were recorded on 500 MHz spectrometer in CD_3OH solvent.

Modeling

A computer model was generated using discover studio version 3.5 software based on NMR data. The dihedral angles ϕ and ψ were maintained at near extended values based on $^{3}J_{NHC^{\alpha}H}$ values and observation of weak d_{NN} and relatively strong $d_{\alpha N}$ NOEs. The θ_1 and θ_2 dihedrals for the Aic residues were fixed at gauche (*g*) and *trans* (*t*) values so that it agree with the observed NOE pattern. The resultant structure was energy minimized with Powell-Reeves Conjugate Gradient (PRCG) method (Macro Model 10.3) using OPLS2005 force-field. The final structure matched with all NMR parameters.

5.5.1 CD spectra of the peptides P1, P2 and P3

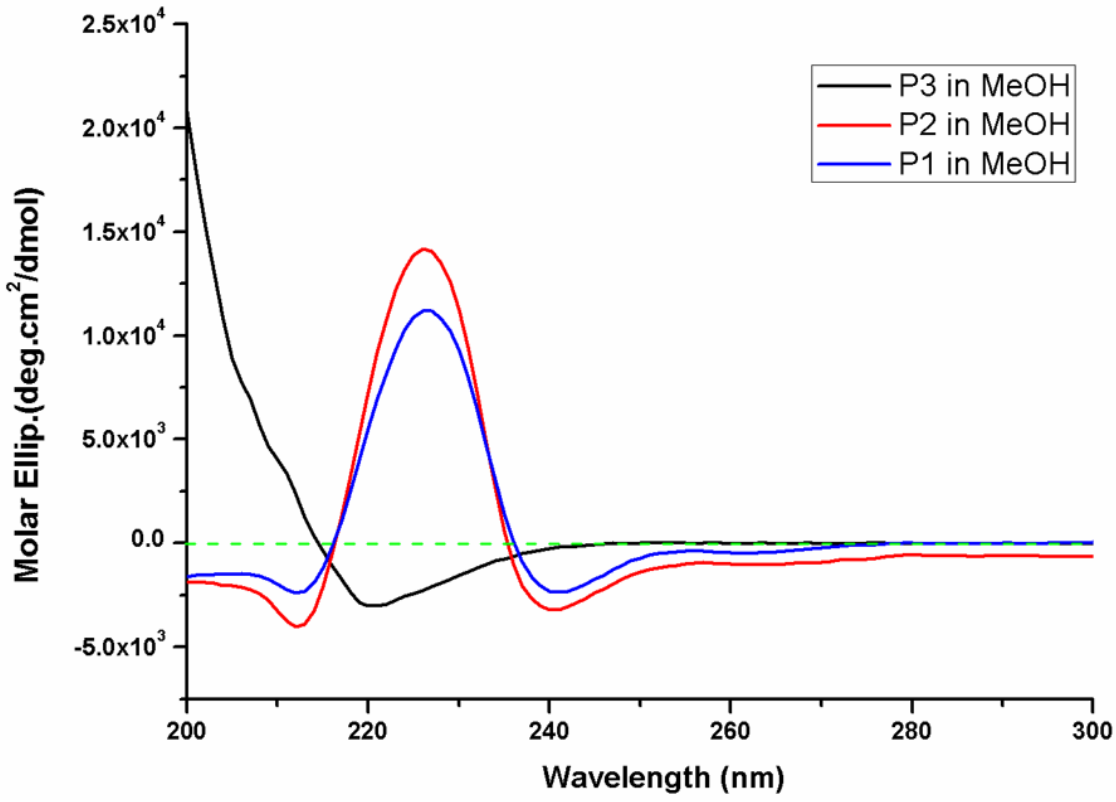

Figure 13: CD signature of peptides **P1**, **P2** and **P3** in methanol.

5.5.2 TGA curve of the peptide P1 and P2

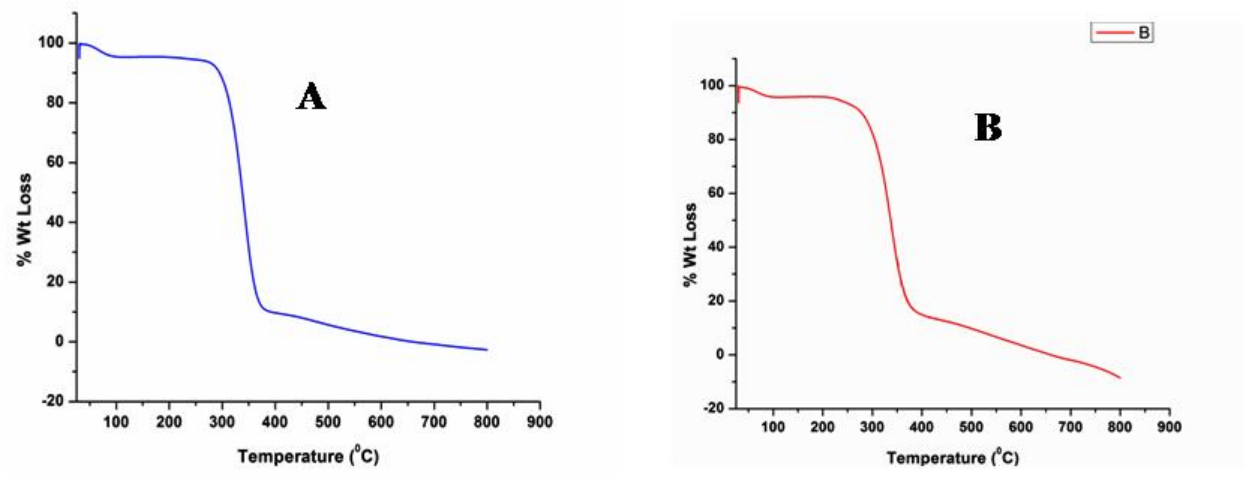

Figure 14 (A,B) Thermogravimetric thermograms of peptide **P1** and **P2** showing high thermal stability.

5.5.3 EDAX analysis of peptides P1, P2 and P3

A

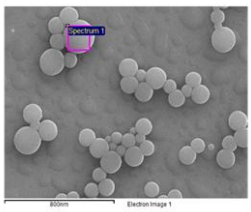

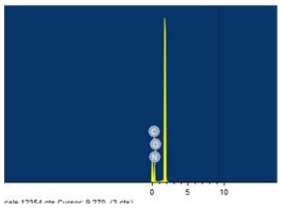

Element	weight%	Atomic%
C K	57.93	62.84
N K	25.07	23.31
O K	17.00	13.85
Total 100		

B

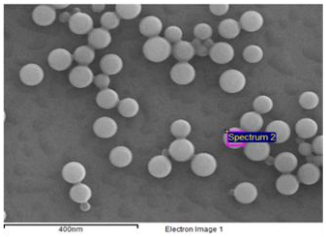

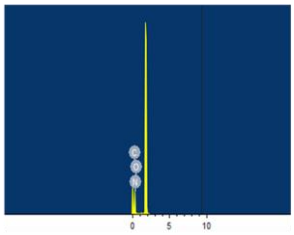

Element	weight%	Atomic%
C K	56.72	61.43
N K	29.14	27.06
O K	14.14	11.50
Total 100		

C

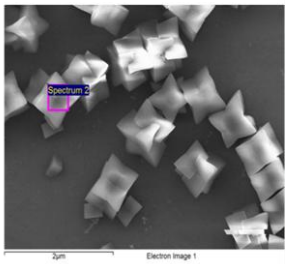

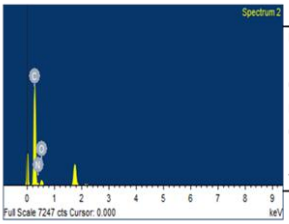

Element	Weight%	Atomic%
C K	67.87	72.26
N K	18.06	16.49
O K	14.07	11.25
Totals	100.00	

Figure 15 A) EDAX analysis of peptide **P1;** B) EDAX analysis of peptide **P2;** C) EDAX analysis of peptide **P3**.

5.5.4 FT-IR spectrum of peptides P1 and P2

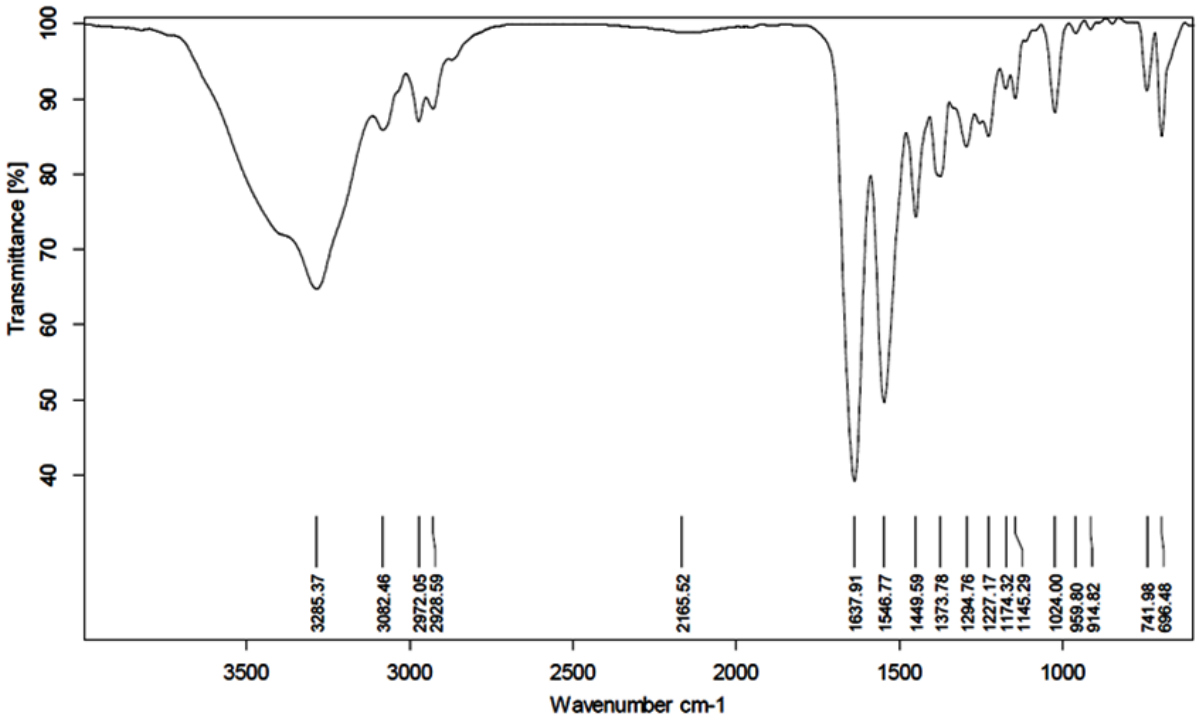

Figure 15 FT-IR spectrum of peptide **P1** recorded using 1 mg/mL in methanol water mixture (6:4)

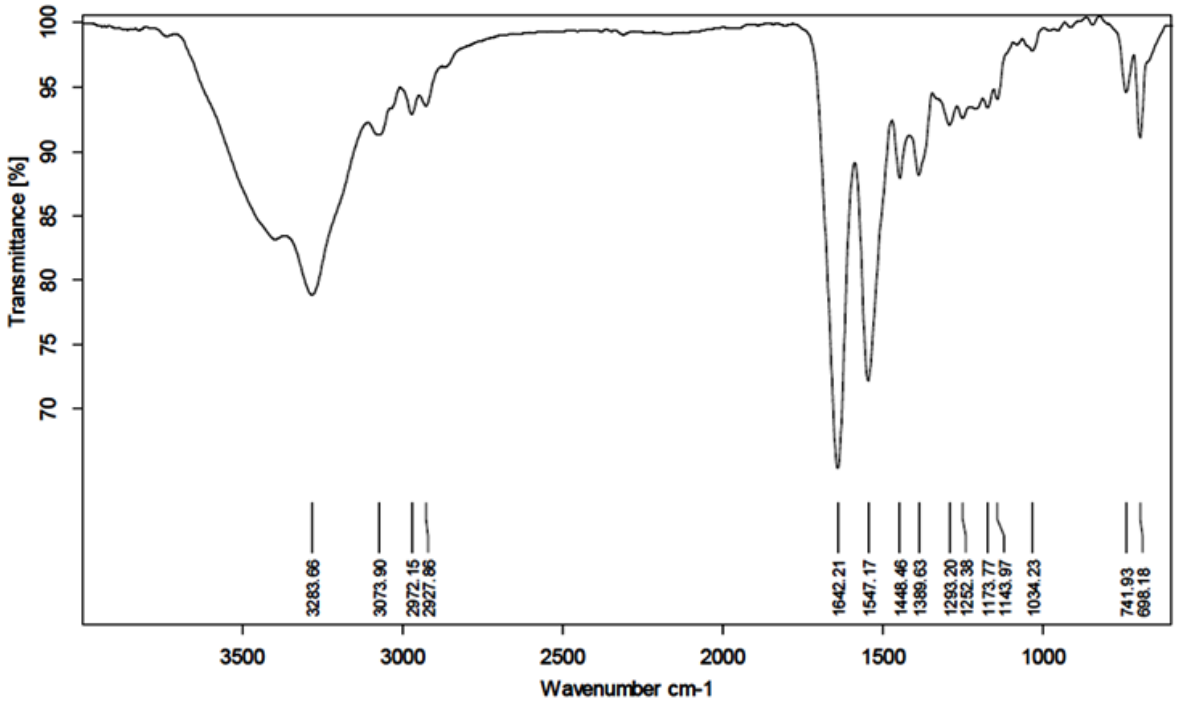

Figure 16. FT-IR spectrum of peptide **P2** recorded using 1 mg/mL in methanol water mixture (6:4)

5.6 References

1. a) Hosseinkhani, H.; Hong, P. -D.; Yu, D. S.; *Chem. Rev.* **2013**, *113*, 4837; b) Koutsopoulos, S.; Zhang, S. *Acta Biomater*. **2013**, *9*, 5162; c) Stephanopoulos, N.; Ortony, J. H.; Stupp, S. I. *Acta Biomater*. **2013**, *61*, 912; d) Hartgerink, J. D.; Beniash, E.; Stupp, S. I. *Science* **2001**, *294*, 1684; e) Hirst, A. R.; Escuder, B.; Miravet, J. F.; Smith, D. K. *Angew. Chem. Int. Ed.* **2008**, *47*, 8002; f) Kuang, Y.; Xu, B. *Angew. Chem. Int. Ed.* **2013**, *52*, 1; g) Zhao, F.; Ma, M. L.; Xu, B. *Chem. Soc. Rev*. **2009,** *38*, 883. h) Cavalli, S.; Albericio, F.; Kros, A. *Chem. Soc. Re*v. **2010**, *39*, 241. i) Gazit, E. *Chem. Soc. Rev*. **2007**, *36*, 1263; j) Branco, M.; Schneider, J. P. *Acta Biomater.* **2009**, *5*, 817. k) Tovar, J. D. *Acc. Chem. Res.* **2013**, *46*, 1527.
2. a) Seebach, D.; Beck, A. K.; Bierbaum, D. J.; *Chem. Biodiv*. **2004**, *1*, 1111; b) Cheng, R. P.; Gellman, S. H.; DeGrado, W. F.; *Chem. Rev.* **2001**, *101*, 3219; c) Horne, W. S.; Gellmann, S. H. *Acc. Chem. Res.* **2008**, *41*, 1399; d) Vasudev, P. G.; Chatterjee, S.; Shamala, N.; Balaram, P. *Chem. Rev*. **2011**, *111*, 657; e) Vasudev, P. G.; Chatterjee, S.; Shamala, N. Balaram, P. *Acc. Chem. Res*. **2009**, *42***,** 1628; f) Balaram, P. *Biopolymers* **2010**, *94*, 733. g) Chatterjee, Vasudev, S. P. G.; Raghothama, S.; Ramakrishnan, C.; Shamala, N.; Balaram, P. *J. Am. Chem. Soc.* **2009**, *131*, 5956; h) Guo, L.; Zhang, W.; Reidenbach, A. G.; Giuliano, M. W.; Guzei, I. A.; Spencer, L. C.; Gellman, S. H. *Angew. Chem. Int. Ed.* **2011**, *50*, 5843; i) Pilsl, L. K. A.; Reiser, O. *Amino Acids* **2011**, *41*, 709; j) Berlicki, L.; Pilsl, L.; Wéber, E.; Mándity, I. M.; Cabrele, C.; Martinek, T. A.; Fülöp, F.; Reiser, O. *Angew. Chem., Int. Ed*. **2012**, *51*, 2208; k) Martinek, T. A.; Mandity, I. M.; Fulop, L.; Toth, G. K.; Vass, E.; Hollosi, M.; Forro, E.; Fülöp, F. *J. Am. Chem. Soc.* **2006**, *128*, 13539; l) Bouillere, F.; Laurent, S. T-.; Kouklovsky, C.; Alezra, V. *Amino Acids* **2011**, *41*, 687; m) Pendem, N.; Nelli, Y. R.; Douat, C.; Fischer, L.; Laguerre, M.; Ennifar, E.; Kauffman, B.; Guichard, G. *Angew. Chem. Int. Ed.* **2013**, *52*, 4147; n) Basuroy, K.; Dinesh, B.; Shamala, N.; Balaram, P. *Angew. Chem. Int. Ed.* **2013**, *52*, 3136.
3. Raguse, T. L.; Lai, J. R. LePlae, P. R.; Gellman, S. H. *Org. Lett.*, **2001**, *3* , 3963.
4. Goodman, J. L.; Petersson, E. J.; Daniels, D. S.; Qiu, J. X.; Schepartz, A. *J. Am. Chem. Soc*. **2007**, *129*, 14746.
5. Horne, W. S.; Price, J. L.; Keck, J. L.; Gellman, S. H. *J. Am. Chem. Soc* **2007**, 129, 4178.
6. Clark, T. D., Buehler, L. K., Ghadiri, M. R. *J. Am. Chem Soc*. **1998**, *120*, 651.

7. a) Hetenyi, A.; Mandity, I. M.; Martinek, T. A.; Toth, G. K.; Fulop, F.; J. *Am. Chem. Soc*. **2005**, *127*, 547; b) Mandity, I. M.; Fulop, L.; Vass, E.; Toth, G.K.; Martinek, T.A.; and Fulop,F. *Org. Lett.*, **2010**, *12* , 5584; c) Martinek, T. A.; Hetenyi, A.; Fulop, L.; Mandity, I. M.; Toth, G. K.; Dekany, I.; Fulop, F. *Angew. Chem. Int. Ed.*. **2006**, *45*, 2396.
8. a) Rua, F.; Boussert, S.; Parella, T.; Diez-Perez, I.; Branchadell, V.; Giralt, E.; Ortuno, R. M.; *Org. Lett.* **2007**, *9*, 3643; b) Gorrea, E.; Nolis, P.; Torres, E.; Silva, E. D.; Amabilino, D. B.; Branchadell, V.; Ortuno, R. M. *Chem. Eur. J.* **2011**, *17*, 4588; c) Torres, E.; Gorrea, E.; Burusco, K. K.; Silva, E. D. Nolis, P.; Rua, F.; Boussert, S.; Diez-Perez, I.; Dannenberg, S.; Izquierdo, S.; Giralt, E.; Jaime, C.; Branchadell, V.; Ortuno, R. M. *Org. Biomol. Chem.* **2010**, *8*, 564; d) Celis, S.; Nolis, P.; Illa, O.; Branchadell, V.; Ortuno, R. M. *Org. Biomol. Chem.* **2013**, *11*, 2839.
9. Pomerantz, W.C.; Yuwono, V.M.; Drake, R.; Hartgerink, J. D.; Abbott, N.L.; Gellman, S.H. *J. Am. Chem. Soc*. **2011**, *133*, 13604.
10. a) Kwon, S.; Jeon, A.; Yoo, S. H.; Chung, I.S.; Lee, H. S. *Angew. Chem. Int. Ed.* **2010**, 49, 8232. b) Kwon, S.; Shin, H. S.; Gong, J.; Eom, J. H.; Jeon, A.; Yoo, S. H.; Chung, I. S.;Cho, S. J.; Lee, H. S. *J. Am. Chem. Soc*. **2011**, *133*, 17618.
11. Seoudi, R.S.; Dowd, A.; Del Borgo, M.P.; Kulkarni, K.; Perlmutter, P.; Aguilar, M.I.; Mechler, A. *Pure Appl Chem*. **2015**, *87*, 1021.
12. Jadhav, S. V.; Gopi, H. N. *Chem. Commun.* **2013**, *49*, 9179
13. Misra, R.; Saseendran, A.; George, G.; Veeresh, K.; Raja, K. M. P.; Raghothama, S.; Hofmann, H.-J; Gopi, H. N. *Chem. Eur. J.* **2017**, *23*, 3764.
14. Misra, R.; Raja, K. M. P.; Hofmann, H.-J.; Gopi, H. N. *Chem. Eur. J*. **2017**, 23, 16644
15. a) Karle, I. L.; Balaram, P. *Biochemistry* **1990**, *29*, 6747. b) Toniolo, C.; Benedetti, E. *Trends Biochem. Sci*. ***1991***, *16*, 350; c) Karle, I. L. *Biopolymers.* **1996**, *40*, 157 d) Kumita, J. R.; Weston, C. J.; Choo-Smith, L.-P.; Wooley, G. A.; Smart, O. S. *Biochemistry* **2003**, *42*, 4492; e) Aravinda, S.; Shamala, N.; Balaram, P. *Chem. Biodiversity* **2008**, *5*, 1238; f) Clayden, J.; Castellanos, A.; Solà, J.; Morris, G. A. *Angew. Chem. Int. Ed.*, **2009**, *48*, 5962.
16. a) Chirgadze, Y. N.; Nevskaya,N. A. *Biopolymers* **1976**, *15*, 627. b) Qian, W.; Bandekar, J.; Krimm, S. *Biopolymers* **1991**, *31*, 193.
17. a) Chatterjee,S.; Vasudev, P. G.; Ananda, K.; Raghothama, S.; Shamala, N. Balaram, P. *J. Org. Chem*. **2008**, 73, 6595; b) Jadhav, S. V.; Bandyopadhyay, A.; Gopi, H. N. *Org. Biomol. Chem.* **2013,** *11*, 509; c) Bandyopadhyay, A.; Jadhav, S. V.; Gopi, H.

N. *Chem. Commun.* **2012**, *48*, 7170. d) Jadhav, S. V.; Misra, R.; Singh, S. K.; Gopi, H. N. *Chem. Eur. J.* **2013**, *19*, 16256

18. Ge, J.; Lei, J.; Zare, R. N. *Nat. Nanotechnol*. **2012**, *7*, 428.
19. Reches, M.; Gazit, E. *Science* **2003**, *300*, 625.
20. Gallivan, J. P.; Dougherty, D. *Proc. Natl. Acad. Sci. USA*.**1999**, 96, 9459
21. a) Ghosh, S.; Reches, M.; Gazit, E.; Verma, S. *Angew. Chem. Int. Ed*. **2007**, *46*, 2002; b) Chen, L. J.; Zhao, G. Z.; Jiang, B.; Sun, B.; Wang, M.; Xu, L.; He, J.; Abliz, Z.; Tan, H. Li, X.; Yang, H. B. *J. Am. Chem. Soc.* **2014**, 136, 5993.

5.7 Appendix I: Mass spectra and ^{1}H NMR for the peptides P1 and P2

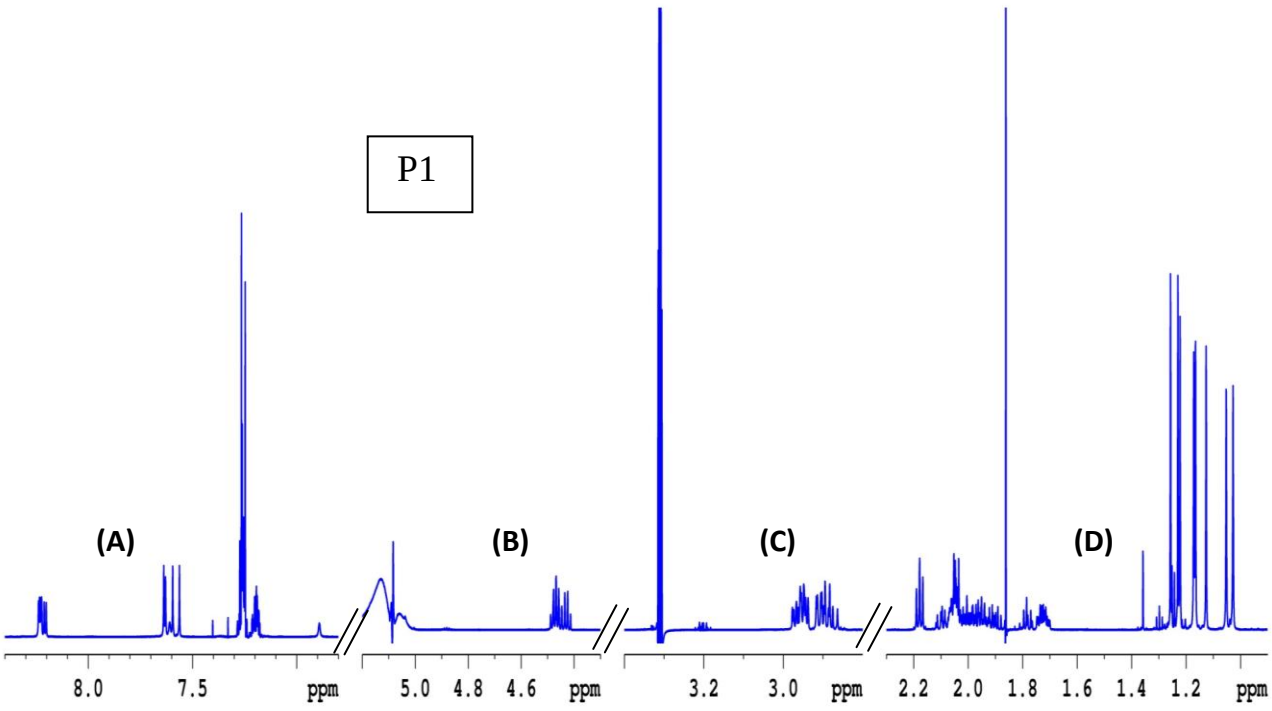

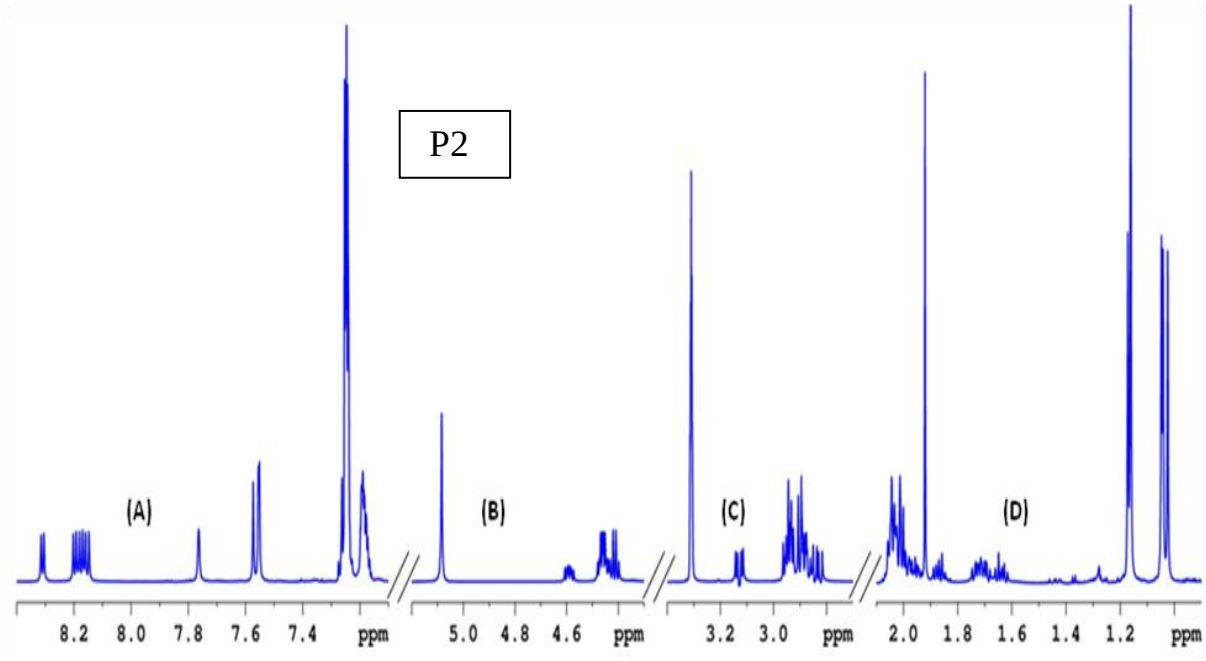
P2
(A)
(B)
(C)
(D)
8.2 8.0 7.8 7.6 7.4 ppm
5.0 4.8 4.6 ppm
3.2 3.0 ppm
2.0 1.8 1.6 1.4 1.2 ppm

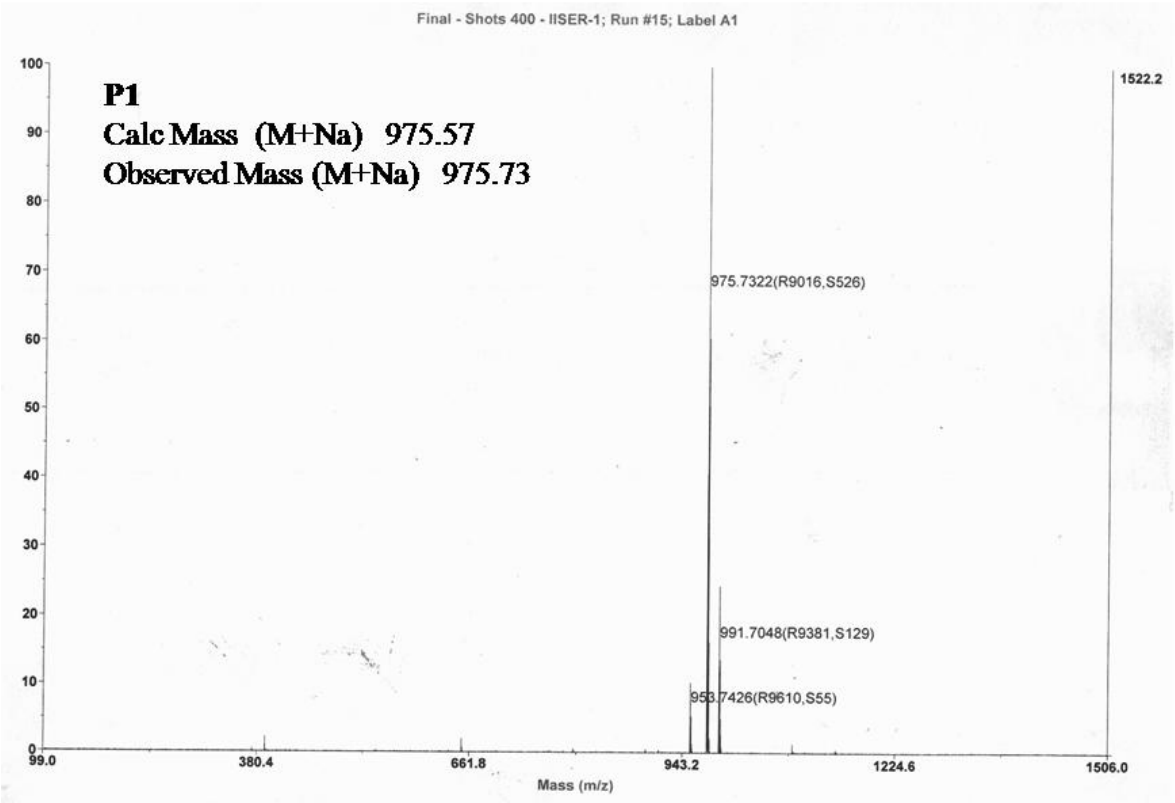
Final - Shots 400 - IISER-1; Run #15; Label A1
P1
Calc Mass (M+Na) 975.57
Observed Mass (M+Na) 975.73
975.7322(R9016,S526)
991.7048(R9381,S129)
953.7426(R9610,S55)
1522.2
Mass (m/z)

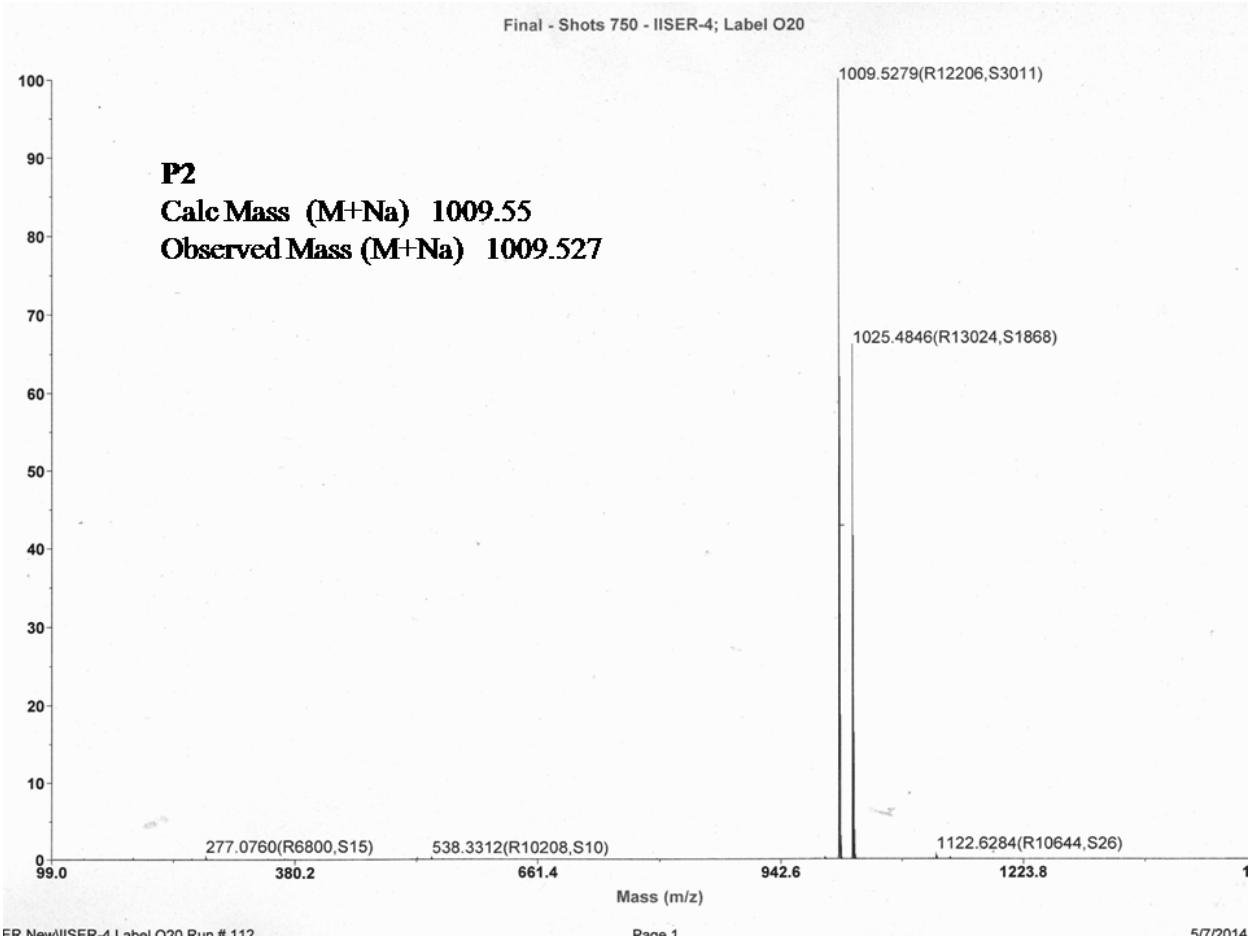
Final - Shots 750 - IISER-4; Label O20
1009.5279(R12206,S3011)
P2
Calc Mass (M+Na) 1009.55
Observed Mass (M+Na) 1009.527
1025.4846(R13024,S1868)
277.0760(R6800,S15)
538.3312(R10208,S10)
1122.6284(R10644,S26)
100
90
80
70
60
50
40
30
20
10
0
99.0
380.2
661.4
942.6
1223.8
Mass (m/z)

Chapter 6

Ambidextrous α,γ-Hybrid Peptide Foldamers with Reversal of Helix Directionality

6.1 Introduction

Helicity is the most common structural feature associated with many kinds of molecules including biopolymers.[1] As proteins are exclusively built from L-amino acids, this stereochemical bias is reflected in their strong preference to right-handed (*P*) helices over the left-handed (*M*) helices. Nevertheless, a recent systematic survey of protein crystal structures revealed the presence of short left-handed helices.[2] Along with helices from chiral amino acids, significant efforts have been made in the literature to build helices completely from achiral amino acids such as Aib and its higher dialkyl substituted analogues.[3,4] Due to their intrinsic conformational restriction, Aib residues ($\phi \sim \pm 60°$ and $\psi \sim \pm 30°$) invariably promote helical conformations. This helix nucleating property of Aib has been widely explored to design α- and 3_{10}-helices. The helices constructed entirely from achiral Aib residues have shown to adopt both (*P*)-and (*M*)-helices. Experimentally characterized α-helix, 3_{10}-helix and racemic right- and left-helices containing Aib residues are shown in Figure 1.

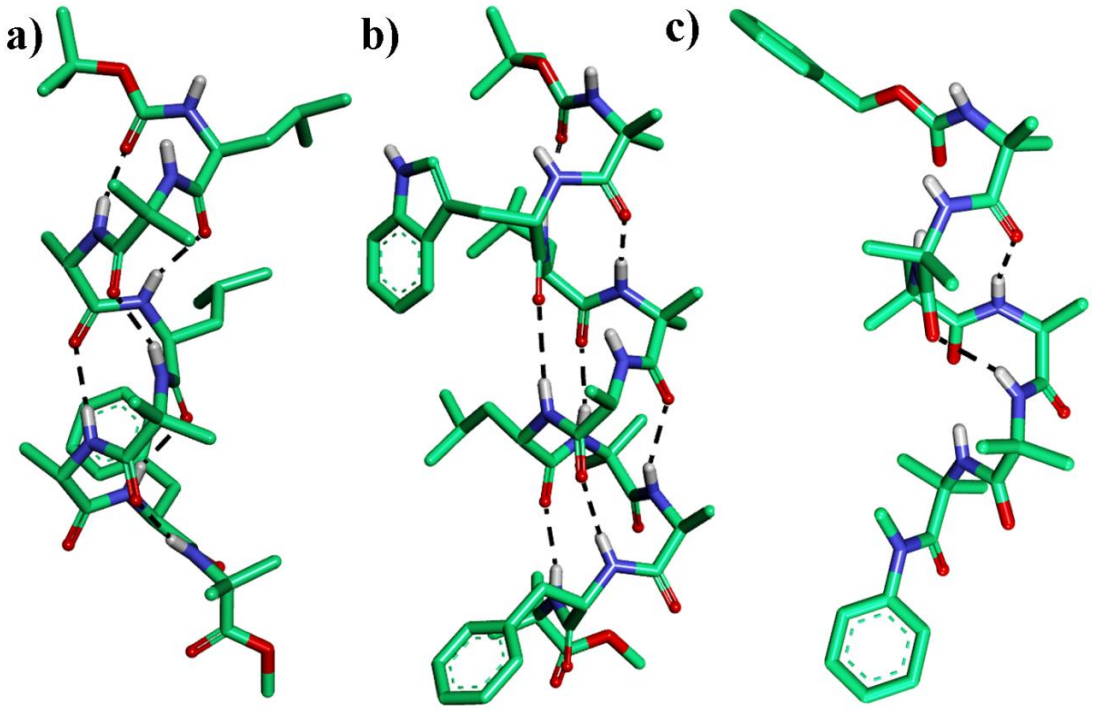

Figure 1 Examples of experimentally characterized helical α-peptide sequence incorporated with Aib amino acid a) 3_{10} helix Boc-(Leu-Aib-Ala)$_2$-Phe-Aib-OMe,[3p] b) α-helix initiated with 3_{10} helix Boc-Aib-Trp-(Leu-Aib-Ala)-Phe-Aib-OMe.[3p] c) Poly Aib peptide, Cbz-Aib$_6$-N(Me)Ph.[3q]

Compared to the limited set of α-peptide helices, foldamers composed of unnatural β- and γ-peptides uncovered various helical types with the distinct intramolecular H-bonding pattern.[5,6] Instructively, the majority of β- and γ-peptides foldamers showed H-bonding between 1→4 residues, similar to the 3_{10}-helices. Moreover, foldamers composed of complete achiral β- and γ-amino acids have not been scrutinized as that of corresponding chiral amino acids. Nonetheless, Seebach and colleagues demonstrated a stair-like 8-helices[7] and uncommon extended sheets from the oligomers of α,α-dialkyl β- amino acids.[8] In continuation, Balaram and colleagues showed 9-helical (1→3, H-bonds) conformations from the oligomers of achiral 3,3-dialkyl substituted γ-amino acid gabapentin (gpn),[9] and 12-helices (1→4, H-bonds) from achiral hybrid peptides composed of Aib and gabapentin (Figure 2a).[10]

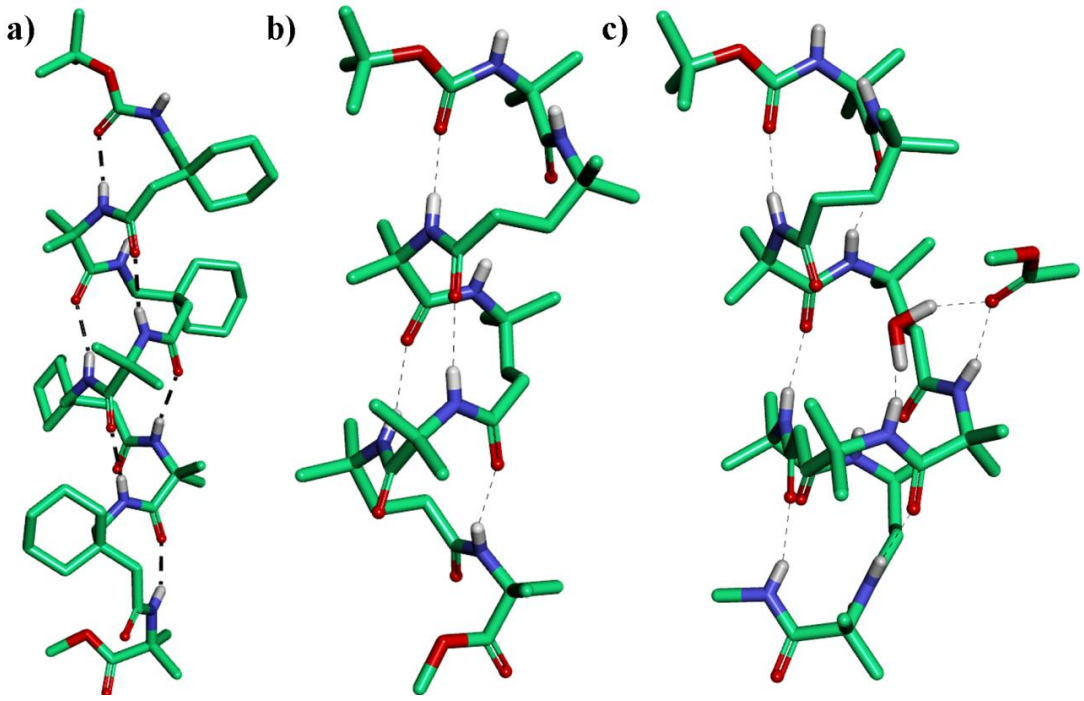

Figure 2 a) The crystal structures of 12-helix for the octapeptides Boc-Gpn-Aib-Gpn-Aib-Gpn-Aib-Gpn-Aib-OMe.[7i] b) The crystal structures of 12-helix of Boc-Aib-Aic-Aib-Aic-Aib-Aic-Aib-OMe.[12] c) The crystal structures of 15/17-helix of Boc-Aib-Aic-Aib-Aic-Aib-Aic-Aib-Aic-Aib-NHMe[12]

In a sharp contrast to the 3_{10}-helices of Aib oligomers, the double homologated Aib (4,4-dimethyl substituted γ-amino acid, Aic,) oligomers have shown to adopt extended sheet type

conformations and spontaneously self-aggregates into fibers.[11] In the Chapter 3 and 4 we showed the different types of helical structures available to the α,γ-hybrid peptides consisting of Aic residues. The 1:1 combination of Aic with helix inducing Aib in 1:1 alternating α,γ-hybrid peptides showed the co-existence of 15/17-helices (1→5 H-bonds) and 12-helices(1→4 H-bonds) in single crystals,[12] analogous to the α- helix (1→5 H-bonds) and 3_{10}-helices(1→4 H-bonds) of α-peptides (Figure2c, 2b). In addition, we have shown the mixed helices and extended sheet types structures in α,γ-hybird peptides composed natural α-amino acids and Aic residues in the Chapters 4 and 5, respectively. The unique structural features of α,γ-hybrid peptides containing 4,4-gem-dimentyl substituted γ-amino acids motived us examine the structural features of 3,3-gem-dimethyl substituted γ-amino acids in α,γ-hybrid peptides.

6.2 Aim and rationale of the work

The remarkable structural features of hybrid peptides composed of 4,4-dimethyl γ-amino acid, motivated us to examine the impact of dimethyl substitutions at the β-position on γ-residues (4-amino-3,3-dimethyl butanoic acid, Adb) and their folding behavior in α,γ-hybrid peptides. In this chapter, we have designed, synthesized and studied the conformational properties of various α,γ-hybrid peptides composed of sterically constrained α-amino acids and Adb.

6.3 Result and discussion

6.3.1 Peptide design and synthesis

The sequences of achiral α,γ-hybrid peptides (**P1**-**P4**) under investigation is shown Scheme 1.

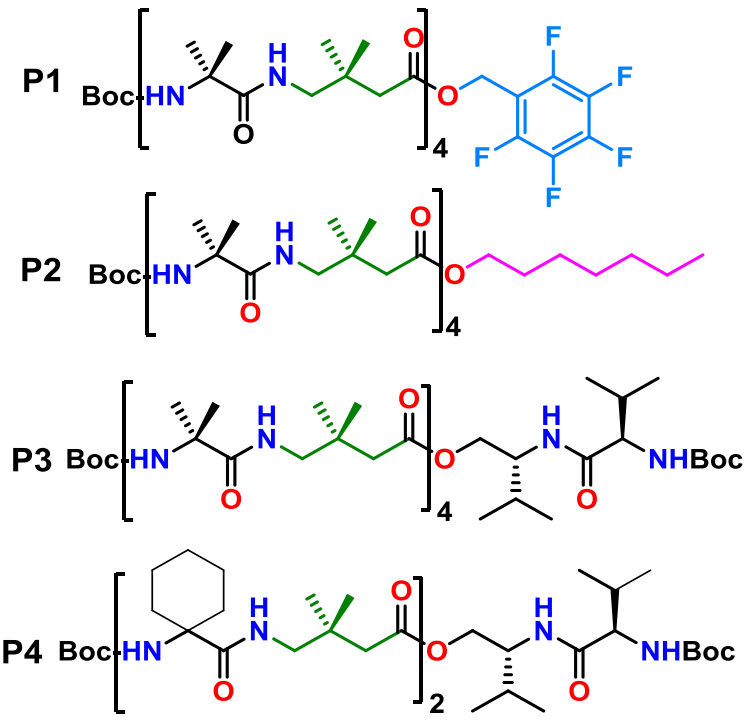

Scheme 1 Sequences of α,γ-hybrid peptides

The 3,3-dimethyl γ-amino acid was synthesized in excellent yield through the Michel addition of nitromethane[13] to 2,2-dimethyl ethyl acrylate, and subsequent transformation of nitro into amine by catalytic hydrogenation. The schematic representation of the Adb synthesis is shown in the Scheme 2. Synthetic details and characterization of Boc-Adb are given in the experiment section.

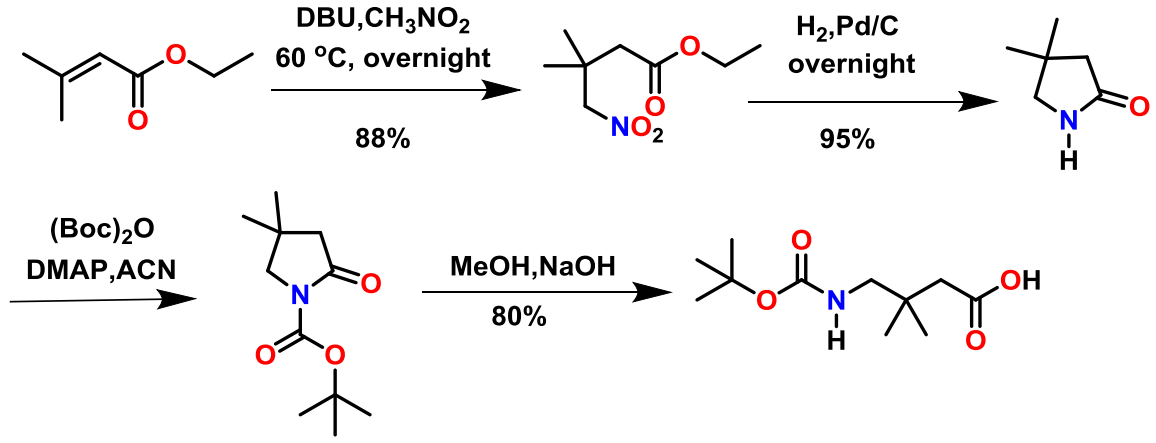

Scheme 2: Synthesis of N- Boc protected 3,3-dimethylbutanoic acid (Adb)

All hybrid peptides were synthesized in solution phase chemistry using EDC/HOBt as coupling agents and purified through reverse phase HPLC. As crystal structures provide

unambiguous conformational behaviour of peptides, we subjected all peptides in the Scheme 1 to crystallization. Initially, the octapeptide **P1** was designed to understand whether this peptide can adopt 12- or 15/17- helix similar to its Aib/Aic analogues.[12] To facilitate the crystallization, we used pentafluorobenzyl ester of Adb at the C-terminus. Based on the structural properties of **P1** other peptides were designed and synthesized. The structural details of **P1** in single crystals are given below.

6.3.2 Crystal structure analysis of peptide P1

Single crystals of **P1** obtained in aqueous MeOH solution yield an interesting structure shown in Figure 3a. The local conformation of Adb residues is described by the backbone torsion angles ϕ(N-C^{γ}), θ_1(C^{γ}-C^{β}), θ_2(C^{β}-C^{α}) and ψ(C^{α}-C=O). The torsion angles of Aib and Adb residues are given in the Table 1. Notably, **P1** adopted an uncommon helix conformation with the co-existence of left- and right-handed helical screw sense, along with a remarkable reversal of helix directionality at the C-terminus. The structure adopted by the peptide **P1** representing a phenomenon observed in macroscopic "tendril perversion".[14] This type of opposite screw sense is a subject of interest, and the co-existence of left- and right-handed helical screw sense is rather unusual in peptide foldamers. Recently, Clayden and colleagues trapped tendril perversion in molecular level by introducing opposite chiral amino acids at the *N*- and *C*-terminus of a helix composed of achiral Aib oligomers.[15] The crystal structure analysis of **P1** reveals three interesting features; the two *N*-terminus residues adopted a left-handed helix screw sense, while middle five residues adopted a right-handed helix screw sense, and finally, the C-terminal Adb ester adopted a left-handed conformation with reversal helix directionality.

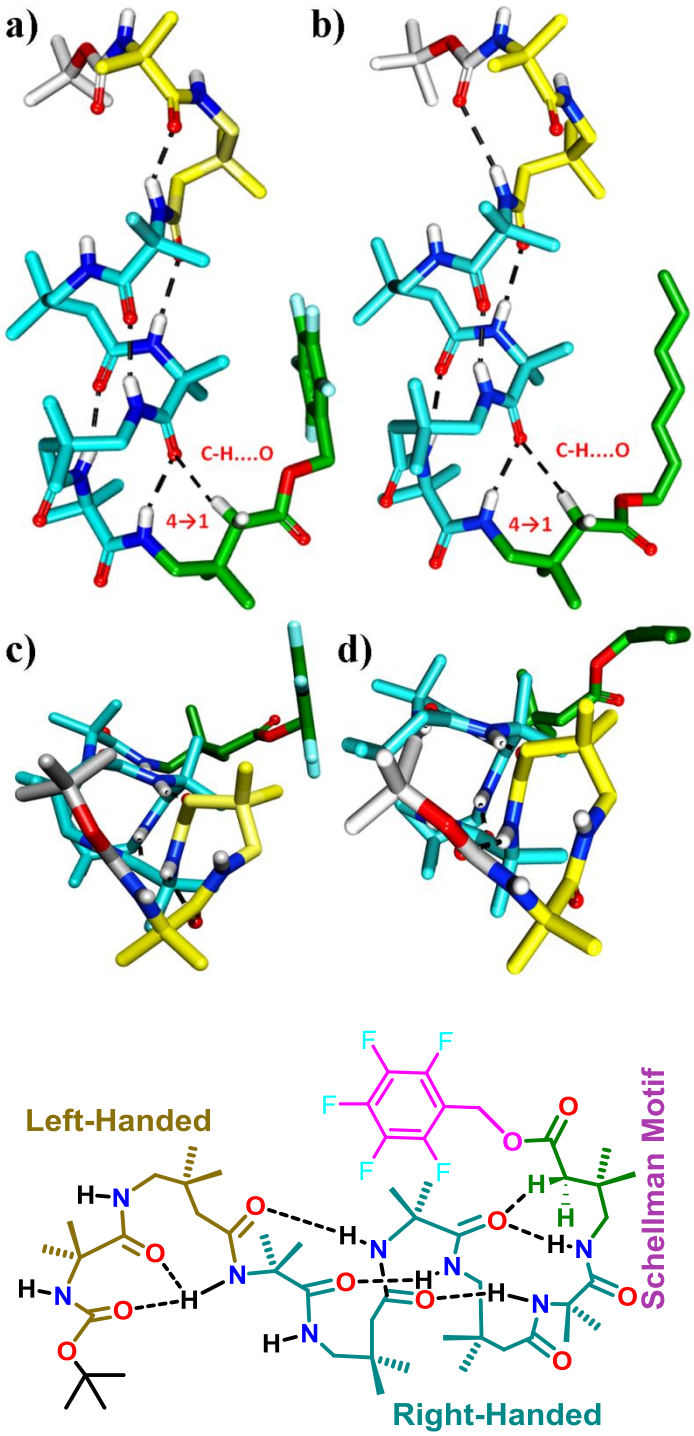

Figure 3 X-ray structure of peptides a) **P1** and b) **P2**. The left- and right-handed helical conformations are highlighted in yellow and cyan, respectively. The helix terminating C-terminal Adb esters are highlighted in green. Top view of **P1** and **P2** are shown in c) and d), respectively. The top views provided a clear distinction of left and right handed helical conformations; e) Chemical structure of **P1** depicting left- and right-handed helical screw sense, and Schellman motif signature along with the intramolecular H-bonds.

Table 1 Torsional Angle Parameters of **P1**

α, γ -	ϕ	θ_1	θ_2	ψ	ω
Aib 1	56	-	-	36	174
Adb 2	114	-56	-76	90	-174
Aib 3	-59	-	-	-35	-175
Adb 4	-126	57	55	-111	-170
Aib 5	-56	-	-	-41	-172
Adb6	-126	52	63	112	-173
Aib 7	-59	-	-	-44	-167
Adb	99	59	176	169	

Table 2 Hydrogen Bond Parameters of **P1**

Intramolecular H-bonds

Donor (D)	Acceptor (A)	D….A (Å)	DH….A (Å)	NH….O (deg)
N3	O3	2.83	2.11	141
N3	O2	3.87	3.19	137
N5	O4	2.82	2.13	161
N6	O5	2.89	2.06	160
N7	O6	2.83	2.10	163
N8	O7	2.85	2.04	159

Intermolecular H-bonds

Donor (D)	Acceptor (A)	D….A (Å)	DH….A (Å)	NH….O (deg)

N1	O8	3.03	2.21	160
N2	O9	3.08	2.23	170

The hydrogen bond parameters of **P1** are tabulated in the Table 2. The *N*-terminus left-handed helix is stabilized by a weak 12-membered H-bond between Boc CO and Aib3NH ($i \rightarrow i+3$) as well as a nine membered H-bond between the Aib 1CO and Aib3 NH ($i \rightarrow i+2$). Interestingly, Adb4 NH does not participate in the canonical H-bonding, and this type of non H-bonding partners have been observed at the junction of left- and right-handed helical fusion.[15,16] The right-handed helix observed from the residues Aib3 to Aib7 is stabilized by 12-membered H-bonds (12-helix) between the residues *i* and *i+3*, which is the most stable helix conformation observed in the α,γ-hybrid peptides composed of γ^4-amino acids.[17] In contrast to the *gauche (g)* and *extended (t)* conformations along C^{γ}-C^{β} and C^{β}-C^{α} bonds adopted by the Aic residues in a 12-helix,[12] the Adb residues have adopted *g, g* conformations similar to γ^4-residues.[16] The C-terminal Adb ester adopted a left-handed helix conformation with reversal of helix direction. Instructively, the torsion variables θ_2 and ψ (C^{β}-C^{α}-C(O)'-O] adopted extended conformation. In addition, the C-terminal twist is stabilized by a 15 membered C-H···O H-bond between Aib6 CO and C^{α}H of Adb8 [C-H···O dist. 2.43Å and ∠ C-H···O is 125°]. The C-terminal helix reversal of **P1** is representing a Schellman motif observed in protein structures.[18] Schellman noted that helices in proteins are often terminated at the C-terminal residue by adopting a left-handed conformation. It is pertinent to note that the helix terminating residue is invariably achiral Gly and less frequently Asn. Similar type of helix termination is often observed in synthetic α-peptide helices containing C-terminal Aib esters.[19] We speculated that the C-H···O H-bond observed at the C-terminus of **P1** and the intermolecular head-to-tail H-bonds between the helices in the crystal packing may be responsible for the helix termination. The unusual structural information obtained from the peptide **P1** motivated us to synthesize peptide **P2** with n-heptanol ester at the C-terminus. The structural analysis of **P2** is given below.

6.3.3 Crystal structure analysis of peptide P2

The unusual left- and right-handed helical screw sense along with the Schellman motif type helix reversal motivated us to design peptide **P2** and examine whether the observed structure

is unique to **P1** or it can persist across other α, γ-hybrid peptides of achiral Aib and Adb. In **P2**, we chose to incorporate n-heptanol ester of Adb to understand the helix reversal is not due to the aromatic π-staking as well as to verify whether the n-alkane can also fold back towards the helix. Single crystals of **P2** grown in aqueous methanol solution yield the structure shown in Figure 3b. Similar to **P1**, **P2** adopted a rare helical conformation associated with left- and right-handed helix screw sense. The first two residues adopted the left-handed helix conformation, stabilized a weak 12-membered H-bond between Boc CO and Aib3 NH and a strong nine membered H-bond between Aib 1 CO and Aib 3 NH. As observed earlier, Adb4NH does not participate in the canonical intramolecular H-bonding. The torsional angles and H-bond parameters are tabulated in the Table 3 and Table 4. Residues from Aib 3 to Aib7 adopted a right-handed 12-helix conformation with similar torsion variables as observed in **P1** (Table 3). As anticipated, the C-terminal Adb ester displayed a Schellman motif type helix terminating property. Interestingly, the n-heptane chain fold back towards *N*-terminus of the helix. In addition, the C-terminal helix reversal is stabilized by a 15 membered C-H···O H-bond between Aib6 CO and $C^{\alpha}H$ of Adb8 [C-H···O dist. 2.49 Å and ∠C-H···O is 149°]. The conformational analysis of n-heptanol ester reveals that except C1-C2, other C-C bonds assumed antiperiplanar conformation. The C1-C2 and ester C-O bonds adopted *gauche* and *anticlinal* conformations, respectively.

Table 3 Torsion Angle (in degree) Parameters of **P2**

α, γ - hybrids	ϕ	θ_1	θ_2	ψ	ω
Aib 1	57	-	-	37	177
Adb 2	125	-56	-66	97	-167
Aib 3	-60	-	-	-39	-177
Adb 4	-125	59	55	-115	-160
Aib 5	-56	-	-	-39	-171
Adb 6	-133	54	59	-106	-176
Aib 7	-56	-	-	-47	-178
Adb	106	65	-177	109	

Table 4: Hydrogen Bond Parameters of P2

Intramolecular H-bonds

Donor (D)	Acceptor (A)	D….A (Å)	DH….A (Å)	NH….O (deg)
N3	O3	2.99	2.59	110
N3	O2	3.29	2.48	157
N5	O4	2.91	2.07	167
N7	O6	2.97	2.13	166
N8	O7	2.85	2.01	169

Intermolecular H-bonds

Donor (D)	Acceptor (A)	D….A (Å)	DH….A (Å)	NH….O (deg)
N1	O8	2.87	2.18	164
N2	O8	2.90	2.09	158

6.3.4 Solution NMR structure of peptide P1

Inspired by the unusual conformation behaviour of the two peptides in single crystal, we thought to investigate the solution structure of peptide **P1** employing 2D NMR (TOCSY and ROESY) technique to understand whether similar type of conformation exists in solution or not. The well dispersed ^{1}H NMR spectrum of peptide **P1** in $CDCl_3$ suggested an ordered structure in solution. The TOCSY spectrum of P1 is shown in Figure 4. The analysis of the ROESY spectrum revealed that strong NH↔NH NOEs between Aib-NH(*i*) and γ-NH(*i+1)* and weak NOEs between γ-NH(*i)* and α-NH(*i+1)*. Along with the sequential NH↔NH,

strong NOEs between$^{\gamma}CH_2$(*i-1)* and Aib-NH(*i*) were also found (Figure 5-8)). Furthermore, DMSO titration experiments revealed that all amide NHs (except the *N*-terminal BocNH) displayed negligible changes in their chemical shifts, thus suggesting their involvement in the intramolecular H-bonding (Figure 9). Using NOEs constrained and H-bonding restrains, the solution structure of peptide **P1** was generated and the superposition of ten lowest energy structures is shown in the Figure 10. Being achiral, peptide **P1** adopted both right and left handed conformations in solution. The average torsion angles measured using solution strcutres of **P1** are tabulated in the Tables 5 and 6.

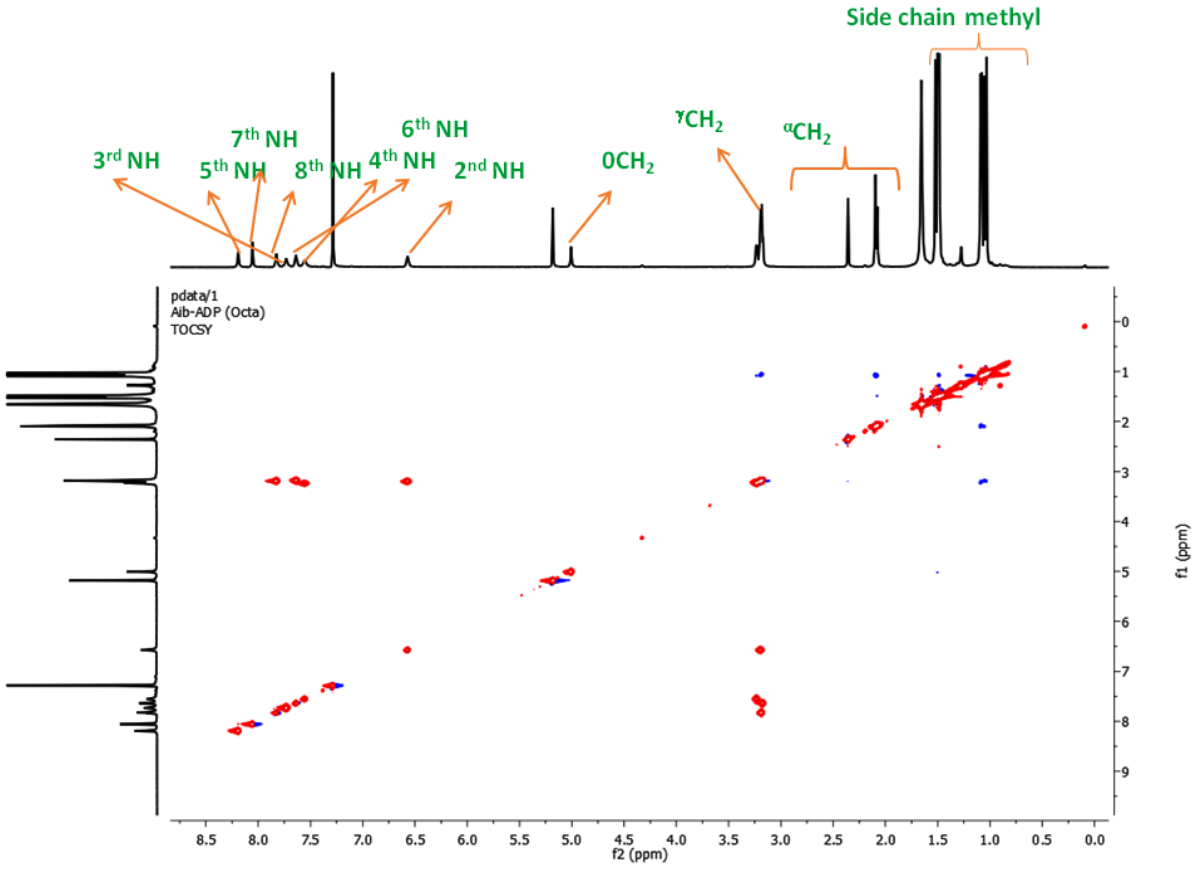

Figure 4 TOCSY spectrum of peptide **P1** (5 mM) in $CDCl_3$.

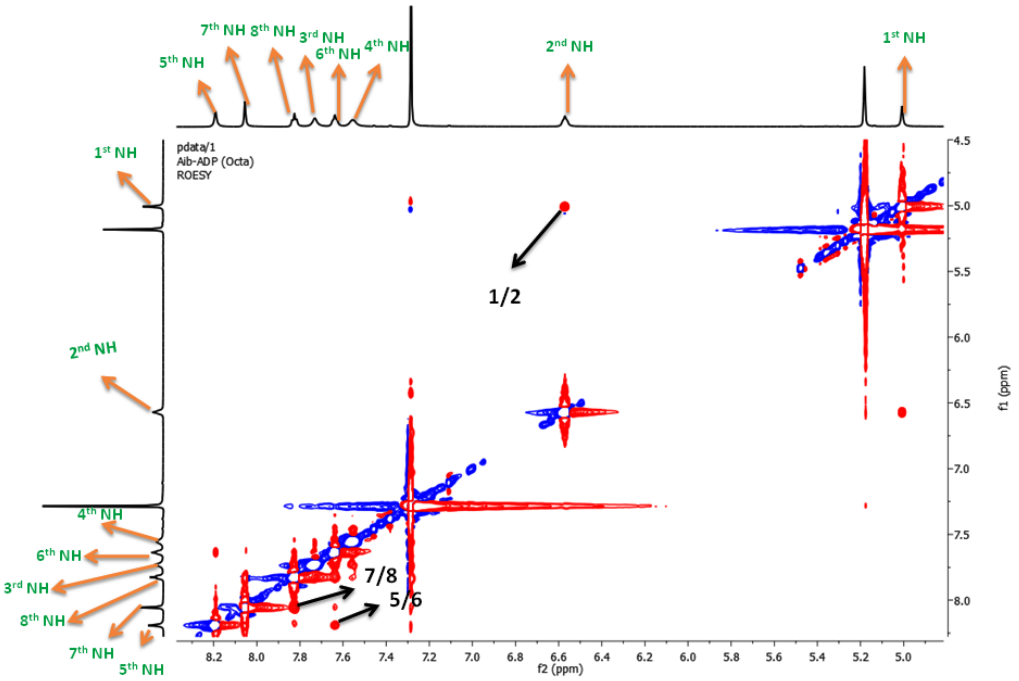

Figure 5 Partial ROESY spectrum of **P1** (5 mM) in $CDCl_3$ showing NH↔NH NOEs.

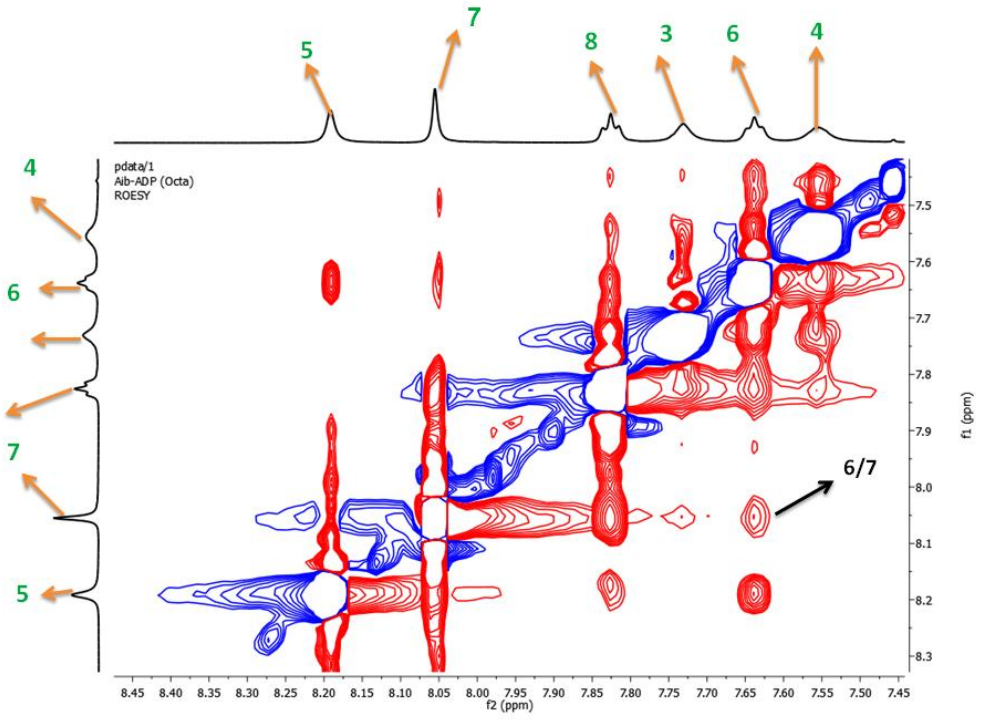

Figure 6 Partial ROESY spectrum of **P1** (5 mM) in $CDCl_3$ showing NH↔NH NOEs.

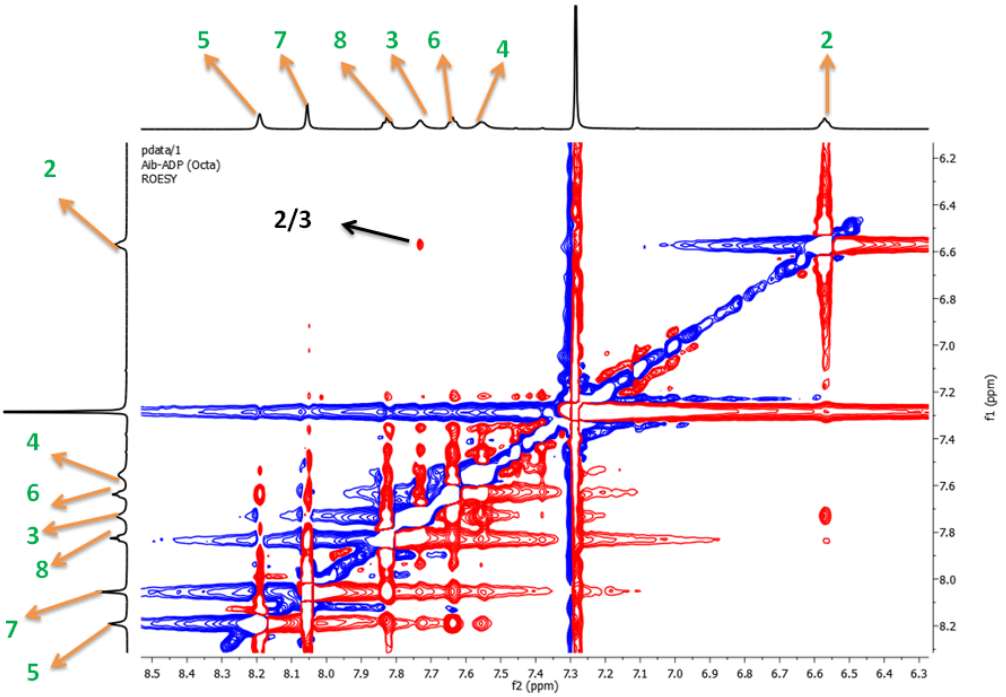

Figure 7 Partial ROESY spectrum of **P1** (5 mM) in $CDCl_3$ showing NH↔NH NOEs.

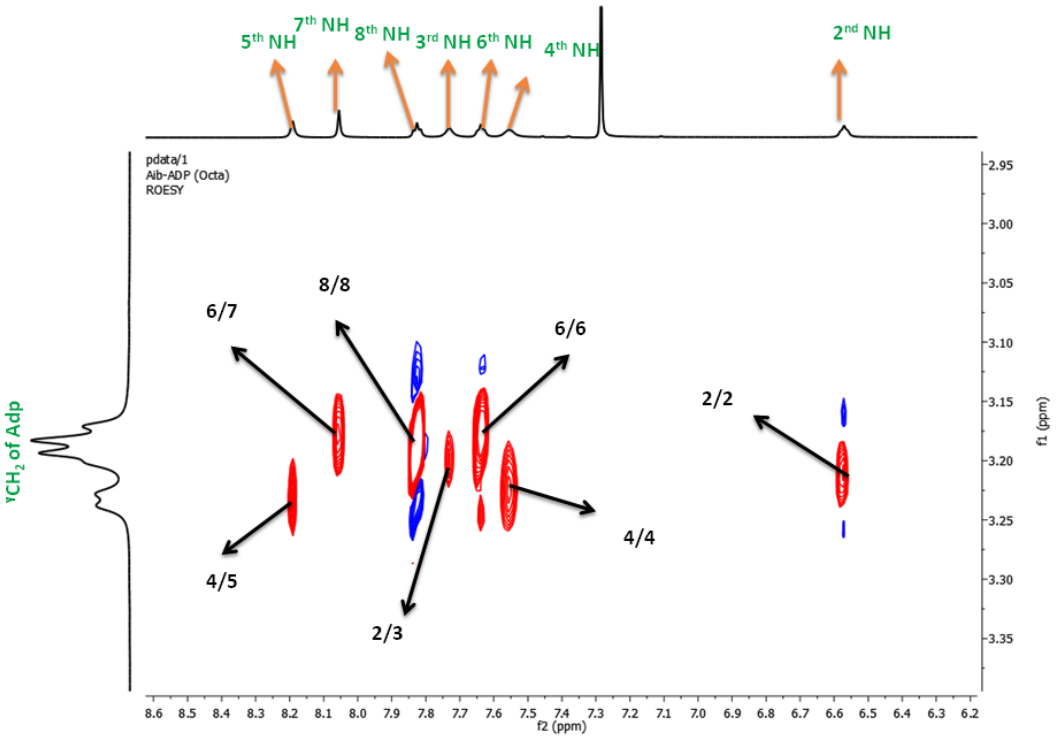

Figure 8 Partial ROESY spectrum of **P1** (5 mM) in $CDCl_3$ showing AibNH↔$^{\gamma}CH_2$ NOEs.

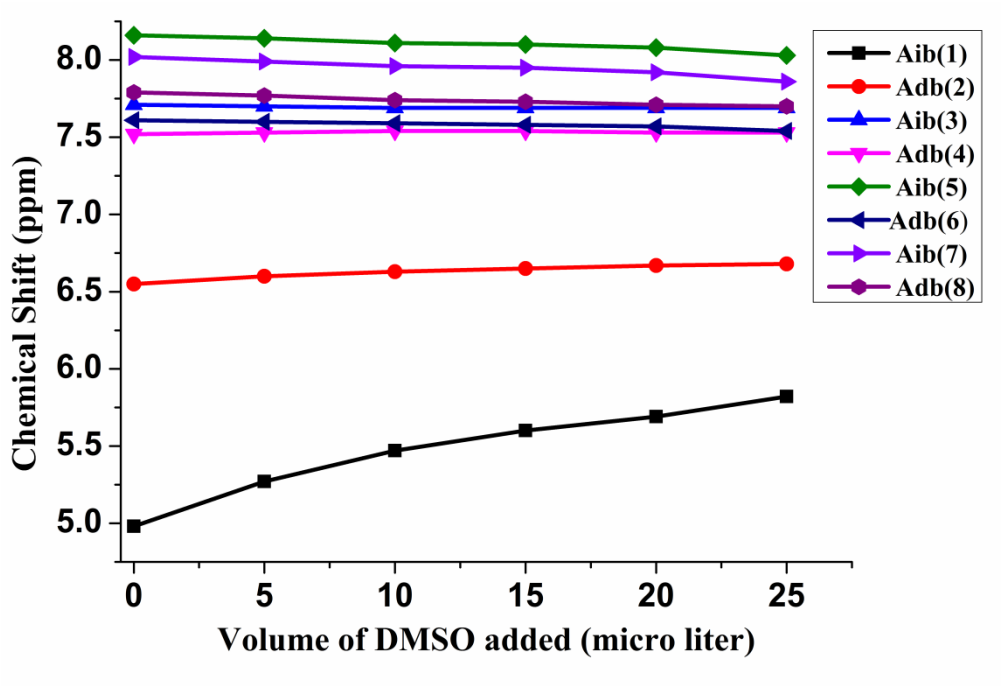

Figure 9 Solvent dependence of NH chemical shifts of peptide **P1** at varying concentrations of $(CD_3)_2SO$.

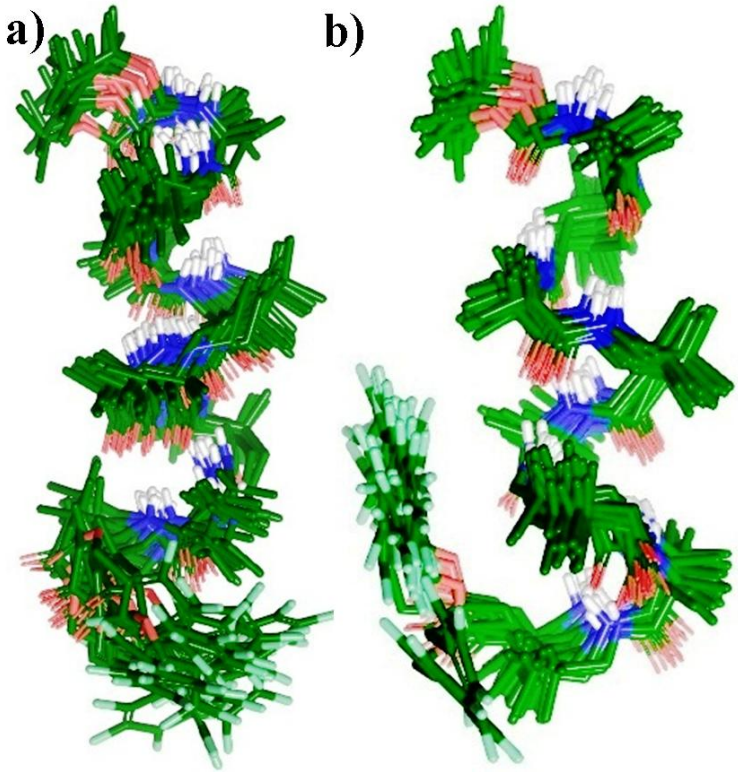

Figure 10 Solution conformations of peptides **P1**, a) right-handed conformation, b) left-handed conformation

Table 5 Dihedral angles (in degrees) measured from the minimized lowest energy conformation of Right handed helix sampled from simulation

Residue	φ	θ_1	θ_2	ψ
Aib(1)	-57			-42
Adp(2)	-128	59	52	-112
Aib(3)	-52			-49
Adp(4)	-123	53	57	-116
Aib(5)	-56			-41
Adp(6)	-129	51.4	62.9	-103
Aib(7)	-57			-42
Adp(8)	150	-51.9	-63.9	75.6

Table 6 Dihedral angles (in degrees) measured from the minimized lowest energy conformation of Left handed helix sampled from simulation

Residue	φ	θ_1	θ_2	ψ
Aib(1)	54			49
Adp(2)	122	-60	-53	116
Aib(3)	55			47
Adp(4)	124	-51	-60	113
Aib(5)	52			48
Adp(6)	131	-54	-60	113
Aib(7)	63			27.

6.3.5 Solution NMR structure of peptide P3

Inspired by the co-existence of opposite helix screw sense and helix terminating property, we sought to investigate whether this property can be explored to design Schellman loops. The helix-Schellman loop-helix structures are often found in proteins.[18] We hypothesize that instead of alkyl or aryl esters, if the C-terminal Adb is esterified with peptide alcohols it may be possible to design Schellman loops. In this context, peptide **P3** was designed (Scheme 1). We chose Boc-Val-Val-ol (dipeptide alcohol) for the C-terminal esterification. As peptide P3 did not yield X-ray quality single crystals, we subjected the peptide to 2D NMR analysis in $CDCl_3$. The analysis of ROESY spectrum of **P3** revealed strong NH↔NH NOEs between Aib1↔Adb2, Aib5↔Adb6, Aib7↔Adb8 and Val9↔Val10, and weak NH↔NH NOEs between Aib2↔Adb3 and Adb4↔Aib5. In addition, medium NOEs between Aib3NH↔C^{γ}HAdb2, Aib5NH↔C^{γ}HAdb4, Aib7NH↔C^{γ}HAdb6, and strong Aib3NH↔C^{α}HAdb2, Aib5NH↔C^{α}HAdb4, Aib7NH↔C^{γ}HAdb6, and Val9NH↔C^{α}H Val10, and a weak NOE between Val 9NH↔C^{γ}HAdb 8 were also observed (Figure11 and Figure12). Further, the DMSO titration studies suggested that except the *N*-terminus Aib1 and Adb 2 NHs, no pronounced chemical shift variation is observed in other amide NHs9 (Figure13). It is fairly surprising that the amide NHs of Val-Val residues are also not exposed to solvent, indicating their involvement in the intramolecular H-bonding. Using unambiguous NH↔NH and other NOEs, the solution structure of **P3** was generated and the superposition of ten lowest energy minimized structures is shown in Figure 14. Instructively, the peptide adopted a continuous right-handed 12-helix conformation up to Aib 7. The C-terminal Adb adopted a left-handed helical conformation. Intriguingly, the Val9 and Val10 NHs are involved in the bifurcated H-bonds with Aib7CO. The average torsion values of NMR derived structures are given in the Table 7. Overall, the structure of **P3** resembling a helix-Schellman loop conformation observed in the protein structures.[17]

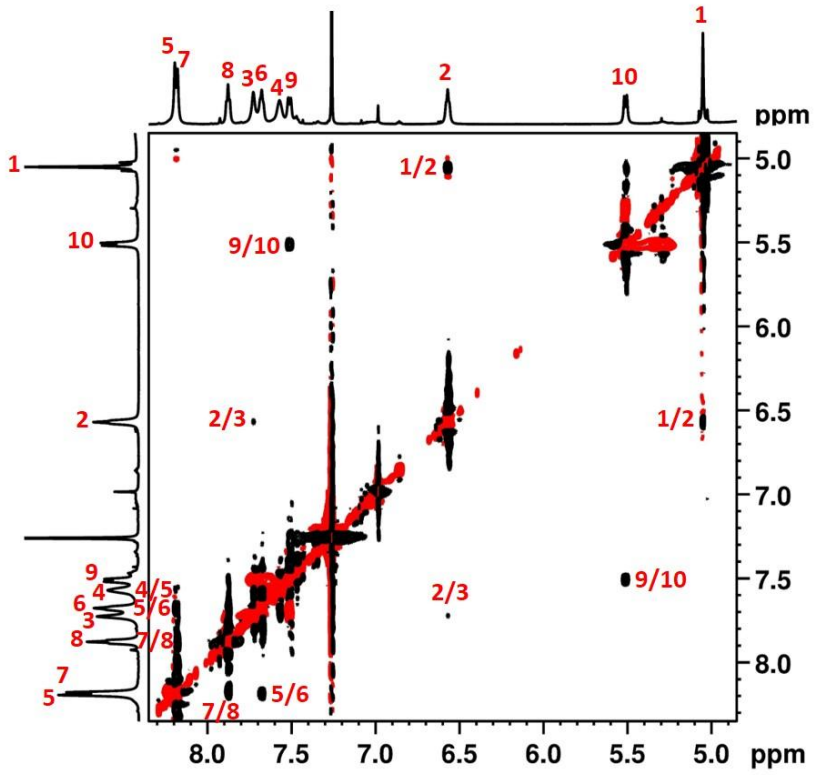

Figure 11 Partial ROESY spectrum of **P3** (5 mM) in $CDCl_3$ showing NH↔NH NOEs.

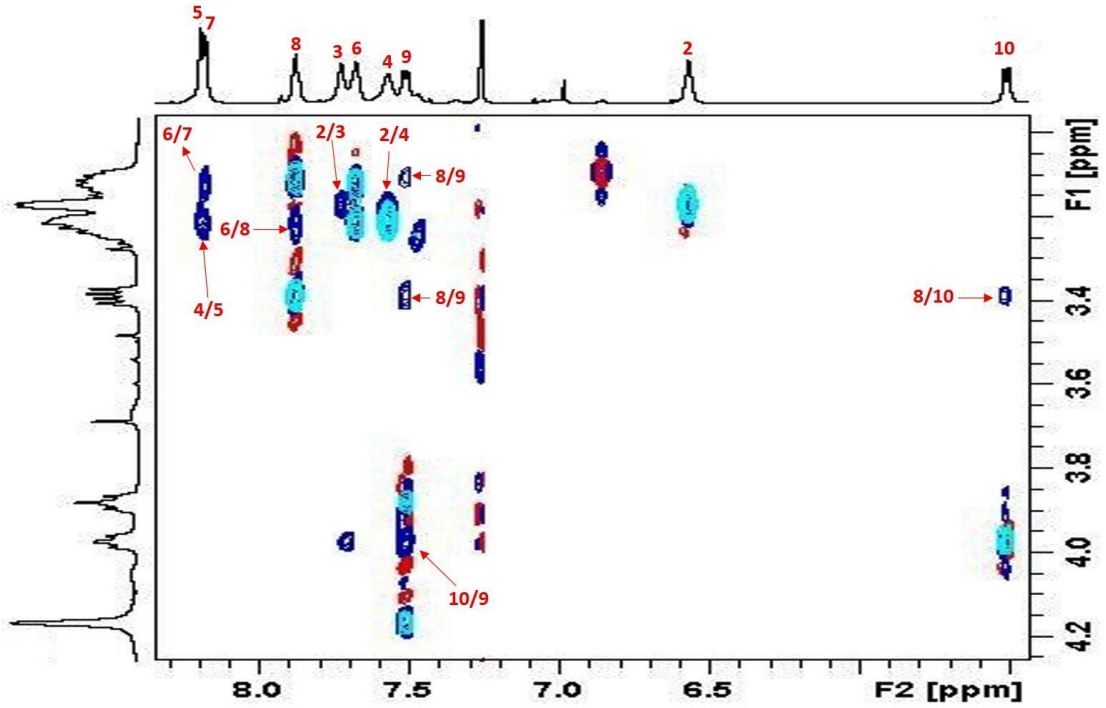

Figure 12 Partial ROESY (overlay with TOCSY, cayn) spectrum of **P3** (5 mM) in $CDCl_3$ showing NH↔$^{\gamma}CH_2$ NOEs of Adp and NH↔$^{\alpha}$CH NOEs of valine.

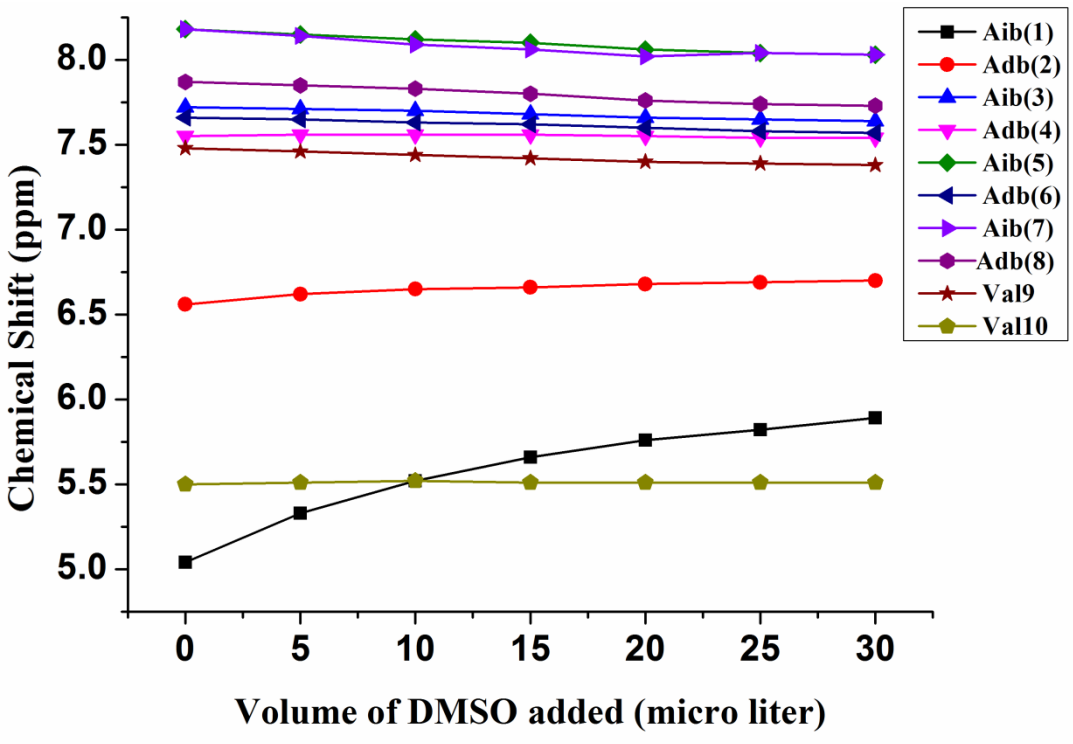

Figure 13 Solvent dependence of NH chemical shifts of the peptide, **P3**, at varying concentrations of $(CD_3)_2SO$.

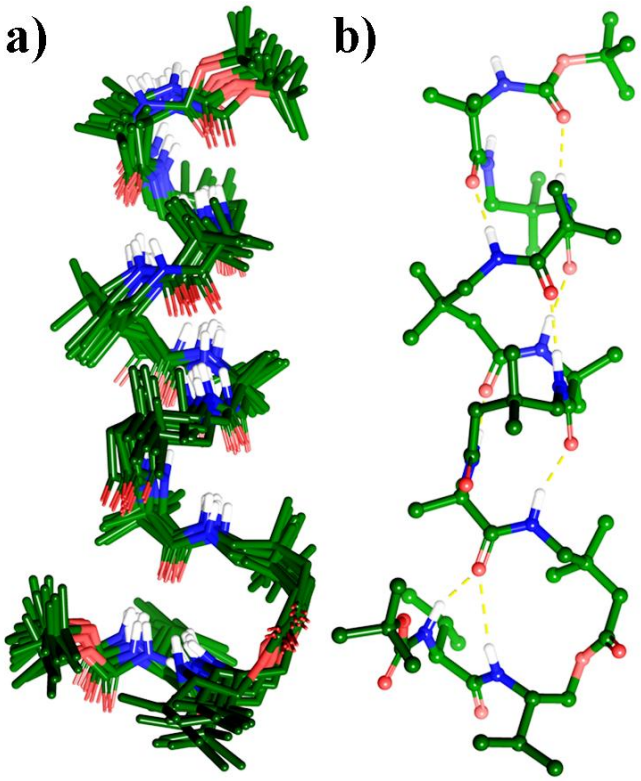

Figure 14: Solution NMR structures of peptide **P3**, a) 10 assembled structure and b) Low energy minimized structure.

Table 7 Backbone torsion angles (in degree) from the minimized lowest energy conformation of peptide **P3** sampled from simulation

Residue	φ	θ1	θ2	ψ
Aib(1)	-57.63			-39.90
Adp(2)	-125.24	60.54	51.26	-113.98
Aib(3)	-53.90			-47.68
Adp(4)	-125.19	52.67	59.35	-113.52
Aib(5)	-53.44			-50.89
Adp(6)	-125.61	52.69	60.80	-120.88
Aib(7)	-65.11			-37.87
Adp(8)	96.33	-179.02	57.74	68.98
Reduced Val(9)	65.11			58.83
Val(10)	-80.51			-18.40

6.3.6 Crystal structure of peptide P4

To realize the helix-Schellman loop type conformation of α,γ-hybrid peptides in single crystals and to support the solution structure of **P3**, we synthesized several α,γ-hybrid peptides from hexa to octapeptides composed of achiral amino acids with Boc-Val-Val-ol ester of C-terminal Adb. Among all the peptides synthesized, the hexapeptide **P4** (Scheme 1) composed of alternating Ac_6c and Adb yield X-ray quality crystals in aprotic $CHCl_3$. The X-ray structure of **P4** is shown in Figure 15. First three residues of **P4** adopted a left-handed 12-helix conformation, while the C-terminal Adb4 adopted a right-handed helical conformation. The torsion angles of Ac_{6C} and Adb residues are given in the Table 8. The H-bond parameters are tabulated in the Table 9. Structural analyses reveal that the C-terminus Boc-Val-Val dipeptide ester adopted a semi-extended type conformation. Notably, the carbonyl of Ac_6c3 participates in three-center H-bonds with amide NHs of Val5 (2→4) and Val6 (1→4)

involving 12 and 15 membered pseudocycles, respectively. Interestingly, the concavity induced at the site of bifurcated H-bonds is occupied by the solvent $CHCl_3$. The crystal structure of **P4** is mimicking helix-Schellman loops in protein structures, and in complete agreement with the solution structure of **P3**. Moreover, the helix terminating property of Adb esters was found to be persistent across the Aib/Adb hybrid peptide foldamers.

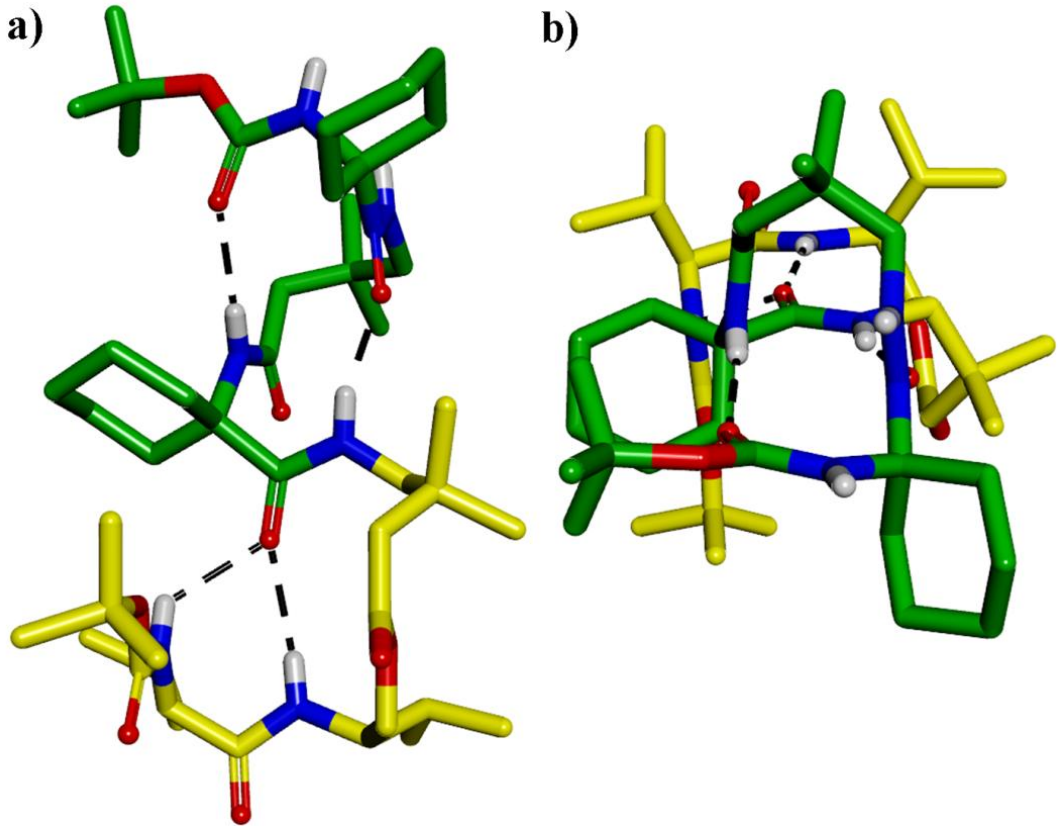

Figure 15 X-ray structure of peptide a) **P1** and b) Top view of **P1**

Table 8: Torsion Angle Parameters of **P4** (in degree)

α, γ - hybrids	ϕ	θ_1	θ_2	ψ	ω
Ac_6 1	53	-	-	46	175
Adb 2	120	-57	-62	120	172
Ac_6 3	61	-	-	40	176
Adb 4	-106	63	80	-44	-
Val 5	-61	-	-	-102	169
Val 6	-47	-	-	-74	178

Table 9: Hydrogen Bond Parameters of **P4**

Intramolecular H-bonds

Donor (D)	Acceptor (A)	D….A (Å)	DH….A (Å)	NH….O (deg)
N3	O2	2.96	2.11	169
N4	O3	2.80	1.97	163
N6	O5	2.88	2.26	129
N5	O5	3.11	2.28	163

Intermolecular H-bonds

Donor (D)	Acceptor (A)	D….A (Å)	DH….A (Å)	NH….O (deg)
N1	O9	2.96	2.12	162
N2	O8	2.94	2.11	160

6.4 Conclusion

In summary, we have demonstrated the unique folding properties of achiral α,γ-hybrid peptides composed of Aib and Adb. The two octapeptides (**P1** and **P2**) have shown to adopt helical conformations with opposite chirality, along with the helix terminating property at the C-terminal Adb esters. Accommodation of three different structural features in a single peptide foldamer is unprecedented. The Schellman motif type helix reversal is consistent across the hybrid peptides studied. The stabilization of the Val-Val dipeptide through three center H-bonds resembling the Schellman loops in protein structures. The study further reveals that the position of dialkyl substitutions on γ-amino acids has a major impact on the folding properties of γ-peptide foldamers and also induces fragility into the 12-helix

conformations of α,γ-hybrid peptides. More importantly, the role of protic solvents in the induction of opposite chirality within the helix cannot be ruled out. Overall, the simple chemistry of amino acid synthesis and the unique structural properties of α,γ-hybrid peptides presented here can be further explored to design novel foldamers.

6.5 Experimental section

General details

All amino acids, Ethyl 3,3-dimethylacrylate, nitro methane, Pd/C, TFA, EDC, HOBt, DIEPA, were commercially available. DCM, DMF, ethyl acetate and pet-ether (60-80 °C) were distilled prior to use. Column chromatography was performed on silica gel (120-200 mesh). Final peptides were purified on reverse phase HPLC (C18 column, MeOH/H_2O 70:30-95:5 as gradient with flow rate 2.5 mL/min). ^{1}H NMR and ^{13}C NMR spectra were recorded on 400 MHz and on 100 MHz respectively, using residual solvent signal as internal standards ($CDCl_3$). Chemical shifts (δ) reported in parts per million (*ppm*) and coupling constants (*J*) reported in Hz. Mass spectra were recorded using MALDITOF/TOF and HRMS Electron Spray Ionization (ESI).

NMR spectroscopy

All NMR studies were carried out by using either 400 or 600 MHz spectrometers. Resonance assignments were obtained by TOCSY and ROESY analysis. All two-dimensional data were collected in phase-sensitive mode by using the time-proportional phase incrementation (TPPI) method. Sets of 1024 and 512 data points were used in the t_2 and t_1 dimensions, respectively. For TOCSY and ROESY analysis, 32 and 72 transients were collected, respectively. A spectral width of 6007 Hz was used in both dimensions. A spin-lock time of 200 and 250 ms were used to obtain ROESY spectra. Zero-filling was carried out to finally yield a data set of 2 K × 1 K. A shifted square-sine-bell window was used before processing.

Molecular Dynamics (MD)

Structure calculation was done using a simulated annealing protocol in vacuum using DESMOND and OPLS 2005 force field with NOE and dihedral constraints. A fully extended peptide molecule (all backbone dihedral angles were kept to be 180˚) was kept in orthorhombic simulation cell of dimensions 40.96*66.43*32.40 Å. The upper limit for

distance was kept at 3 Å and 4 Å for strong and medium NOEs. All the lower distance limits were taken to be 1.8 Å. 1 Kcal/Mol force constant was used for all the constraints. NOE potentials (appropriate for treating ambiguous NOE assignments) used are having the following form,

E_{NOE} = fc * (lower - d)^2, if d < lower;

E_{NOE} = 0, if lower <= d <= upper;

E_{NOE} = fc * (upper - d)^2, if upper < d <= upper + sigma;

E_{NOE} = fc * (a + beta * (d - upper) + c / (d - upper)), if d > upper + sigma;

where d is the distance and fc is the force constant.

Values of sigma and beta used in the calculation are 0.5 and 1.5 respectively. The values a and c are determined automatically such that potential is continuous and differential everywhere.

Before production run simulation, a default NVT relaxation was done as implemented in DESMOND. NVT ensemble was used for the production run simulation. Berendsen thermostat with a relaxation time of 1 ps was used. A RESPA integrator was used in which for all the bonded interactions and near nonbonded interactions a time step of 1 fs was used and far nonbonded interaction time step of 3 fs was used. A cutoff of 9 Å was used for short range electrostatic interactions. A smooth particle mesh ewald method was used for treating long range electrostatic interactions. Simulated annealing was done in 6 stages. First stage consist simulation for 30 ps at 10 K. In the second stage, temperature was linearly increased to 100 K till 100 ps. In the third stage, temperature was linearly increased to 300 K till 200 ps. In the fourth stage, temperature was linearly increased to 400 K till 300 ps. In the fifth stage, temperature was maintained at 400 k till 500 ps. In the sixth stage, temperature was linearly decreased to 300 K till 1000 ps and maintained at 300 k till 1200 ps. 20 minimum energy structures were taken from the trajectory between 1000 ps and 1200 ps. The lowest energy structure from the trajectory between 1000 ps and 1200 ps was taken and minimized using a steepest descent method using a convergence gradient threshold of 0.05 kcal/mol/Å.

6.5.1 Crystal structure information

Crystal structure analysis of P1

Crystals of peptide were grown by slow evaporation from a solution of aqueous methanol. A single crystal (0.24 × 0.09 × 0.12 mm) was mounted on loop with a small amount of the paraffin oil. The X-ray data were collected at 100K temperature on a Bruker APEX(II) DUO CCD diffractometer using Mo K_α radiation (λ = 0.71073 Å), ω-scans (2θ = 56.804), for a total of 15327 independent reflections. Space group P-1, a = 12.4211(17), b = 14.978(2), c = 18.010(2), α = 86.938(3), β = 72.999(3), γ = 73.465(3),V = 3070.1(7)Å^3, triclinic, Z = 2 for chemical formula C_{53} H_{86} F_5 N_8 O_{12}, with one molecule in asymmetric unit; ρcalcd = 1.214 g cm^{-3}, μ = 0.096 mm^{-1}, F (000) = 1280, The structure was obtained by direct methods using SHELXS-97.[1] The final R value was 0.0611 (wR2 = 0.1421) 4923 observed reflections ($F_0 \geq 4\sigma$ ($|F_0|$)) and 558 variables, S = 0.895.The largest difference peak and hole were 0.474 and -0.506eÅ^3, respectively.CCDC No 1535091

Crystal structure analysis of P2

Crystals of peptide were grown by slow evaporation from a solution of aqueous methanol. A single crystal (0.34 × 0.06 × 0.18 mm) was mounted on loop with a small amount of the paraffin oil. The X-ray data were collected at 100K temperature on a Bruker APEX(II) DUO CCD diffractometer using Mo K_α radiation (λ = 0.71073 Å), ω-scans (2θ = 57.728), for a total of 16084 independent reflections. Space group P-1, a = 13.932(10), b = 14.137(10), c = 17.651(14), α = 103.854(18), β = 100.946(19), γ = 108.442(17),V = 3066(4)Å^3, triclinic, Z = 2 for chemical formula C_{53} H_{93} N_8 O_{12}, with one molecule in asymmetric unit; ρcalcd = 1.120 g cm^{-3}, μ = 0.079 mm^{-1}, F (000) = 1342, The structure was obtained by direct methods using SHELXS-97.[1] The final R value was 0.1173 (wR2 = 0. 0.2192) 5639 observed reflections ($F_0 \geq 4\sigma$ ($|F_0|$)) and 679 variables, S = 1.128.The largest difference peak and hole were 0.295 and -0.445 Å^3, respectively. CCDC No 1535092

Crystal structure analysis of P4

Crystals of peptide were grown by slow evaporation from a solution of chloroform. A single crystal (0.31 × 0.04 × 0.20 mm) was mounted on loop with a small amount of the paraffin oil. The X-ray data were collected at 100K temperature on a Bruker APEX(II) DUO CCD diffractometer using Mo K_α radiation (λ = 0.71073 Å), ω-scans (2θ = 57.14), for a total of 15677 independent reflections. Space group P 21, a = 11.261(3), b = 20.461(5), c = 14.368(4), γ = 108.903(6),V = 3132.1(14)Å^3, monoclinic, Z = 2 for chemical formula C_{47} H_{85} Cl_3 N_6 O_{13}, with one molecule in asymmetric unit; ρcalcd = 1.112gcm^{-3}, μ = 0.202mm^{-1}, F

(000) = 4599, The structure was obtained by direct methods using SHELXS-97.[1] The final R value was 0.1173 (wR2 = 0. 0.2310) 6854 observed reflections ($F_0 \geq 4\sigma$ ($|F_0|$)) and 637variables, S = 1.212.The largest difference peak and hole were 0.846 and -0.436 $Å^3$, respectively. CCDC No 1535094

6.5.2 Synthesis of γ-amino acid (Adb) and peptides

Synthesis of N- Boc protected 3,3-dimethylbutanoic acid (Adb)

Ethyl 3,3-dimethylacrylate (6.4 g, 50 mmol) was dissolved in neat nitro methane (13.5 mL, 250 mmol, 5 quivalents) and 1,8-diazabicyclo[5.4.0]undec-7-ene (DBU, 11.2 mL, 75 mmol, 1.5 quivalents) were added. The mixture was heated at 60 °C overnight, and the nitromethane was evaporated under reduced pressure. Ethyl acetate (300 mL) and 1M HCl (2x100 mL) were added to the resulting residue, and the organic phase was separated. The acidic aqueous layer was washed twice with ethyl acetate, the combined organic phase was dried over Na_2SO_4, and the solvent was evaporated under reduced pressure. The product, 3, 3-dimethyl-4-nitro-butyric acid ethyl ester was collected (7.56 g, 80 % yield) as colorless oil. The suspension of activated Pd/C (20% by weight) and 3,3-dimethyl-4-nitro-butyric acid ethyl ester (3.78 g, 20 mmol) in MeOH (40 mL) and acetic acid (5 mL) was stirred at room temperature in the presence of hydrogen. After completion of the reaction (TLC, ~36 hrs), Pd/C was filtered through the bed of celite and the filtrate was evaporated to dryness under vacuum to get gummy 4,4-dimethyl-2-pyrrolidinone (2.14 g, 95 % yield,) as oil. The amide NH group of 4,4-dimethyl-2-pyrrolidinone was further protected with Boc group and then hydrolyzed using NaOH (2.0 M) in MeOH to get final product *N*-Boc protected 3,3-dimethylbutanoic acid (3.21 g, 80 % yield in two step).

Synthesis of peptide P1-P4

Synthesis of all the peptides were carried out by conventional solution phase methods using racemization free fragment condensation strategy. The Boc group was used for the N-terminal protection and the C-terminus was protected as a benzyl ester. Couplings were carried out using *N*-Ethyl-*N′*-(3-dimethylaminopropyl) carbodiimide hydrochloride (EDC) and 1-hydroxybenzotriazole (HOBt). N-terminal protecting groups was removed with trifluoroacetic acid C-terminal benzyl group was deprotected by catalytic hydrogenation. Then $(Aib\text{-}Adp)_4$–COOH was further reacted with pentafluorobenzyl bromide and heptyl bromide in presence of potsium carbonate and DMF as solvent to obtain compound **P1** and

P2. For compound **P3** (Aib-Adp)$_4$–COOH was reacted with Boc-Val-Valol in presence of DCC and DMAP. Finally, all the peptides were purified by RP-HPLC using MeOH/H_2O system.

Structural data of the γ-amino acid (Adb) and peptides:

3,3-dimethylbutanoic acid (Adb)

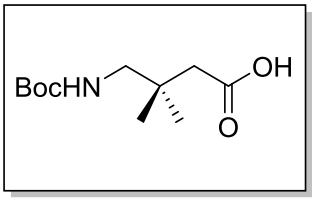

^{1}H NMR (400 MHz, DMSO-d_6) δ 11.94 (s, 1H), 6.86 – 6.55 (t, 1H), 2.86 (d, J = 6.4 Hz, 2H), 2.06 (s, 2H), 1.37 (s, J = 1.2 Hz, 9H), 0.89 (s, 6H). ^{13}C NMR (101 MHz, DMSO) δ 173.53, 156.54, 77.89, 50.55, 44.05, 34.82, 28.70, 25.07. HR-MS m/z calculated value for $C_{11}H_{21}NO_4$ is $[M+Na]^+$ 254.1368 and observed 254.1370.

PeptideP1

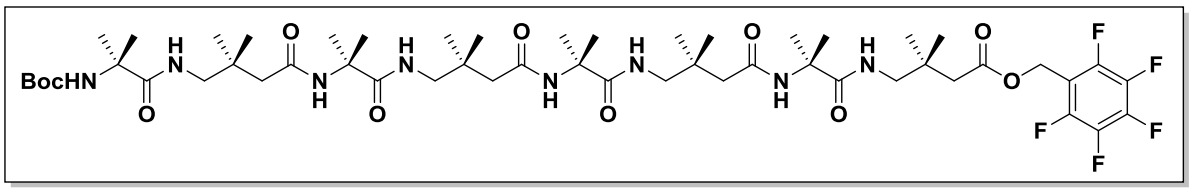

^{1}H NMR (600 MHz, Chloroform-d) δ 8.17 (s, 1H), 8.03 (s, 1H), 7.80 (t, J = 6.5 Hz, 1H), 7.71 (s, 1H), 7.61 (t, J = 6.5 Hz, 1H), 7.59 – 7.49 (m, 1H), 6.55 (t, J = 6.2 Hz, 1H), 5.16 (s, 2H), 4.98 (s, 1H), 3.27 – 3.04 (m, 8H), 2.33 (s, 2H), 2.06 (d, J = 11.3 Hz, 6H), 1.56 – 1.36 (m, 33H), 1.11 – 0.92 (m, 24H). MALDI TOF/TOF- *m/z* calcd. for $C_{52}H_{83}F_5N_8O_{11}$ $[M+Na]^+$ 1113.59, obsrvd. 1113.76.

PeptideP2

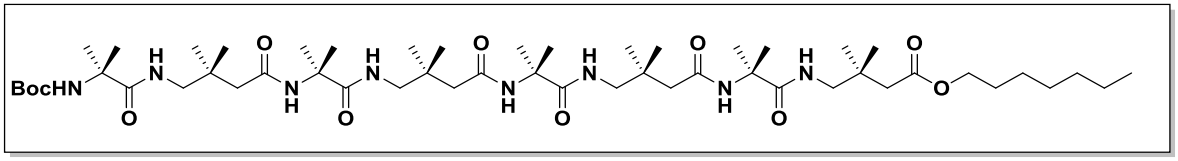

^{1}H NMR (400 MHz, Chloroform-d) δ 8.15 (s, 1H), 8.06 (s, 1H), 7.76 – 7.68 (m, 2H), 7.63 (t, J = 6.5 Hz, 1H), 7.53 (d, J = 7.7 Hz, 1H), 6.59 (t, J = 6.1 Hz, 1H), 5.06 (s, 1H), 4.03 (t, J = 6.8 Hz, 2H), 3.25 – 3.08 (m, 8H), 2.28 (s, 2H), 2.11 – 2.00 (m, 6H), 1.69 (s, 5H), 1.50 – 1.43

(m, 27H), 1.35 – 1.21 (m, 9H), 1.04 (dd, *J* = 12.3, 6.5 Hz, 24H), 0.90 – 0.83 (m, 3H). MALDI TOF/TOF- *m/z* calcd. for $C_{52}H_{96}N_8O_{11}$ $[M+Na]^+$ 1031.70, obsrvd. 1031.85.

PeptideP3

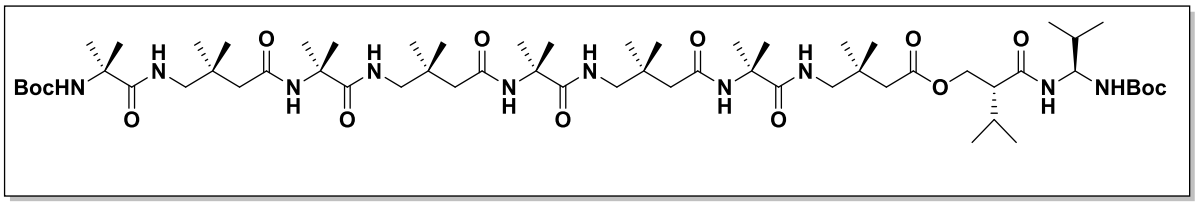

^{1}H NMR (600 MHz, Chloroform-*d*) δ 8.21 (d, *J* = 9.8 Hz, 2H), 7.90 (t, *J* = 6.5 Hz, 1H), 7.75 (s, 1H), 7.70 (t, *J* = 6.6 Hz, 1H), 7.59 (s, 1H), 7.54 (d, *J* = 9.3 Hz, 1H), 6.59 (t, *J* = 6.4 Hz, 1H), 5.53 (d, *J* = 9.2 Hz, 1H), 5.06 (d, *J* = 15.7 Hz, 1H), 4.19 (d, *J* = 2.8 Hz, 2H), 4.03 – 3.96 (m, 1H), 3.90 (tt, *J* = 9.2, 3.2 Hz, 1H), 3.29 – 3.09 (m, 10H), 2.15 – 2.05 (m, 9H), 1.57 – 1.41 (m, 57H), 1.11 – 0.99 (m, 32H), 0.98 – 0.90 (m, 15H). MALDI TOF/TOF- *m/z* calcd. for $C_{60}H_{110}N_{10}O_{14}$ $[M+Na]^+$ 1217.81, obsrvd. 1217.99.

Peptide P4

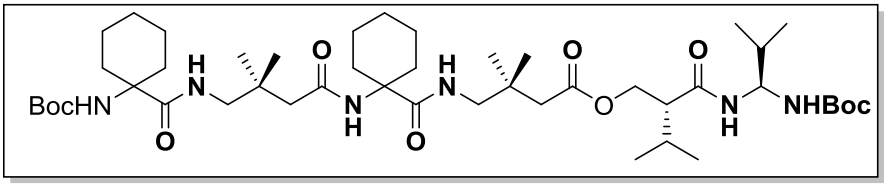

^{1}H NMR (400 MHz, Chloroform-*d*) δ 7.68 (s, 1H), 7.49 (d, *J* = 9.0 Hz, 2H), 6.87 (d, *J* = 7.7 Hz, 1H), 5.38 (d, *J* = 9.2 Hz, 1H), 4.87 (s, 1H), 4.25 (d, *J* = 10.7 Hz, 1H), 4.11 (d, *J* = 7.4 Hz, 1H), 3.98 (t, *J* = 8.2 Hz, 1H), 3.87 (td, *J* = 9.2, 4.8 Hz, 1H), 3.54 – 3.41 (m, 1H), 3.27 – 3.06 (m, 2H), 3.01 (d, *J* = 14.2 Hz, 1H), 2.30 (dd, *J* = 31.5, 14.5 Hz, 2H), 2.20 – 2.00 (m, 4H), 1.99 – 1.72 (m, 9H), 1.72 – 1.54 (m, 7H), 1.50 – 1.20 (m, 22H), 1.11 – 0.84 (m, 25H). MALDI TOF/TOF- *m/z* calcd. for $C_{46}H_{82}N_6O_{10}$ $[M+Na]^+$ 901.75, obsrvd. 901.7.

6.6 References

1. a) Cintas, P. *Angew. Chem. Int. Ed.* **2002**, *41*, 1139; b) Rickhaus, M.; Mayor, M.; Juríčka, M. *Chem. Soc. Rev.*, **2016**, *45*, 1542; c) Wang, Y. Xu, J. Wang, Y.; Chen, H. *Chem. Soc. Rev*., **2013**, *42*, 2930.
2. Novotny,M.; Kleywegt, G. J. *J. Mol. Biol.*, **2005**, *347*, 231.

3. a) Aravinda, S.; Shamala,N.; Balaram, P., *Chem. Biodiversity* **2008**, *5*, 1238; b) Venkatraman, J.; Shankaramma, S. C.; Balaram, P. *Chem. Rev*. **2001**, *101*, 3131; c) Karle, I. L.; Balaram, P. *Biochemistry* **1990**, *29*, 6747; d) Toniolo, C.; Crisma, M.; Formaggio, F.; Peggion, C. Biopolymers **2001**, *60*, 396; e) LeBailly, B. A. F.; Clayden, J. *Chem. Commun*., **201**6, *52*, 4852; f) Crisma, M.; De Zotti, M.; Formaggio, F.; Peggion, C.; Moretto, A.; Toniolo,C. *J. Pept. Sci*. **2015**, 21, 148.
4. a) Clayden,J.; Castellanos, A.; Solá, J.; Morris G. A. *Angew. Chem. Int. Ed.* **2009**, *48*, 5962; b) Solá, J.; Morris, G. A.; Clayden, J. *J. Am. Chem. Soc.* **2011**, 133, 3712. c) Solà, J.; Helliwell, M.; Clayden, J. *Biopolymers* **2011**, *95*, 62; d) De Poli, M.; Zawodny,W.; Quinonero, O.; Lorch, M.; Webb, S. J.; Clayden, J. *Science*, **2016**, *352*, 575; e) Ousaka, N.; Inai, Y.; Kuroda, R. *J. Am. Chem. Soc*., **2008**, *130*, 12266. f) Solà, J.; Helliwell, M.; Clayden J. *J. Am. Chem. Soc*., **2010**, 132 , 4548; g) Pike, S.J.; Boddaert, T.; Raftery, J.; Webb, S. J.; Clayden, J. *New J. Chem.*, **2015**, *39*, 3288; h) Benedetti, E; Saviano, M; Iacovino, R; Pedone, C; Santini, A; Crisma, M; Formaggio, F; Toniolo, C; Broxterman, Q B; Kamphuis, J. *Biopolymers* **1998**, *46*, 433; i) Pengo, B; Formaggio, F; Crisma, M; Toniolo, C; Bonora, G M; Broxterman , QB; Kamphuis, J; Saviano, M; Iacovino, R; Rossi, F; Benedetti, E. *J. Chem. Soc*., Perkin Trans. **1998**, *2*, 1651; j) Inai, Y; Tagawa, K; Takasu, A; Hirabayashi, T; Oshikawa, T; Yamashita, M. *J. Am. Chem. Soc.* **2000**, *122*, 11731; k) Inai, Y; Ishida, Y; Tagawa, K; Takasu, A; Hirabayashi, T. *J. Am. Chem. Soc*. **2002**, *124*, 2466; l) Komori, H; Inai, Y; *J. Org. Chem*. **2007**, *72*, 4012. m) Ousaka, N; Inai, Y; Kuroda, R. *J. Am. Chem. Soc*. **2008**, *130*, 12266; n) Ousaka, N; Inai Y. *J. Org. Chem*. **2009**, *74*, 1429. o) Demizu, Y; Yamagata, N; Sato, Y; Doi, M; Tanaka, M; Okuda, H; Kurihara, M. *J. Pept. Sci*. **2010**, *16*, 153; p) Karle, I.L; Flippen-anderson, J.L.; Gurunath, R.; Balaram, P. Protein Science **1994**, *3*, 1547; q) Dannecker-Doring, I.; Linden, A.; Heimgartner, H. *Helv. Chim. Acta.* **2011**, *94*, 993.
5. a) Seebach, D.; Beck, A. K.; Bierbaum, D. J. *Chem. Biodiversity* **2004**, *1*, 111; b) Horne, W. S.; Gellman,S. H. *Acc. Chem. Res.* **2008**, *41*, 1399; c) Cheng, R. P.; Gellman, S. H.; DeGrado,W. F. *Chem. Rev.* **2001**, *101*, 3219; d) Fülöp, F.; Martinek,T. A.; Tóth, G. K. *Chem. Soc. Rev.* **2006**, *35*, 323; e) Guichard, G.; Huc, I. *Chem. Commun.* **2011**, *47*, 5933; f) Vasudev, P. G.; Chatterjee, S.; Shamala, N.; Balaram, P. *Chem. Rev.* **2011**, *111*, 657; g) Martinek, T. A.; Fülöp, F. *Chem. Soc. Rev.* **2012**, *41*, 687. h) Bouillère, F.; Thétiot-Laurent, S.; Kouklovsky, C.; Alezra,V. *Amino Acids* **2011**, *41*, 687. i) Baldauf, C. ; Hofmann, H.-J.; *Helv. Chim. Acta* **2012**, *95*, 2348; j)

Goodman, C. M.; Choi, S.; Shandler, S.; DeGrado, W. F.; *Nat. Chem. Biol*. **2007**, *3*, 252; k) *Foldamers: Structure, Properties and Applications (Eds.: S. Hecht, I. Huc)*, Wiley-VCH, Weinheim, **2007**; l) Gellman, S. H. *Acc. Chem. Res*. **1998**, *31*, 173; m) Pilsl, L. K. A.; Reiser, O. *Amino Acids* **2011**, *41*, 709.

6. a) Shin, S.; Lee, M.; Guzei, I. A.; Kang,Y. K.; Choi, S. H. *J. Am. Chem. Soc.* **2016**, *138*, 13390; b) Collie, G. W.; Pulka-Ziach, K.; Lombardo,C. M.; Fremaux, J.; Rosu, F.; Decossas, M.; Mauran, Mauran,L.; Lambert, O.; Gabelica,V.; Mackeret, C. D.; Guichard, G. *Nature Chemistry*, **2015, *7***, 871; c) Basuroy ,K.; Dinesh, B.; Reddy, M.; Chandrappa, S.; Raghothama, S.; Shamala, N.; Balaram, P. *Org. Lett*., **2013**, *15* , 4866; d) De Pol, S.; Zorn, C.; Klein, C. D.; Zerbe, O.; Reiser, O. *Angew. Chem., Int. Ed.* **2004**, *43*, 511; e) Baldauf, C.; Günther, R.; Hofmann, H.-J. *Biopolymers* **2006**, *84*, 408; f) Lee, M.; Shim, J.; Kang, P.; Guzei, I. A.; Choi, S. H.; *Angew. Chem., Int. Ed*. **2013**, *52*, 12564. g) Baldauf, C.; Günther, R.; Hofmann, H.-J. *J. Org. Chem.* **2006**, *71*, 1200 h) Sharma, G. V. M.; Jadhav, V. B.; Ramakrishna, K. V. S.; Jayaprakash, P.; Narsimulu, K.; Subash,V.; Kunwar, A. C.; *J. Am. Chem. Soc.* **2006**, *128*, 14657; i) Vasudev, P. G.; Ananda, K.; Chatterjee, S.; Aravinda, S.; Shamala, N.; Balaram, P. *J. Am. Chem. Soc.* **2007**, *129*, 4039; j) Guo, L.; Almeida, A. M.; Zhang, W.; Reidenbach, A. G.; Choi, S. H.; Guzei, I. A;. Gellman, S. H. *J. Am. Chem. Soc.* **2010**, *132*, 7868; k) Guo, L.; Zhang, W.; Guzei, I. A.; Spencer, L. C.; Gellman, S. H. *Org. Lett*. **2012**, *14*, 2582; l) Basuroy, K.; Dinesh, B.; Shamala, N.; Balaram, P. *Angew. Chem., Int. Ed*. **2012**, *51*, 8736; m) Bandyopadhyay, A.; Jadhav, S. V.; Gopi, H. N. *Chem. Commun.* **2012**, *48*, 7170; n) Basuroy, K.; Dinesh, B.; Shamala, N.; Balaram, P. *Angew. Chem., Int. Ed.* **2013**, *52*, 3136; o) Giuliano, M. W.; Maynard, S. J.; Almeida, A. M.; Guo, L.; Guzei, I. A.; Spencer, L. C.; Gellman, S. H.; *J. Am. Chem. Soc*. **2014**, *136*, 15046; p) Sonti, R.; Dinesh, B.; Basuroy, K.; Raghothama, S.; Shamala, N.; Balaram, P. *Org. Lett*. **2014**, *16*, 1656. q) Fisher, B.
7. Abele, S.; Seiler, P.; Seebach, D. *Helv. Chim. Acta*, **1999**, *82*, 1559.
8. Seebach, D.; Sifferlen,T.; Bierbaum, D. J.; Rueping, M.; Jaun,B.; Schweizer, B. Schaefer, J.; Mehta, A. K.; Connor, R. D. O' Meier, B. H.; Ernst, M.; Glättli, A. *Helv. Chim. Acta* **2002**, *85*, 2877 .
9. Vasudev, P. G.; Shamala N.; Ananda, K.; Balaram, P. *Angew. Chem. Int. Ed*. **2005**, *44*, 4972.
10. Chatterjee, S.; Vasudev, P. G.; Ragothama, S.; Ramakrishna, C.; Shamala, N.; Balaram, P. *J. Am. Chem. Soc.* **2009**, *131*, 5956.

11. Jadhav, S. V.; Gopi, H. N. *Chem. Commun*. **2013**, *49*, 9179.
12. Misra, R. Saseendran, A.; George, G.; Veeresh, K.; Raja, K. M. P.; Raghothama, S.; Hofmann, H.-J; Gopi, H. N. *Chem. Eur. J*. **2017**, *23*, 3764.
13. Kumar, M. G.; Mali, S. M.; Gopi, H. N. *Org. Biomol. Chem*. **2013**, *11*, 803.
14. Goriely, A.; Tabor, M. *Phys. Rev. Lett*. **1998**, *80*, 1564.
15. Tomsett, M.; Maffucci, I.; Le Bailly, B. A. F.; Byrne, L.; Bijvoets, S. M.; Lizio, M. G.; Raftery, J.; Butts, C. P.; Webb, S. J.; Contini, A.; Clayden, J. *Chem. Sci.* **2017**, *8*, 3007.
16. Banerjee, A.; Raghothama, S.; Karle, I. L.; Balaram P. *Biopolymers*. **1996**, *39*, 279.
17. a) Baldauf, C.; Günther, R.; Hofmann, H.-J. *J. Org. Chem*. **2006**, *71*, 1200; b) Jadhav, S. V.; Bandyopadhyay, A.; Gopi, H. N. *Org. Biomol. Chem*. **2013**, *11*, 509; c) Fisher, B. F.; Gellman, S. H. *J. Am. Chem. Soc.* **2016**, *138*, 10766.
18. Schellman, C. In *Protein Folding;* Jaenicke, R., Ed.; Elsevier/North-Holland Biochemical Press: Amsterdam, **1980**, 53.
19. a) Aravinda, S.; Shamala, N.; Bandyopadhyay A.; Balaram, P. *J. Am. Chem. Soc*. **2003**, *125*, 15065; b) Pike, S.; Raftery, J. J.; Webb S. J.; Clayden, J, *Org. Biomol. Chem*., **2014**, *12*, 4124; c) Ousaka, N.; Inai Y. *J. Am. Chem. Soc*. **2006**, *128*, 14736; d) Shepherd,N. E.; Hoang, H. N.; Abbenante, G.; Fairlie, D. P. *J. Am. Chem. Soc*. **2009**, *131*, 15877; e) Maurizot,V.; Dolain, C.; Leydet,Y.; Le´ger, J. M.; Guionneau, P.; Huc, I. *J. Am. Chem. Soc*. **2004**, *126*, 10049; f) Aravinda,S.; Shamala, N.; Pramanik, A.; Das, C.; Balaram, P. *Biochem. Biophys. Res. Commun*., *273*, 933. g) Karle I. L. *Biopolymers (peptide science)* **2001**, *60*, 351; h) Datta, S.; Shamala, N.; Banerjee, A.; Pramanik, A.; Bhattacharyya, S.; Balaram P. *J. Am. Chem. Soc*. **199**7, *119*, 9246; i) Kumaki, J.; Kawauchi,T.; Okoshi, K.; Kusanagi, H.; Yashima, E. *Angew. Chem. Int. Ed*. **2007**, *46*, 5348.

6.7 Appendix I Mass spectra and ^{1}H NMR spectra for the monomer Adb and peptides P1 to P4

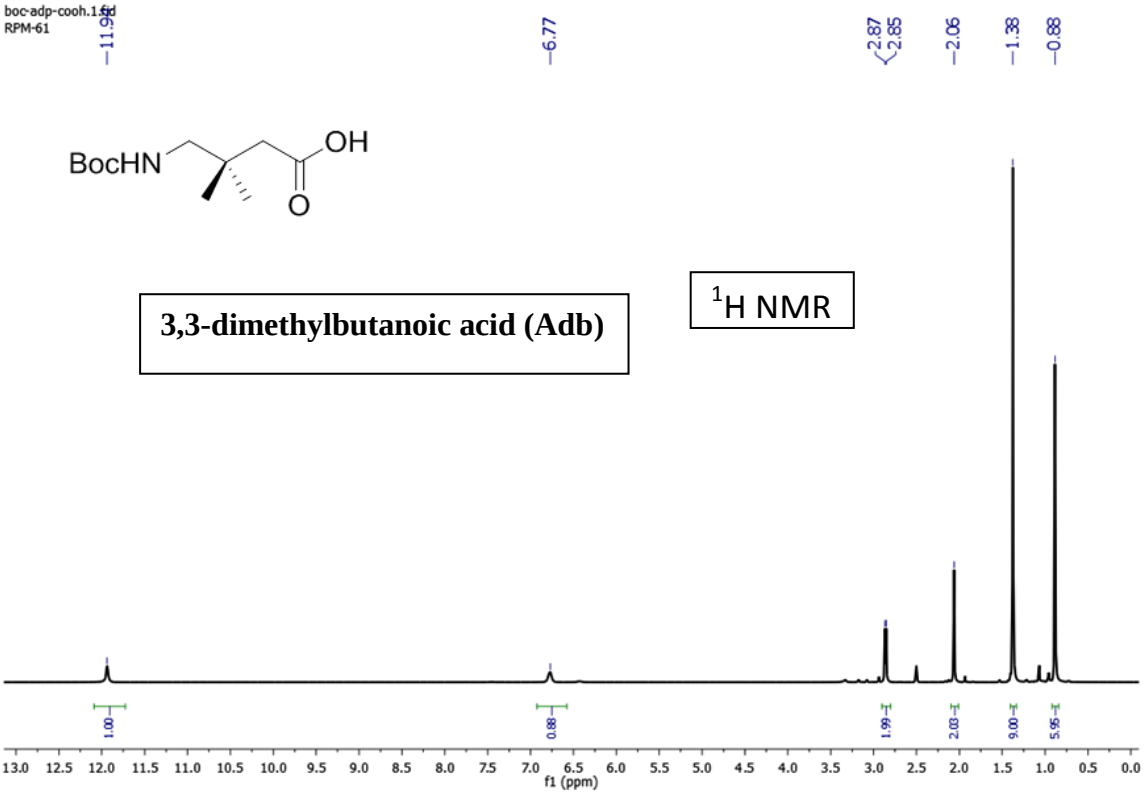

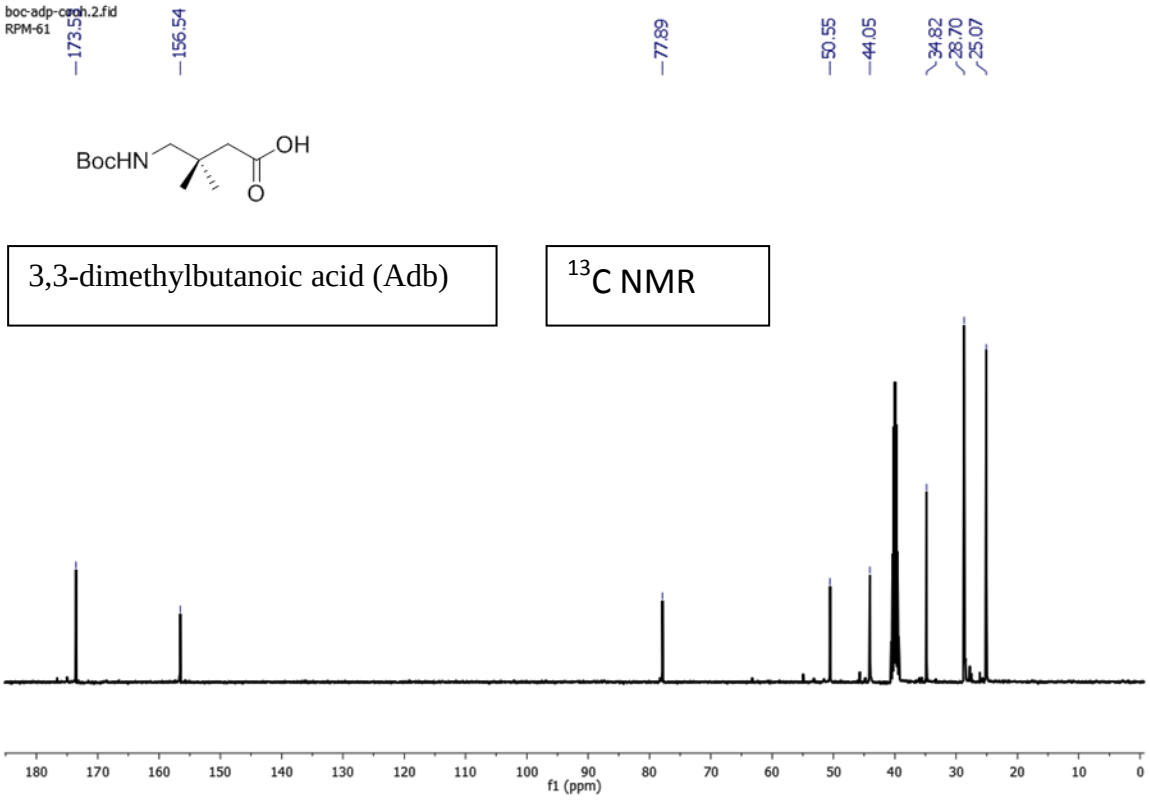

3,3-dimethylbutanoic acid (Adb)

^{13}C NMR

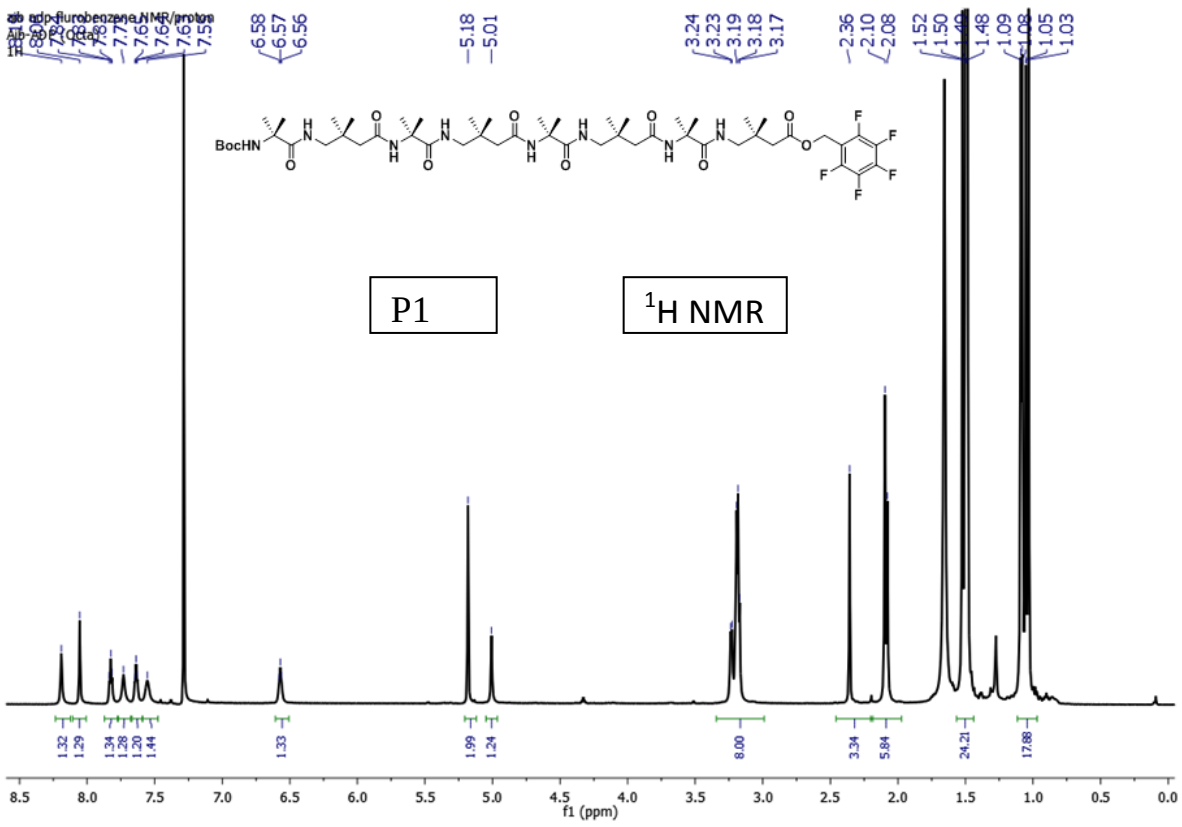
BocHN
P1
1H NMR
f1 (ppm)

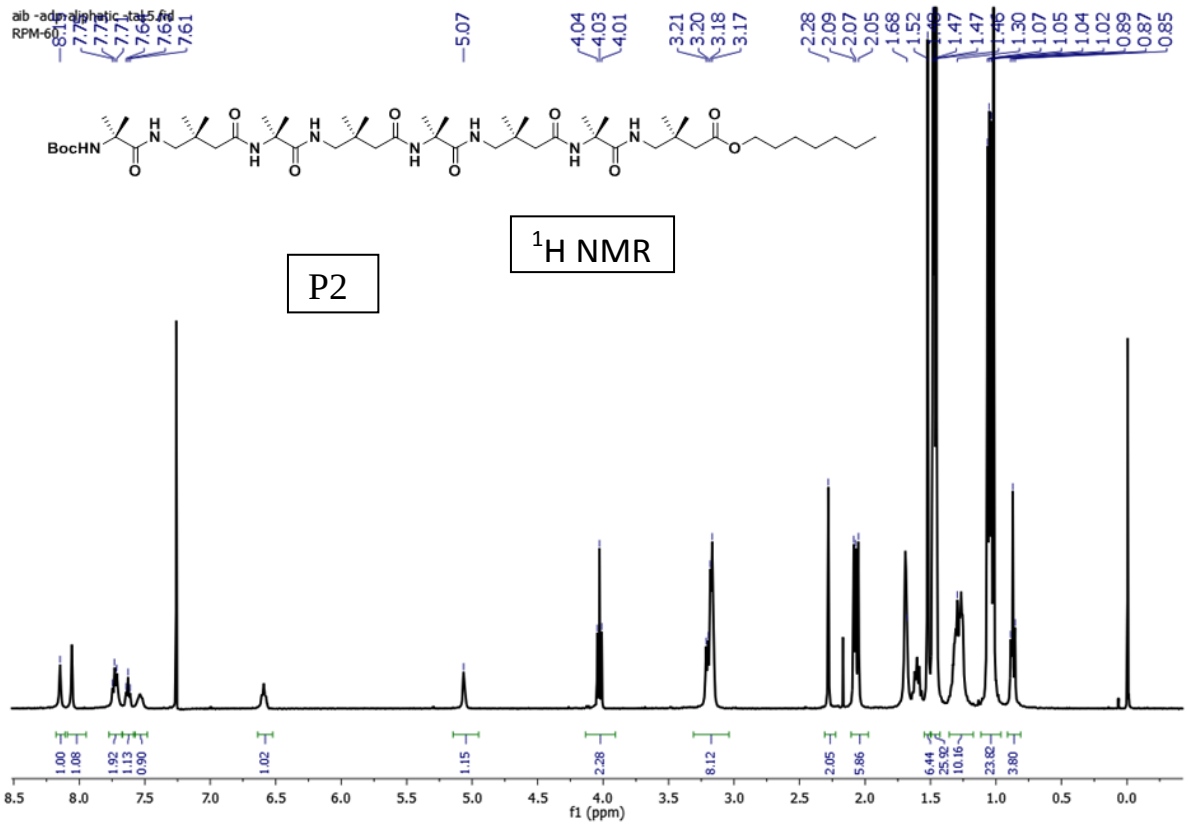
aib -adm aliphatic -tal5.fid
RPM-60
8.13
7.78
7.77
7.71
7.64
7.62
7.61
5.07
4.04
4.03
4.01
3.21
3.20
3.18
3.17
2.28
2.09
2.07
2.05
1.68
1.52
1.47
1.47
1.46
1.30
1.07
1.05
1.04
1.02
0.89
0.87
0.85
BocHN
P2
1H NMR
1.00
1.08
1.92
1.13
0.90
1.02
1.15
2.28
8.12
2.05
5.86
6.44
25.92
10.16
23.82
3.80
8.5
8.0
7.5
7.0
6.5
6.0
5.5
5.0
4.5
4.0
3.5
3.0
2.5
2.0
1.5
1.0
0.5
0.0
f1 (ppm)

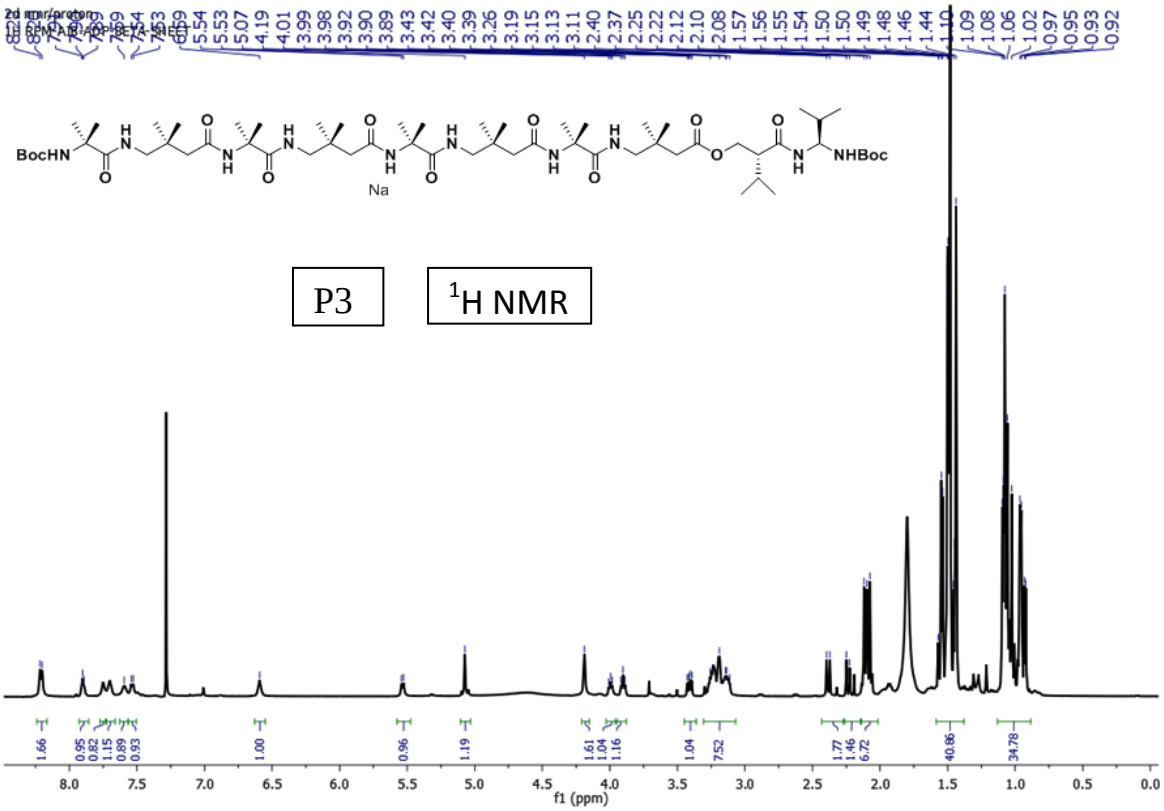
BocHN
NHBoc
Na
P3
1H NMR
f1 (ppm)

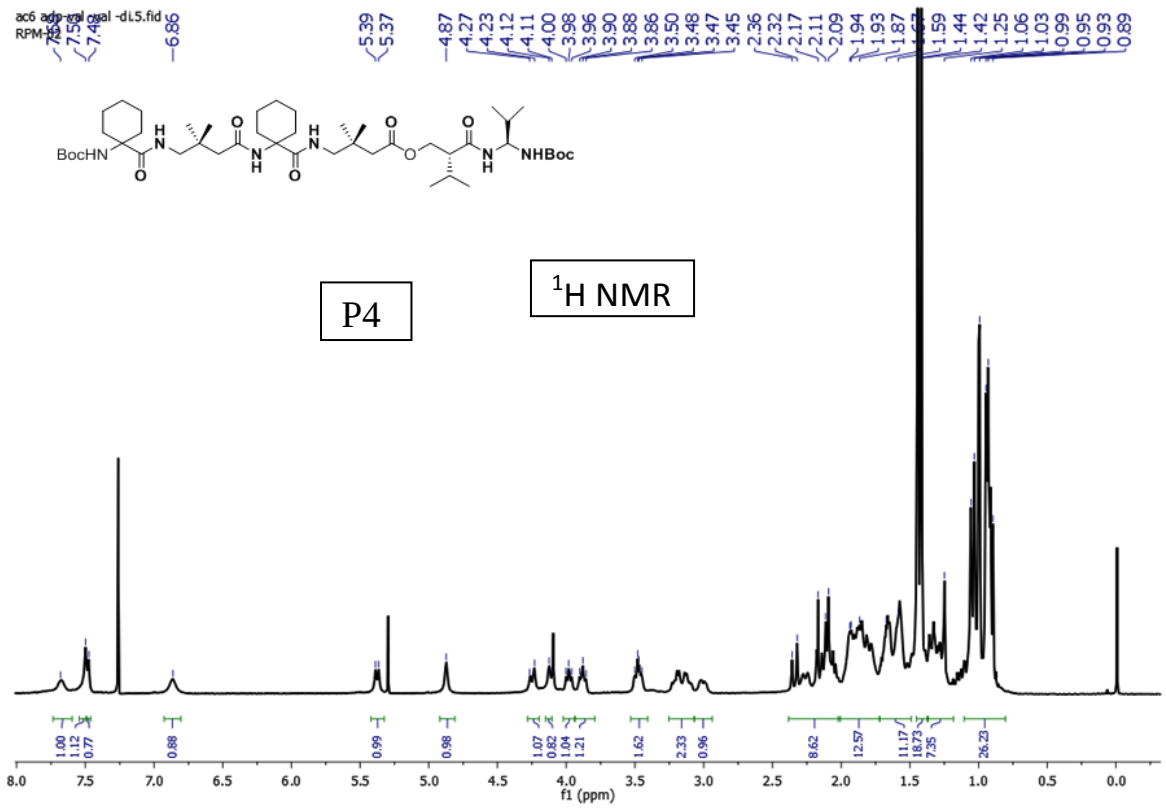
BocHN
NHBoc
P4
1H NMR
f1 (ppm)

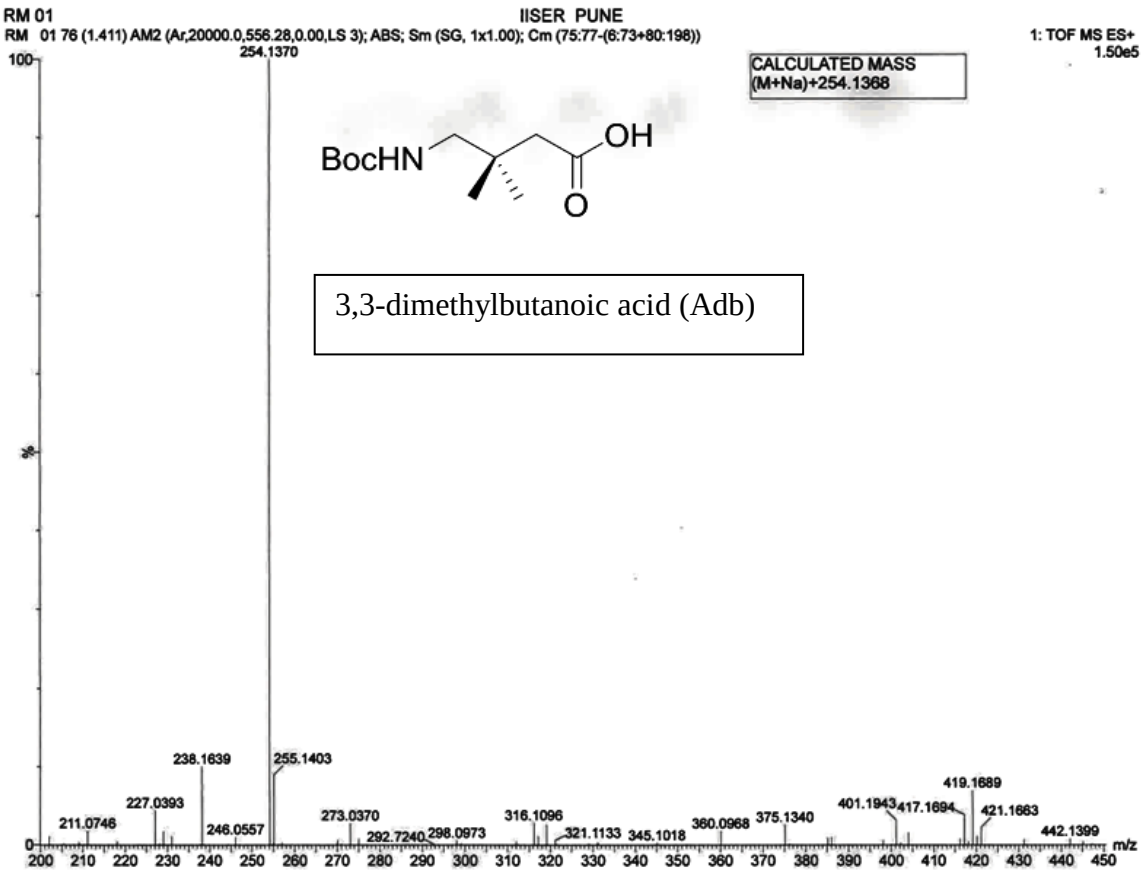
RM 01
IISER PUNE
RM 01 76 (1.411) AM2 (Ar,20000.0,556.28,0.00,LS 3); ABS; Sm (SG, 1x1.00); Cm (75:77-(6:73+80:198))
1: TOF MS ES+
1.50e5
CALCULATED MASS
(M+Na)+254.1368
BocHN
OH
O
3,3-dimethylbutanoic acid (Adb)
254.1370
238.1639
255.1403
227.0393
211.0746
246.0557
273.0370
292.7240
298.0973
316.1096
321.1133
345.1018
360.0968
375.1340
401.1943
417.1694
419.1689
421.1663
442.1399
m/z

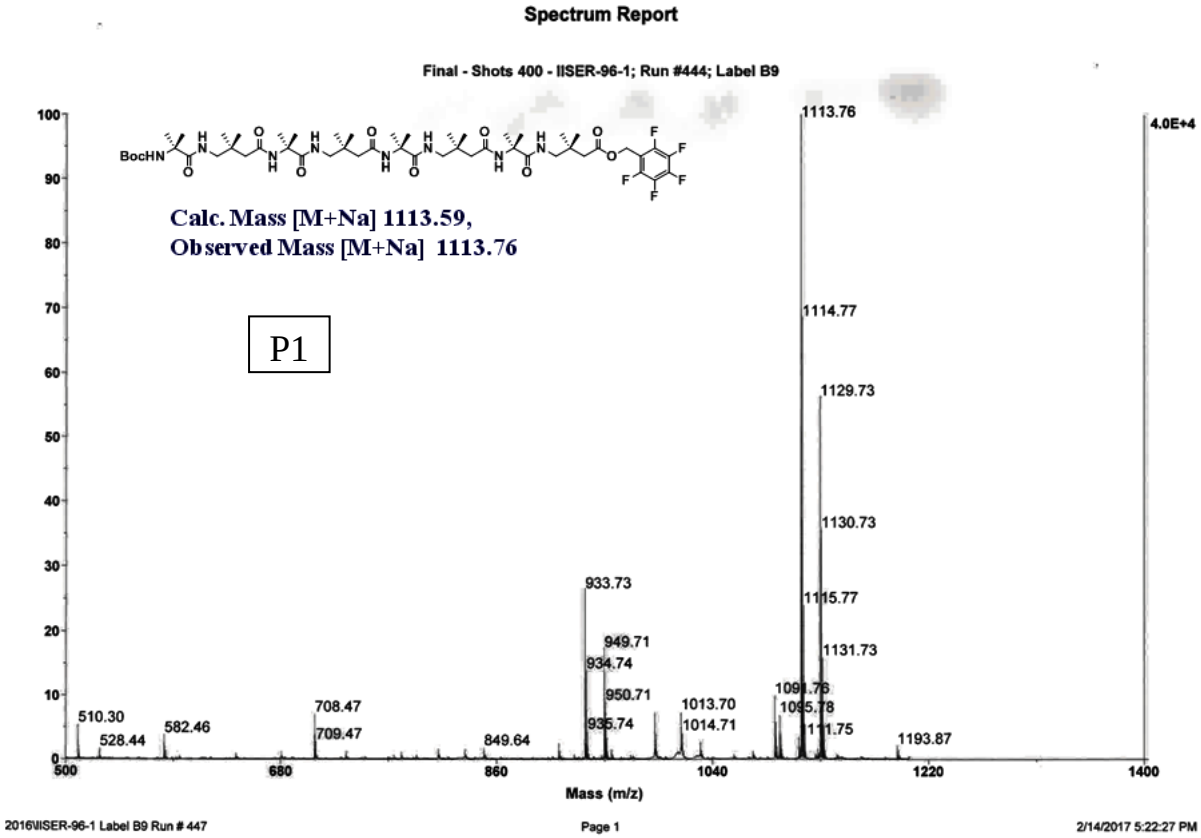
Spectrum Report
Final - Shots 400 - IISER-96-1; Run #444; Label B9
BocHN
Calc. Mass [M+Na] 1113.59,
Observed Mass [M+Na] 1113.76
P1
1113.76
4.0E+4
1114.77
1129.73
1130.73
933.73
1115.77
949.71
1131.73
934.74
950.71
1013.70
1014.71
708.47
709.47
510.30
528.44
582.46
849.64
935.74
1193.87
Mass (m/z)
2016\IISER-96-1 Label B9 Run # 447
Page 1
2/14/2017 5:22:27 PM

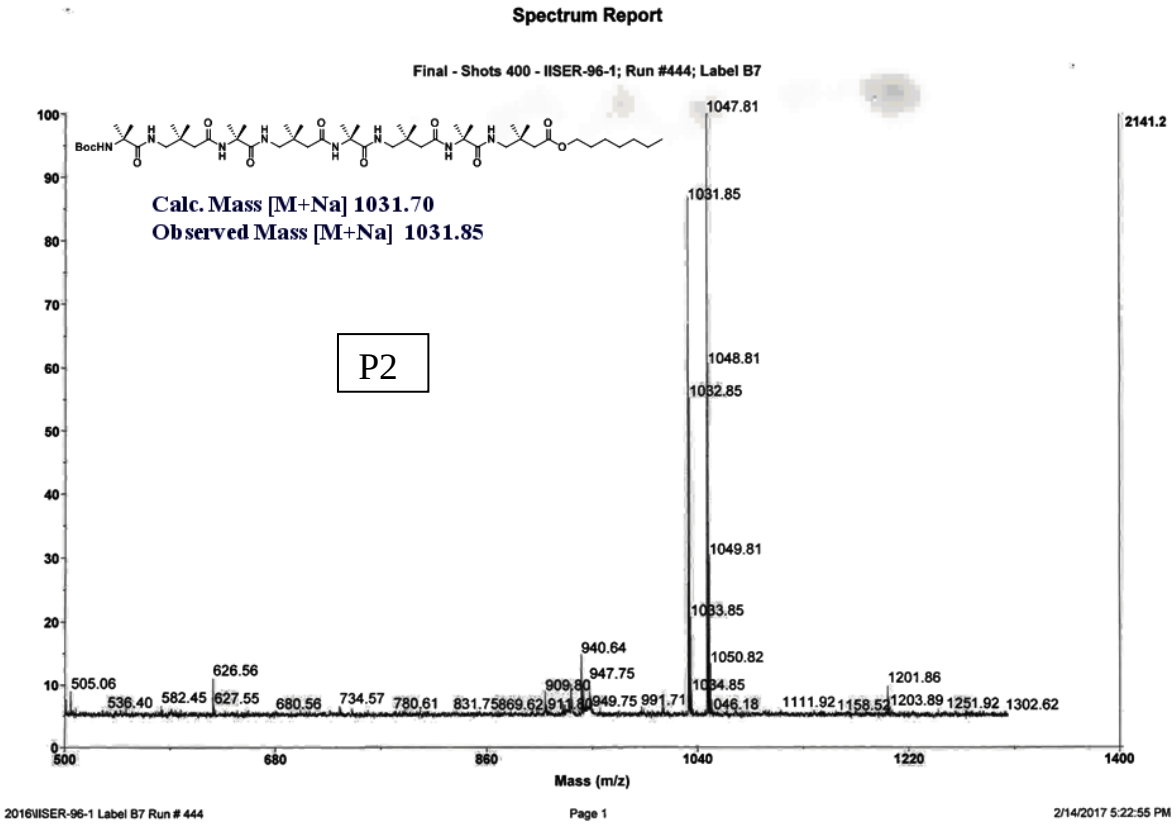
Spectrum Report
Final - Shots 400 - IISER-96-1; Run #444; Label B7
BocHN
Calc. Mass [M+Na] 1031.70
Observed Mass [M+Na] 1031.85
P2
1047.81
2141.2
1031.85
1048.81
1032.85
1049.81
1033.85
940.64
1050.82
947.75
626.56
505.06
1201.86
536.40
582.45
627.55
680.56
734.57
780.61
831.75
869.62
909.80
949.75
991.71
1034.85
1046.18
1111.92
1158.52
1203.89
1251.92
1302.62
Mass (m/z)
2016\IISER-96-1 Label B7 Run # 444
Page 1
2/14/2017 5:22:55 PM

Spectrum Report

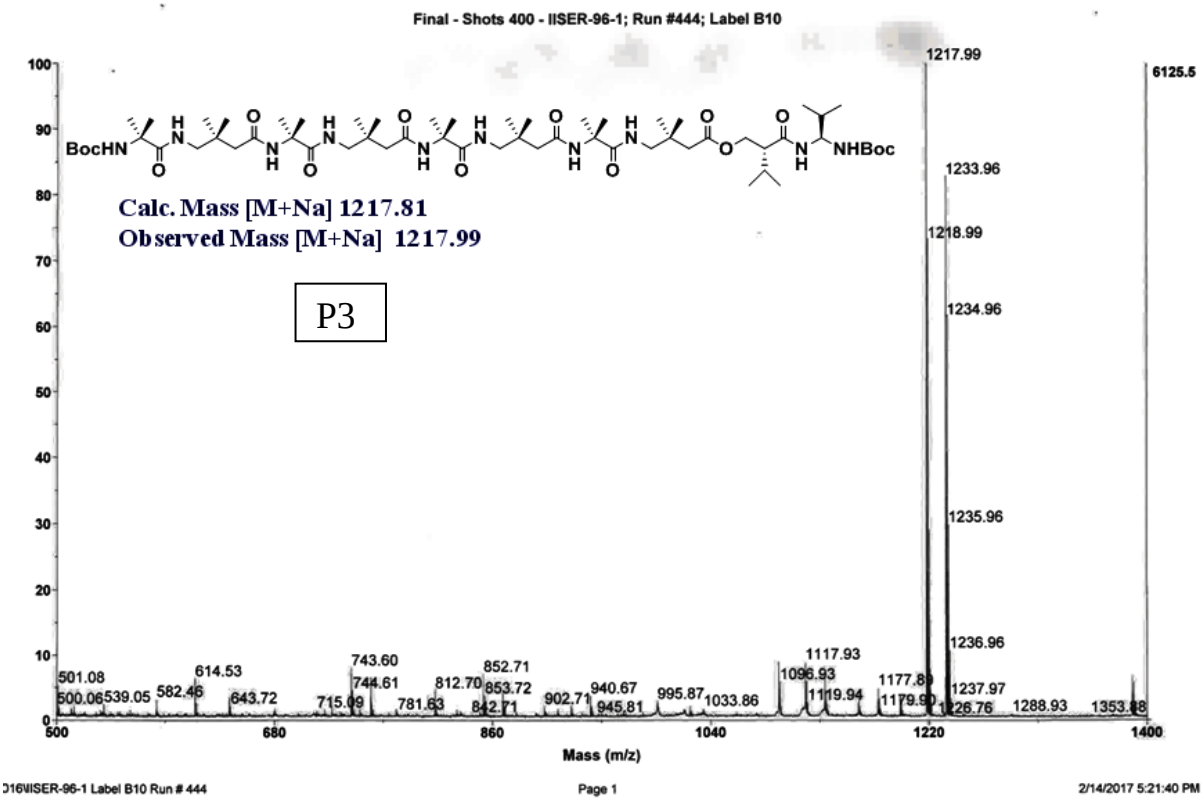

Spectrum Report

~~A-07~~ RM-01

Final - Shots 400 - IISER-96-1; Run #459; Label D8

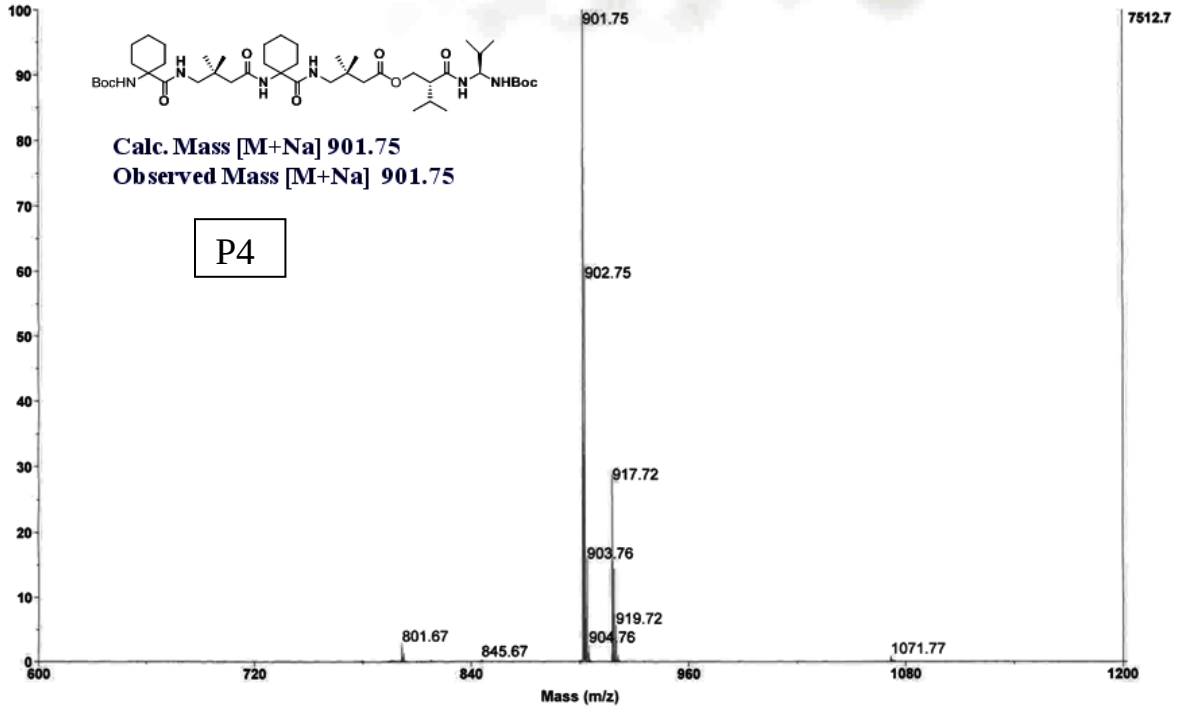

2016\IISER-96-1 Label D8 Run # 459 Page 1 2/21/2017 11:35:02 AM